UNIVERSITY OF SOUTHAMPTON

INVESTIGATION ON THE ROLE OF LIPIDS IN THE REGULATION OF PROTEIN FUNCTION

MARIA-NEFELI TSALOGLOU BSc DHons

THESIS SUBMITTED FOR THE DEGREE OF DOCTOR OF PHILOSOPHY

FACULTY OF SCIENCE
SCHOOL OF CHEMISTRY

MARCH 2008

To my grandparents,

Χρυσούλα & Βασίλη

Κούλα & Αντώνη

Λιλή & Ντίνο

UNIVERSITY OF SOUTHAMPTON

ABSTRACT

FACULTY OF SCIENCE

CHEMISTRY

Doctor of Philosophy

INVESTIGATION ON THE ROLE OF LIPIDS IN REGULATION OF PROTEIN FUNCTION

By Maria-Nefeli Tsaloglou

Type II amphiphiles have been shown *in vitro* to activate the catalytic activity of the rate-determining enzyme of lipid metabolism CTP: phosphocholine cytidylyltransferase (CCT). Membrane stored curvature elastic stress has been suggested as a regulator of CCT activity. It has been postulated that Type II lipids, which form membranes with high curvature elastic stress, activate CCT by increasing the partitioning of CCT onto the membrane. Conversely, Type I lipids inhibit CCT activity by decreasing stored elastic energy.

This investigation was undertaken to further support that the stored elastic stress regulates the activity of CCT. The effect of 28 different lipidic systems on CCT was studied *in vitro* using a ^{14}C radiochemical assay. Our results were consistent with the predictions resulting from the hypothesis.

The effect of two Type I amphiphiles hexadecylphosphocholine and hexadecylammonium bromide on phospholipid metabolism of transfected GFP-HeLa cells was studied *in vivo*. Membrane lipids were quantified by electrospray ionisation mass spectrometry and cells were sized using a novel optical microscopy image analysis method. Both drugs inhibited CCT and decreased cell size, thus suppressing phospholipid metabolism as predicted by our hypothesis.

Finally, a study was conducted into whether the catalytic activity of phosphofructokinase (PFK-1), a major regulatory enzyme of glycolysis, is regulated via membrane stored curvature elastic stress analogously to CCT. A novel ^{33}P radiochemical assay was developed and, for the first time, PFK-1 kinetics in the presence of membranes were investigated for the bacterium *Bacillus stearothermophilus*. Large unilamellar vesicles consisting in di-oleoyl phosphocholine/oleic acid (50:50) and di-oleoyl phosphocholine (100%) both activated the enzyme, as predicted by our hypothesis but less markedly than in the case of CCT.

Overall, our studies have raised important questions on how lipid compositional diversity might be controlled *in vivo* and have provided important evidence supporting the membrane stored elastic stress hypothesis of enzyme regulation.

Declaration

This thesis is the result of work done whilst registered as a postgraduate student at the University of Southampton.

_____

Maria-Nefeli Tsaloglou

Contents

Appendices

Acknowledgements

I am indebted to George Attard for being an excellent supervisor, inspiring and terrifying, with his generous funding, his relentless scientific creativity and for allowing me ample experimental freedom. Above all, I thank him for heartfelt conversations when I was under the weather with serious illness.

There are not enough words to thank Marcus Dymond for teaching me experimental techniques, explaining me innumerable times the same things, helping with analyses and exegeses, correcting my thesis and being my kind of normal person. I hope it suffices to him to know that although I do not believe in mentors, I consider him to be the closest to one I will ever have.

Also, I would like to thank Geoffrey Luckhurst for inspiring to do a PhD with his integrity, professionalism and elegant views on science.

Past and present members of our research group have contributed to my work with advice, saying a kind word at stressful times or just by their mere presence. Daniele Malleo wrote a Matlab script for me and Grielof Koster assisted with mass spectrometry. Staff at Chemistry stores and administration made sure I always had chemicals and consumables, and Rosemary Bell of the Radiation Protection Service advised me on radiochemicals.

My fellow Argonauts Nota, Hugo, Clelia, Maria, Charlotte, Chris G. and Chris V. and many others went through this postgraduate journey with me.

Jilly Cooper, David Lynch, mavros gatos, marilena, lidia tigria and people kept me company with their stories during the lonely times of writing up.

Amalia, Clelia, Claire, Charis, Eirini, Elena, Freddy, Giannis G., Giannis Z., Jenny, Mihalis, Melpo, Melenia, Myrto, Nota, Periklis, Phil and Thanos helped just by being my friends. My other Alexandros also assisted with picture backgrounds.

My partner in life and crimes against science Alexandros knows how essential he has been to me finishing this. Αν δεν είχα και σένα, τί θα ήμουν στη γή!
My family: my parents Olga and Giannis, my brother Antonis, my aunt Teresa and my grandparents have always been there for me and made me who I am. A special thanks to my parents with pride in their achievements and love. They have supported me and nudged me forward through everything, so this would not have been possible without them.
I dedicate this thesis to my grandparents who filled me up with love and amazing stories, gave up their own well-being and in one case their life for me to be physically and financially free. This is for all the missed goodbyes I never got the chance to say.

Chapter 1

Introduction

Table of Contents

I.1. Biological membranes: an overview

I.1.1. Membranes in cells

Biological membranes have been classically considered as asymmetric bilayer walls that encapsulate cells and act as dynamic barriers to the surrounding extra-cellular environment. They compartmentalise cell organelles and provide cells with structural support (Barenholz and Cevc 2000; Hianik 2006).

The cellular area, including all cell contents except nuclei, enclosed by the plasma membrane is termed as the cytoplasm (Thain and Hickman 1996). The latter consists in approximately 80 percent water by mass (Shepherd 2006). However, it has been shown that that water amount is not enough to allow hydration of all cellular contents, therefore the cytoplasm is in fact a gel (Trevors and Pollack 2005).

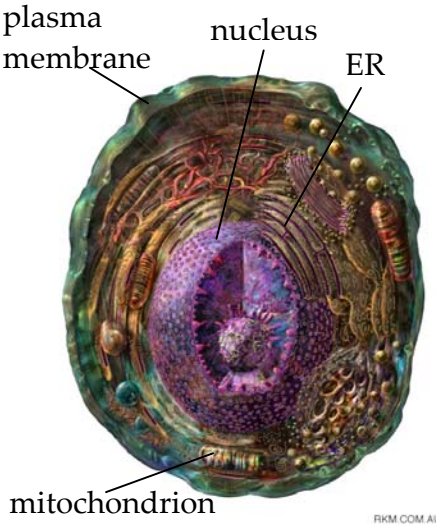

Figure I.1- Diagram of an animal cell, purchased from RK Media.

The cytosol, cell cytomatrix, or micro-trabecular lattice is the proteinaceous matrix in which metabolic enzymes are organised in clusters onto a cytoskeletal scaffolding (Srere 2000). The plasma membrane is further supported by a 50 nm to 2 μm contractile actin cortex of cytoskeleton (Charras, Hu et al. 2006).

The nucleus, the cell organelle where genetic material resides, is surrounded by the nuclear envelope. Also, endoplasmic reticulum (ER) is a convoluted network of membranous stacks, or cisternae, and the energy-supplying mitochondria are also membrane-enclosed. Consequently, the presence of membranes is essential in cells and is not solely restricted in the plasma membrane, but expanded in internal membranes of cell organelles.

I.1.2. Biomembranes: models and composition

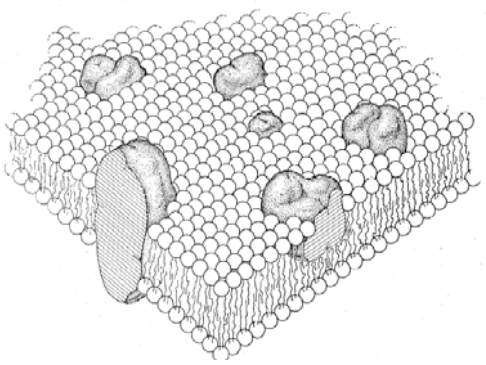

Figure I.2- The fluid mosaic model as illustrated in original publication (Singer and Nicolson 1972).

According to the fluid mosaic model, proposed in a historic publication by Singer and Nicholson some 35 years ago, cell or plasma membranes are dynamic mixtures of lipids and membrane proteins (Singer and Nicolson 1972). The key point of the model was that embedded proteins form a "mosaic" structure in a fluid phospholipid bilayer.

Current theories of lipid bilayer organisation still use the fluid mosaic model as a backbone but have introduced many new elements as modern experimental tools provided with insights into membrane architecture. Various experimental methods including nuclear magnetic resonance (Chan, Feigenson et al. 1972) and deuterium magnetic resonance (Seelig and Seelig 1974) have confirmed the 2D fluidity of membranes due to hydrocarbon chains being less ordered and mobile in the centre of the bilayer than closer to the lipid-water interface. Also, the advent of increasingly powerful computers in the past twenty years has provided with computational tools such as molecular dynamics (MD) for structure and function study of bilayers at the atomic level (Figure I.3). Nowadays, biomembranes are regarded as a 5 nm complex heterogeneous smectic phases of lipids, proteins and carbohydrates held together by hydrophobic and physical interactions (Janmey and Kinnunen 2006).

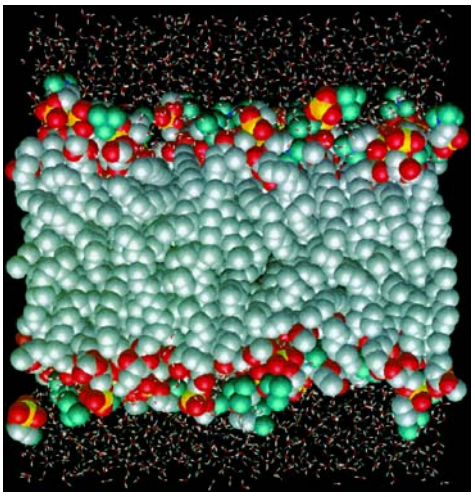

Figure I.3- Plasma membrane MD simulated image (Tieleman, Marrink et al. 1997).

Hundreds of different lipid species are present in the plasma membrane, but the most abundant constituents are phospholipids.

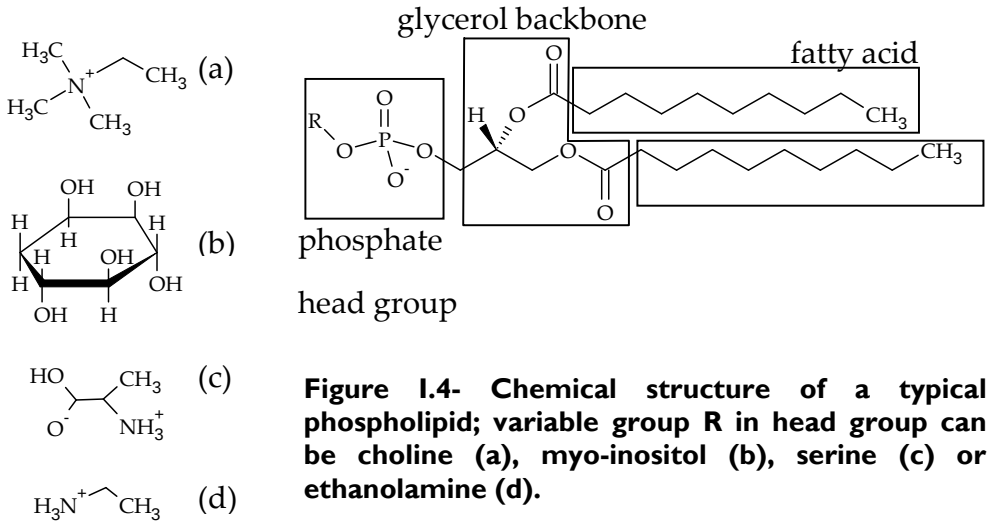

Figure I.4- Chemical structure of a typical phospholipid; variable group R in head group can be choline (a), myo-inositol (b), serine (c) or ethanolamine (d).

Phospholipids or lipids, from the Hellenic "λιποειδή", are highly diverse in both function and property. They are derivatives of phosphatidic acid and consist of a glycerol backbone with one carbon phosphorylated, and the other two esterified by simple fatty acids, forming diacyl glycerols (Figure I.4). The phosphate can be esterified with an amino acid, an aliphatic amine, a choline residue, or a carbohydrate residue (Bergethon 1990). Variation in head group esterification, as well as the chain length and degree of unsaturation of the fatty acid chains, contribute to the large diversity of possible phospholipid structures. A typical cell membrane consists of 70 percent phosphatidyl choline (PtdCho), 20 percent phosphatidyl ethanolamine (PtdEth), and 10 percent of mainly phosphatidyl serine (PtdSer) and phosphatidyl inositol (PtdIns) (Boon and Smith 2002).

An example of the phospholipid nomenclature used in this thesis for the compound with two singly unsaturated 18 carbon atom chains and a phosphatidyl choline head group is the systematic name 1,2-di-octadecanoyl-sn-glycero-3-phosphatidyl choline, the common name 1,2-di-oleoyl-sn-glycero-3-phosphatidyl choline (DOPC) and the chemical abbreviation PC18:1/18:1.

The most important property of lipids is amphipathicity. An amphiphile (Figure I.5) according to International Union of Pure and Applied Chemistry is "a molecule that consists of two parts of contrasting character that are hydrophilic and hydrophobic, or lipophobic and lipophilic" (Baron 2001).

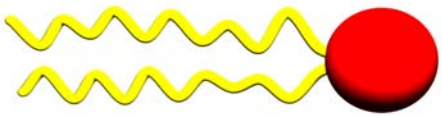

Figure I.5- An amphiphile with a red hydrophilic head group and yellow hydrophobic tail.

Upon mixing with water, three types of amphiphilic behaviour can occur. At a low amphiphile concentration, amphiphiles exist as monomers. Then, amphiphile monomers spontaneously form micelles at their critical micellar concentration (CMC). Further addition of amphiphiles above the CMC leads to lyotropic liquid crystal behaviour, where micelles fuse into larger, more ordered aggregates. These aggregates termed as liquid crystal phases are fluid and show long range orientational order, unlike other liquids. They can be characterised optically by cross polarising optical microscopy. Many different phases have been identified, but biological membranes adopt the fluid lamellar (L_α), that shows a tightly packed infinite three-dimensional mesh (Figure I.6). Side-chains of adjacent amphiphiles are arranged in two sheets, termed as lamellae, stacked on top of each other and separated by a water-excluding area (Seddon 1990).

Figure I.6- PovRay© image of a L_α phase, courtesy of Steve Hant.

In biological systems, reactions occur in constant temperature (T) and free energy (ΔG), enthalpy (ΔH) and entropy (ΔS) are related by $\Delta G=\Delta H-T\Delta S$, as suggested by Gibbs in 1875. When $\Delta G<0$, the reaction is thermodynamically favourable, may occur spontaneously and is termed as exergonic. Exergonic reactions are characterised by considerable energy release ($\Delta H<0$) and/or increase in disorder ($\Delta S>0$). Conversely, when $\Delta G>0$, the reaction is endergonic.

According to the simplest model of hydrophobic hydration, when any solute molecule is dissolved in water a solvation sphere, or clathrate cage, forms around it and new hydrogen and Van der Waals bonds are created in an exothermic process (Frank and Evans 1945). Hydrocarbons are hydrophobic, non-polar molecules that do not easily dissolve in water. During hydrophobic hydration, each water molecule in the clathrate cage forms one more hydrogen bond that in bulk water (Mancena 1996) but the volume of configuration space available for hydrogen bonding is reduced by the presence of the hydrocarbon (Chandler 2005). Therefore, the presence of a hydrocarbon causes $\Delta S<0$ for the system in RT. Formation of the clathrate cage compensates this entropy gain and allows water molecules to maintain more of their hydrogen bonds. In fact, the transfer of one mole of the simplest hydrocarbon methane from a non-polar medium to water requires 2.6 kcal of free energy at 25°C (Kauzmann 1959). Overall, accommodation of a hydrocarbon in water shows $\Delta G>0$ (Widom, Bhimalapuran et al. 2003).

Nowadays, the idea of a rigid clathrate structure has been completely dismissed for extended hydrophobic surfaces. For larger hydrophobes or large molecules with hydrophobic subunits, formation of larger aggregates, containing more than one molecule is enthalpically favourable and exothermic ($\Delta H<0$). It allows more water molecules to interact with each other ($\Delta S>0$) and minimises the disruption due to the presence of non-polar molecules. In lipid amphiphiles, the collective decrease in ΔH from sequestering the alkyl chains away from water and the loss of hydrogen bonding is so large that it drives the formation of aggregates in an exergonic process, despite the immiscibility of hydrocarbons in water (Yaminsky and Vogler 2001). Consequently, the hydrophobic effect during formation of aggregates and liquid crystal phases of lipid amphiphiles in water satisfies the hydrophilic requirement of lipid head groups to be solvated and the hydrophobic need of alkyl tails to be distanced from the aqueous phase (Atkins 2002).

I.1.3. Physical properties of membranes

Biomembrane amphiphile composition and thermodynamic conditions, such as temperature, pressure, pH, salt concentration and osmotic pressure, can change the interfacial curvature of the lipid bilayer (Shearman, Ces et al. 2006).

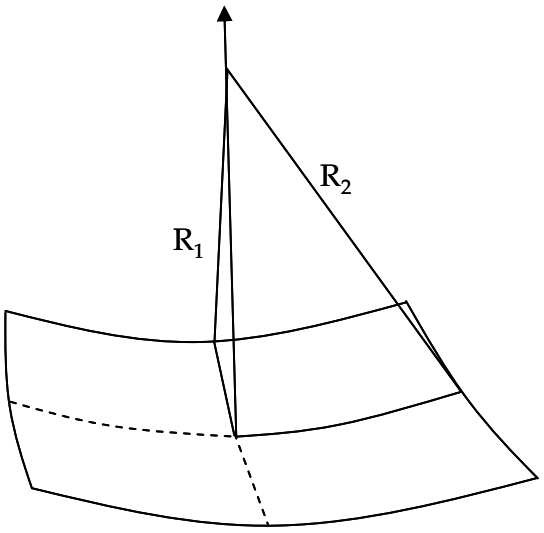

Figure I.7- Principal curvatures, c_1 and c_2 at one point on a monolayer, where $c_1=1/R_1$ and $c_2=1/R_2$ (Shearman, Ces et al. 2006).

An increase in temperature would cause the lipid hydrocarbon chains of a single flat monolayer to splay. Therefore, the monolayer becomes more curved. Curvature for any point in the monolayer can be quantified by extending a normal to the surface. The two principal curvatures, c_1 and c_2, can be thus identified (Figure I.7). Gaussian curvature, K, at that point is equal to the product of c_1 and c_2. Alternatively, the mean curvature of the monolayer, H, is inversely proportional to twice the sum of c_1 and c_2. In a flat monolayer, both H and K are zero, whereas a cone would have only K equal to zero.

Lipids can be thus classified into three categories according to mean curvature and phase behaviour (Gruner 1985) as seen in Figure I.8 overleaf. Positive curvature is by convention when a monolayer spontaneously bends away from the aqueous polar environment and towards the hydrocarbon region. Lipids can also be characterized by their critical packing parameter, ζ:

$\zeta = \upsilon / a_0 l_c$,

where υ is the cylindrical volume of the chains, a_0 is the cross sectional area of the head group and l_c the maximum length of the hydrocarbon chains.

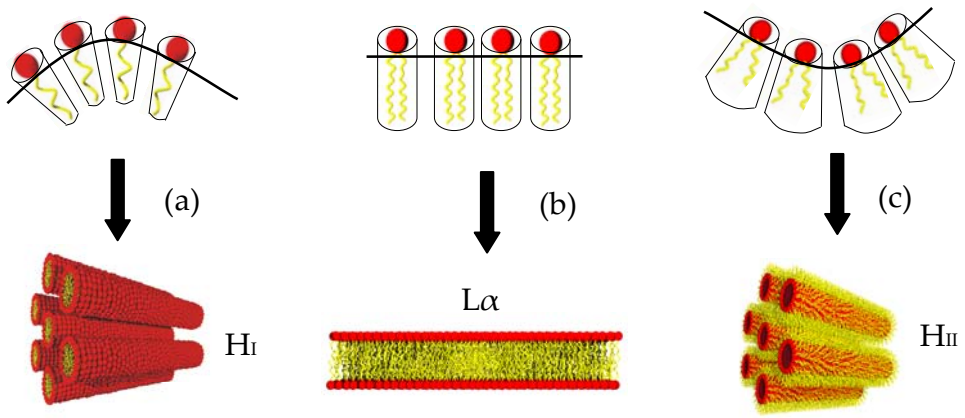

Figure I.8- Classification of lipids according to phase behaviour and curvature as (a) Type I with positive curvature forming hexagonal liquid crystal phases, (b) Type 0 with null curvature favoring lamellar phases and (c) Type II with negative curvature preferably aggregating to inverse hexagonal phases.

For a conical molecule, ζ is equal to 1/3, for a cylinder is 1 whereas for an inverted cone, or wedge, ζ is 3/2.

The lateral stress model of lyotropic crystal behaviour includes the contribution of ζ, but also takes into account the total free energy of the system. The total free energy of a bilayer is directed by membrane curvature, hydration forces, packing of the hydrocarbon chains and electrostatic interactions between the head groups (Kirk, Gruner et al. 1984).

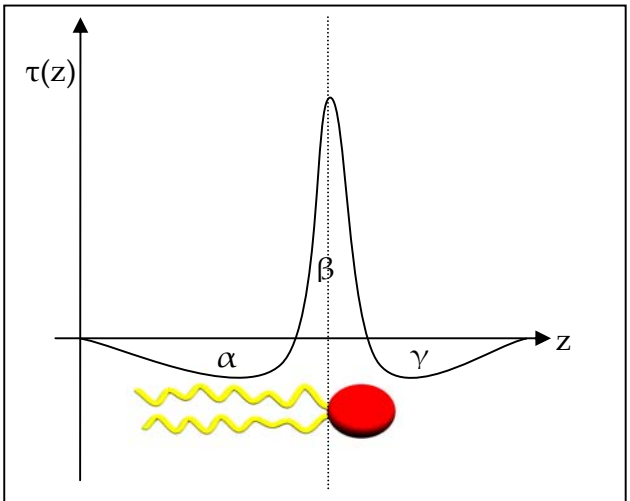

Figure I.9- The lateral stress profile of an amphiphile within an aggregate, where α is the hydrocarbon zone, β the water-hydrocarbon interface, and γ the head group region. For Type I amphiphiles, α>γ, for Type 0, α=γ and for Type I, α<γ.

The spontaneous mean curvature of a monolayer c_0 depends on the distribution of lateral stresses across the monolayer and thus, on the balance of areas α, β and γ in the lateral stress profile (Figure I.9).

In the hydrocarbon zone α, repulsions occur between the chains but cis unsaturation improves lateral packing of the chains and increases the area of α (Ollila, Hyvoenen et al. 2007). In the interfacial region β, the main force contributing to $\tau(z)$ is the hydrophobic effect. In the head group area γ, electrostatic and hydration interactions are the main contributing forces. Electrostatic repulsions or attractions can occur depending on head group charge, whilst lipid head group hydration decreases the packing density by introducing membrane defects (Barenholz and Cevc 2000).

A flat bilayer comprising only of Type 0 amphiphiles is at equilibrium with H_0 and $\tau(z)$ both at zero. However, curvature frustration occurs in a symmetric bilayer when each monolayer has the propensity to bend to opposite directions due to the presence of lipid molecules of different typology. Curvature frustration can be quantified by the monolayer bending rigidity κ_M of a bilayer and the torque tension τ, which are related to the lateral stress $\tau(z)$[1] by:

$$\tau = \int z\,\tau(z)dz = -2\kappa_M c_0 ,$$

where c_0 is monolayer spontaneous curvature as previously described.

The stored elastic stress of a membrane is equal to the summed lateral stresses of its component amphiphiles, which are quantified by the curvature elastic energy, g_c per amphiphile (Helfrich 1981):

$$g_c = 1/2\kappa_M A(c_1 + c_2 - 2c_o)^2 + \kappa_G A c_1 c_2 ,$$

where A is the cross-sectional area per molecule and κ_G the Gaussian curvature modulus. Physically this means that a bilayer consisting of two monolayers would be constrained to remain flat, but with an inherent stored elastic stress, proportional to the spontaneous mean curvatures of the two component monolayers (Attard, Templer et al. 2000).

[1] Lateral stress $\tau(z)$ is equal to the negative of lateral pressure $\pi(z)$.

I.1.4. Use of vesicles as models of membranes

Phospholipid vesicles, or liposomes, are closed membrane systems that are prepared from phospholipids rehydrated in water (Papahadjopoulos 1973). They comprise of a single lipid bilayer, of which the composition depends on the surface to volume ratio of the constituent lipid species.

Multi-lamellar vesicles form when further liposomes are internalised inside a liposome. When sonicated, multi-lamellar vesicles are provided with enough energy so as to rupture and reform, resulting to small and/or large unilamellar vesicles (SUVs and LUVs) (Chapman, Fluck et al. 1968; DeKruijff, Cullis et al. 1975). Both are highly curved and asymmetric compared to planar bilayers of the same composition (Feigenson and Chan 1974). SUVs range from 4 to 20 nm in diameter, whereas LUVs are larger, ranging from 50 to 10 μm (Gradzielski 2003).

Advantages of using vesicles in biochemical and biophysical research include the accurate and easy control of membrane composition, as well as their high stability and amenability in harsh experimental methods such as ultracentrifugation. Vesicles have also been long used as systems for drug delivery in antimicrobial and cancer chemotherapy (Gregoriades 1980).

For the *in vitro* experiments in this thesis, LUVs were used as a viable model of cell membranes. Their size and distribution was determined by right angle light scattering (Matsuzaki, Murase et al. 2000).

I.2. Enzymes, membranes and lipids

Membrane proteins can be integral or peripheral. They are termed as integral, or intrinsic, when they are inserted across the plane of the plasma membrane, spanning the wall and connecting with the hydrophobic inner part. They usually act as receptors, and a typical example is calcium ATPase (EC 3.6.3.8), which is found on the inner mitochondrial membrane and is responsible for the catalysis of adenosine triphosphate (ATP). Peripheral or extrinsic proteins sit on the surface of the cell membrane and may be bound to integral proteins.

Both types of membrane protein show structural motifs in their secondary structure, which allow them to interact with membranes. The motifs are predominantly α-helices and β-barrels, both stabilised by hydrogen bonds. Alpha helices are the most common feature of proteins where a chain of amino acids coils around its long axis with 3.6 subunits per turn, while β-barrels form when proteins fold back along themselves in an anti-parallel fashion. Proteins can interact with membranes by hydrophobic and electrostatic contacts, and also via ionic bridges mediated by ions, such as calcium.

Enzymes are proteins with the specific function of catalysing metabolic reactions. They can be located in the plasma membrane or the cytoplasm. However, enzymes themselves can be regulated, amongst others by lipids or by the presence of membranes in *in vitro* assays. Examples of enzymes that have been found to be modulated by lipids are CTP: Phosphocholine cytidylytransferase (CCT, EC 2.7.7.15), phosphofructokinase-1 (PFK-1, EC 2.7.1.11) and phospholipase A_2 (PLA_2, EC 3.1.1.4).

I.3. General thesis overview

I.3.1. *In vitro* investigation

I.3.1.1. CCT

A carbon-14 radiochemical assay was used to investigate the effect of 28 different lipidic systems on CCT.

I.3.1.2. PFK-1

A phosphorus-32 assay (Sola-Penna, dos Santos et al. 2002) was modified for use with phosphorus-33. Conditions were optimised for assaying PFK-1 from *Bacillus stearothermophilus* and a kinetic investigation was undertaken in the absence of lipids, in DOPC (100%) and in a DOPC/OA (50:50) binary mixture of vesicles.

I.3.2. *In vivo* investigation

HeLa cells were used to study the mechanism of lipid regulation of membranes by investigating the effect of Type I amphiphiles on cell membrane composition by mass spectrometry and cell size by microscopy.

I.4. References

Atkins, P., de Paula, J. (2002). Atkins' Physical Chemistry, 7th edition, Oxford University Press.

Attard, G. S., R. H. Templer, et al. (2000). "Modulation of CTP:phosphocholine cytidylyltransferase by membrane curvature elastic stress." Proc. Natl. Acad. Sci. U. S. A. **97**(16): 9032-9036.

Barenholz, Y. and G. Cevc (2000). "Structure and properties of membranes." Phys. Chem. Biol. Interfaces: 171-241.

Baron, M. (2001). "Definitions of basic terms relating to low-molar-mass and polymer liquid crystals. (IUPAC recommendations 2001)." Pure and Applied Chemistry **73**(5): 845-895.

Bergethon, P. R., Simons, E.R. (1990). Biophysical Chemistry:Molecules to Membranes. New York, Springer- Verlag.

Boon, J. M. and B. D. Smith (2002). "Chemical control of phospholipid distribution across bilayer membranes." Med. Res. Rev. **22**(3): 251-281.

Chan, S. I., G. W. Feigenson, et al. (1972). "Anisotropic and restricted molecular motion in lecithin bilayers." Biochem. Biophys. Res. Commun. **46**(4): 1488-1493.

Chandler, D. (2005). "Interfaces and the driving force of hydrophobic assembly." Nature **437**: 640-647.

Chapman, D., D. J. Fluck, et al. (1968). "Physical studies of phospholipids. X. The effect of sonication on aqueous dispersions of egg yolk lecithin." Bioch. Biophys. Acta, Biomembranes **163**(2): 255-261.

Charras, G. T., C.-K. Hu, et al. (2006). "Reassembly of contractile actin cortex in cell blebs." J. Cell Biol. **175**(3): 477-490.

DeKruijff, B., P. R. Cullis, et al. (1975). "Differential scanning calorimetry and phosphorus-31-NMR studies on sonicated and unsonicated phosphatidylcholine liposomes." Bioch. Biophys. Acta, Biomembranes **406**(1): 6-20.

Feigenson, G. W. and S. I. Chan (1974). "Nuclear magnetic relaxation behavior of lecithin multilayers." J. Am. Chem. Soc. **96**(5): 1312-1319.

Frank, H. S. and M. W. Evans (1945). "Free volume and entropy in condensed systems." J. Chem. Phys. **13**: 507-532.

Gradzielski, M. (2003). "Vesicles and vesicle gels-structure and dynamics of formation." J.Phys.Condens.Matter **15**: R655-R697.

Gregoriades, G. (1980). Liposomes in biological systems. G. Gregoriades and A. Allison, Wiley.

Gruner, S. M. (1985). "Intrinsic curvature hypothesis for biomembrane lipid composition: a role for nonbilayer lipids." Proc. Natl. Acad. Sci. U. S. A **82**(11): 3665-3669.

Helfrich, W. (1981). Amphiphilic mesophases made of defects. Physics of Defects, Les Houches, France, Proceedings of the Les Houches Summer School of Theoretical Physics.

Hianik, T. (2006). "Structure and physical properties of biomembranes and model membranes." Acta Physica Slovaca **56**(6): 687-806.

Janmey, P. A. and P. K. J. Kinnunen (2006). "Biophysical properties of lipids and dynamic membranes." Trends Cell Biol. **16**(10): 538-546.

Kauzmann, W. (1959). "Some factors in the interpretation of protein denaturation." Advan. Protein Chem. **14**: 1-63.

Kirk, G. L., S. M. Gruner, et al. (1984). "A thermodynamic model of the lamellar to inverse hexagonal phase transition of lipid-membrane systems." Biochemistry **23**: 1093-1102.

Mancena, R. L. (1996). "Hydrogen-bonding behaviour in the hydrophobic hydration of simple hydrocarbons in water." J. Chem. Soc., Faraday Trans **92**(14): 2547-2554.

Matsuzaki, K., O. Murase, et al. (2000). "Optical characterization of liposomes by right angle light scattering and turbidity measurement." Bioch. Biophys. Acta, Biomembranes **1467**(1): 219-226.

Ollila, S., M. T. Hyvoenen, et al. (2007). "Polyunsaturation in lipid membranes: Dynamic properties and lateral pressure profiles." J. Phys. Chem. B **111**(12): 3139-3150.

Papahadjopoulos, D. (1973). "Phospholipids as model membranes. Monolayers, bilayers, and vesicles." BBA Library **3**(Form Funct. Phospholipids, 2nd Ed.): 143-169.

Seddon, J. M. (1990). "Structure of the inverted hexagonal (HII) phase, and non-lamellar phase transitions of lipids." Biochim. Biophys. Acta **1031**(1): 1-69.

Seelig, A. and J. Seelig (1974). "Dynamic structure of fatty acyl chains in a phospholipid bilayer measured by deuterium magnetic resonance." Biochemistry **13**(23): 4839-4845.

Shearman, G. C., O. Ces, et al. (2006). "Inverse lyotropic phases of lipids and membrane curvature." J. Phys.-Condensed Matter **18**(28): S1105-S1124.

Shepherd, V. A. (2006). "The cytomatrix as a cooperative system of macromolecular and water networks." Curr. Topics Devel. Biol. **75**: 171-223.

Singer, S. J. and G. L. Nicolson (1972). "Fluid mosaic model of structure of cell-membranes." Science **175**(4023): 720-731.

Sola-Penna, M., A. C. dos Santos, et al. (2002). "A radioassay for phosphofructokinase-1 activity in cell extracts and purified enzyme." J. Biochem. Biophys. Meth. **50**(2-3): 129-140.

Srere, P. A. (2000). "Macromolecular interactions: tracing the roots." **25**(3): 150-153.

Thain, M. and M. Hickman (1996). Penguin Dictionary of Biology, Penguin Books.

Tieleman, D. P., S. J. Marrink, et al. (1997). "A computer perspective of membranes: molecular dynamics studies of lipid bilayer systems." Bioch.Biophys.Acta **1331**(3): 235-270.

Trevors, J. T. and G. H. Pollack (2005). "Hypothesis: the origin of life in a hydrogel environment." Progr. Biophys. .Mol. Biol. **89**(1): 1-8.

Widom, B., P. Bhimalapuran, et al. (2003). "The hydrophobic effect." Phys. Chem. Chem. Phys. **5**: 3085-3093.

Yaminsky, V. V. and E. A. Vogler (2001). "Hydrophobic hydration." Curr. Op. Coll. Inter. Sc. **6**: 342-349.

Chapter II

Regulation of CCTα activity by membrane lipid composition

Table of Contents

II.1. Introduction

II.1.1. Phosphatidyl choline biosynthesis

Phosphatidylcholine (PtdCho), or lecithin from the Hellenic λέκιθος, is a major constituent of cell membranes and was first isolated from egg yolk by Gobley in 1847 (Chatagnon and Chatagnon 1957). Its biosynthetic pathway was first elucidated in the 1950's by Eugene Kennedy at the University of Chicago in three historic papers (Kennedy and Weiss 1956; Borkenhagen and Kennedy 1957; Borkenhagen and Kennedy 1959). The three enzymes involved in this three step pathway are choline kinase (CK, EC 2.7.1.32), CTP: phosphocholine cytidylytransferase (CCT, EC 2.7.7.15) and CTP-choline diacylglycerol phosphocholine transferase (CCP, EC 2.7.8.2).

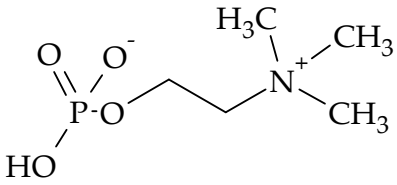

Figure II.1- Structure of phosphocholine (PC).

During the first biosynthetic step of the Kennedy pathway, CK phosphorylates choline to phosphocholine (PC). CK also phosphorylates ethanolamine and is thus also referred as choline/ethanolamine kinase β (Aoyama, Liao et al. 2004). In higher eukaryotes, choline is not synthesised de novo as its only source is the hydrolysis of PtdCho. Therefore, choline has to be acquired in the diet and is an essential component of culture media for animal cells (Eagle 1955) and was classified in 1998 as an essential nutrient for humans (Blusztajn 1998).

CCT catalyses the second step of the Kennedy pathway, during which PC is converted to CDP-choline. This reaction is both rate-determining (Vance, Trip et al. 1980; Whitehead, Trip et al. 1981) and regulatory in PtdCho biosynthesis (Vance and Choy 1979; Sleight and Kent 1980).

Lastly, CDP-choline is condensed with diacyl glycerol (DAG) by CCP to form PtdCho. A diagram of the Kennedy pathway follows in Figure II.2.

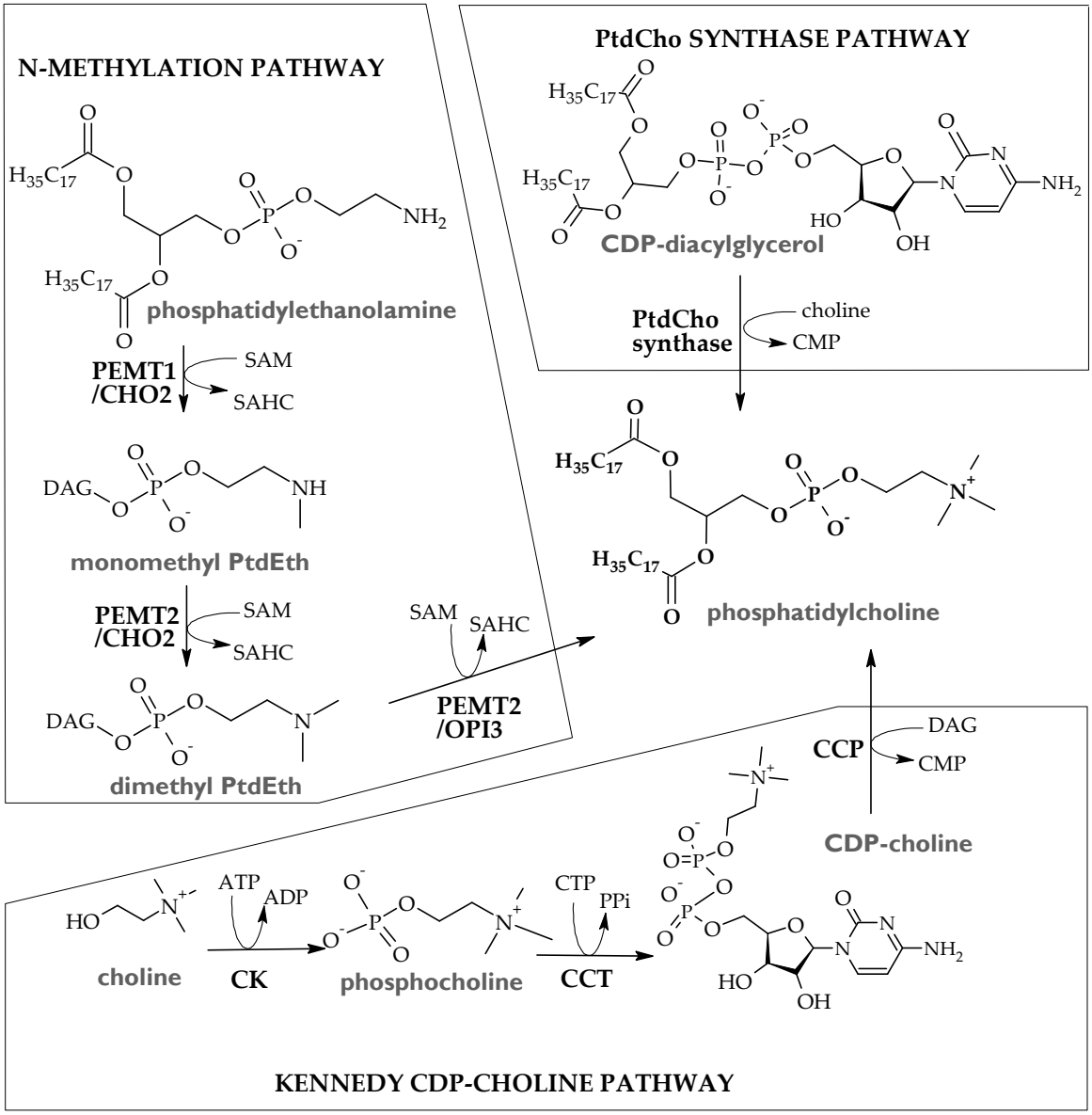

Figure II.2- Major pathways of phosphatidylcholine (PtdCho) biosynthesis. Main biosynthetic route in eukaryotes is via the Kennedy pathway, catalysed by choline kinase (CK), CTP: Phosphocholine cytidylytransferase (CCT) and CTP-choline diacylglycerol phosphocholine transferase (CCP). CCT is the rate-determining enzyme of that route. A minor route in eukaryotes, but predominant in prokaryotes and yeast, is the N-methylation pathway, catalysed by eukaryotic phosphatidyl ethanolamine N-methyltransferase (PEMT1 or CHO2) and phosphatidyl N-methylethanolamine N-methyltransferase (PEMT2 or OPI3). The most recently determined route is the PtdCho synthase pathway in prokaryotes. Minor routes in eukaryotes by base exchange from other phospholipids and by lyso-PtdCho acylation are not shown in this diagram. In fungi, both the Kennedy and N-methylation pathways have been observed.

An alternative pathway for PtdCho biosynthesis is via the S-adenosylmethionine (SAM) dependent methylation of phosphatidyl ethanolamine (PtdEth). In eukaryotes, phosphatidyl ethanolamine N-methyltransferase (PEMT1, EC 2.1.1.17) catalyses the first methylation of PtdEth to monomethyl PtdEth. The latter is then methylated twice to form PtdCho by phosphatidyl N-methylethanolamine N-methyltransferase (PEMT2, EC 2.1.1.71) (Hirata, Viveros et al. 1978). In yeast, equivalent enzymes for PEMT1 and PEMT2 have been isolated, CHO2 and OPI3 respectively (Kodaki and Yamashita 1987). The substrate of this route, PtdEth is biosynthesised by a pathway also uncovered by Eugene Kennedy (Kennedy and Weiss 1956). Interestingly, the analogous enzyme to CCT in this pathway, CTP: phosphoethanolamine cytidylytransferase (CET, EC 2.7.7.14), is not the rate-determining enzyme, but regulation occurs at multiple sites of the pathway (Bladergroen and van Golde 1997).

A completely novel biosynthetic pathway for PtdCho was recently described in the bacterium *Sinorhizobium meliloti* (de Rudder, Lopez-Lara et al. 2000). In the latter choline-dependent route, PtdCho synthase (EC 2.7.8.24) catalyses the direct condensation of CDP-DAG with choline to form PtdCho.

In every organism, one of the three pathways of PtdCho biosynthesis is predominant. Firstly, in higher eukaryotes of kingdoms plantae and animalia, the Kennedy CDP-choline pathway prevails. The exception is in rat and human liver cells that show significant N-methylation activity (Vance, Walkey et al. 1997). Solely in eukaryotes, two further minor pathways can yield PtdCho. First, base exchange enzymes catalyse the head group exchange of other phospholipids to form PtdCho (Kanfer 1980). Second, lyso-PtdCho can be acylated by 1 or 2-acylglycerol-3-phosphorylcholine acyltransferase (EC 2.3.1.62 or EC 2.3.1.23) to form PtdCho (Brumley and van den Bosch 1977).

Secondly, in kingdom fungi, PtdCho biosynthesis occurs mainly through the N-methylation pathway (Carman and Henry 1989). An exception is *Saccharomyces cerevisiæ* of kingdom fungi, which has been shown to use both the Kennedy and N-methylation pathways (Carman and Zeimetz 1996).

Thirdly, for kingdom prokaryotæ, it was originally believed that PtdCho was not contained as a membrane phospholipid with the exception of few highly specialised species (Heath, Jackowski et al. 2002). However, in a thorough review of PtdCho biosynthesis published by Geiger and co-workers, it was estimated from genomic data that more than 10 per cent of bacteria contain PtdCho in their membranes (Sohlenkamp, Lopez-Lara et al. 2003). Most bacterial species, such as *Rhodobacter sphaeroides* (Arondel, Benning et al. 1993), use the N-methylation pathway for PtdCho synthesis.

In order to investigate further the Kennedy pathway of PtdCho biosynthesis, human cervical cells of the HeLa cell line were used for the *in vivo* research described in this thesis (see chapter IV).

II.1.2. CCT

In mammals, three protein isoforms of CCT have been isolated: CCTα, CCTβ_1 and CCTβ_2 (Jackowski 2002). CCTα is coded by the PCYT1A gene in humans and Pcyt1a in mice (Kalmar, Kay et al. 1994), whilst CCTβ_1 (Lykidis, Murti et al. 1998) and CCTβ_2 (Lykidis, Baburina et al. 1999) are splice variants of the PCYT1B gene in humans and Pcyt1b in mice.

CCT isoform gene expression is not uniform in mammalian tissues. CCTα is expressed in all tissues that have been investigated (Kalmar, Kay et al. 1994), CCTβ_2 is in brain tissue, whereas CCTβ_1 only in foetal tissue, placenta, ovaries and testes (Lykidis, Baburina et al. 1999).

All three isoforms have three functional domains in common: lipid, phosphorylation and catalytic (Figure II.3). However, CCTα shows a nuclear localisation domain that is not present in CCTβ isoforms. Hence, CCTα cell localisation can be both in (Wang, MacDonald et al. 1995) and outside the nucleus (Houweling, Chui et al. 1996) whereas CCTβ proteins reside outside the nucleus, mostly associated with the endoplasmic reticulum (Lykidis, Murti et al. 1998).

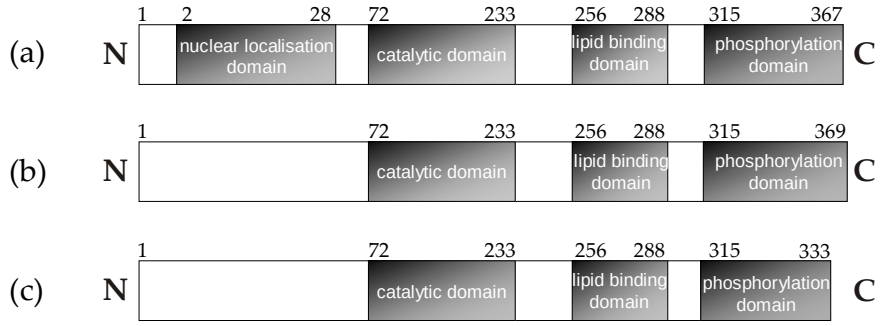

Figure II.3-The functional domains of the genes coding for (a) CCTα (Wang and Kent 1995; Friesen, Liu et al. 2001), (b) CCTβ$_2$ (Lykidis, Jackson et al. 2001) and (c) CCTβ$_1$ (Lykidis, Baburina et al. 1999). Diagram adapted from original publication (Jackowski and Baburina 2002).

Since rat CCTα was used for the *in vitro* experiments of this thesis (Luche, Rock et al. 1993), discussion will focus on that isoform, which has been purified and characterised in many different organisms, including yeast *Streptococcus pneumoniae* (Kwak 2002), eukaryote *Plasmodium falciparum* (Yeo, Larvor et al. 1997), nematode *Caenorhabditis elegans* (Friesen, Liu et al. 2001), mammalian liver from *Rattus norvegicus* (Weinhold, Rounsifer et al. 1986) and human HeLa cells (Kalmar, Kay et al. 1994). Mammalian CCTα from *R. norvegicus* is a homodimer or homotetramer held together by cysteine disulfide bonds (Weinhold, Rounsifer et al. 1986; Cornell 1989).

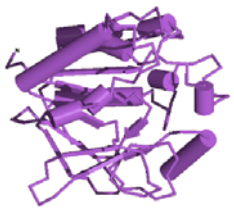

Figure II.4- CCTα from *S. pneumoniae* resolved at 1.5 Å (Kwak 2002).

Each 367 amino acid monomer has a molecular weight of approximately 42 kDa in the presence of either Triton X-100 micelles or lipid vesicles (Cornell 1989). However, oligomerisation is not dependent on membranes as the dimer interface includes only the nuclear localisation and catalytic domains (Xie, Smith et al. 2004)

Figure II.5- Mammalian CCTα helical domain 1PEH spanning residues 267 to 288 (Dunne, Cornell et al. 1996).

The mammalian CCTα site of reversible binding with membranes has been identified as an 11-residue repeat motif on an 78 Å amphipathic α-helix in the region from residues 236 to 293 (Kalmar, Kay et al. 1990; Johnson and Cornell 1994; Dunne, Cornell et al. 1996), which can be partially immersed into one of the two leaflets of a lipid bilayer (Johnson, Aebersold et al. 1997). CCTα membrane association causes transition of the corresponding peptide from a random coil to the amphipathic α-helix (Johnson and Cornell 1994; Dunne, Cornell et al. 1996; Johnson, Rao et al. 1998). Many studies have shown that although the membrane binding domain is discrete from the catalytic domain (Friesen, Campbell et al. 1999), binding to membranes is a prerequisite for catalytic activity (Choy, Lim et al. 1977; Choy, Farren et al. 1979; Feldman and Weinhold 1987; Yang, Boggs et al. 1995; Lykidis, Jackson et al. 2001) and thus alters the rate of PtdCho biosynthesis (Kent 1990; Vance 1990; Tronchere, Record et al. 1994). Finally, truncation of the α-helical domain leads to CCTα inhibition (Yang, Boggs et al. 1995; Friesen, Campbell et al. 1999; Lykidis, Jackson et al. 2001), suggesting an activating role for the membrane binding domain.

The CCTα catalytic mechanism involves the formation of a penta-coordinate transition state of substrate PC with conserved lysine and arginine amino acid residues on the catalytic domain (Kwak 2002; Helmink, Braker et al. 2003).

II.1.3. Regulation of CCTα activity

CCTα is an example of an ambiquitous enzyme (Wilson 1978) since it can be localised both on membranes, plasma or organelle, and in the cytoplasm and intra-organelle space. Membrane partitioning of the enzyme is a reversible switch for catalytic activity, and in consequence for PtdCho biosynthesis in cells. CCTα has been extensively reviewed in the literature (Kent 1997; Jackowski 2002; Jackowski and Baburina 2002; Jackowski and Fagone 2005). Also, there are numerous thorough reviews on lipid biosynthesis (Kent 1995; Vance 2002; Hatch and Choy 2004; Vance and Vance 2004) and its regulation (Kent 1990; Tijburg, Geelen et al. 1990; Vance 1990; Tronchere, Record et al. 1994; Clement and Kent 1999).

The term "*ambiquitous*" later evolved to "*amphitropic*" (Burn 1988) to describe a new class of proteins that are not distinctly cytoplasmic, integral or peripheral, and includes phospholipase A_2 and protein kinase C (Johnson 1999). CCTα is part of a sub-group of amphitropic proteins, whereby membrane interaction mediates catalytic activity via an amphipathic α-helix (Cornell and Taneva 2006).

CCTα ambiquiticity, or amphitropism, and the role of membrane binding on enzyme activity and PtdCho biosynthesis have been the subject of considerable study and review that has thus led to the evolution of several competing hypotheses for the regulation of enzyme activity. Overall, mechanisms suggested in the literature can be distinguished into lipid-dependent and lipid independent, but all agree on that "*this fascinating enzyme can be active or inactive, is phosphorylated and dephosphorylated, moves on and off membranes and, perhaps, travels around the cell*" (Kent 1997).

II.1.3.1. Lipid independent mechanisms

II.1.3.1.1. **The translocation hypothesis**

The first and perhaps most well-characterised hypothesis, translocation is intertwined with protein amphitropism and relocalisation. In fact, CCTα was one of the first proteins for which regulation by translocation was shown (Sleight and Kent 1980). It was later put forward as the main regulatory mechanism for PtdCho biosynthesis by Vance and co-workers (Vance and Pelech 1984) to explain why rat CCTα was catalytically activated when bound to cellular membranes, but remained inactive in the cytoplasm, which acted like a protein reservoir (Pelech, Pritchard et al. 1983). Further evidence supporting the hypothesis has been presented for bovine CCTα (Bladergroen, Wensing et al. 1998).

Translocation has been suggested to be triggered by enzyme dephosphorylation, treatment with DAG, or an excess of PC substrate (Tronchere, Record et al. 1994). However, a year later it was shown by two separate groups that a mutant enzyme lacking the phosphorylation could bind to membranes without significant alteration in PtdCho biosynthetic rate (Houweling, Jamil et al. 1994; Wang and Kent 1995). Evidence for CCTα feedback regulation by increasing PC concentration in membranes (Jamil, Yao et al. 1990) and DAG (Pelech, Pritchard et al. 1983) could be used to support either of the lipid dependent mechanisms.

It can be concluded that translocation is modulated by factors covered in the more complex and recent hypotheses of lipid-dependency and phosphorylation. Therefore, it is an important link in CCTα regulation but not a regulatory mechanism in itself.

II.1.3.1.2. **Regulation by phosphorylation**

CCTα regulation by dephosphorylation of the carboxyl terminal domain (Figure II.3) is the main lipid independent hypothesis in the literature. In rat CCTα, phosphorylation sites have been identified on a strip of 19 serine amino acid residues terminating on the carboxyl terminus (Macdonald J. I. S. and Kent C. 1993). The carboxyl or phosphorylation domain can interact with lipids but not in the same manner as the membrane binding domain, being only affected by anionic lipids (Lykidis, Jackson et al. 2001). Truncation of the phosphorylation domain removes the phosphorylation ability of the enzyme but does not affect maximal catalytic activity (Cornell, Kalmar et al. 1995). Thus, it has been suggested that the phosphorylation domain contributes to negative cooperativity of lipids to CCTα activity (Yang and Jackowski 1995).

According to this hypothesis, hyperphosphorylation of the carboxyl terminal domain triggers deactivation of the enzyme, while dephosphorylated CCTα is catalytically active (Pelech and Vance 1982). First indications for this hypothesis came from a potential correlation of CCTα and protein kinase C (PKC), since cAMP and its analogues are inhibitors of PKC. Results that cAMP analogues inhibited (Pelech, Pritchard et al. 1983) while phorbol esters activated CCTα (Kinzel, Kreibich et al. 1979; Guy and Murray 1982) were dismissed when cAMP showed no effect on the phosphorylation state of CCTα (Jamil, Utal et al. 1992).

The first supporting evidence came when treatment of HeLa cells with fatty acids (Wang, MacDonald et al. 1993) and of Chinese ovary cells with phospholipase C (Watkins and Kent 1991) hyperphosphorylated the enzyme and caused its complete translocation to its inactive cytoplasmic form. The most recent study available showed that oxysterols decreased PtdCho synthesis by increasing CCTα phosphorylation in murine lung epithelial cells (Agassandian, Zhou et al. 2005).

However phosphorylation is not necessary for binding to membranes. Later studies using solely oleic acid indicated that CCTα first translocates from the cytoplasm, then associates with membranes and lastly is dephosphorylated (Houweling, Jamil et al. 1994). Also, site-directed mutagenenis of the serine residues replacing them with alanine caused a ten-fold increase to CCTα translocation on membranes and a eight-fold increase in enzyme activity (Wang and Kent 1995).

Consequently, the phosphorylation hypothesis cannot solely explain CCTα regulation, at least not with the available experimental evidence.

II.1.3.2. Lipid-dependent mechanisms

As discussed in section II.1.2, CCTα activity is dependent on the presence of lipids, with evidence that fatty acids stimulate CCTα first produced in the 1960s (Fiscus and Schneider 1966). Two hypotheses have been since proposed for the lipid-dependent regulation of CCTα activity: the electrostatic and the stored elastic stress.

II.1.3.2.1. The electrostatic hypothesis

In membranes, electrostatic interactions can create catalytic sites by localised charge accumulation, affect molecule recognition and transport, as well as cause conformational changes to interacting molecules (Cevc 1990). Although the membrane interior is not charged, cell membrane surfaces have a net negative charge because of polar and ionised groups on protruding glycoproteins and on membrane bound or adsorbed molecules.

The Gouy-Chapman electrical double layer membrane approximation has been the classically used model to predict the electrostatic potential on the membrane surface. It models charges confined on an infinitely narrow flat surface and relies on a simple Poisson-Boltzmann equation where ion distribution is controlled by coulombic forces. Interfacial structure, hydration effects and non-electrostatic interactions are neglected. Modern theories include a modified Poisson-Boltzmann equation where interionic interactions but a universal theory of membrane electrostatics is not available as of yet.

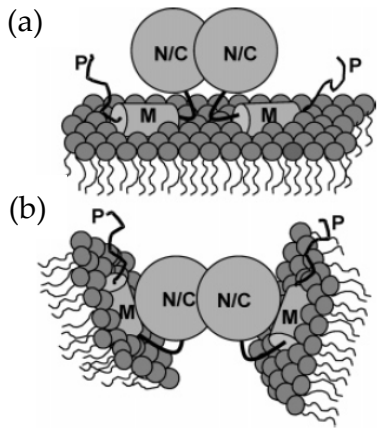

Figure II.6- Two modes of CCTα interaction with membranes according to the electrostatic hypothesis. In (a) the CCTα homodimer interacts with one LUV while in (b) a cross-bridge forms between separate vesicles. M is the membrane domain, N/C the N-terminal and catalytic domain and P the phosphorylation domain. Diagram reproduced from original publication (Taneva, Patty et al. 2005).

The electrostatic model for CCTα regulation initially postulated that CCTα is activated by anionic lipids while lipid dependence of stabilising interactions is attributed more to negative charge density than head group structure itself (Cornell 1991). A cross-bridging mode is suggested that occurs only with anionic amphiphiles and is not a prerequisite for enzyme activation (Figure II.8). Packing density of membranes, fatty acid length,

CCTα preference to curved surfaces and Triton X-100 presence were used to explain CCTα activation by neutral or cationic lipids (Cornell 1991; Cornell and Northwood 2000).

The suggested mechanism is sequential: an initial electrostatic interaction positions the protein at the bilayer surface, followed by hydrophobic interactions between anionic lipids and cationic residues of the amphipathic α-helix (Arnold 1996). Electrostatic interactions are necessary for binding while hydrophobic interactions are attributed essential solely for activation, but lipid polymorphism of membranes is disregarded as a hypothesis (Cornell and Arnold 1996).

Anionic lipids phosphoglycerol (PG) and phosphoinositol (PI) activated CCTα in Triton X-100 mixed micelles and supported this hypothesis (Cornell 1991). However, neutral lipids, like oleyl alcohol and monoacyl glycerol strongly activated CCTα *in vitro* and in cell cultures (Cornell and Vance 1987), contradicting the charge argument but not otherwise explained. Also, it has been shown that CCTα partioning is not due to packing defects as maintained in the electrostatic hypothesis (Drobnies, Van der Ende et al. 1999).

Overall, the electrostatic hypothesis is supported by some of the experimental evidence available. Its main drawback is that it is largely descriptive of biochemical observations and does not offer a biophysical explanation, not taking into account steric and repulsions and splay of chains at the hydrocarbon zone of lipids. Cornell and co-workers, who first suggested the electrostatic hypothesis, have upgraded the concept of curvature and elimination of packing stress as more important to electrostatics in their more recent publications (Davies, Epand et al. 2001; Johnson, Xie et al. 2003; Cornell and Taneva 2006). Therefore, some of the attributes of the electrostatics now make part of the stored elastic stress hypothesis, but the electrostatic hypothesis as such cannot fully explain experimental data for CCTα activation in membranes.

II.1.3.2.2. **The stored elastic stress hypothesis**

The stored elastic stress hypothesis is the most recently suggested (Attard, Templer et al. 2000). It correlates CCTα dependency on lipids and the lateral stress model of lyotropic liquid crystal behaviour (see section I.I.3), according to which lipids can be distinguished into Types I, II and 0. Membrane lipid composition is postulated to modulate CCTα membrane association, and in consequence affect catalytic activity. Each lipid type is predicted to have a different lateral stress profile depending on its chemical structure (Figure II.6) comparing di-oleoyl-phosphatidate (DOPA, PA18:1/18:1), di-oleoyl-phosphatidyl choline (DOPC, PC18:1/18:1) and di-stearoyl-phosphatidate (DSPA, PA18:0/18:0).

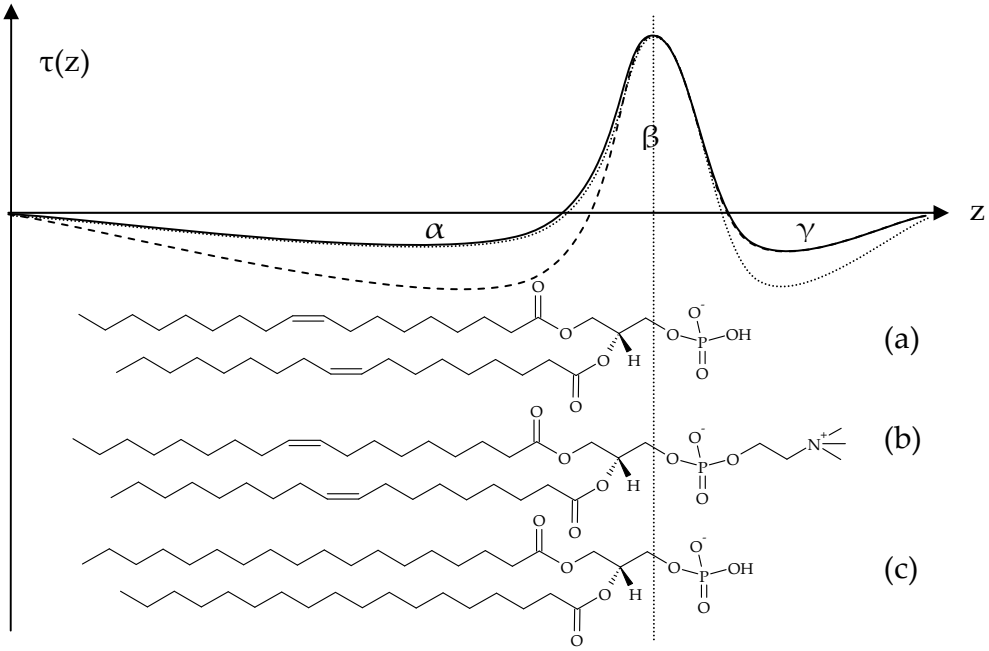

Figure II.7- Lateral stress profiles for (----) DOPA (PA18:1/18:1) (a), (.....) DOPC (PC18:1/18:1) (b) and (____) DSPA (PA18:0/18:0) (c), where α is the hydrocarbon zone, β the water-hydrocarbon interface, and γ the head group region.

DOPA and DSPA have the same phosphate head group but α for DOPA is larger because of its two unsaturated chains. Thus, DOPA is more Type II than DSPA. On the other hand, DOPC shows the same degree of unsaturation with DOPA, but because of the larger phosphocholine head group, its γ is larger, so DOPC is less Type II than DOPA.

It was first pointed out in 1993 that Type II amphiphiles activated CCTα (Jamil, Hatch et al. 1993). A biophysical explanation was later proposed by Attard and co-workers (Attard, Templer et al. 2000). They suggested that the α-helix in the membrane binding domain of the enzyme becomes submersed into an amphiphilic monolayer, relieving part of the membrane curvature elastic energy, g_c, for Type II amphiphiles (Figure II.7). For a membrane containing Type II di-oleoyl-phosphatidyl ethanolamine (DOPE, PE18:1/18:1), it was calculated that 19 or more lipids would become relaxed due to a single molecule of CCTα partitioning into the membrane. The latter would be a very significant contribution to the total stored elastic stress, τ, of the bilayer. However, g_c cannot be released for membranes containing Type I amphiphiles due to their cross-sectional area, A. Consequently, the stored elastic stress hypothesis proposes that the sign and magnitude of τ modulates membrane association and thus catalytic activity of CCTα.

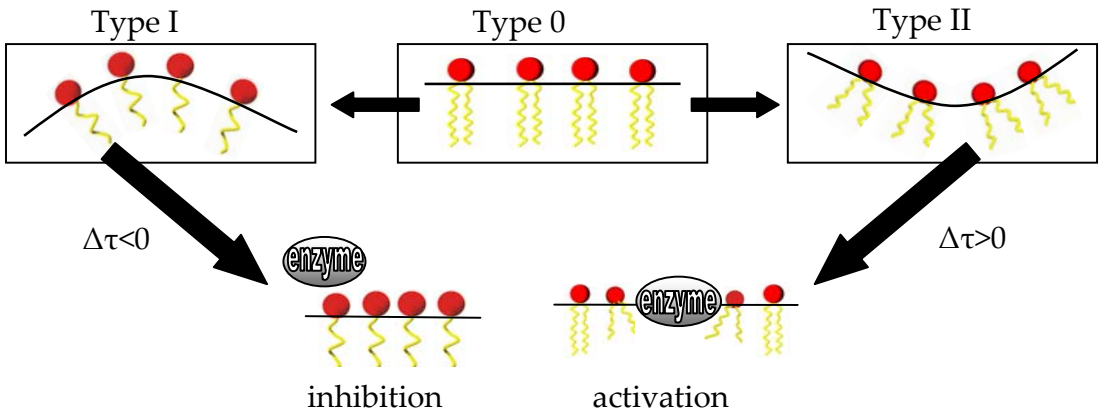

Figure II.8- Diagram summarising the stored elastic stress hypothesis for CCTα. Type II lipids activate CCTα by increasing τ in the monolayer, while Type I have the opposite effect. This is because insertion of the α-helix through CCTα partitioning to membranes allows the hydrocarbon chains to splay, contributing negatively to τ and therefore relieving the stored elastic stress. Consequently, partitioning of the helix into the bilayer is energetically more favourable for membranes with more positive values of τ, and thus higher stored elastic stress.

Assuming that only the chains of a lipid annulus surrounding the α-helix are allowed to splay by enzyme partitioning, and only locally cylindrical interfacial curvature is allowed and g_c released upon CCTα binding is:

$g_c = \kappa A (2 c_1 c_0 - c_1^2/2)$,

where κ is the bending rigidity of the monolayer, c_1 is the principal curvature of the monolayer at the interface and c_0 is the spontaneous curvature of the monolayer (see section I.I.3). This g_c is smaller than the total stored elastic curvature energy released for a locally spherical energy, therefore CCTα is modelled as a cylinder.

The membrane/water partition coefficient, K, for CCTα with cylindrical curvature is:

$$K = K_0 \exp\left[\frac{n\kappa A(2c_1c_0 - 1/2c_1^2)}{k_B T}\right],$$

where K_0 is a factor that includes invariant free energy contributions with respect to enzyme partitioning, n is number of amphiphiles surrounding the binding domain, k_B is the Boltzmann constant and T is temperature. Then, the relative activity of the enzyme, S, in the presence of binary large unilamellar vesicles (LUVs) is:

$$S = \exp\left[\frac{n(x)\kappa(x)A(x)(2c_1c_0(x) - 1/2c_1^2) - n(0)\kappa(0)A(0)(2c_1c_0(0) - 1/2c_1^2)}{k_B T}\right],$$

where $c_0(x)$ and $c_0(0)$, κ(x) and κ(0), A(x) and A(0) depend on mole composition of the two amphiphiles in the binary system. Using experimental values for c_0, κ and A for DOPC (PC18:1/18:1), and DOPE (PE18:1/18:1) and a Type I amphiphile, it was calculated with reasonable agreement that in DOPC/X binary membranes CCTα will be activated by DOPE and deactivated by a Type I amphiphile (Attard, Templer et al. 2000).

At the time of writing this thesis, it is extremely hard to measure g_c for an amphiphile. Therefore, exact juxtaposition of experimental enzyme assay results and theoretical predictions is not easily achieved.

However, whether an amphiphile would activate or inhibit the enzyme can be predicted from the lyotropic liquid crystal phases it preferentially forms and its lateral stress profile.

Stabilising interactions of amphipathic α-helical domains with lipid bilayers have also been reported for a number of different proteins and peptides: apolipoprotein A (Tytler, Epand et al. 1994); sarcoplasmic reticulum calcium ATPase (Navarro, Toivio-Kinnucan et al. 1984; Cheng, Lepock et al. 1986); rhodopsin (Wiedmann, Pates et al. 1988); dolichyl-phosphomannose synthase (Jensen and Schutzbach 1988); frog skin magainin and bacterial toxins (Sansom 1998). In fact, the stored elastic stress hypothesis has been suggested as a universal mechanism to explain membrane incorporation and conformation to proteins with amphipathic helices (Gruner 1985). Nonetheless, application of this hypothesis using spectroscopic and simulation studies is extremely complex because the stored elastic stress of a bilayer cannot be measured experimentally.

Helix formation for peptides in membranes has been shown to be entropically favourable suggesting it is a driving force for protein membrane binding (Wieprecht, Apostolov et al. 1999; Wieprecht, Beyermann et al. 2002). Studies probing membrane surfaces by deuterium NMR (Watts 1988) have showed that CCTα partitioning is not due to phase separations of bilayer components (Drobnies, Van der Ende et al. 1999). A conformational change is indicated from evidence that the membrane binding domain folds from a random coil in solution to an α-helix upon binding to a membrane (Johnson, Rao et al. 1998), increasing CCTα affinity for the CTP substrate (Yang, Boggs et al. 1995).

From early experiments on rat liver CCTα, it has been shown that addition of appropriate phospholipid mixtures is required for maximal catalytic activity (Weinhold, Rounsifer et al. 1986; Feldman and Weinhold 1987). Evidence for activation by Type II lipids DOPA (Cornell and Vance 1987), DAG (Jamil, Hatch et al. 1993), OA (Weinhold and Barrett 1998), DOPE (Attard, Templer et al. 2000), monolein (Nakano, Karno et al. 2005) is available.

Inhibition by Type I amphiphiles has also been shown in the literature for hexadecyl phosphocholine (HDPC) (Boggs, Rock et al. 1998), phosphatidyl serine (PS) and fatty acids (Arnold 1996).

When CCTα oligomerisation is considered, the stored elastic stress hypothesis still applies since each protein subunit of the homodimer or homotetramer can be laterally arranged on top of the bilayer with all α-helical domains protruding down into the membrane.

Consequently, the stored elastic stress hypothesis can be used to explain all available experimental evidence in the literature. However, a more consistent study of a range of Type II, 0 and I amphiphiles with variable degrees of charge and unsaturation is required to firmly support the hypothesis. The latter is presented in this chapter.

II.1.3.3. Other hypotheses

Calpains are proteinases that can degrade CCTα at two sites, one of which within the catalytic domain (Zhou, Ryan et al. 2003). Interestingly, CCTα is much more stable than other targets of the calpains by formation of protecting and stabilising interactions with a protein termed calmodulin (Chen and Mallampalli 2007). Thus, it has been hypothesised that calmodulin may infer some regulatory role in PtdCho biosynthesis.

All aforementioned hypotheses involved CCTα control at the cellular level. On the other hand, evidence of CCTα modulation at a transcriptional and post-transcriptional level has been reported. Colony stimulating factor 1, a growth factor for cell culture media, has been shown to cause an increase in CCTα mRNA, leading to enhanced rates of PtdCho biosynthesis both in a murine macrophage cell line (Tessner, Rock et al. 1991) and in rat liver cells (Houweling, Tijburg et al. 1993). Unfortunately, the exact mechanism of control has not been yet elucidated.

II.2. Experimental

II.2.1. Materials

The majority of the phospholipids were purchased from Avanti Lipids (Alabama, USA) except for OA, CHOL and DOPS, which were from Sigma (Dorset, UK). Namely, the following phospholipids were employed: DOPC, OA, DOPA, DOPE, OPA, DOPS, OPS, DES, DESP, C18:0 CER, C18:1 CER, DOG, C6:0 PG, SM, CHOL, OLEOYL COA and DPHPC. Other chemicals used such as dCTP, DTT, $MgCl_2$, Bis Tris, PtdCho and pure water were also from Sigma (Dorset, UK). CCTα enzyme expressed and purified by the Suzanne Jackowski Group at St. Jude Children Research Hospital (Memphis, USA). TLC plates used were 20 by 20 cm, of silica gel with fluorescent indicator UV_{254} from Machery Nagel. The ACS Scintillation Cocktail and phosphoryl [methyl-14C] choline (1.85 MBq, 50 μCi) were purchased by Amersham Biosciences (Buckinghamshire, UK).

II.2.2. Methods

II.2.2.1. Preparation of LUVs

Appropriate volumes of lipid for each composition were decanted into 3 mL brown HLPC vials to a total lipid amount of 2.54 μmoles. Pure water (200 μL) was added to each vial and the samples were lyophilised to dryness. Standard buffer (169.3 μL, 150 mM Bis Tris, 10 mM $MgCl_2$ of pH 7.0 at 37 °C) was pipetted into the vials, which were then vortexed for 10 minutes and rested for 20 minutes. The samples were subsequently sonicated for 20 minutes and allowed to rest for a further 20 minutes. Four freeze-thaw cycles were carried out. Before use in the assay, a 10 μM solution of each vesicle system in standard buffer was sized using a Coulter N4 PLUS Particle Sizer (Attard Group). For the type I amphiphiles, CTAB, SDS, HDPC, C16EO8 and DHDMAB, the vesicles were allowed at least five hours in a 37 °C water bath and were then used in the radiochemical assay.

II.2.2.2. Radiochemical Assay

A radiochemical enzyme assay was performed in triplicate for each amphiphile system, including two controls, without lipid and without enzyme. The concentrations in each 50 μL experiment were 3.26 mM PtdCho, 4 mM DTT, 10.00 μg/mL CCT, 2.98 mM dCTP, and 3 mM lipid solution in chloroform.

Purified rat CCT*α* was kindly donated by Prof. Jackowski from St. Jude Children's Research Hospital, Memphis, USA. CCT was acquired in aliquots of 200 μL of 0.44 mg/mL CCT, WT His in 50 mM Tris, 500 mM NaCl and 50% glycerol at pH 8.0. Before the assay, the appropriate volume from the 0.44 mg/mL solution was diluted with buffer (197.3 mM Bis Tris, 13.5 mM $MgCl_2$ of pH 7.0 at 37 °C) to a final CCT*α* concentration of 0.1056 mg/ mL.

The vesicles were allowed to thaw for one hour before each assay, and were diluted to 5 mM with the addition of standard buffer (338.6 μL, 150 mM Bis Tris, 10 mM $MgCl_2$ of pH 7.0 at 37 °C) in each sample.

DTT (10 μL, 60 mM), CCT (14.2 μL, 0.1056 mg. mL-1), dCTP (29.8 μL, 15.01 mM) and standard buffer (40.5 μL, 150 mM Bis Tris, 10 mM $MgCl_2$ of pH 7.0 at 37 °C) were added to a 94.5 μL final volume. The solution was vortexed and divided to three 31.5 μL aliquots, for the purposes of the triplicate experiment. Then, the appropriate vesicular solution (10 μL, 15 mM) was added to each of the three aliquots. The reaction was initiated by the addition of ^{14}C-^{12}C-PtdCho (8.5 μL, 19.15 mM) in each experiment. PtdCho (^{14}C) was purchased at 50 μCi/mL (0.907 mM). A 1:1 dilution with ^{12}C PtdCho (37.4 mM) was made to a total PtdCho concentration of 19.15 mM.

The vials were transferred in a 37 °C water bath, were allowed to incubate for 15 minutes, and then immersed in liquid nitrogen. The reaction was quenched by the addition of EDTA (15 μL, 160 mM). Approximately half the amount of experiment (30 μL) was spotted on UV TLC plates. TLC chromatography was performed in

14% ammonia solution in methanol (90:10). The plates were viewed under UV light and two spots were seen, of which the uppermost corresponded to the product CDP-choline. Each spot was cut out separately for each fraction and inserted into liquid scintillation vials with the addition of ACS Scintillation Cocktail (4 mL). Radioactive decay was measured using the LS6500 Beckman Liquid Scintillation Counter (School of Chemistry, Radiochemical Lab).

After the end of the assay the radionuclide content was disposed following the local rules of the School of Chemistry, University of Southampton under the Radiation Protection Act.

II.3. CCTα kinetics in LUVs

A saturation kinetics assay was run in order to establish an assay incubation time for CCTα in LUVs.

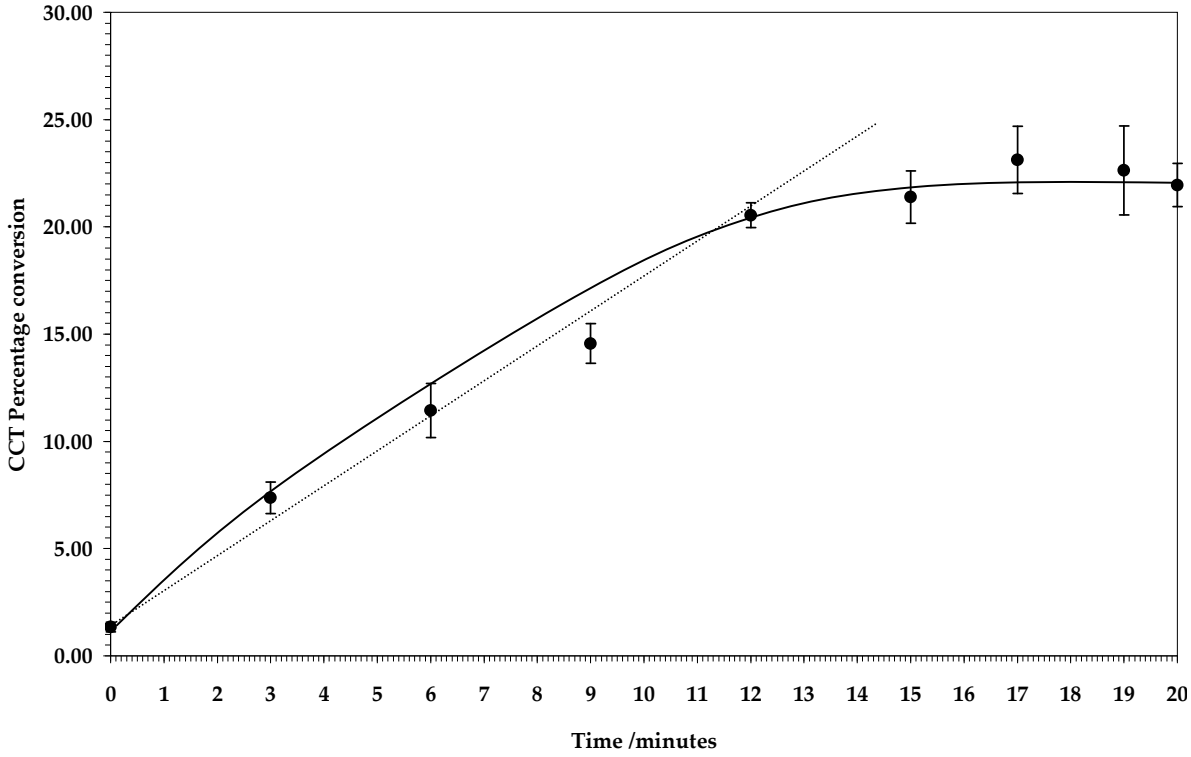

Figure II.9- Plot of CCT percentage conversion as a function of time (Assay 7) in DOPC/OA (50:50) vesicles.

CCTα percentage conversion reached a plateau at approximately 20 percent between 12 and 20 minutes in DOPC/OA (50:50). The presence of OA has been shown to cause maximal catalytic activity for CCTα both in the literature (Weinhold, Rounsifer et al. 1986; Cornell 1991; Jamil, Hatch et al. 1993) and in unpublished results from our lab. Also, a DOPC/OA (50:50) composition is the maximum OA composition that can be used because phase separations occur in more OA present. Thus, a 15 minute incubation time is adequate in order for enzyme conversion to be within the linear range of CCTα activity for less activating LUV binary systems than DOPC/OA (50:50).

II.4. Effect of Type II amphiphiles on CCTα

The effect of 28 different amphiphiles in binary LUV systems in DOPC on enzyme activity was investigated using a carbon-14 PC CCTα radiochemical assay (Experimental in section II.2). A challenge for *in vitro* CCTα studies is the presence of lipid contaminants in the enzyme either from endogenous lipids in crude enzyme extracts, and to detergents in the purified enzyme preparation from plasmids. The His-tagged CCTα used in our studies has been purified of all lipid contaminants and detergents using a nickel affinity column (Lykidis, Jackson et al. 2001). In order to investigate whether Type II amphiphiles activate CCTα activity according to the stored elastic stress hypothesis, two different approaches were employed. The first approach involved examining the effect of changing the type and length of the hydrocarbon chain (area α in lateral stress diagram) to enzyme activity. The five head group types studied were:

- phosphate (PA)
- phosphatidyl serine (PS)
- phosphatidyl ethanolamine (PE)
- phosphatidyl glycerol (PG)
- phosphatidyl choline (PC)

The second approach involved studying the effect of varying head group type and size (area γ in lateral stress diagram) on enzyme activity. Three different chain lengths were used:

- di-oleyl (DO or 18:1/18:1)
- di-palmitoyl (DP or 16:0/16:0)
- di-phytanoyl (DPH)

Finally, four amphiphiles of biological importance were studied as a speculative addition to examine *in vivo* CCTα effects.

DOPC was present in all investigated systems, which were binary LUVs. Before each experiment, size of LUVs was confirmed by right angle light scattering to be at least 1000 nm in diameter (see section I.I.4).

DOPC was used as a positive control and as a baseline of CCTα relative activity between systems to ease comparison. It must be noted that DOPC itself is CCTα activating compared to the negative control of no LUVs present. Consequently, assay results are presented as both absolute CCTα activitity in (nmoles.mg^{-1}.min^{-1}) and relative activity to 100 percent DOPC.

II.4.1. Hydrocarbon chain changes

II.4.1.1.1. Phosphate head group

Three amphiphiles with a phosphate head group were investigated:

- 1,2-di-oleoyl-sn-glycero-3-phosphate (DOPA, PA18:1/18:1)
- 1-oleoyl-sn-glucero-3-phosphate (OPA, PA18:1)
- 1,2-dipalmitoyl-sn-glycero-3-phosphate (DPPA, 16:0/16:0)

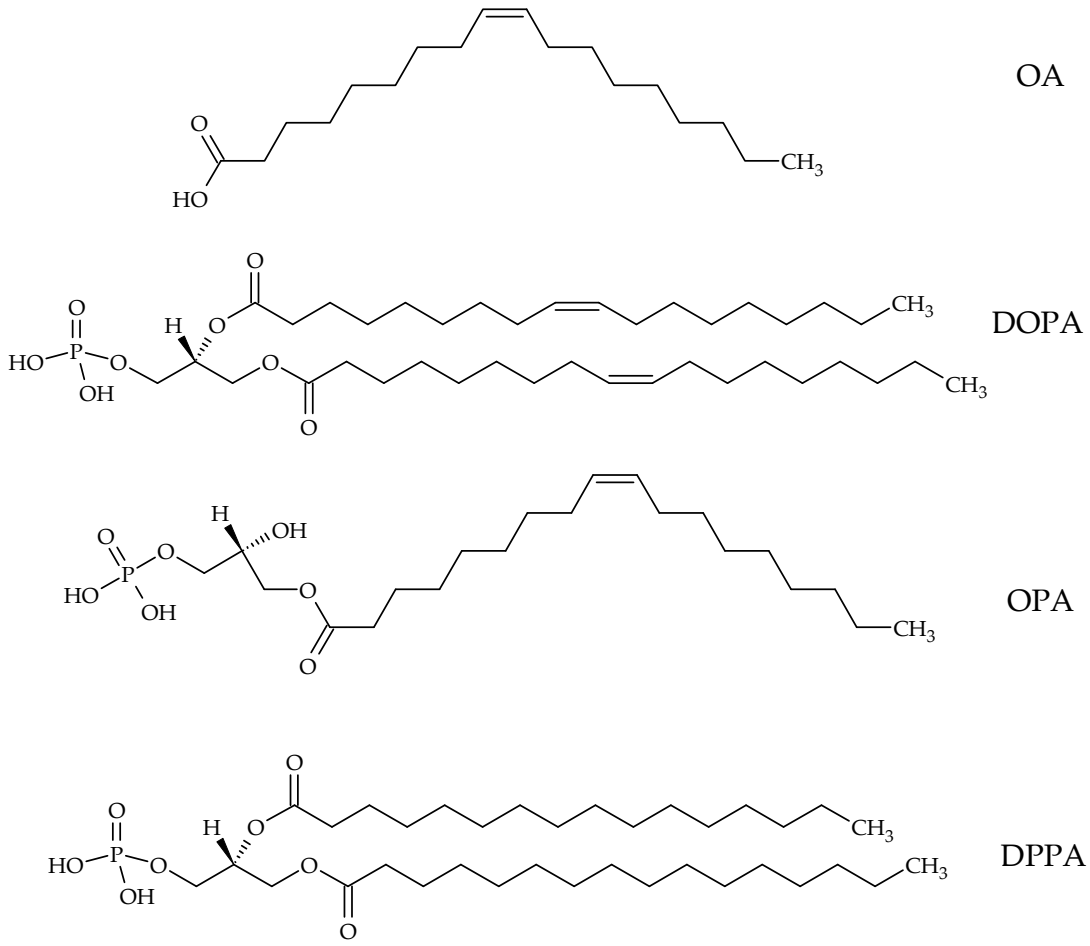

Figure II.10- Chemical structures for OA, DOPA (PA18:1/18:1), OPA (PA18:1) and DPPA (PA16:0/16:0).

Since DOPA, OPA and DPPA all show a phosphate head group, they are singly anionic and charged, as seen from their chemical structures (Figure II.10). Oleic acid (OA, 18:1) is also grouped here, although it does not have a phosphate head group.

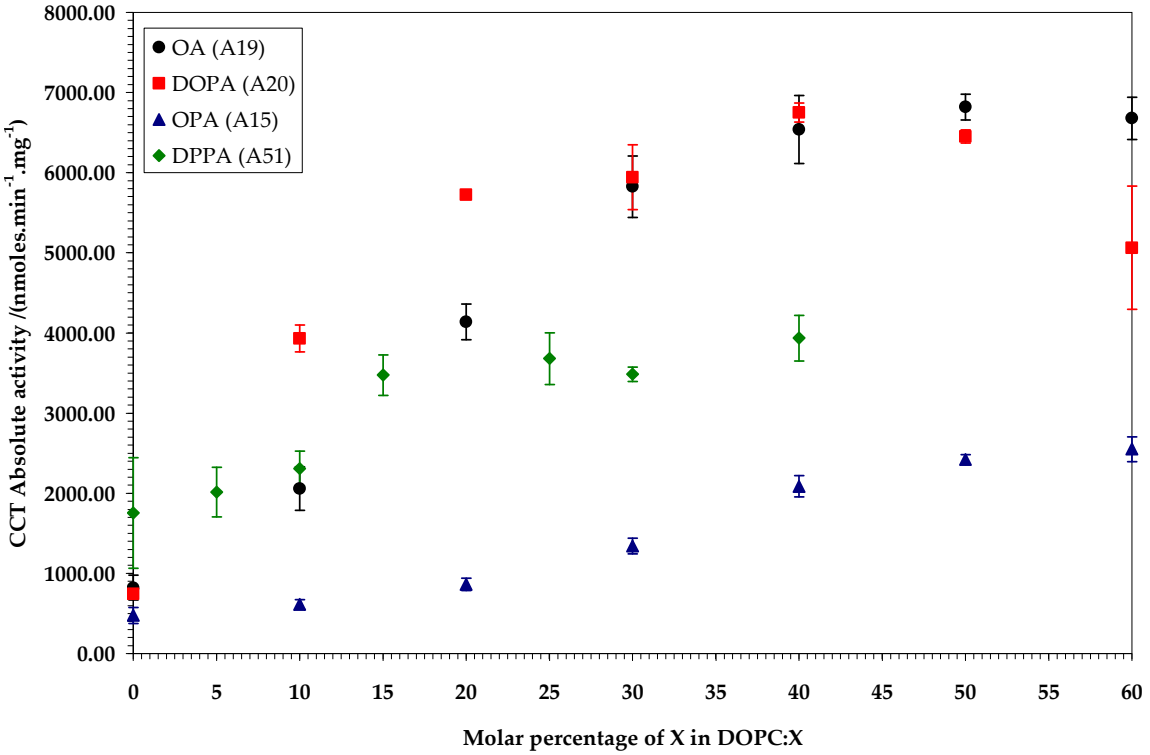

Figure II.11- Plot of CCT absolute activity against molar % of amphiphile X in DOPC: X vesicles.

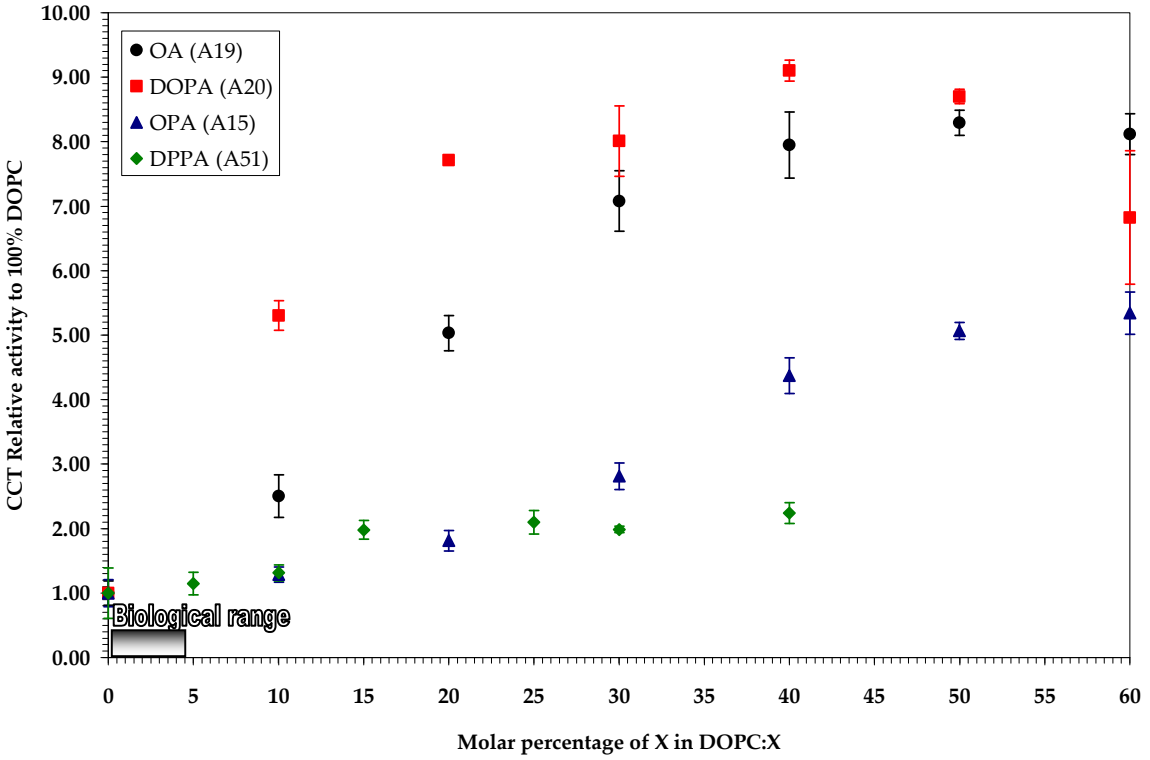

Figure II.12- Plot of CCT relative activity to 100% DOPC against molar % of amphiphile X in DOPC: X vesicles.

Considering their lateral stress diagrams (Figure II.6), their head group regions γ should be identical, but because of the variation in their hydrocarbon regions, zones α will be different. OPA will have the least pronounced α due to its only one fatty acid chain, followed by DPPA with two 16:0 chains. Finally, DOPA would show the largest α since it has two 18:1 chains. DOPA should have a larger α than DPPA since it has longer and more unsaturated chains. According to the lateral stress model of lyotropic crystal behaviour (see section I.I.3) DOPA would the most negative curvature when aggregating followed by DPPA and then OPA. Consequently, their ranking according to increasing Type II character would be OPA, DPPA and lastly DOPA. In fact, DOPA and OPA have been shown to be Type II and Type 0 respectively under physiological conditions (Kooijman, Chupin et al. 2003). OA is harder to compare as it is not a phospholipid, lacking the phosphate head group, but a fatty acid with only one cis C18:1 chain. However, it DOPC/OA LUVs have been shown to form inverse hexagonal phases due to specific interactions between DOPC and negatively charged OA head groups (Ferreira, Bentley et al. 2006). Thus, the binary system can be classified as a Type II amphiphile.

Overall, all four systems showed an activating effect on CCTα (Figures II.11-12). DOPC/DOPA was the most CCTα activating system, followed closely by DOPC/OA, then DOPC/OPA, and finally DOPC/DPPA. Previous experiments in our lab (Attard, Templer et al. 2000; Fagone 2003) and in the literature (Cornell and Vance 1987; Feldman and Weinhold 1987) have also shown that DOPA and OA strongly activate CCTα in LUVs.

These results are in line with the stored elastic stress hypothesis, since these amphiphiles modulated enzyme activity following the exact trend of their Type II characters.

Although anionic DOPA, OPA and DPPA activated CCTα, the electrostatic hypothesis argument of charge is not supported by this evidence since three amphiphiles with identical head group charge activated CCTα completely differently, with a maximal ten-fold difference between DOPA and DPPA.

II.4.1.1.2. **Phosphatidyl serine head group**

The effect of the anionic head group PS on CCTα was investigated for three amphiphiles:

- 1,2-di-oleoyl-sn-glycero-3-phosphatidyl-serine (DOPS, PS18:1/18:1)
- 1-oleoyl-sn-glycero-3-phosphatidyl-serine (OPS, PS18:1)
- 1,2-dipalmitoyl-sn-glycero-3-phosphatidyl-serine (DPPS, PS16:0/16:0)

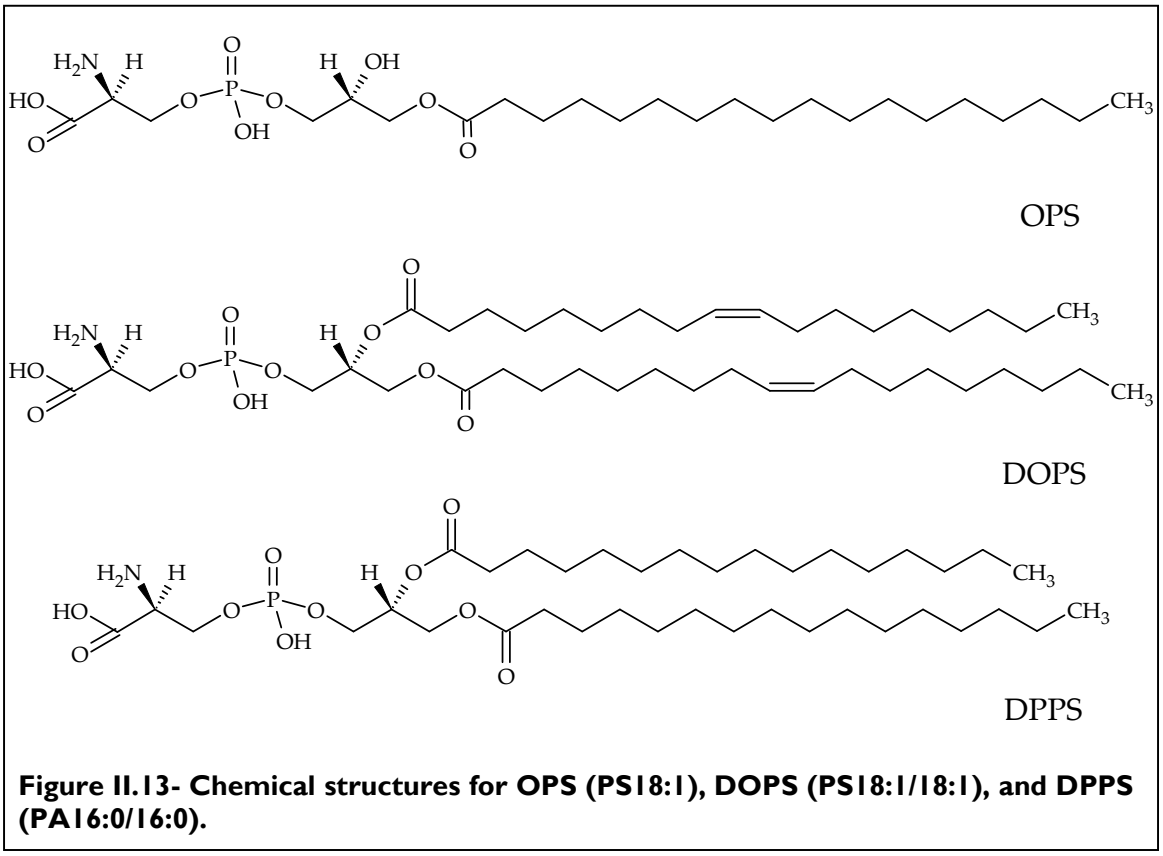

Figure II.13- Chemical structures for OPS (PS18:1), DOPS (PS18:1/18:1), and DPPS (PA16:0/16:0).

OPS, DOPS and DPPS all have the singly anionic phosphatidyl serine head group (Figure II.13). Comparing their lateral stress profiles, their head group γ region would be the same but α would vary due to their different fatty acid chains. Hence, using the same argument as for the phosphate head group amphiphiles, their ranking by increasing Type II character would be OPS, DPPS and DOPS.

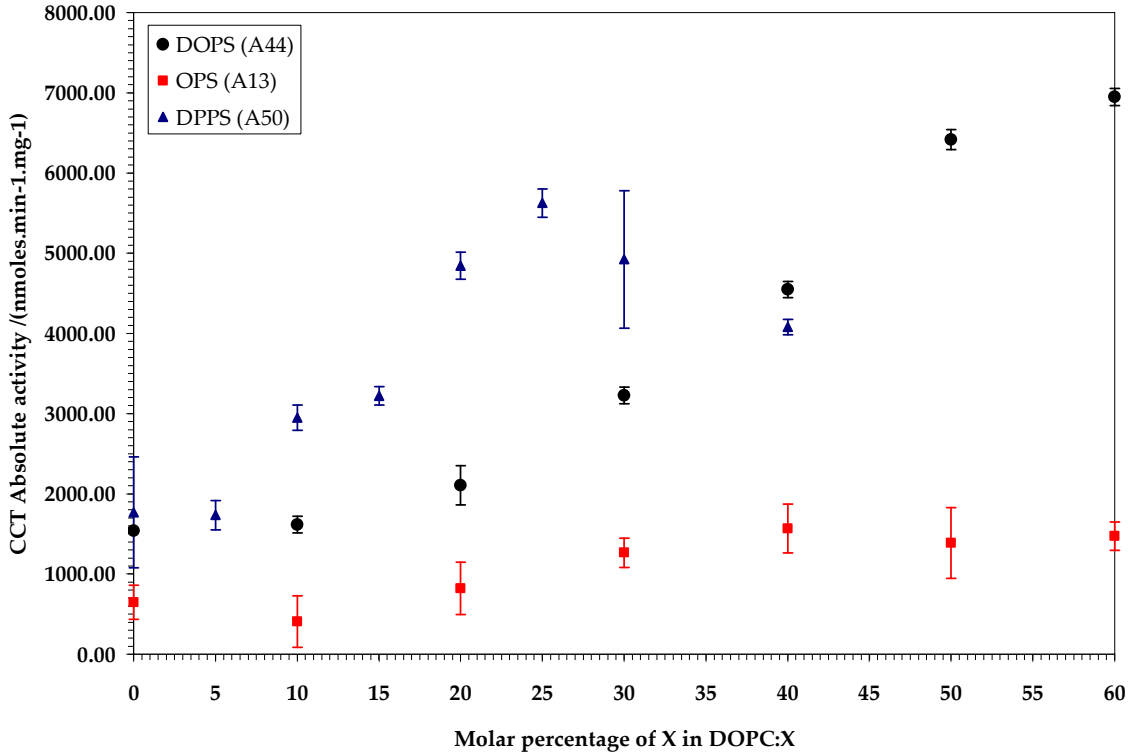

Figure II.14- Plot of CCT absolute activity against molar % of amphiphile X in DOPC: X vesicles.

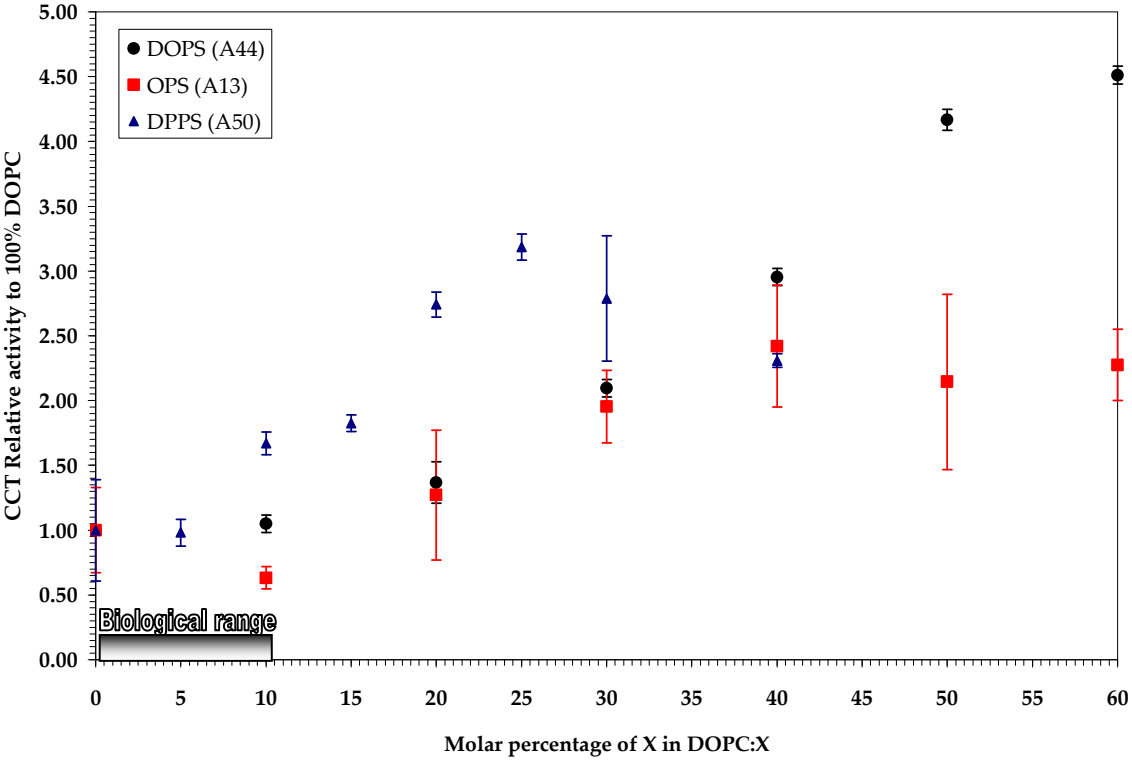

Figure II.15- Plot of CCT relative activity to 100% DOPC against molar % of amphiphile X in DOPC: X vesicles.

According to our results, all three binary systems activated CCTα, while DOPC/DPPS was the least activating (Figures II.14-15). DOPC/OPS was slightly more activating reaching a maximal relative activity to 100% DOPC of 4.68±0.63 compared to 4.51±0.07 for DOPC/DOPS. Therefore, within error, the two systems activated CCTα to the same degree, although DOPC/OPS reached the same relative activity at a smaller concentration. The stored elastic stress hypothesis fits these results as Type II DPPS, DOPS and OPS all increased CCTα activity in LUVs. The DOPC/OPS system was considerably more activating than in DPPS, which does not follow their typology trend and does not support the hypothesis. However, DPPS is not molten at the 37°C of the assay since its gel to fluid transition temperature at pH 7 is at 54°C (Marsh 1990). This means that although DPPS is a Type II amphiphile, it may not show Type II characteristic lyotropic behaviour at the temperature of our experiment.

OPS has been recently shown to be Type I in physiological temperature (Marsh 2007). However, OPS in the presence of lithium ions and protons forms inverse hexagonal phases, similar to those for DOPS (Cevc, Seddon et al. 1985). That is because cationic lithium ions and protons interact with the PS head group, thus increasing γ region in the lateral stress diagram of OPS. Since our assay buffer contains 10 mM $MgCl_2$ and substrate phosphocholine is purchased as a calcium salt, similar interactions may be occurring between magnesium or calcium ions and PS head groups. In fact, our own phase studies on DOPC/DOPS in assay buffer and phosphocholine showed the formation of inverse hexagonal phase in mixtures with more that 35 molar percentage of DOPS.

The fact that all three anionic amphiphiles activated the enzyme supports the electrostatic hypothesis. Unfortunately, their very different activation trends of a two-fold maximal difference between DOPS and OPS are not in line with the charge argument.

II.4.1.1.3. **Phosphatidyl ethanolamine head group**

The following two amphiphiles with the neutral zwitterionic phosphatidyl ethanolamine head group were investigated:

- 1,2-di-oleoyl-sn-glycero-3-phosphatidyl-ethanolamine (DOPE, PE18:1/18:1)
- 1,2-di-O-phytanyl-sn-glycero-3-phosphatidyl-ethanolamine (DPHPE)

DOPE results were kindly contributed by Dymond in our research lab.

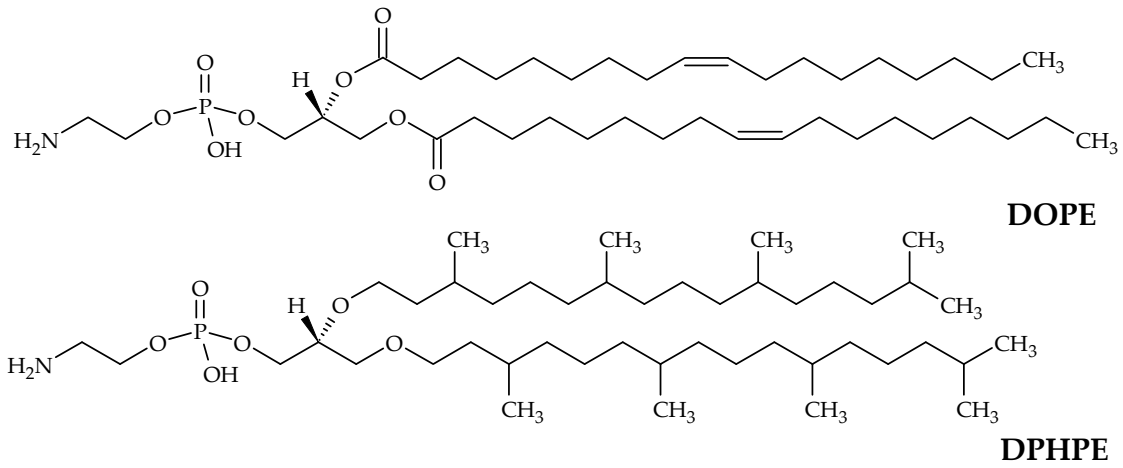

Figure II.16- Chemical structures for DOPE (PE18:1/18:1), and DPHPE.

These two amphiphiles show the same uncharged head group and thus area γ in their lateral stress profiles should be identical. However, their fatty acid chains are very different, with DPHPE showing highly methylated ether linked phytanyl chains. Using space filling chemical models, the distance between the two chains (C1 to C8) for DPHPE was calculated as 5.68 Å compared to 3.12 Å for DOPE (C1 to C22). Therefore, α for DPHPE would be larger as its chains splay further apart than the two C18:1 chains of DOPE. Hence, DPHPE is more Type II than DOPE.

According to our results, DPHPE is more activating than DOPE (Figures II.17-18). The stored elastic stress hypothesis is thus supported by these data since DPHPE, being more Type II than DOPE, increased CCTα activity much more strongly than DOPE. On the other hand, data are not in line with the electrostatic hypothesis since two neutral lipids activated the enzyme quite strongly.

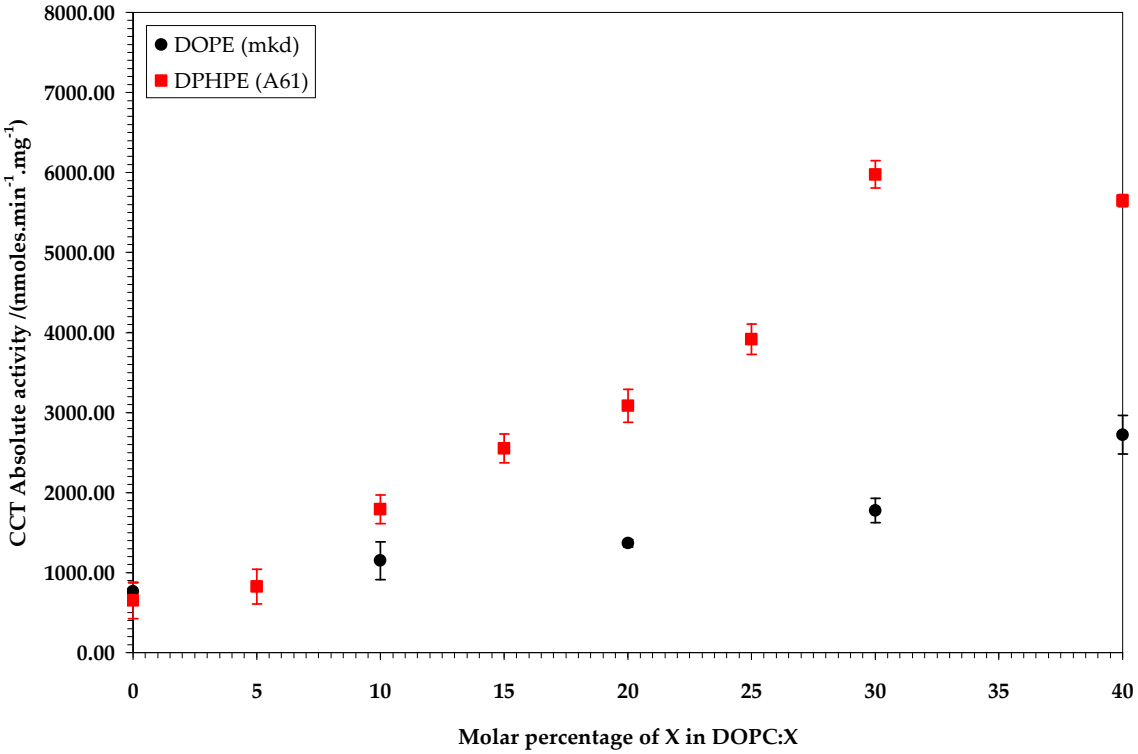

Figure II.17- Plot of CCT absolute activity against mol % of amphiphile X in DOPC: X vesicles.

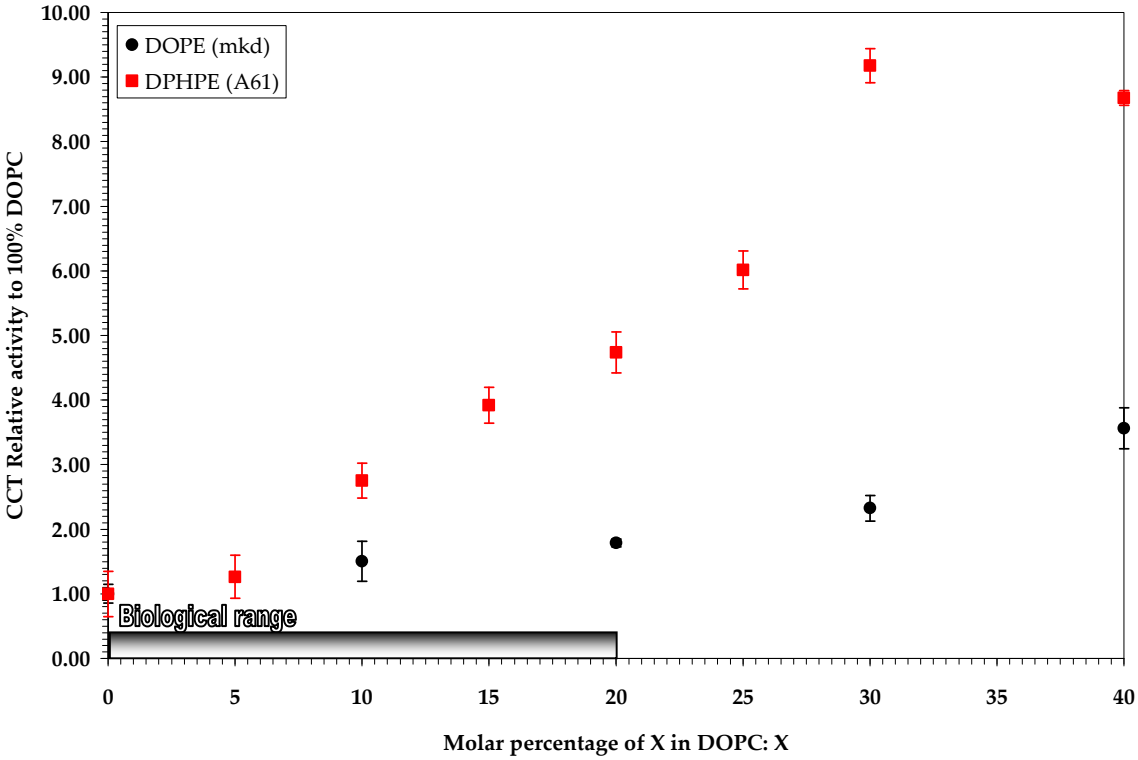

Figure II.18- Plot of CCT relative activity to 100% DOPC against molar % of amphiphile X in DOPC: X vesicles.

II.4.1.1.4. **Phosphatidyl glycerol head group**

The following three diacyl glycerols (DAGs) were studied:

- 1-palmitoyl-2-oleoyl-sn-glycerol (POG, 16:0/18:1)
- 1-stearoyl-2-arachidonoyl-sn-glycerol (SAG, 18:0/20:4)
- 1,2-di-oleoyl-sn-glycerol (DOG, 18:1/18:1)

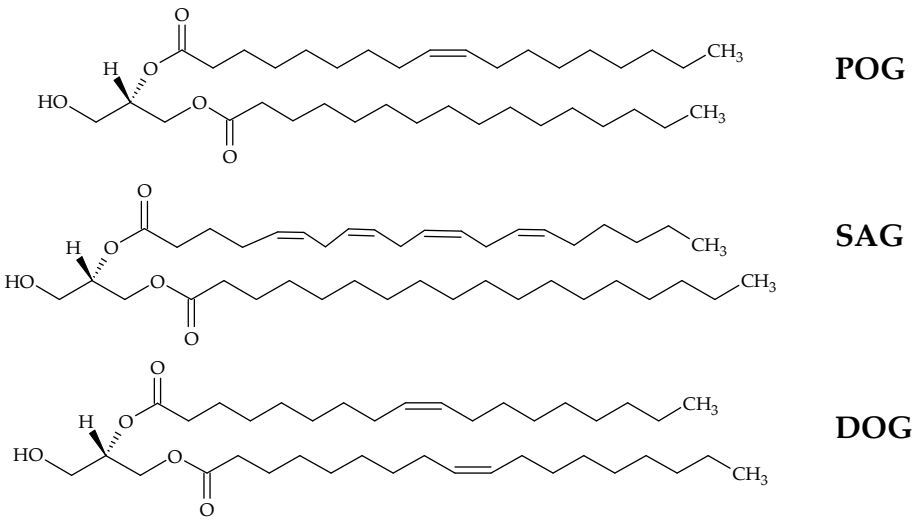

Figure II. 19- Chemical structures for (POG, 16:0/18:1), (SAG, 18:0/20:4) and (DOG, 18:1/18:1).

All three amphiphiles have the same head group and charge but their chains show large variation. Therefore in their lateral stress profiles, γ would be the same but α would vary with SAG having the largest, followed by DOG, then POG. That is because SAG has four double bonds; therefore its chains would splay the most, and DOG has two unsaturated chains while POG only has one. Therefore, their ranking in increasing Type II character should be POG, DOG and SAG.

Our results show DOPC/DOG as the most CCTα activating, causing a very marked maximum at only 2% DOG, followed by SAG and lastly POG (Figures II.20-21). The maximum of DOG at such a small mole percentage followed by a gradual decrease, suggest that a phase separation has occurred. Results for DOPC/SAG show very slight activation at a maximum of about 2.5 relative to DOPC. In DOPC/POG almost no change in CCTα activity occurred compared to DOPC.

DAGs form cubosomes, a phase that is not completely understood, when mixed with DOPC (Seddon 1990; Shearman, Khoo et al. 2007). DOPC is preferentially hydrated by water added during the vesicle preparation, trapping a small amount of DAGs, while the remainder phases out. This argument is supported by the sizing results of LUVs by light scattering at 90° for DOG (Figure II.20), which show very small particles at the 4 mole percent.

DOPC/DOG mole fraction	% of LUVs	Exact diameter/nm
100:0	83.4	1858.0 ± 214.3
	13.4	378.9 ± 78.2
98:2	83.8	2000.0 ± 137.0
	16.2	158.7 ± 13.6
96:4	100.0	509.4 ± 91.2
94:6	73.3	2000.0 ± 137.0
	26.7	246.2 ± 37.5
92:8	78.7	1954.9 ± 140.9
	21.3	250.4 ± 40.7
90:10	96.2	659.6 ± 106.3
	3.8	10.0 ± 0.9

Figure II.20- Light scattering sizing results for DOPC/DOG (A17).

Sizing data for SAG and POG LUVs showed that the majority of the samples in all fractions had a size larger than 1000 nm, with the exception of DOPC/POG (90:10) that had 68.2 percent of its sample with an average size of 462.3 ± 110.6 nm.

The stored elastic stress hypothesis is not supported by results for DAGs. However, formation of cubosomes hinders data analysis since LUVs forming do not have the expected size and composition. The experimental method must be improved in order to correct this phase separation. Especially DOPC/DOG illustrated variability between experiments, and was in fact the only binary system out of all studied with poor reproducibility.

These data would be the hardest to justify by the electrostatic hypothesis, as none of its arguments can explain the maximal activity for 2 mole percent DOG.

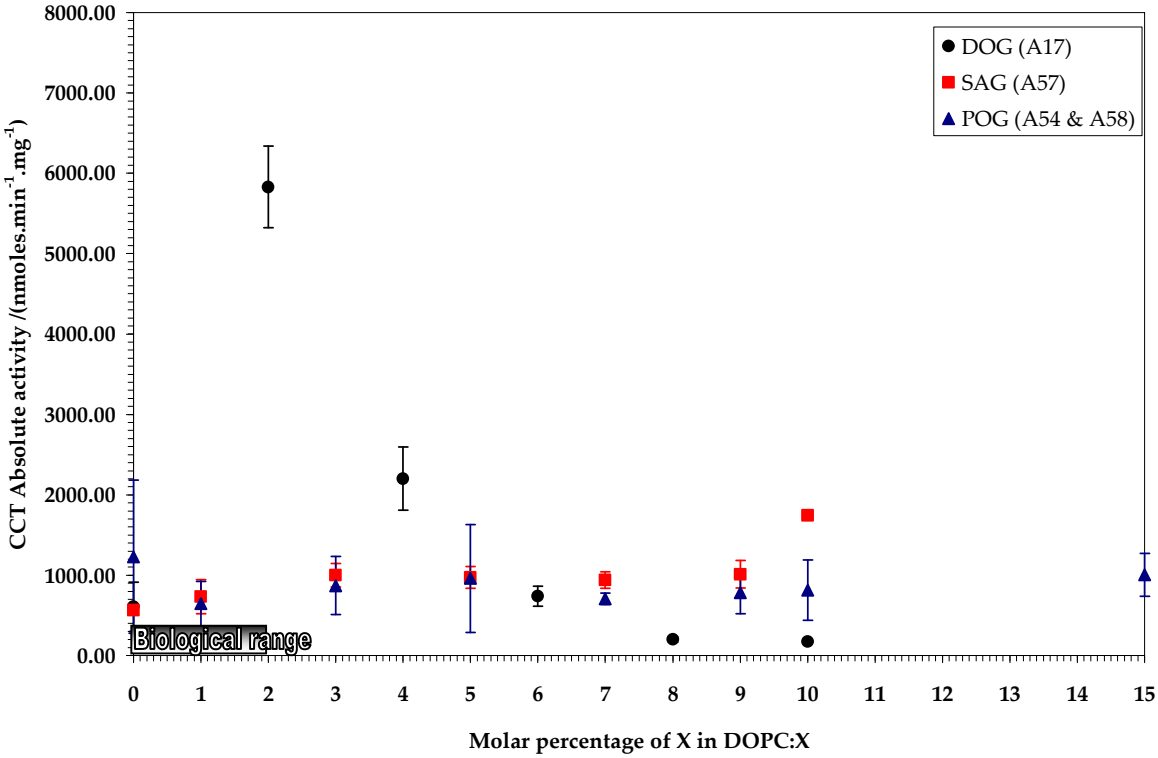

Figure II.21-Plot of CCT absolute activity against molar % of amphiphile X in DOPC: X vesicles.

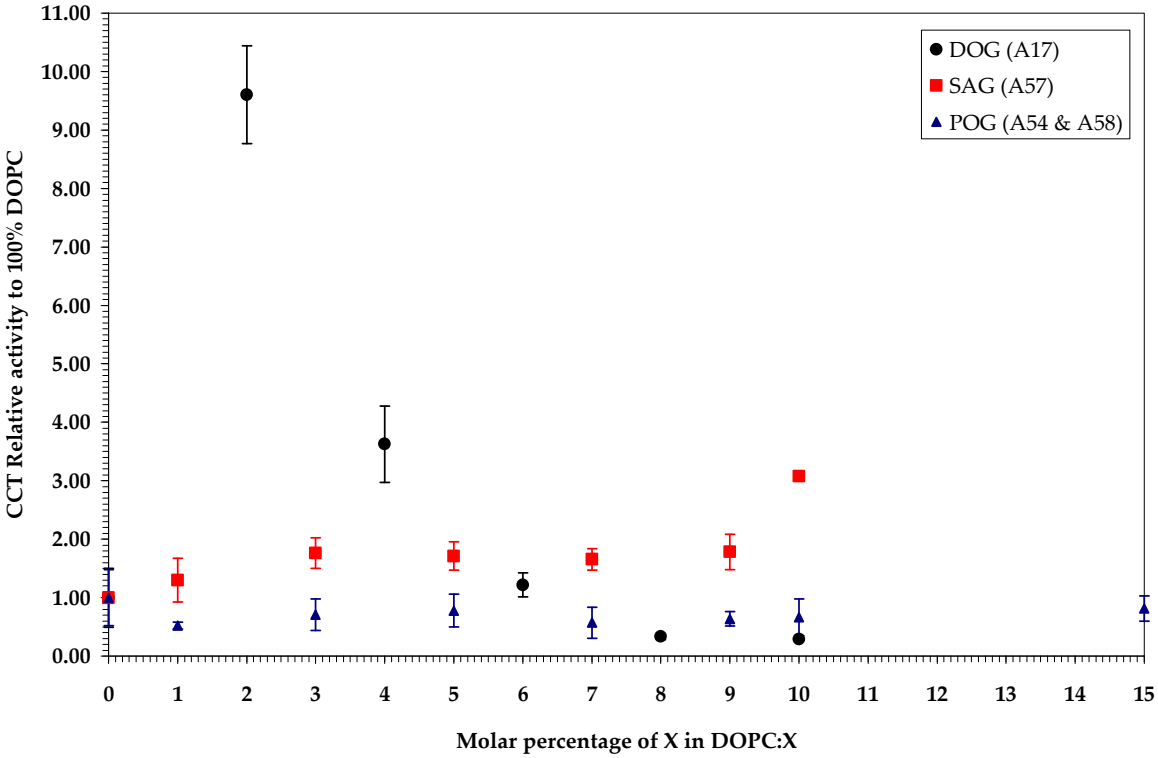

Figure II.22- Plot of CCT relative activity to 100% DOPC against molar % of amphiphile X in DOPC: X vesicles.

II.4.1.1.5. **Phosphatidyl choline head group**

The effect of the zwitterionic head group PC was assayed for:

- N-Stearoyl-D-erythro-Sphingosylphosphorylcholine (SM)
- 1,2-di-O-phytanyl-sn-glycero-3-phosphatidyl-choline (DPHPC)

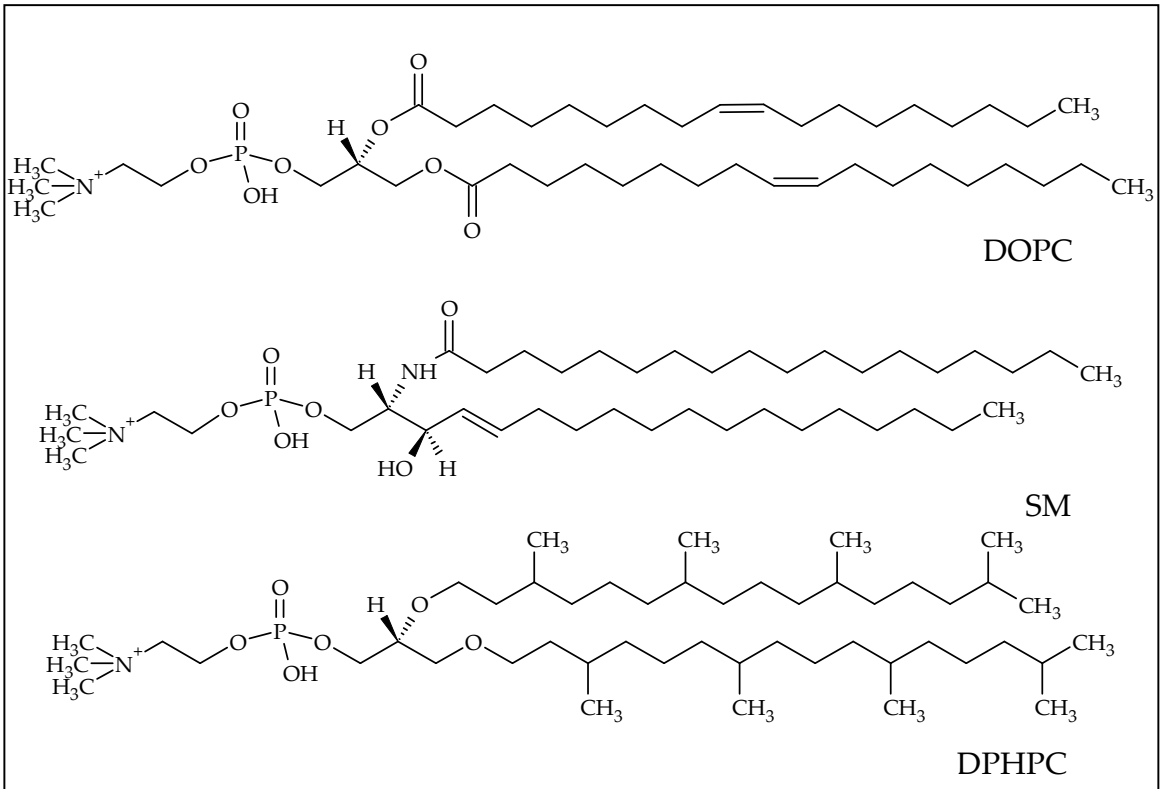

Figure II.23- Chemical structures for DOPC, SM and DPHPC.

Since DOPC, SM and DPHPC have the head group, γ in their lateral stress diagram would be identical. However, SM has two completely saturated hydrocarbon chains while DPHPC has the extensive branching, characteristic for the phytanyl chain. Hence, DPHPC would have a more pronounced α, rendering it more Type II compared to SM. DOPC has two 18:1 chains, and thus would have a larger α to SM. The same argument as for DOPE and DPHPE applies when comparing α for DOPC and DPHPC (see section II.3.1.1.3). Consequently, their ranking according to increasing Type II character would be SM, DOPC and DPHPC. In fact, SM aggregates to a lamellar phase in physiological temperature (Kihara, Mitsutake et al. 2007), hence is a Type 0 lipid.

The results illustrate a maximum relative activity to 100 percent DOPC at 3.46 for DOPC/DPHPC (40:60) while SM is not activating or slightly deactivating for CCTα. These data are in agreement with the literature as SM has been shown before to inhibit CCTα activity (Sohal and Cornell 1990; Vivekananda, Smith et al. 2001). Since DOPC is used as a positive control, its relative activity to 100 percent DOPC is always 1.

Results for both SM and DPHPC are in line with the stored elastic stress hypothesis. The electrostatic hypothesis is supported by the SM data, since as an uncharged species, it did not activate the enzyme, but contradictory, DPHPC, with the same uncharged head group as SM, promoted CCTα catalytic activity considerably.

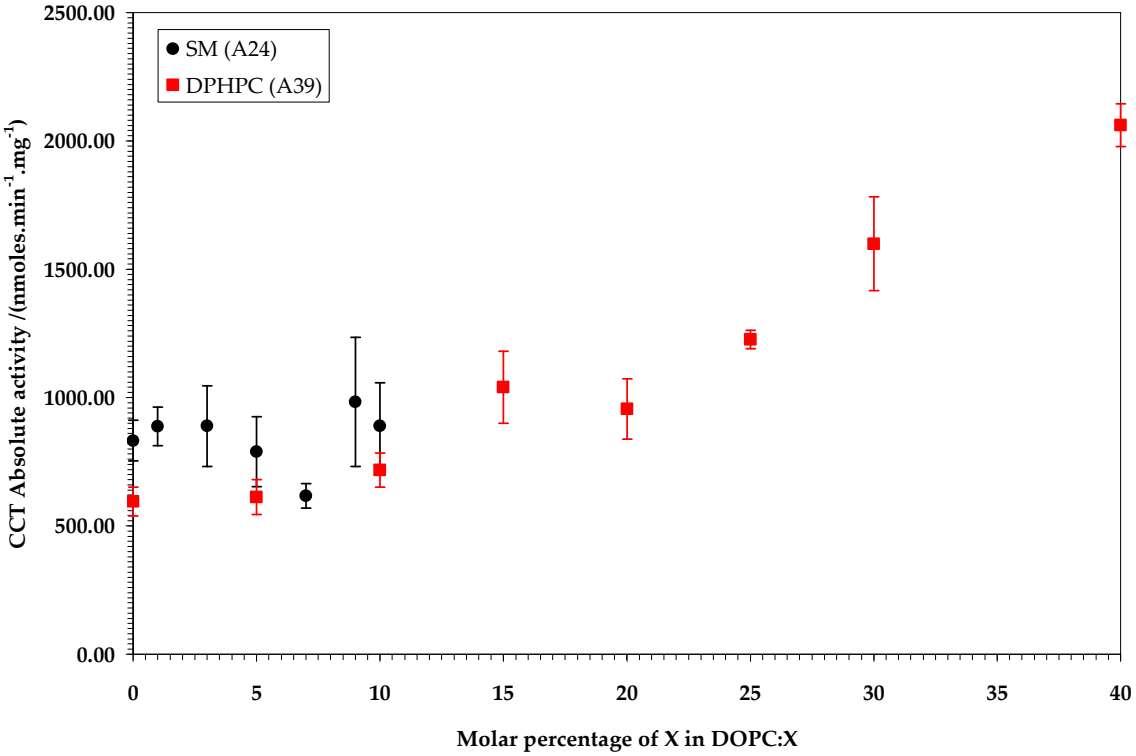

Figure II.24- Plot of CCT absolute activity against molar % of amphiphile X in DOPC: X vesicles.

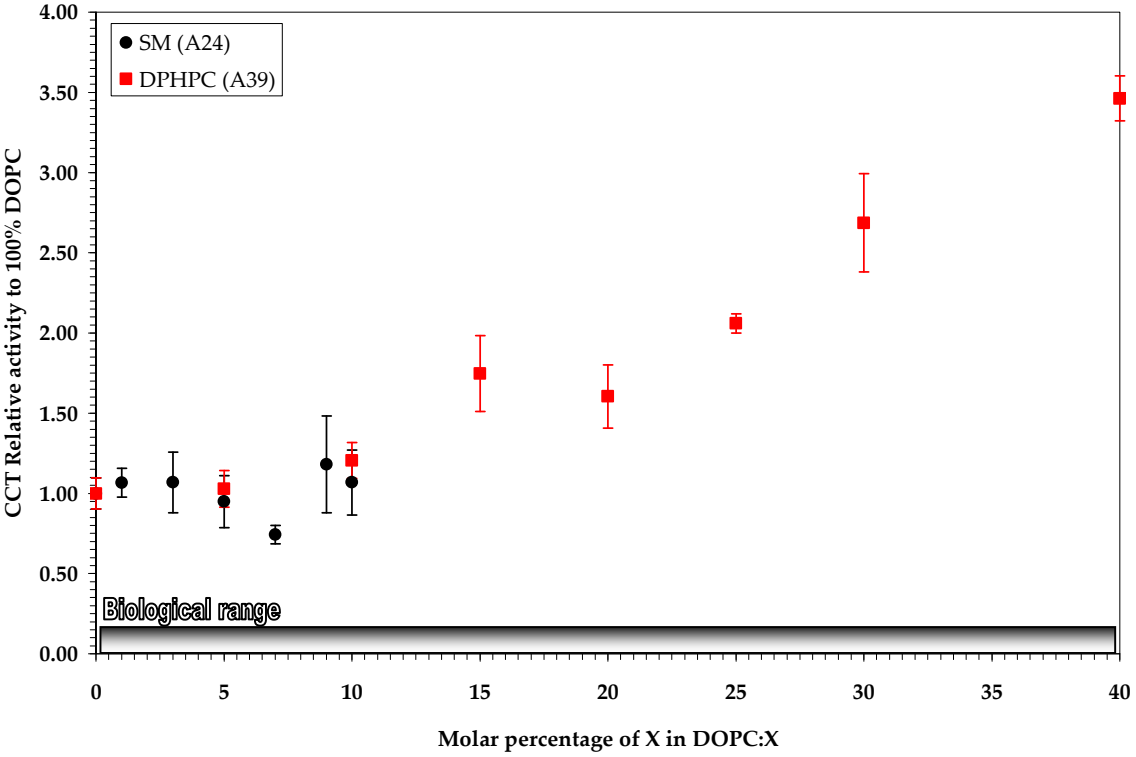

Figure II.25- Plot of CCT relative activity to 100% DOPC against molar % of amphiphile X in DOPC: X vesicles.

II.4.1.1.6. **Effect of unsaturation in chain**

In order to investigate how unsaturation in the fatty acid chains of amphiphile would modulate enzyme activity, two species were investigated:

- N-Stearoyl-D-erythro-Sphingosine, (C18:0 CER)
- N-Oleoyl-D-erythro-Sphingosine, (C18:1 CER)

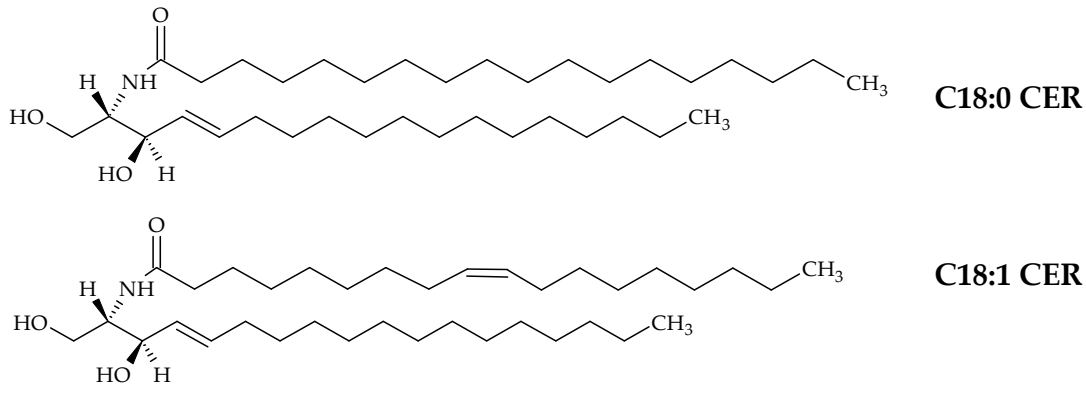

Figure II.26- Chemical structures for C18:0 and C18:1 CER.

These two amphiphiles only differ on one degree of unsaturation in one of their fatty acid chains. Hence, α would be larger for C18:1 CER, making it more Type II than its completely saturated counterpart.

From our results, C18:1 CER activated CCTα with a maximal relative activity to 100% DOPC equal to 5.95± .36 at DOPC/C18:1 CER (60:40) while all, C18:0 CER showed a very slight activation with a maximal relative activity equal to 2.53± 0.31 at the same mole percent (Figures II.27-28).

The stored elastic stress model completely agrees with these results illustrating how introducing unsaturation in an otherwise identical structure, can change lyotropic liquid crystal behaviour and in consequence modulate CCTα catalytic activity.

The electrostatic hypothesis is not supported by these data since two neutral amphiphiles not only activated CCTα but also to varying degrees.

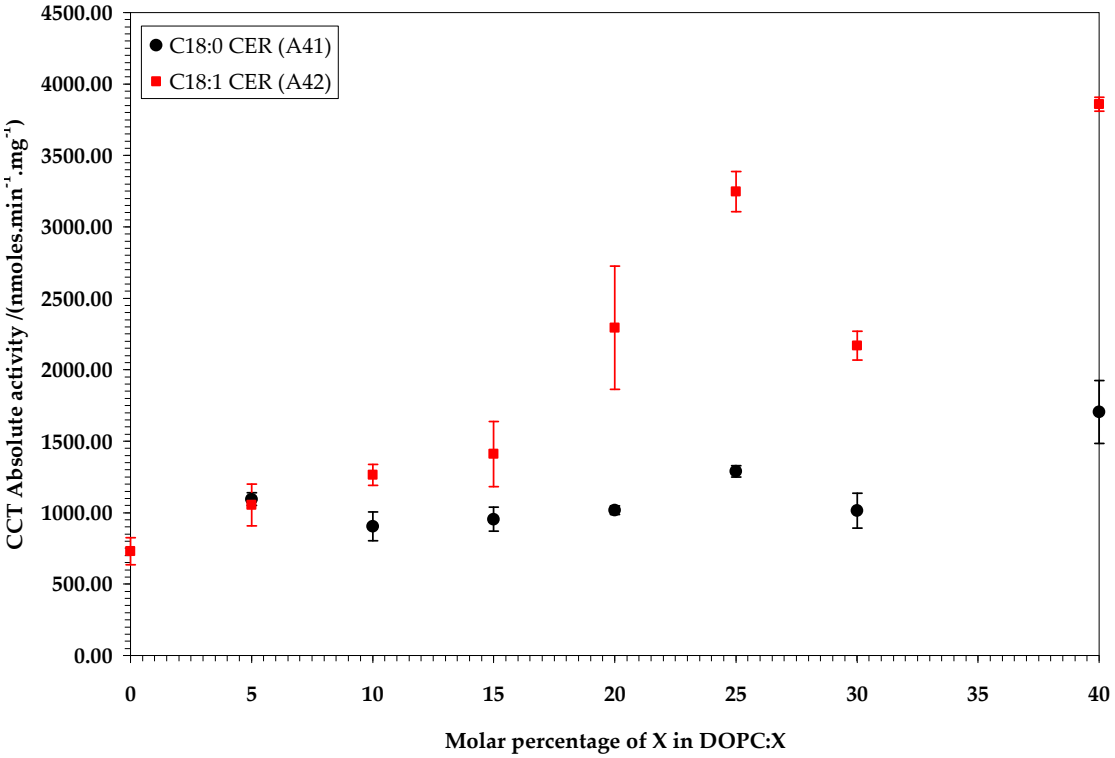

Figure II.27- Plot of CCT absolute activity against molar % of amphiphile X in DOPC: X vesicles.

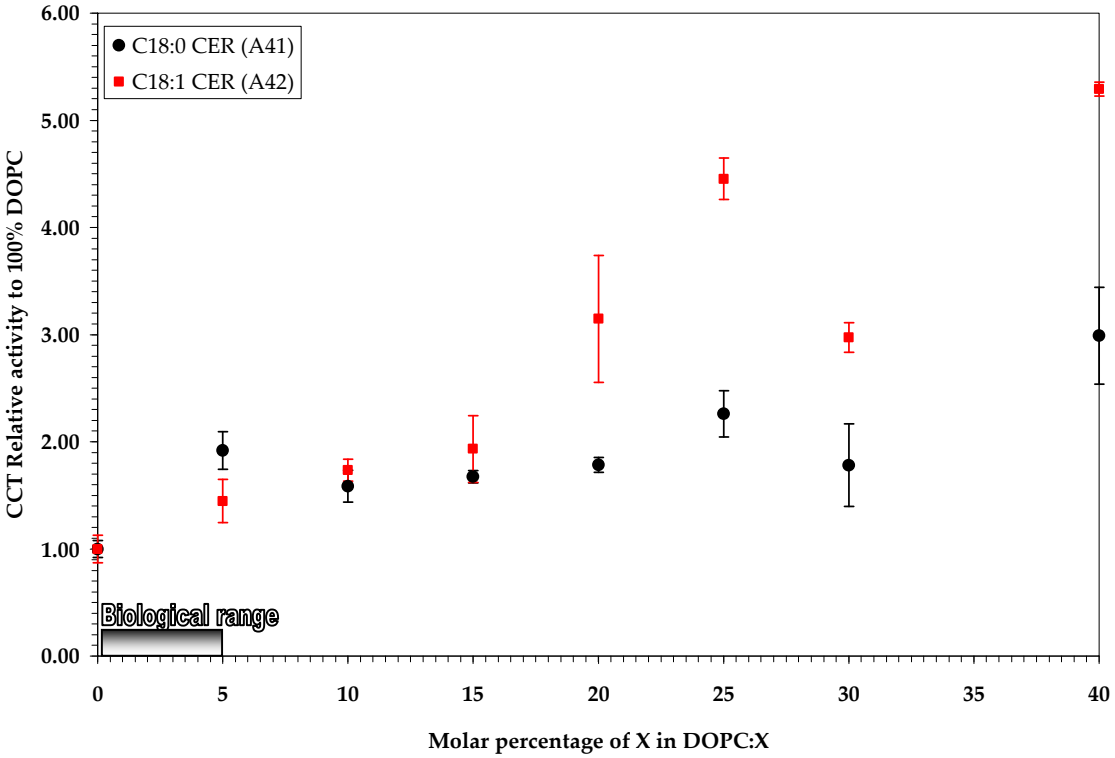

Figure II.28- Plot of CCT relative activity to 100% DOPC against molar % of amphiphile X in DOPC: X vesicles.

II.4.2. Head group changes

II.4.2.1.1. Di-oleoyl chain

Amphiphiles DOPA, DOPS, DOPE and DOG all show two di-octadecanoyl, or di-oleoyl chains. For chemical structures, see Figures II.10, II.13, II.16 and II.19, respectively. Therefore, their hydrocarbon chain cross sections should be identical, as well α as in their lateral stress profiles, γ but would vary because of their different head groups. Considering head group size DOG has the smaller head group with only an alcohol group, followed by DOPA that has a larger phosphate head group. DOPE is the next larger with a PE while DOPS is the largest of all with the three carbon atom long PS. Therefore, in increasing α order DOG would be first, then DOPA, DOPE and DOPS. DOPA and DOPS are anionic, while DOG and DOPE are zwitterionic. Steric repulsions will occur between the anionic head groups in a monolayer, increasing the head group cross-sectional area even further. Consequently, all four amphiphiles would be Type II, but in order of increasing Type II character DOPC would show the least, then DOPE, DOPS and DOPA and DOG.

Our data showed that DOPA is by far the most CCTα activating, followed by DOPS, then DOPE (Figures II.29-30). DOG showed a maximal activity at the 2 mole percent fraction but then activity fell sharply, as discussed in II.3.1.1.3.

These data support the stored elastic stress hypothesis since all four Type II amphiphiles activated the enzyme, and in fact following their exact order of Type II behaviour. The electrostatic hypothesis is in line with the results for anionic DOPA and DOPS that activated CCTα, and zwitterionic DOPE. However, it cannot explain data for DOG that is uncharged but strongly enhanced enzyme activity.

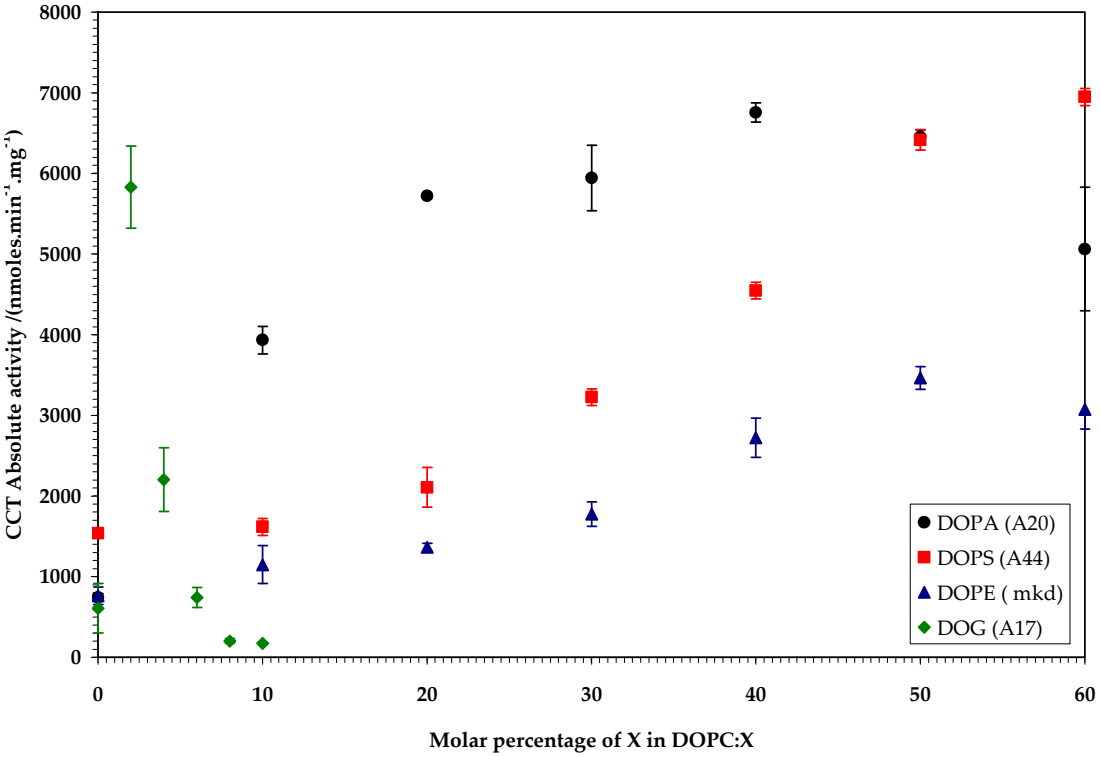

Figure II.29- Plot of CCT absolute activity against molar % of amphiphile X in DOPC: X vesicles.

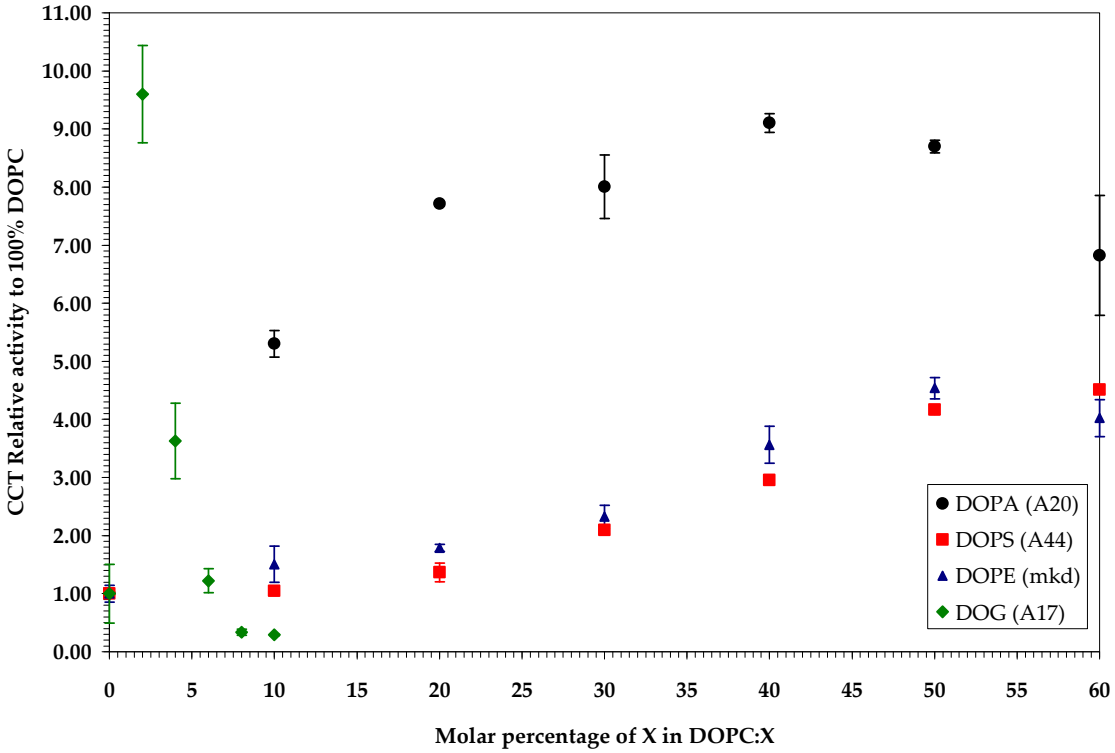

Figure II.30- Plot of CCT relative activity to 100% DOPC against molar % of amphiphile X in DOPC: X vesicles.

II.4.2.1.2. **Dipalmitoyl chain**

DPPS and DPPA both have a di-palmitoyl, or di-hexadecanoyl chain, as seen in Figures II.10 and II.13 respectively. Both are anionic and they only differ in that the PS head group is larger than the phosphate one. In their lateral stress profiles, α would be equal, and γ would be larger for PS. Thus, DPPS should be less Type II than DPPA. It must be noted that treating γ as purely steric would be a gross oversimplification since factors like charge screening that can affect it. Especially for the PS head group, for which is has been shown that changes in phase transition temperature are caused by interactions of lithium cations and protons (Cevc, Seddon et al. 1985).

Our data showed that DPPS was at least two-fold more CCTα activating. These results are not in line with the stored elastic stress hypothesis, but it must be noted that during the vesicle preparation for both lipids, and especially DPPA, two phases formed when in aqueous solution. This is because DPPS is in the L_β and not the Lα phase at 37 °C (Marsh 1990), the temperature of our experiment. Hence, as DPPS phases out of the vesicles, LUVs will not have the desired composition.

With respect to the electrostatic hypothesis, results for both amphiphiles agree. However, since they both carry a single negative charge, enzyme activation should be the same between the two. The latter is contradicted by our data.

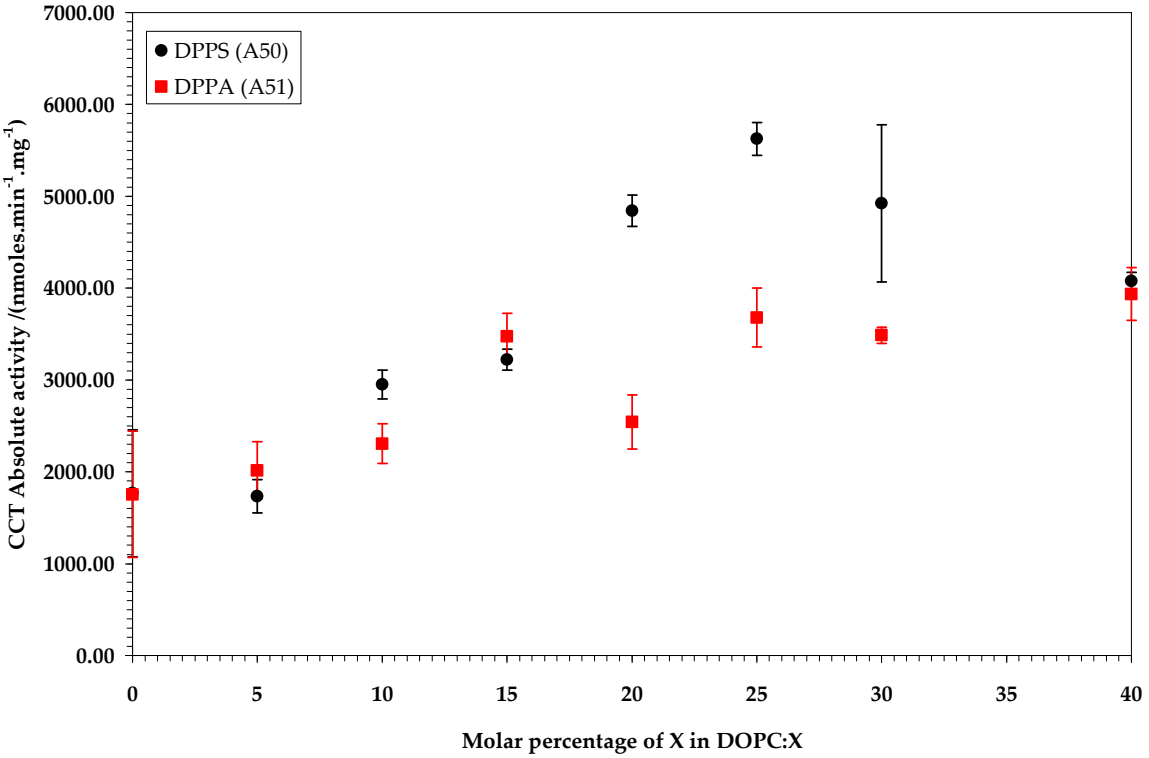

Figure II.31- Plot of CCT absolute activity against molar % of amphiphile X in DOPC: X vesicles.

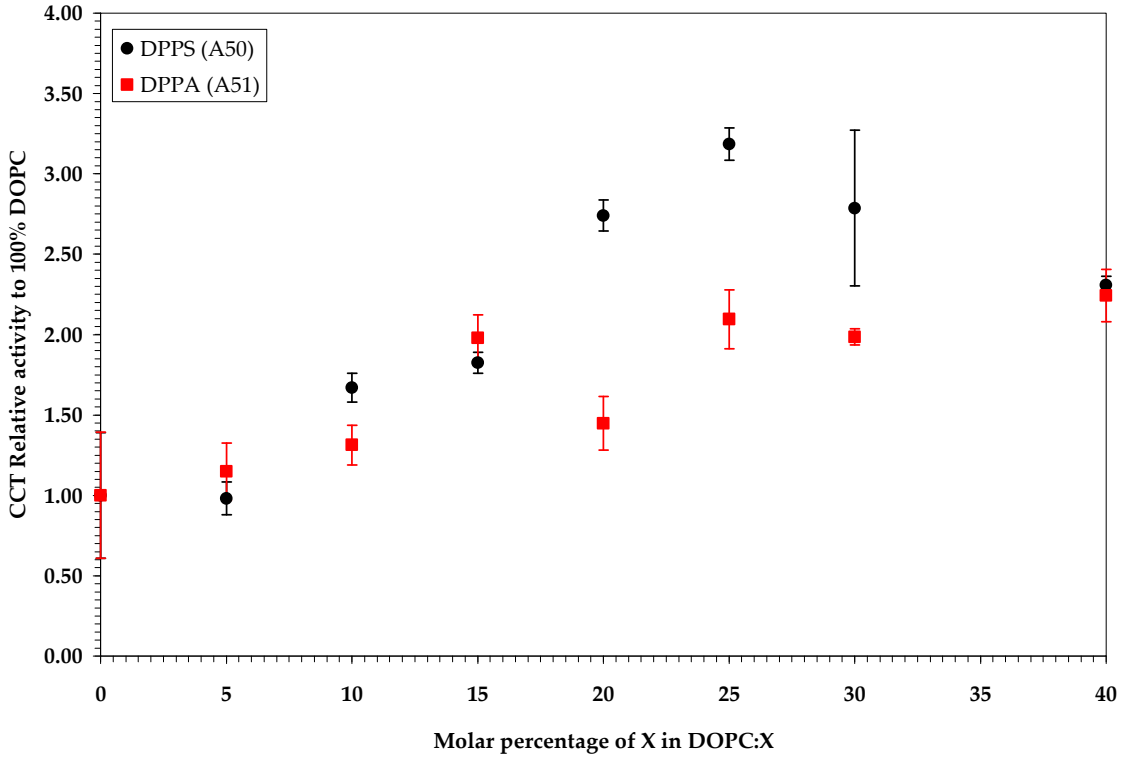

Figure II.32- Plot of CCT relative activity to 100% DOPC against molar % of amphiphile X in DOPC: X vesicles.

II.4.2.1.3. **Diphytanoyl chain**

DPHPE and DPHPC both illustrate the characteristic phytanyl chain, as seen in Figures II.16 and II.23, respectively. The latter highly branched chain is predominant in membrane lipids of hyperthermophilic archaebacteria that grow optimally at 80 to 105 °C (Minamikawa and Hato 1997). Interestingly, ether-linked phytanyl phospholipid analogs have been found to cause apoptosis in human HL60 cells (Hoffman, Stanley et al. 1984).

In their lateral stress profiles, α would be equal but γ should be larger for DPHPC due to its larger PC head group. Since DPHPC is anionic compared to the zwitterionic DPHPE, steric repulsions will occur between the DPHPC monomers in a monolayer. Also, DPHPC should have α identical to DOPC, but γ larger since the DPH chain are bulkier than DO (see section II.3.1.1.3). Taking all these parameters into consideration, DPHPC should be less Type II than DPHPE due to its very large head group cross-sectional area.

Our results showed that DPHPE has at least four-fold more CCTα activating that DPHPC (Figures II.33-34). Also, DPHPC was slightly more activating than DOPC. This is line with the stored elastic stress hypothesis since the more Type II amphiphile activated the enzyme more strongly. The electrostatic hypothesis is not supported here because a zwitterionic was markedly more CCTα activating than an anionic lipid.

It must be noted that the last data point for DOPC/DPHPE, at a 40:60 molar ratio, may be due to a phase change. Thus, phase studies for this particular binary mixture should be done as further work to this thesis to clarify this point.

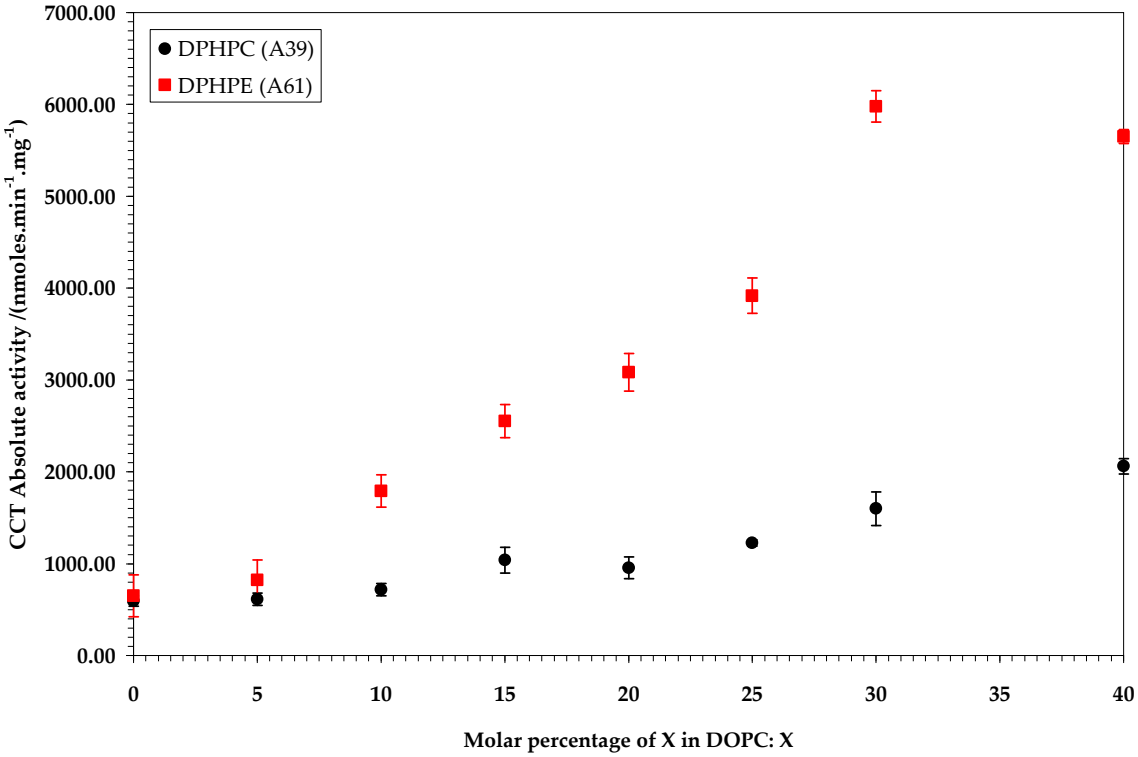

Figure II.33- Plot of CCT absolute activity against molar % of amphiphile X in DOPC: X vesicles.

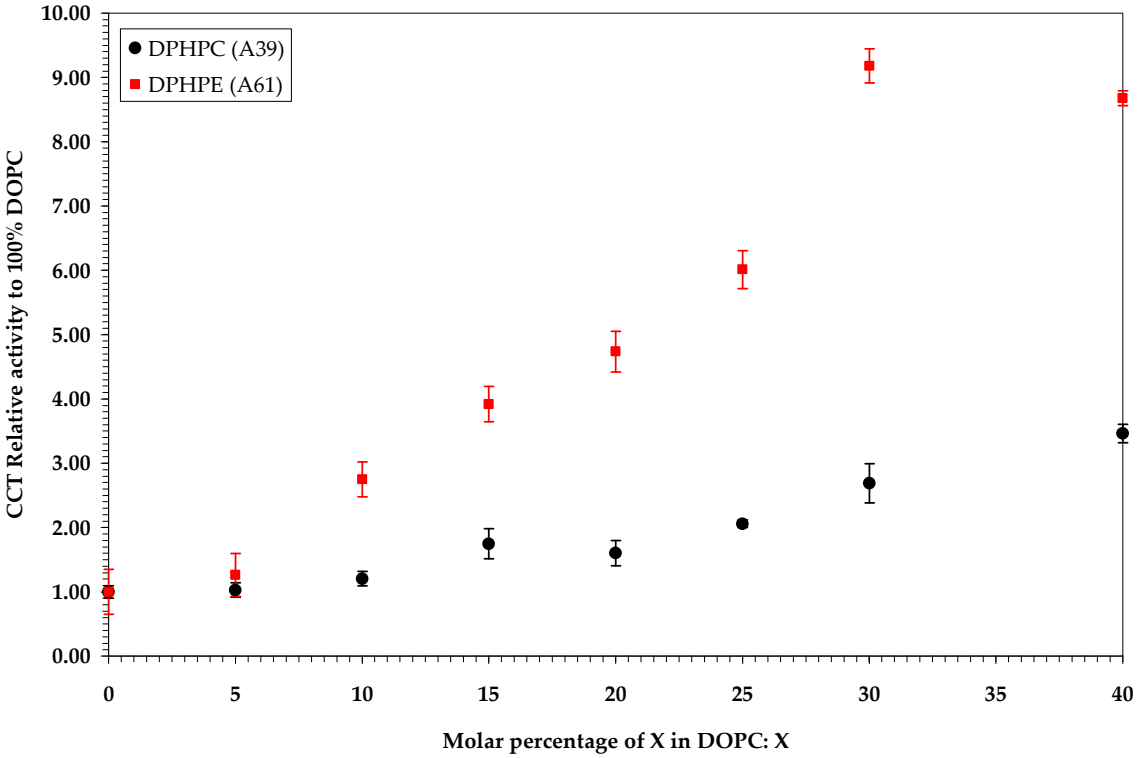

Figure II.34- Plot of CCT relative activity to 100% DOPC against molar % of amphiphile X in DOPC: X vesicles.

II.4.2.1.4. **Effect of phosphorylation to head group**

Phosphorylation changes to the head group area of amphiphiles was investigated in two species:

- D-erythro-sphingosine (DES)
- D-erythro-sphingosine-phosphate (DESP)

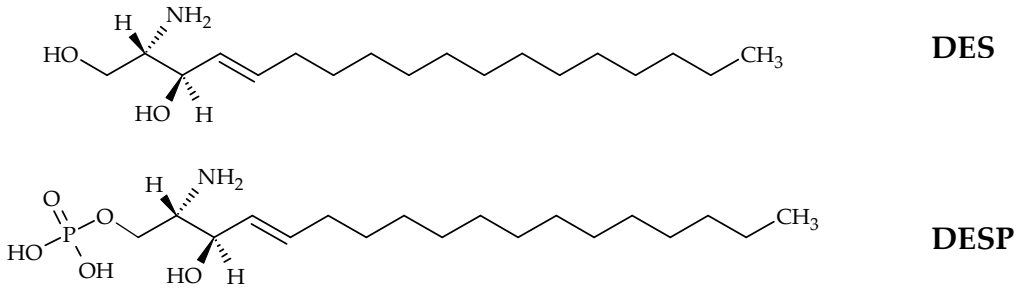

Figure II.35- Chemical structures for DES and DESP.

DES is neutral while DESP is anionic. Considering their lateral stress profiles, α would be equal but γ should be larger for DESP due to its larger phosphate head anionic group. Thus, DESP should be less exhibit less Type II behaviour than DES. Also, magnesium ions in the assay buffer could potentially bridge between the phosphate head groups anionic DESP, decreasing its Type II character even further, similarly to DOPS (Cevc, Seddon et al. 1985).

However, both species are more soluble and easily hydrated than DOPA, the most activating Type II species treated so far. That is because they have only one chain and lack the glycerol backbone. The pKa of the terminal hydroxyl group on DES is 14.15 at 25 °C (Dawson, Elliott et al. 1959).

Consequently, it is difficult to firmly categorise DES and DESP according to their typology lack of phase studies, but comparison between them is still feasible.

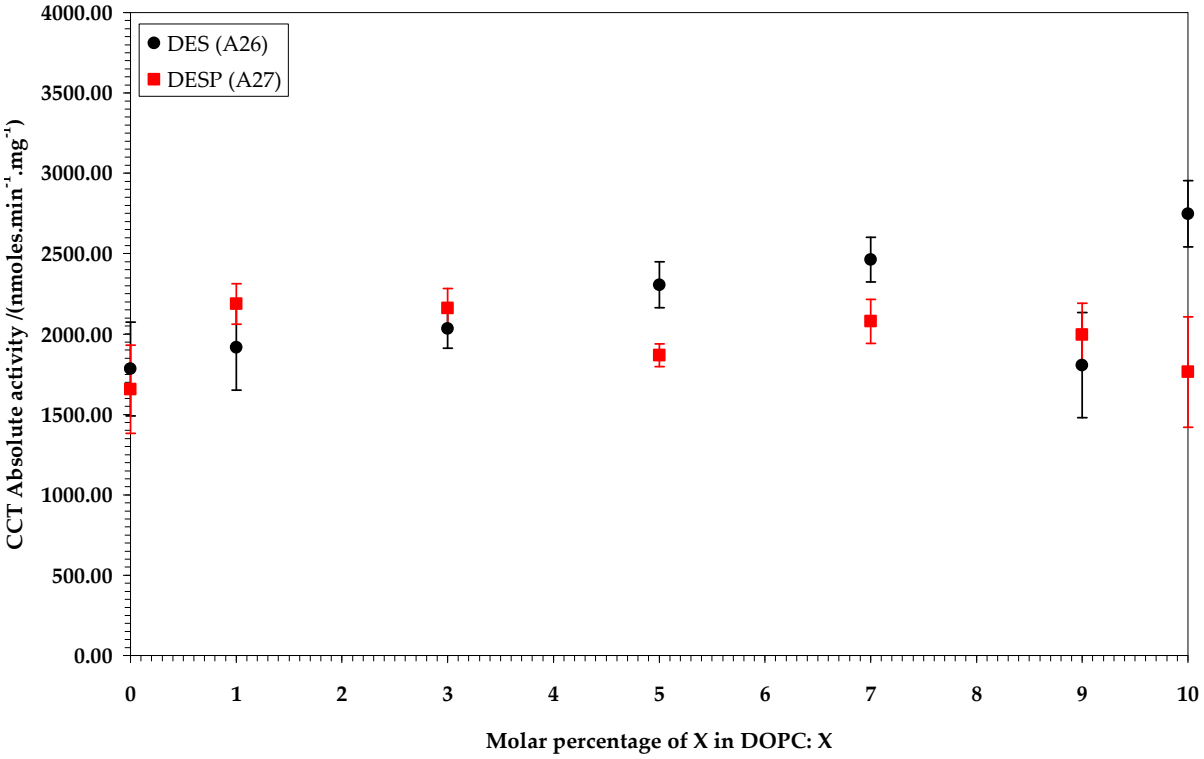

Figure II.36- Plot of CCT absolute activity against molar % of amphiphile X in DOPC: X vesicles.

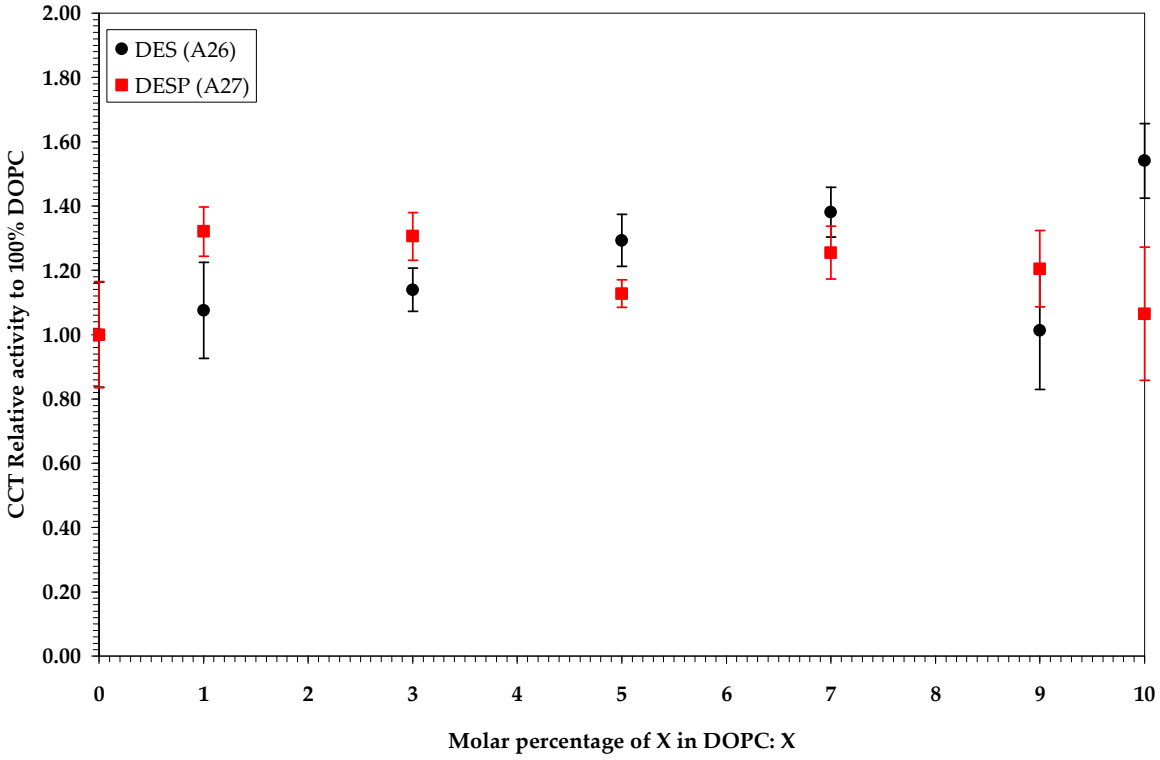

Figure II.37- Plot of CCT relative activity to 100% DOPC against molar % of amphiphile X in DOPC: X vesicles.

From our results, both DES and DESP slightly increased CCTα activity in the assay (Figures II.36-37). DES was more steeply activating with maximal relative activity to 100% at 1.44±0.11 compared to 1.11±0.11 for DES. Overall, there was not significant difference between the two amphiphiles within error. The results verify the stored elastic stress hypothesis, as in fact DES, being more Type II, is more activating than DESP, albeit marginally so.

The electrostatics hypothesis is supported by data for DES but not for DESP, but having so similar values and trends is not in agreement.

Overall, DES and DESP are good candidates for phase studies, since phase transition temperatures are available for neither species. Interestingly, DES is a pharmacological inhibitor of protein kinase C, an amphitropic protein, as well an *in vivo* inhibitor of calmodulin, a regulator of CCTα activity (Khan, Mascarella et al. 1991).

II.4.3. Amphiphiles of biological interest

The remaining Type II amphiphile systems investigated were:

- Cholesterol (CHOL)
- 1,2-Dihexanoyl-sn-Glycero-3-[Phospho-rac-(1-glycerol)] (C6:0 PG)
- 1,2-Dioctanoyl-sn-Glycerol (C8:0 DG)
- oleoyl coenzyme A (O COA).

These systems were chosen for either having a critical role in metabolism or showing a unique structure.

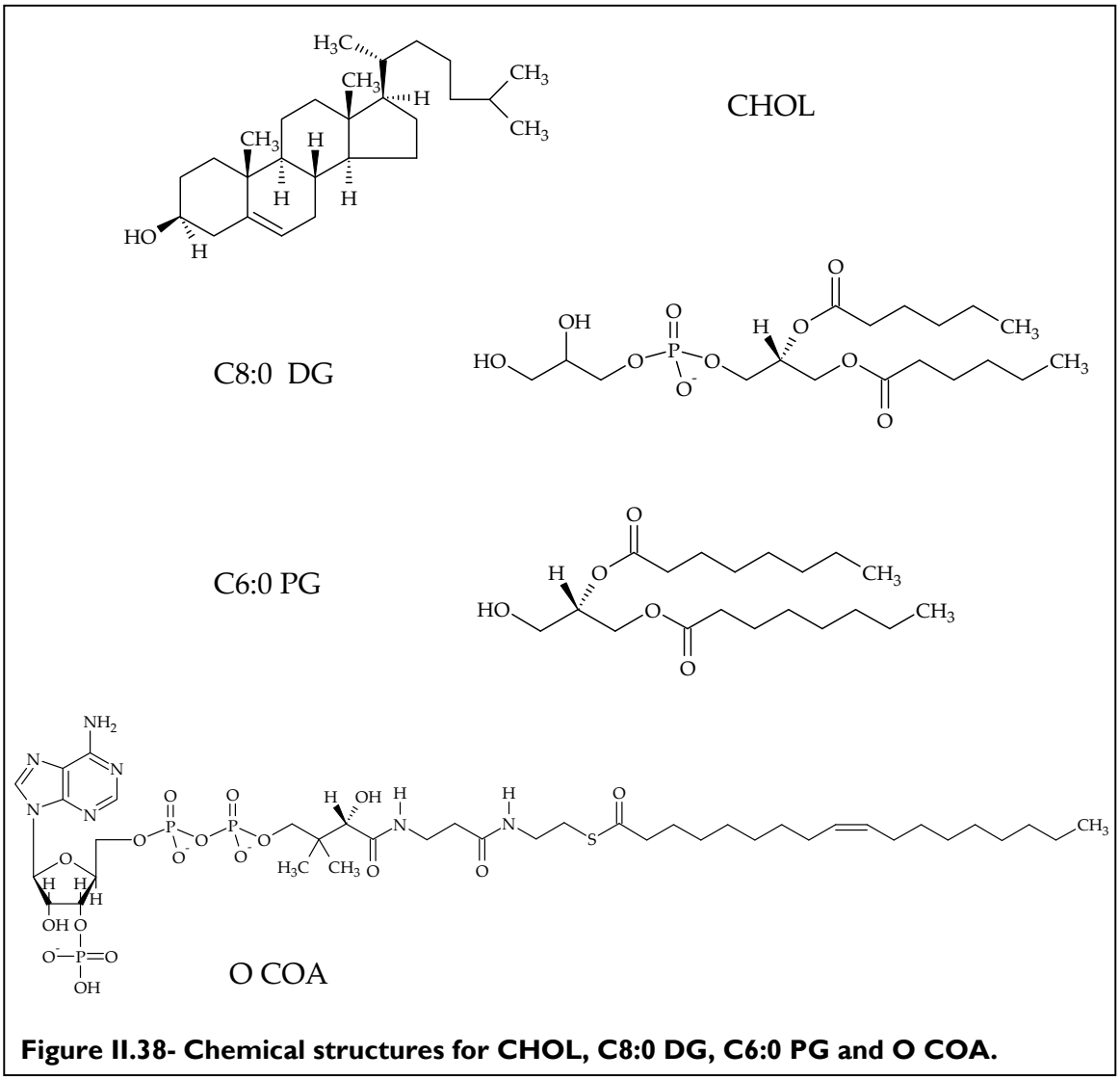

Figure II.38- Chemical structures for CHOL, C8:0 DG, C6:0 PG and O COA.

CHOL and C6:0 PG are neutral, while O COA and C8:0 DG are anionic. In fact, O COA has three negative charges. It is not feasible to compare the lateral stress profiles of these four amphiphiles. However, CHOL should be Type II since it is soluble in both water and chloroform (Dawson, Elliott et al. 1959) and has a large cross-sectional area overall due to its sterol nucleus. On the other hand, O COA should be Type I because of its comparably large head group with only one fatty acid chain. It is harder to attribute typology to C6:0 PG and C8:0 DG due to their short chains and small head groups.

Our results showed that CHOL, C6:0 PG and C8:0 DG activated CCTα while O COA had no or slightly inhibitory effect (Figures II.39-40). Results for CHOL and O COA are in line with the stored elastic stress hypothesis as the Type II CHOL activated CCTα about two-fold more than O COA.

The electrostatic hypothesis is contradicted by results for CHOL and O COA. CHOL is neutral and yet activated the enzyme while O COA is triply anionic and failed to activate the enzyme. The hypothesis is supported for anionic C8:0 DG that promoted CCTα catalysis but fails for neutral C6:0 PG, which was also enzyme activating.

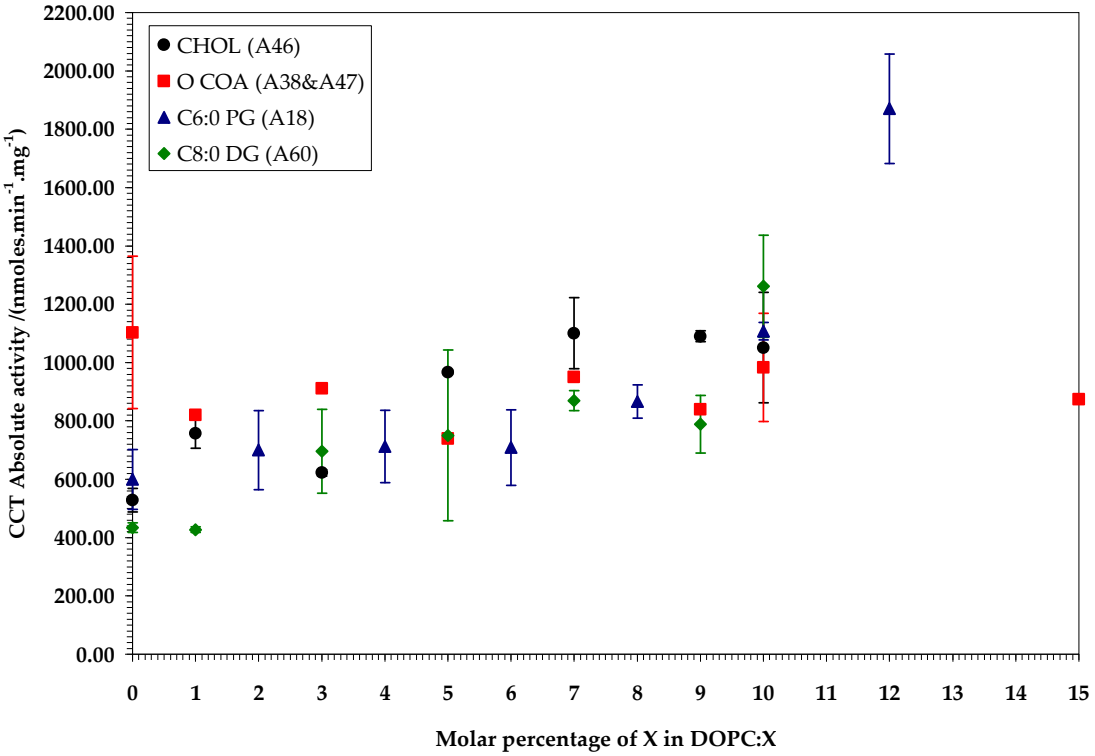

Figure II.39- Plot of CCT absolute activity against molar % of amphiphile X in DOPC: X vesicles.

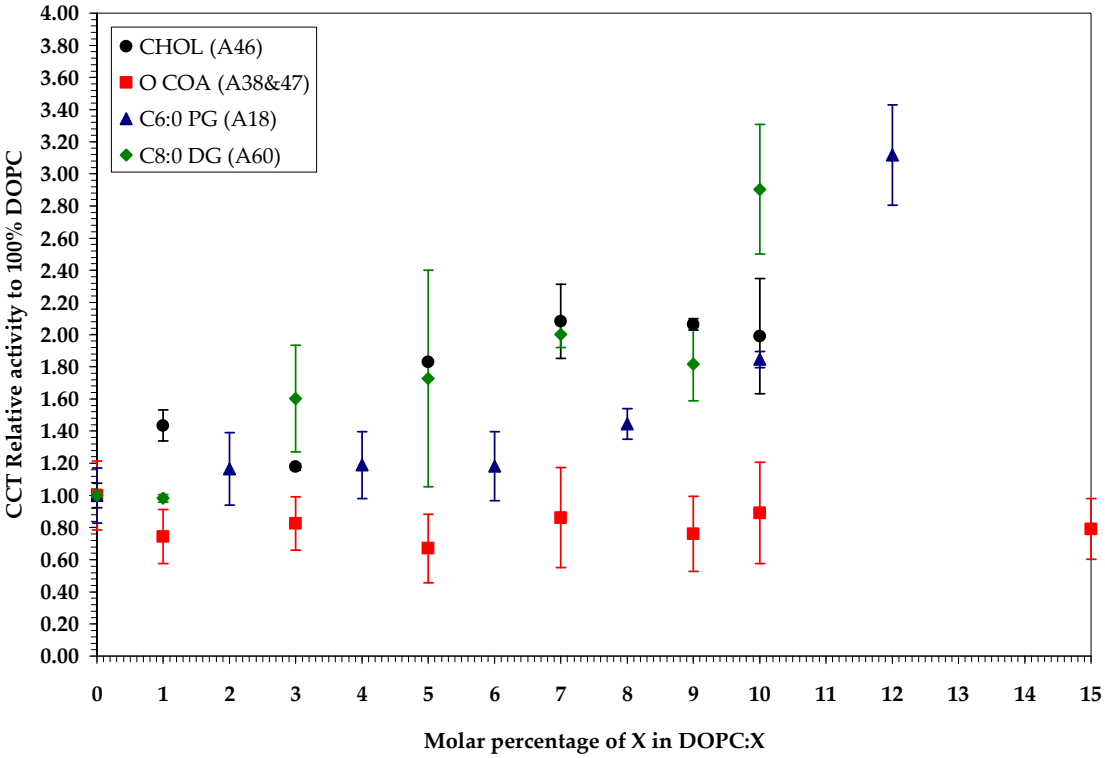

Figure II.40- Plot of CCT relative activity to 100% DOPC against molar % of amphiphile X in DOPC: X vesicles.

II.5. Effect of Type I amphiphiles on CCTα

Five Type I amphiphiles, that would preferentially form hexagonal liquid crystal phases (see section I.1.3), were assayed in LUVs or in micelles.

II.5.1. LUV tertiary systems

In LUVs, the following amphiphiles were studied in tertiary systems of DOPC/DOPE/X, where DOPC/DOPE (80:20):

- hexadecyl-trimethyl ammonium bromide (CTAB)
- sodium dodecyl sulphate (SDS)
- hexadecyl phosphatidylcholine (HDPC)
- di-hexadecyl-di-methyl ammonium bromide (DHDMAB)
- octaethylene glycol monohexadecyl ether (C16EO8)

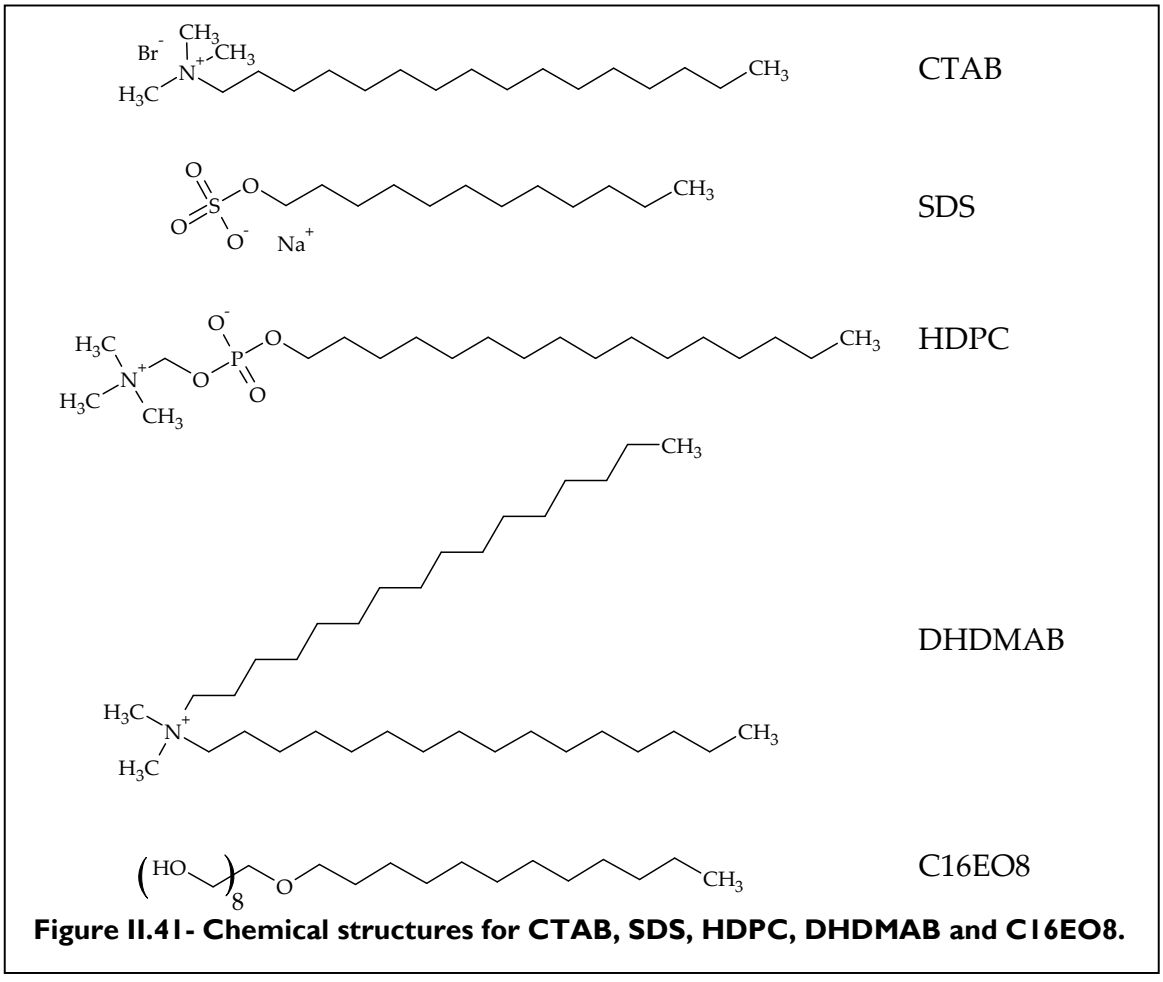

Figure II.41- Chemical structures for CTAB, SDS, HDPC, DHDMAB and C16EO8.

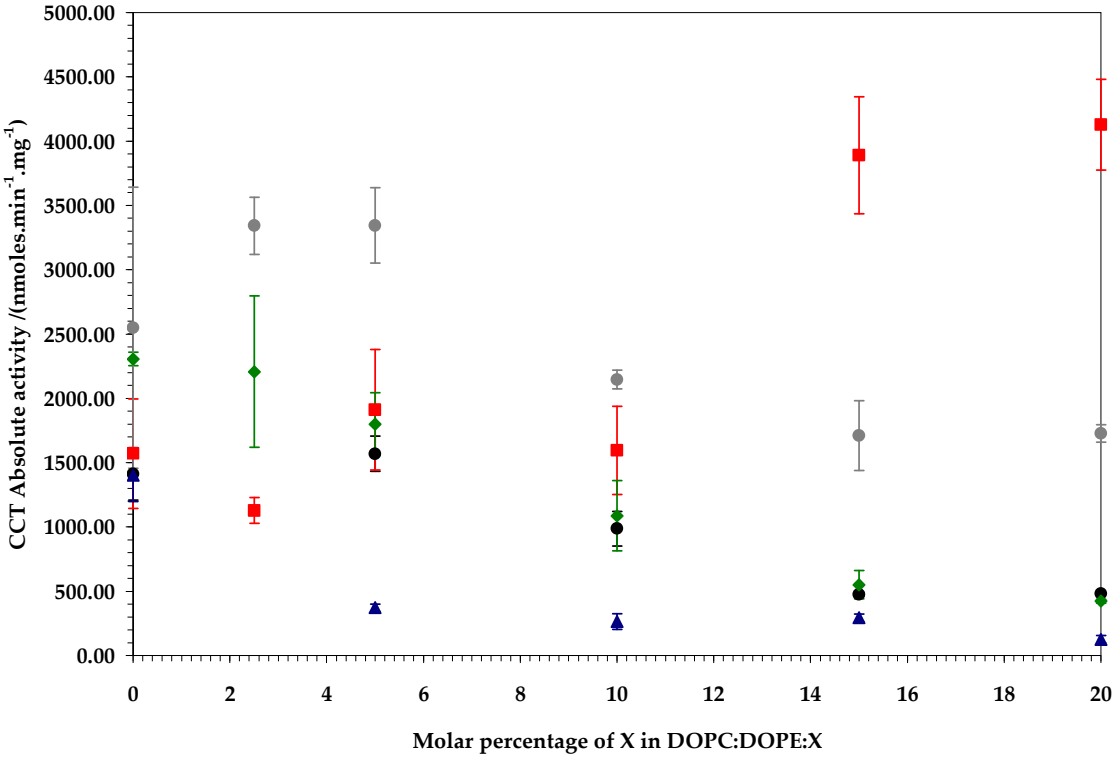

Figure II.42- Plot of CCT absolute activity against molar % of X in DOPC: DOPE: X vesicles.

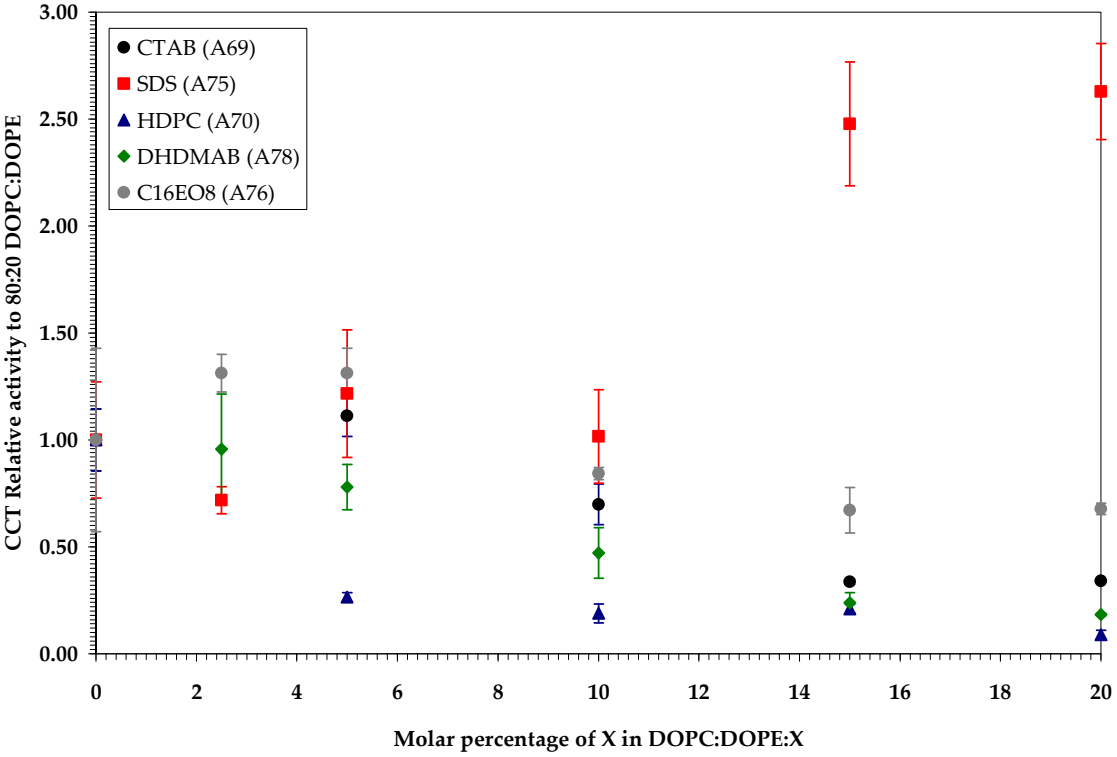

Figure II.43- Plot of CCT relative activity to 100% DOPC against molar % of X in DOPC: X vesicles.

Considering charge, CTAB and DHDMAB are cationic, SDS is anionic, HDPC is zwitterionic and C16EO8 is neutral. DHDMAB has been found to be Type 0 by phase studies conducted in our lab (Dymond, personal communication) while the other four species can be classified as Type I due to their single hydrocarbon saturated chains and small head groups.

Our results showed deactivation for all species except SDS that was quite CCTα activating (Figures II.42-43). The latter result is not supportive of the stored elastic stress hypothesis, since it is a Type I amphiphile. However, SDS has shown spurious results in past experiments in our lab (Dymond and Fagone, personal communication). Also, the dodecyl sulphate cation on SDS could potentially bridge with magnesium anions in the assay buffer, in similar fashion to OPS. DHDMAB had a deactivating effect contradictory to the stored elastic stress hypothesis, albeit a Type 0 amphiphile. On the other hand, CTAB and HDPC decreased the activity of the enzyme, in accordance with the hypothesis as they are both strongly Type I. C16EO8 showed an initial activation by the smallest C16EO8 fraction followed by a mild deactivating effect.

All results in this section are in line with the electrostatic hypothesis since SDS, the only anionic species activated CCTα, while the cationic and neutral species did not.

II.5.2. Micellar solutions

CTAB and SDS micellar solutions were also assayed. The ranges of concentrations studied were based on literature values for critical micellar concentration (CMC) of CTAB and SDS (Figure II.44-45).

CMC of CTAB /mM	Conditions	Method	Reference
0.85	In aqueous solution at 20°C	Electron spin resonance	(Li, Li et al. 1997)
0.166	In Tris-HCl at 27°C	Surface tension measurement	(Yu, Lu et al. 2005)
0.143	In Tris-HCl at 35°C	Surface tension measurement	(Yu, Lu et al. 2005)
1.05	In aqueous solution at 20°C	Electromotive force measurements	(Yao, Tjandra et al. 2003)
1.20	In aqueous solution at 55°C	Osmotic coefficient measurement	(Dearden and Woolley 1987)

Figure II.44- Values for CMC of CTAB from the literature.

CMC of SDS /mM	Conditions	Method	Reference
8.0	In pure water at 25°C	Conductimetry and spectrophotometry	(Benito, Garcia et al. 1997)
8.08	In pure water at 25°C pH 7.0	Micellar electrokinetic chromatography	(Fuguet, Rafols et al. 2005)
8.1	In pure water at 25°C	Capillary electrophoresis	(Lin 2004)

Figure II.45- CMC values of SDS with corresponding conditions and methods.

Our results showed no effect on CCTα within error for cationic CTAB (Figure II.46) and for SDS a slight activation is observed, but quite large error bars. However, the apparent peak in SDS absolute activity at 1 mM becomes negligible, if it is considered that an absolute activity of about 1000 $nmol.min^{-1}mg^{-1}$ occurs in DOPC vesicles only.

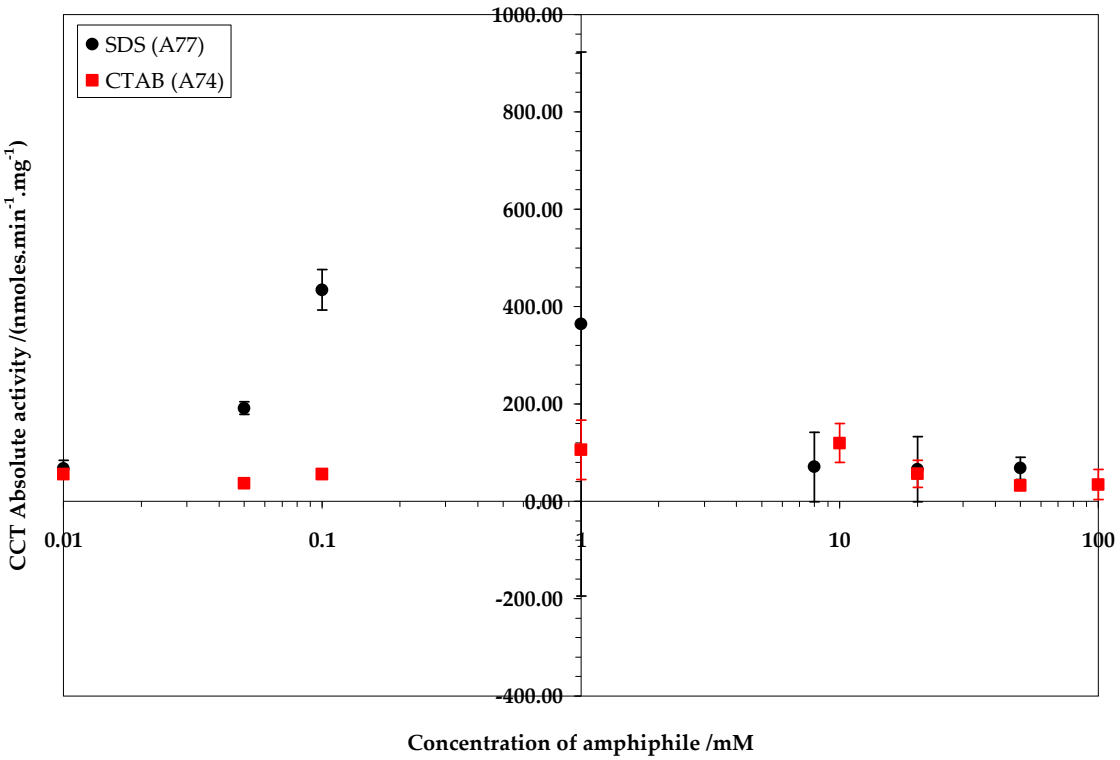

Figure II.46- Plot of CCT absolute activity against molar % of X in DOPC: DOPE: X vesicles.

It can be thus concluded that variation of the charge on detergent micelles did not affect CCTα activity, which is completely against the charge argument of the electrostatic hypothesis. However, the hypothesis states that binding to membranes and enzyme activation are two separate events, independent to each other. Comparing LUV and micellar results for SDS, an increase in CCTα activity was observed in the presence of LUVs, that did not occur for micelles. If enzyme activation was independent of binding to membranes, then the same enzyme activation should occur in both micelles and LUVs, in order for the electrostatic hypothesis to be supported, which was not the case with our results.

II.6. Conclusions and further work

A reference table was constructed which summarises all the lipidic systems studied in this chapter (Figure II.47). In order the compare and assess the overall effect of the 28 investigated binary amphiphile systems, a ranking table of relative activity to 100% DOPC (S) was prepared for mole% 5, 10, 15, 20, 30 and 40 of amphiphile in DOPC (Figure II.48 overleaf).

DOPC/X System	Typology	Head group charge	Head group pKa	Thesis relevant pages
DOPA	II	Anionic	(PO_4) ~4.0 in 0.1 M NaCl	pp. II.27-30
OPA	0/II	Anionic		
DPPA	II	Anionic		
OA	II	Neutral		
DOPS	II	Anionic	(PO_4) ~5.0 in 0.1 M NaCl	pp. II.31-33
OPS	II	Anionic		
DPPS	II	Anionic		
DOPE	II	Zwitterionic	(PO_4) ~9.6 in 0.1 M NaCl	pp. II.34-35
DPHPE	II	Zwitterionic		
POG	II	Neutral	(PO_4) ~3.2 in 0.1 M NaCl	pp. II.36-38
SAG	II	Neutral		
DOG	II	Neutral		
DOPC	0/II	Zwitterionic	(PO_4) ~1.0 in 0.1 M HCl	pp. II.39-41
SM	0	Zwitterionic		
DPHPC	II	Zwitterionic		
C18:0 CER	II	Neutral	N/A	pp. II.42-43
C18:1 CER	II	Neutral		
DES	II	Neutral	(OH) ~ 14.15 at 25 °C (Dawson, Elliott et al. 1959)	pp. II.50-52
DESP	II	Anionic		
CHOL	II	Neutral	N/A	pp. II.53-55
C6:0 PG	II	Neutral		
C8:0 DG	II	Anionic		
O COA	I	Anionic		
CTAB	I	Cationic	N/A	pp. II.56-58
SDS	I	Anionic		
HDPC	I	Zwitterionic		
DHDMAB	0	Cationic		
C16EO8	I	Neutral		

Figure II.47- Reference table summarising all lipidic systems studied. Typology information based on phase behaviour and pKa values from Marsh 1990, unless otherwise stated.

LIPID	S at 5 mole percent	LIPID	S at 10 mole percent	LIPID	S at 15 mole percent	LIPID	S at 20 mole percent	LIPID	S at 30 mole percent	LIPID	S at 40 mole percent
DOPA	3.00*	DOPA	5.30	DOPA	6.50*	DOPA	7.71	DPHPE	9.18	DOPA	9.10
C18:0 CER	1.92	C8:0 DG	2.90	DPHPE	3.92	OA	5.03	DOPA	8.01	DPHPE	8.68
CHOL	1.83	DPHPE	2.75	OA	3.70*	DPHPE	4.74	OA	7.08	OA	7.95
C8:0 DG	1.73	OA	2.50	C6:0 PG	3.50*	C18:1 CER	3.15	C18:1 CER	2.97	OPA	4.37
DOG	1.60	CHOL	1.99	C8:0 DG	3.35*	DPPS	2.74	OPA	2.81	DOPE	1.14
OA	1.60*	C6:0 PG	1.85	CHOL	2.20*	SDS	2.63	DPPS	2.79	DPHPC	3.46
C18:1 CER	1.45	C18:1 CER	1.73	DPPA	1.98	OPA	1.81	DPHPC	2.69	C18:0 CER	2.99
C16EO8	1.31	DPPS	1.67	C18:1 CER	1.93	DOPE	0.35	DOPE	0.85	DOPS	2.95
DPHPE	1.26	C18:0 CER	1.59	DPPS	1.82	C18:0 CER	1.78	OPS	2.16	OPS	2.76
SDS	1.21	DES	1.54	DPHPC	1.75	DPHPC	1.60	DOPS	2.09	SM	1.01
OPA	1.20*	DOPE	0.43	C18:0 CER	1.67	OPS	1.45	DPPA	1.99	DOG	
C6:0 PG	1.19*	SDS	1.02	DES	1.60*	DPPA	1.45	C18:0 CER	1.78	DPPS	
DES	1.16	DPPA	1.31	OPA	1.55*	DOPS	1.37	SM	1.01	C6:0 PG	
DPPA	1.15	OPA	1.29	SDS	2.48	SM	1.01	C16EO8		C18:1 CER	
DESP	1.13	DPHPC	1.20	DOPE	0.76	CTAB	0.34	DOG		C8:0 DG	
CTAB	1.11	CTAB	0.70	DOPS	1.20*	DHDMAB	0.18	C6:0 PG		DPPA	
DPHPC	1.03	DESP	1.06	SM	1.01	C16EO8	0.68	C8:0 DG		CHOL	
SM	1.01	DOPS	1.05	DESP	0.90*	HDPC	0.09	CHOL		DES	
DOPS	1.00*	SM	1.01	O COA	0.79	DOG		DES		DESP	
DPPS	0.98	O COA	0.89	OPS	0.77	C6:0 PG		DESP		O COA	
DHDMAB	0.96	OPS	0.83	CTAB	0.34	C8:0 DG		O COA		SDS	
O COA	0.67	C16EO8	0.84	C16EO8	0.67	CHOL		SDS		CTAB	
DOPE	0.36	DHDMAB	0.47	DHDMAB	0.24	DES		CTAB		HDPC	
OPS	0.28	DOG	0.29	HDPC	0.21	DESP		HDPC		DHDMAB	
HDPC	0.27	HDPC	0.19	DOG	0.20*	O COA		DHDMAB		C16EO8	

Figure II.48- Ranking tables of relative activity (S) to 100% DOPC for investigated systems at 5, 10, 15, 20, 30 and 40 mole% in DOPC, expect for SDS, CTAB, HDPC, C16EO8 and DHDMAB where activity is relative to DOPC/DOPE (80:20). Annotated values with asterisk have been estimated by extrapolation of trend lines, while cells in grey were too far outside the experimental range to be estimated.

DOPA was the most activating phospholipid for CCTα for all fractions, with the exception of DPHPE at 30 mole%. The latter was also one of the most activating systems along with OA, C8:0 DG, C6:0 PG and OPA. For SM and O COA, S showed little or no effect with increasing mole% of amphiphile being very close to unity for both in most. SDS has a surprisingly strong CCTα activator at 20 mole%.

In the majority of systems, that is 22 out of 28 of our results are consistent with the predictions resulting from the stored elastic stress hypothesis. It would have been ideal to have a ranking of theoretical relative activities for all our binary systems and thus compare between hypothesis and experimental evidence. Alas, curvatures for all our investigated amphiphiles are not available in the literature and therefore only a semi-quantititative assessment was feasible.

Type II amphiphiles DOPA, OPA, OA, DPPA, DOPS, OPS, DPPS, DPHPE, DOPE, DOG, POG, SAG, SM, DPHPC, C18:0 and C18:1 CER, DES, DESP, CHOL and O COA all promoted enzyme catalysis and followed the order of their semi-quantitative Type II character as presented in result discussion. Unfortunately, it is harder to assess typology for C6:0 PG and C8:0 DG, but both appeared to activate the enzyme at all mol%. DPPS not as activating as expected from its Type II character compared to DOPS and OPS, but that could be due to phase separations at our experimental temperature. The same argument of same separation could be applied to DOG which had maximal S at only 2 mole% and then showed little or no activation at higher fractions, which was supported by light scattering sizing data.

Type I amphiphiles CTAB, HDPC, C16EO8 and DHDMAB all inhibited CCTα catalytic activity, but SDS data was the only contradictory to the stored elastic stress hypothesis.

The electrostatic hypothesis cannot be as successfully used to explain our data, since results for only 11 of the 28 systems are in line with the hypothesis. Anionic

lipids DOPA, OPA, DPPA, DOPS, OPS, DPPS, DESP, C6:0 PG, DPHPC, O COA and SDS increased CCTα activity and zwiterionic SM inhibited the enzyme supporting the hypothesis. However, amphiphiles showing the same charged head group did not activate CCTα with the same potency as the hypothesis postulates, for all the studied head groups, that is phosphate, PS, PE, acyl glycerol and PC. For example, comparing anionic DOPA and OPA, both with a phosphate head group, DOPA has almost twice the maximal S at 9.02 ± 0.16 than 5.22 ± 0.31 for OPA. The hypothesis is also not verified by results for O COA since it has three negative charges but an inhibiting effect on the enzyme.

Also, the charge density argument of the hypothesis, an example of which is that a smaller anionic head group would be more activating than a larger one fails if one compares SDS, showing the smallest of all head groups with DOPA. DOPA has a larger charge density, but yet it activated CCTα much more efficiently than SDS in all mole%.

Neutral lipids DOPE and DPHPE were both CCTα activators, which is against the hypothesis. In fact, DPHPE was one of the strongest activators of the 25 amphiphiles. Similarly for CHOL, OA, DOG, POG, SAG, DES, C18:0 and C18:1 CER. Zwiterionic DPHPC also very potentlty promoted CCTα catalysis. Comparing C18:0 and C18:1 CER, it cannot be explained why one of the two would be more activating without any change in the overall electrostatics of the molecule.

Finally, different CCTα activation in LUVs and micelles undermines the argument of the electrostatic hypothesis that binding to membranes and activation are two separate independent events.

Since a dephosphorylated cDNA of CCT was used for cloning the enzyme used in these experiments, it is not possible to draw major conclusions with respect to the phosphorylation hypothesis. However, since binding to membranes has been

shown a prerequisite for enzyme activity (see section II.1.2), and our results using a dephosphorylated enzyme showed very high CCTα catalytic rates, the partition coefficient of the enzyme contributed by the phosphorylation cannot be that significant.

Unfortunately, the nature of these data does provide not evidence to support or contradict the translocation and other hypotheses mentioned in section II.1.3, but as reviewed most of the CCTα literature favours a lipid-dependent mechanism of CCTα regulation. Consequently, the stored elastic stress hypothesis can be used to explain the majority of our results in a robust manner, which is not the case for the electrostatic hypothesis that is contradicted by the majority of data.

Future work could include the investigation of further lipid systems, especially amphiphiles not involved in phospholipid biosynthesis. The benefit of that is that most of the investigated amphiphiles in our study are metabolic intermediates in mammalian metabolism, and thus would affect phospholipid biosynthesis in other nodes of regulation. A potential candidate is monogalactosyl diacyl glycerol, ubiquitous in plant chloroplasts but absent in animal membrane, hence just its effect as an amphiphile could be assessed. Also, ternary and quaternary amphiphile systems could be studied in order to move closer to the natural complexity of biological membranes. Finally, charged latex beads could be assayed so as to assess the effect of charge on enzyme activity with respect to the electrostatic hypothesis.

II.7. References

Agassandian, M., J. Zhou, et al. (2005). "Oxysterols inhibit phosphatidylcholine synthesis via ERK docking and phosphorylation of CTP:phosphocholine cytidylyltransferase." J. Biol. Chem. 280(22): 21577-21587.

Aoyama, C., H. Liao, et al. (2004). "Structure and function of choline kinase isoforms in mammalian cells." Progr. Lipid Res. 43(3): 266-281.

Arnold, R. S. a. C., R.B. (1996). "Lipid regulation of CTP:phosphocholine cytidylyltransferase: electrostatic, hydrophobic, and synergistic interactions of anionic phospholipids and diacylglycerol." Biochemistry 35 (30)(30): 9917 -9924.

Arondel, V., C. Benning, et al. (1993). "Isolation and functional expression in Escherichia coli of a gene encoding phosphatidylethanolamine methyltransferase (EC 2.1.1.17) from *Rhodobacter sphaeroides*." J.Biol.Chem. 268(21): 16002-16008.

Attard, G. S., R. H. Templer, et al. (2000). "Modulation of CTP:phosphocholine cytidylyltransferase by membrane curvature elastic stress." Proc. Natl. Acad. Sci. U. S. A. 97(16): 9032-9036.

Benito, I., M. A. Garcia, et al. (1997). "Spectrophotometric and conductimetric determination of the critical micellar concentration of sodium dodecyl sulfate and cetyltrimethylammonium bromide micellar systems modified by alcohols and salts." Colloids Surfaces A: Physicochem. Eng. Aspects 125(2-3): 221-224.

Bladergroen, B. A. and L. M. van Golde (1997). "CTP:phosphoethanolamine cytidylyltransferase." Biochim. Biophys. Acta 1348(1-2): 91-99.

Bladergroen, B. A., T. Wensing, et al. (1998). "Reversible translocation of CTP:phosphocholine cytidylyltransferase from cytosol to membranes in the adult bovine liver around parturition." Bioch. Biophys. Acta, Lipids and Lipid Metabolism 1391(2): 233-240.

Blusztajn, J. K. (1998). "Choline, a vital amine." Science 281(5378): 794-795.

Boggs, K., C. O. Rock, et al. (1998). "The antiproliferative effect of hexadecylphosphocholine toward HL60 cells is prevented by exogenous lysophosphatidylcholine." Biochim. Biophys. Acta - Lipids and Lipid Metabolism 1389(1): 1-12.

Borkenhagen, L. F. and E. P. Kennedy (1957). "The enzymatic synthesis of cytidine diphosphate choline." J. Biol. Chem. 227(2): 951-962.

Borkenhagen, L. F. and E. P. Kennedy (1959). "The enzymatic exchange of L-serine with O-phospho-L-serine catalyzed by a specific phosphatase." J. Biol. Chem. 234(4): 849-853.

Brumley, G. and H. van den Bosch (1977). "Lysophospholipase--transacylase from rat lung: isolation and partial purification." J. Lipid Res. 18(4): 523-532.

Burn, P. A. (1988). "Amphitropic proteins: a new class of membrane proteins." Trends Biochem. Sci. 13(3): 79-83.

Carman, G. M. and S. A. Henry (1989). "Phospholipid biosynthesis in yeast." Annu. Rev. Biochem. 58: 635-669.

Carman, G. M. and G. M. Zeimetz (1996). "Regulation of phospholipid biosynthesis in the yeast *Saccharomyces cerevisiae*." J. Biol. Chem. 271(23): 13293-13296.

Cevc, G. (1990). "Membrane Electrostatics." Bioch. Biophys. Acta 1031(3): 311-382.

Cevc, G., J. M. Seddon, et al. (1985). "Thermodynamic and structural-properties of phosphatidylserine bilayer-membranes in the presence of lithium ions and protons." Biochim. Biophys. Acta 814(1): 141-150.

Chatagnon, C. and P. Chatagnon (1957). "19th Century chemical research on brain tissue constituents: French pioneers. III. Theodore Nicolas Gobley." Ann. Med. Psychol. 115(2): 256-75.

Chen, B. B. and R. K. Mallampalli (2007). "Calmodulin binds and stabilises the regulatory enzyme, CTP:phosphocholine cytidylyltransferase." J. Biol. Chem. 282(46): 33494-33506.

Cheng, K. H., J. R. Lepock, et al. (1986). "The role of cholesterol in the activity of reconstituted Ca-ATPase vesicles containing unsaturated phosphatidylethanolamine." J. Biol. Chem. 261(11): 5081-5087.

Choy, P. C., S. B. Farren, et al. (1979). "Lipid requirements for the aggregation of CTP:phosphocholine cytidylyltransferase in rat liver cytosol." Can. J. Biochem. 57(6): 605-612.

Choy, P. C., P. H. Lim, et al. (1977). "Purification and characterization of CTP: cholinephosphate cytidylytransferase from rat liver cytosol." J. Biol. Chem. 252(21): 7673-7677.

Clement, J. M. and C. Kent (1999). "CTP:phosphocholine cytidylyltransferase: insights into regulatory mechanisms and novel functions." Biochem. Biophys. Res. Commun. 257(3): 643-650.

Cornell, R. (1989). "Chemical cross-linking reveals a dimeric structure for CTP:phosphocholine cytidylyltransferase." J. Biol. Chem. 264(15): 9077-9082.

Cornell, R. and D. E. Vance (1987). "Binding of CTP:phosphocholine cytidylyltransferase to large unilamellar vesicles." Bioch. Biophys. Acta, Lipids and Lipid Metabolism 919(1): 37-48.

Cornell, R. B. (1991). "Regulation of CTP-phosphocholine cytidylyltransferase by lipids .1. Negative surface-charge dependence for activation." Biochemistry 30(24): 5873-5880.

Cornell, R. B. (1991). "Regulation of CTP-phosphocholine cytidylyltransferase by lipids .2. Surface curvature, acyl chain-length, and lipid-phase dependence for activation." Biochemistry 30(24): 5881-5888.

Cornell, R. B. and R. S. Arnold (1996). "Modulation of the activities of enzymes of membrane lipid metabolism by non-bilayer-forming lipids." Chem. Phys. Lipids 81(2): 215-227.

Cornell, R. B., G. B. Kalmar, et al. (1995). "Functions of the C-terminal domain of CTP: phosphocholine cytidylyltransferase. Effects of C-terminal deletions on enzyme activity, intracellular localization and phosphorylation potential." Biochem. J. 310(2): 699-708.

Cornell, R. B. and I. C. Northwood (2000). "Regulation of CTP:phosphocholine cytidylyltransferase by amphitropism and relocalization." Trends Biochem. Sci. 25(9): 441-447.

Cornell, R. B. and S. G. Taneva (2006). "Amphipathic helices as mediators of the membrane interaction of amphitropic proteins, and as modulators of bilayer physical properties." Current Protein & Peptide Science 7(6): 539-552.

Davies, S. M. A., R. M. Epand, et al. (2001). "Regulation of CTP: phosphocholine cytidylyltransferase activity by the physical properties of lipid membranes: An important role for stored curvature strain energy." Biochemistry 40(35): 10522-10531.

Dawson, R. M. C., D. C. Elliott, et al. (1959). Data for biochemical research. London, Oxford University Press.

de Rudder, K. E. E., I. M. Lopez-Lara, et al. (2000). "Inactivation of the gene for phospholipid N-methyltransferase in *Sinorhizobium meliloti*: phosphatidylcholine is required for normal growth." Mol. Microbiol. 37(4): 763-772.

Dearden, L. V. and E. M. Woolley (1987). "Osmotic coefficients of alkyltrimethylammonium bromides in water and in aqueous sodium bromide solutions at 55 DegC." J. Phys. Chem. 91(9): 2404-2408.

Drobnies, A. E., B. Van der Ende, et al. (1999). "CTP:phosphocholine cytidylyltransferase activation by oxidized phosphatidylcholines correlates with a decrease in lipid order: A 2H NMR analysis." Biochemistry 38(47): 15606-15614.

Dunne, S. J., R. B. Cornell, et al. (1996). "Structure of the membrane binding domain of CTP:phosphocholine cytidylyltransferase." Biochemistry 35(37): 11975-11984.

Eagle, H. (1955). "Nutrition needs of mammalian cells in tissue culture." Science 122: 501-504.

Fagone, P. (2003). Modulation of CCTa by membrane biophysics, PhD Thesis. School of Chemistry. University of Southampton.

Feldman, D. and P. Weinhold (1987). "CTP:phosphorylcholine cytidylyltransferase from rat liver. Isolation and characterization of the catalytic subunit." J. Biol. Chem. 262(19): 9075-9081.

Ferreira, D. A., M. V. L. B. Bentley, et al. (2006). "Cryo-transmission electron microscopy investigation of phase behaviour and aggregate structure in dilute dispersions of monoolein and oleic acid." Intern. J. Pharmaceutics 310(1-2): 203-212.

Fiscus, W. G. and W. C. Schneider (1966). "The role of phospholipids in stimulating phosphorylcholine cytidyltransferase activity." J. Biol. Chem. 241(14): 3324-3330.

Friesen, J. A., H. A. Campbell, et al. (1999). "Enzymatic and cellular characterization of a catalytic fragment of CTP:phosphocholine cytidylyltransferase alpha." J. Biol. Chem. 274(19): 13384-13389.

Friesen, J. A., M. F. Liu, et al. (2001). "Cloning and characterization of a lipid-activated CTP:phosphocholine cytidylyltransferase from Caenorhabditis elegans: identification of a 21-residue segment critical for lipid activation." Biochim. Biophys. Acta 1533(2): 86-98.

Fuguet, E., C. Rafols, et al. (2005). "Critical micelle concentration of surfactants in aqueous buffered and unbuffered systems." Analytica Chimica Acta 548(1-2): 95-100.

Gruner, S. M. (1985). "Intrinsic curvature hypothesis for biomembrane lipid composition: a role for nonbilayer lipids." Proc. Natl. Acad. Sci. U. S. A 82(11): 3665-3669.

Guy, G. R. and A. W. Murray (1982). "Tumor promoter simulation of phosphatidyl choline turnover in HeLa cells." Cancer Res. 42(5): 1980-1985.

Hatch, G. M. and P. C. Choy (2004). "Phospholipid biosynthesis." Adv. Mol. Cell Biol. 33: 357-385.

Heath, R. J., S. Jackowski, et al. (2002). Fatty acid and phospholipid metabolism in prokaryotes. New Comprehensive Biochemistry. 36: 55-92.

Helmink, B. A., J. D. Braker, et al. (2003). "Identification of lysine 122 and arginine 196 as important functional residues of rat CTP:phosphocholine cytidylyltransferase alpha." Biochemistry 42(17): 5043-5051.

Hirata, F., O. H. Viveros, et al. (1978). "Identification and properties of two methyltransferases in conversion of phosphatidylethanolamine to phosphatidylcholine." Proc. Natl. Acad. Sci. U. S. A 75(4): 1718-1721.

Hoffman, D. R., J. D. Stanley, et al. (1984). "Cytotoxicity of ether-linked phytanyl phospholipid analogs and related derivatives in human HL-60 leukemia cells and polymorphonuclear neutrophils." Res. Comm. Chem. Pathol. Pharmac. 44(2): 293-306.

Houweling, M., Z. Chui, et al. (1996). "CTP:phosphocholine cytidylyltransferase is both a nuclear and cytoplasmic protein in primary hepatocytes." Eur. J. Cell Biol. 69(1): 55-63.

Houweling, M., H. Jamil, et al. (1994). "Dephosphorylation of CTP-phosphocholine cytidylyltransferase is not required for binding to membranes." J. Biol. Chem. 269(10): 7544-7551.

Houweling, M., L. B. M. Tijburg, et al. (1993). "Evidence that CTP:choline-phosphate cytidylyltransferase is regulated at a pretranslational level in rat liver after partial hepatectomy." Eur. J. Biochem. 214(3): 927-33.

Jackowski, S. (2002). "CTP:phosphocholine cytidylyltransferase." Lipids: Glycerolipid Metabolizing Enzymes: 109-124.

Jackowski, S. and I. Baburina (2002). "Lipid interaction with cytidylyltransferase regulates membrane synthesis." Special Publication - Royal Society of Chemistry 283: 163-176.

Jackowski, S. and P. Fagone (2005). "CTP:Phosphocholine Cytidylyltransferase: Paving the Way from Gene to Membrane." J. Biol. Chem. 280(2): 853-856.

Jamil, H., G. M. Hatch, et al. (1993). "Evidence that binding of CTP:phosphocholine cytidylyltransferase to membranes in rat hepatocytes is modulated by the ratio of bilayer- to non-bilayer-forming lipids." Biochem. J. 291(2): 419-427.

Jamil, H., A. K. Utal, et al. (1992). "Evidence that cyclic AMP-induced inhibition of phosphatidylcholine biosynthesis is caused by a decrease in cellular diacylglycerol levels in cultured rat hepatocytes." J. Biol. Chem. 267(3): 1752-1760.

Jamil, H., Z. M. Yao, et al. (1990). "Feedback regulation of CTP:phosphocholine cytidylyltransferase translocation between cytosol and endoplasmic reticulum by phosphatidylcholine." J. Biol. Chem. 265(8): 4332-4339.

Jensen, J. W. and J. S. Schutzbach (1988). "Modulation of dolichyl-phosphomannose synthase activity by changes in the lipid environment of the enzyme." Biochemistry 27: 6315-6320.

Johnson, J. E., R. Aebersold, et al. (1997). "An amphipathic alpha-helix is the principle membrane-embedded region of CTP:phosphocholine cytidylyltransferase. Identification of the 3-(trifluoromethyl)-3-(m-[125I]iodophenyl) diazirine photolabeled domain." Bioch. Biophys. Acta 1324(2): 273-284.

Johnson, J. E. and R. B. Cornell (1994). "Membrane-binding amphipathic alpha-helical peptide derived from CTP:phosphocholine cytidylyltransferase." Biochemistry 33(14): 4327-35.

Johnson, J. E., Cornell, R. B. (1999). "Amphitropic proteins: regulation by reversible membrane interactions (Review)." Mol. Memb. Biol. 16(3): 217 - 235.

Johnson, J. E., N. M. Rao, et al. (1998). "Conformation and lipid binding properties of four peptides derived from the membrane-binding domain of CTP:phosphocholine cytidylyltransferase." Biochemistry 37(26): 9509-9519.

Johnson, J. E., M. Xie, et al. (2003). "Both acidic and basic amino acids in an amphitropic enzyme, CTP:phosphocholine cytidylyltransferase, dictate its selectivity for anionic membranes." J. Biol. Chem. 278(1): 514-522.

Kalmar, G., R. Kay, et al. (1990). "Cloning and expression of rat liver CTP: phosphocholine cytidylyltransferase: an amphipathic protein that controls phosphatidylcholine synthesis." Proc. Natl. Acad. Sci. U. S. A 87(16): 6029-6033.

Kalmar, G. B., R. J. Kay, et al. (1994). "Primary structure and expression of a human CTP:phosphocholine cytidylyltransferase." Bioch. Biophys. Acta, Gene Structure and Expression 1219(2): 328-334.

Kanfer, J. N. (1980). "The base-exchange enzymes and phospholipase-D of mammalian tissue." Can. J. Biochem. 58(12): 1370-1380.

Kennedy, E. P. and S. B. Weiss (1956). "The function of cytidine coenzymes in the biosynthesis of phospholipides." J. Biol. Chem. 222(1): 193-214.

Kent, C. (1990). "Regulation of phosphatidylcholine biosynthesis." Prog. Lipid.Res. 29(2): 87-105.

Kent, C. (1995). "Eukaryotic phospholipid biosynthesis." Annu. Rev. Biochem. 64: 315-343.

Kent, C. (1997). "CTP:phosphocholine cytidylyltransferase." Biochim. Biophys. Acta 1348(1-2): 79-90.

Khan, W. A., S. W. Mascarella, et al. (1991). "Use of D-erythro-sphingosine as a pharmacological inhibitor of protein kinase C in human platelets." Biochem. J. 278(387-392).

Kihara, A., S. Mitsutake, et al. (2007). "Metabolism and biological functions of two phosphorylated sphingolipids, sphingosine 1-phosphate and ceramide 1-phosphate." Progr. Lipid Res. 46(2): 126.

Kinzel, V., G. Kreibich, et al. (1979). "Stimulation of choline incorporation in cell cultures by phorbol derivatives and its correlation with their irritant and tumor-promoting activity." Cancer Res. 39(7): 2743-2750.

Kodaki, T. and S. Yamashita (1987). "Yeast phosphatidylethanolamine methylation pathway. Cloning and characterization of two distinct methyltransferase genes." J. Biol. Chem. 262(32): 15428-15435.

Kooijman, E. E., V. Chupin, et al. (2003). "Modulation of membrane curvature by phosphatidic acid and lysophosphatidic acid." Traffic 4(3): 162-174.

Kwak, B.-Y., Yong-Mei Zhang,Y.-M., Yun, M. , Heath, R.J., Rock, C.O., Jackowski, S., Park H.W. (2002). "Structure and mechanism of CTP:phosphocholine

cytidylyltransferase (LicC) from *Streptococcus pneumoniae*." J. Biol. Chem. 277(6): 4343-4350.

Li, F., G.-Z. Li, et al. (1997). "Studies on cetyltrimethylammonium bromide (CTAB) micellar solution and CTAB reversed microemulsion by ESR and 2H NMR." Colloids Surfaces A: Physicochem. Engin. Aspects 127(1-3): 89.

Lin, C.-E. (2004). "Determination of critical micelle concentration of surfactants by capillary electrophoresis." J. Chromatogr. A 1037(1-2): 467-478.

Luche, M. M., C. O. Rock, et al. (1993). "Expression of rat CTP:phosphocholine cytidylyltransferase in insect cells using a baculovirus vector." Arch. Biochem. Biophys. 301(1): 114-18.

Lykidis, A., I. Baburina, et al. (1999). "Distribution of CTP:phosphocholine cytidylyltransferase (CCT) isoforms. Identification of a new CCTb splice variant." J. Biol. Chem. 274(38): 26992-27001.

Lykidis, A., P. Jackson, et al. (2001). "Lipid activation of CTP:phosphocholine cytidylyltransferase alpha: Characterization and identification of a second activation domain." Biochemistry 40(2): 494-503.

Lykidis, A., K. G. Murti, et al. (1998). "Cloning and characterization of a second human CTP:phosphocholine cytidylyltransferase." J. Biol. Chem. 273(22): 14022-14029.

Macdonald J. I. S. and Kent C. (1993). "Baculovirus-mediated expression of rat liver CTP:phosphocholine cytidylyltransferase." Protein Express. Purif. 4(1): 1-7.

Marsh, D. (1990). CRC Handbook of lipid bilayers, CRC Press.

Marsh, D. (2007). "Lateral pressure profile, spontaneous curvature frustration and the incorporation and conformation of proteins in membranes. ." Biochem J 93: 3884-3899.

Minamikawa, H. and M. Hato (1997). "Phase behavior of synthetic phytanyl-chained glycolipid/water systems." Langmuir 13(9): 2564-2571.

Nakano, M., T. Karno, et al. (2005). "Detection of bilayer packing stress and its release in lamellar-cubic phase transition by time-resolved fluorescence anisotropy." J. Phys. Chem. B 109(10): 4754-4760.

Navarro, J., M. Toivio-Kinnucan, et al. (1984). "Effect of lipid composition on the calcium/adenosine 5'-triphosphate coupling ratio of the Ca2+-ATPase of sarcoplasmic reticulum." Biochemistry 23: 130-135.

Pelech, S. L., P. H. Pritchard, et al. (1983). "Fatty acids promote translocation of CTP:phosphocholine cytidylyltransferase to the endoplasmic reticulum and stimulate rat hepatic phosphatidylcholine synthesis." J. Biol. Chem. 258(11): 6782-6788.

Pelech, S. L. and D. E. Vance (1982). "Regulation of rat liver cytosolic CTP: phosphocholine cytidylyltransferase by phosphorylation and dephosphorylation." J. Biol. Chem. 257(23): 14198-14202.

Sansom, M. S. P. (1998). "Peptides and lipid bilayers: dynamic interactions." Curr. Op. Coll. Interf. Sci. 3(5): 518-524.

Seddon, J. M. (1990). "An inverse face-centered cubic phase formed by diacylglycerol-phosphatidylcholine mixtures." Biochemistry 29(34): 7997-8002.

Shearman, G. C., B. J. Khoo, et al. (2007). "Calculations of and evidence for chain packing stress in inverse lyotropic bicontinuous cubic phases." Langmuir 23(13): 7276-7285.

Sleight, R. and C. Kent (1980). "Regulation of phosphatidylcholine biosynthesis in cultured chick embryonic muscle treated with phospholipase C." J. Biol. Chem. 255(22): 10644-10650.

Sohal, P. S. and R. B. Cornell (1990). "Sphingosine inhibits the activity of rat liver CTP:phosphocholine cytidylyltransferase." J. Biol. Chem. 265(20): 11746-11750.

Sohlenkamp, C., I. M. Lopez-Lara, et al. (2003). "Biosynthesis of phosphatidylcholine in bacteria." Progr. Lipid Res. 42(2): 115-162.

Taneva, S. G., P. J. Patty, et al. (2005). "CTP:phosphocholine cytidylyltransferase binds anionic phospholipid vesicles in a cross-bridging mode." Biochemistry 44(26): 9382-9393.

Tessner, T. G., C. O. Rock, et al. (1991). "Colony-stimulating factor 1 regulates CTP:phosphocholine cytidylyltransferase mRNA levels." J. Biol. Chem. 266(25): 16261-16264.

Tijburg, L., M. J. H. Geelen, et al. (1990). "Regulation of the biosynthesis of triacylglycerol, phosphatidylcholine and phosphatidylethanolamine in the liver." Bioch. Biophys. Acta 1004(1): 1-19.

Tronchere, H., M. Record, et al. (1994). "Phosphatidylcholine cycle and regulation of phosphatidylcholine biosynthesis by enzyme translocation." Biochim. Biophys. Acta 1212(2): 137-151.

Tytler, E. M., R. M. Epand, et al. (1994). "Cross-sectional molecular shapes of amphipathic a helixes control membrane stability." Pept.: Chem., Struct. Biol., Proc. Am. Pept. Symp., 13th: 444-445.

Vance, D. E. (1990). "Phosphatidyl choline biosynthesis." Biochem. Cell Biol. 68(10): 1151-1165.

Vance, D. E. (2002). Phospholipid biosynthesis in eukaryotes. Biochemistry of Lipids, Lipoproteins and Membranes (4th edition). D. E. Vance and J. E. Vance, Elsevier Science: 205-232.

Vance, D. E. and P. C. Choy (1979). "How is phosphatidyl choline biosythesis regulated?" Trends Biochem. Sci. 4: 145-147.

Vance, D. E. and S. L. Pelech (1984). "Enzyme translocation in the regulation of phosphatidylcholine biosynthesis." Trends Biochem. Sci. 9(1): 17-20.

Vance, D. E., E. M. Trip, et al. (1980). "Poliovirus increases phosphatidylcholine biosynthesis in HeLa cells by stimulation of the rate-limiting reaction catalyzed by CTP: phosphocholine cytidylyltransferase." J. Biol. Chem. 255(3): 1064-1069.

Vance, D. E., C. J. Walkey, et al. (1997). "Phosphatidylethanolamine N-methyltransferase from liver." Bioch. Biophys. Acta 1348(1-2): 142-150.

Vance, J. E. and D. E. Vance (2004). "Phospholipid biosynthesis in mammalian cells." Biochem. Cell Biol. 82(1): 113-128.

Vivekananda, J., D. Smith, et al. (2001). "Sphingomyelin metabolites inhibit sphingomyelin synthase and CTP:phosphocholine cytidylyltransferase." Am J Physiol Lung Cell Mol Physiol 281(1): L98-107.

Wang, Y. and C. Kent (1995). "Effects of altered phosphorylation sites on the properties of CTP:phosphocholine cytidylyltransferase." J. Biol. Chem. 270(30): 17843-17849.

Wang, Y. and C. Kent (1995). "Identification of an inhibitory domain of CTP:phosphocholine cytidylyltransferase." J. Biol. Chem. 270(32): 18948-18952.

Wang, Y., J. I. MacDonald, et al. (1993). "Regulation of CTP:phosphocholine cytidylyltransferase in HeLa cells. Effect of oleate on phosphorylation and intracellular localization." J. Biol. Chem. 268(8): 5512-5518.

Wang, Y., J. I. S. MacDonald, et al. (1995). "Identification of the nuclear localization signal of rat liver CTP:phosphocholine cytidylyltransferase." J. Biol. Chem. 270(1): 354-360.

Watkins, J. D. and C. Kent (1991). "Regulation of CTP:phosphocholine cytidylyltransferase activity and subcellular location by phosphorylation in Chinese hamster ovary cells. The effect of phospholipase C treatment." J. Biol. Chem. 266(31): 21113-21117.

Watts, A. (1988). "Probing membrane surfaces by deuterium NMR." Studia Biophys. 127(1-3): 29-36.

Weinhold, P., M. Rounsifer, et al. (1986). "The purification and characterization of CTP:phosphorylcholine cytidylyltransferase from rat liver." J. Biol. Chem. 261(11): 5104-5110.

Weinhold, P. A. and D. Barrett (1998). "Studies on the regulation of CTP:phosphocholine cytidylyltransferase using permeabilized HEP G2 cells: evidence that both active and inactive enzyme are membrane-bound." Biochim. Biophys. Acta 1391(3): 307-319.

Whitehead, F. W., E. Trip, et al. (1981). "Semliki forest virus does not Inhibit phosphatidylcholine biosynthesis in Bhk-21 Cells." Can. J. Biochem. 59(1): 38-47.

Wiedmann, T. S., R. D. Pates, et al. (1988). "Lipid-protein interactions mediate the photochemical function of rhodopsin." Biochemistry 27: 6469-6474.

Wieprecht, T., O. Apostolov, et al. (1999). "Thermodynamics of the alpha-helix-coil transition of amphipathic peptides in a membrane environment: implications for the peptide-membrane binding equilibrium." J. Mol. Biol. 294(3): 785-794.

Wieprecht, T., M. Beyermann, et al. (2002). "Thermodynamics of the coil-a-helix transition of amphipathic peptides in a membrane environment: the role of vesicle curvature." Biophys. Chem. 96(2-3): 191-201.

Wilson, J. E. (1978). "Ambiquitous enzymes- Variation in intracellular distribution as a regulatory mechanism." Trends Biochem. Sci. 3(6): 124-125.

Xie, M., J. L. Smith, et al. (2004). "Membrane binding modulates the quaternary structure of CTP:phosphocholine cytidylyltransferase." J. Biol. Chem. 279(27): 28817-28825.

Yang, W., K. P. Boggs, et al. (1995). "The association of lipid activators with the amphipathic helical domain of CTP:phosphocholine cytidylyltransferase accelerates catalysis by increasing the affinity of the enzyme for CTP." J. Biol. Chem. 270(41): 23951-23957.

Yang, W. and S. Jackowski (1995). "Lipid activation of CTP:phosphocholine cytidylyltransferase is regulated by the phosphorylated carboxyl-terminal domain." J. Biol. Chem. 270(28): 16503-16506.

Yao, J., W. Tjandra, et al. (2003). "Hydroxyapatite nanostructure material derived using cationic surfactant as a template." J. Mater. Chem. 13(12): 3053-3057.

Yeo, H. J., M. P. Larvor, et al. (1997). "*Plasmodium falciparum* CTP:phosphocholine cytidylyltransferase expressed in *Escherichia coli*: Purification, characterization and lipid regulation." Biochem. J. 324: 903-910.

Yu, L., T. Lu, et al. (2005). "Studies on the effects of amino acids on micellization of CTAB via surface tension measurements." Colloids Surfaces A: Physicochem. Engin. Aspects 257-258: 375-379.

Zhou, J., A. J. Ryan, et al. (2003). "Oxidized lipoproteins inhibit surfactant phosphatidylcholine synthesis via calpain-mediated cleavage of CTP:phosphocholine cytidylyltransferase." J. Biol. Chem. 278(39): 37032-37040.

Chapter III

Effect of Type I amphiphiles on HeLa PtdCho metabolism

Table of Contents

III.1. Background

III.1.1. In vivo studies of metabolism

III.1.1.1. Use of mammalian cell lines

Cell cultures have been employed since the turn of the century to investigate biological processes in neurobiology and molecular biology. Tissue culture methods now offer an alternative to animal experimentation for the research of drug activities and the design of new forms of therapy. Continuous or immortal cell lines have an unlimited life span as long as basic cell survival conditions are met (Allen, Caviedes et al. 2005). One example is the HeLa cell strain, which was chiefly used to develop and test the Salk vaccine against poliomyelitis (Brown and Henderson 1983).

Figure III.1- Henrietta Lacks (1920-1951).

This immortal line of human negroid cervix epitheloid carcinoma cells was derived from cervical cancer cells of Henrietta Lacks (Figure III.1), and hence were named HeLa. The patient died in 1951 but her cells were propagated by George Otto Gey (Gey, Coffman et al. 1952). Although there is no record of the patient's consent, HeLa cells have been used extensively in cancer research ever since, and are commercially available to purchase with none of the profits being awarded to Henrietta Lacks's descendants (Masters 2002).

The most important advantage of the HeLa cell line is resilience since it was originally derived from a rare high-grade adenocarcinoma. HeLa cells can grow under relatively simple culture conditions without an excessive cost of maintenance. However, some have argued that the cell line is not pure and that

sub-lines and false cell lines litter the literature (Gartler 1967; Gartler 1968). In fact more than a hundred cross-contaminants have been reported (Nelson-Rees and Flandermeyer 1976; Nelson-Rees, Daniels et al. 1981). Another drawback is that HeLa cells are adherent, which limits the experiments that can be performed in real time as cells have to be detached by means of a lytic protein, trypsin, or by scraping. Both methods can potentially introduce variability to the results that is not based on the tested parameter studied, for example incubation with a drug.

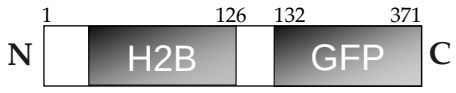

Figure III.2- The H2B-GFP chimeric protein. GFP tag is fused to the carboxyl terminal of the human histone H2B. Diagram adapted from original publication (Kanda, Sullivan et al. 1998).

More recently, the line has been genetically modified to include the green fluorescence protein (GFP) gene of the jellyfish *Aequorea victoria* fused to human histone H2B, without affecting either cell morphology or growth rate (Kanda, Sullivan et al. 1998). Cells then emit a stable green fluorescent signal at 509 nm with a shoulder at 540 nm (Chalfie, Tu et al. 1994). Therefore, DNA-specific stain dyes, such as 4,6-diamidino-2-phenyl-indole (DAPI), are not required to visualise cell nuclei, since the fluorescence can mark nuclear chromatin in living cells. This alternative to traditional labelling of nuclear components has been particularly useful in live microscopy where the dynamics of nuclear architecture of living cells can be monitored in the absence of toxic dyes like DAPI (Zink, Sadoni et al. 2003; Zink, Fischer et al. 2004).

In our experiments, the transfected GFP-HeLa cell line was used to investigate the effect of two amphiphiles, hexadecylphosphatidyl choline (HDPC) and hexadecyl trimethylammonium bromide (CTAB), on lipid metabolism by quantitation of membrane lipids using electrospray ionisation mass spectrometry (ESI-MS). The bright GFP fluorescence displayed by the cells allowed cell sizing by microscopy, and provided with valuable insight on size variation during the cell cycle.

III.1.1.2. Lipid synthesis during the cell cycle

In eukaryotic cells, cell division occurs in four distinct stages that are collectively termed as the cell cycle (Nelson 2000). Although the duration for each stage varies with cell type, in cultured mammalian cell systems the cycle is 16 to 24 hours long, with each cell being at a different stage at any given point. Blocking agents can be used to synchronise the majority of the cells in a culture at the same point of the cycle, which enables the study of metabolic events occurring at each individual phase. Three commonly used blocking agents are shown in Figure III.3.

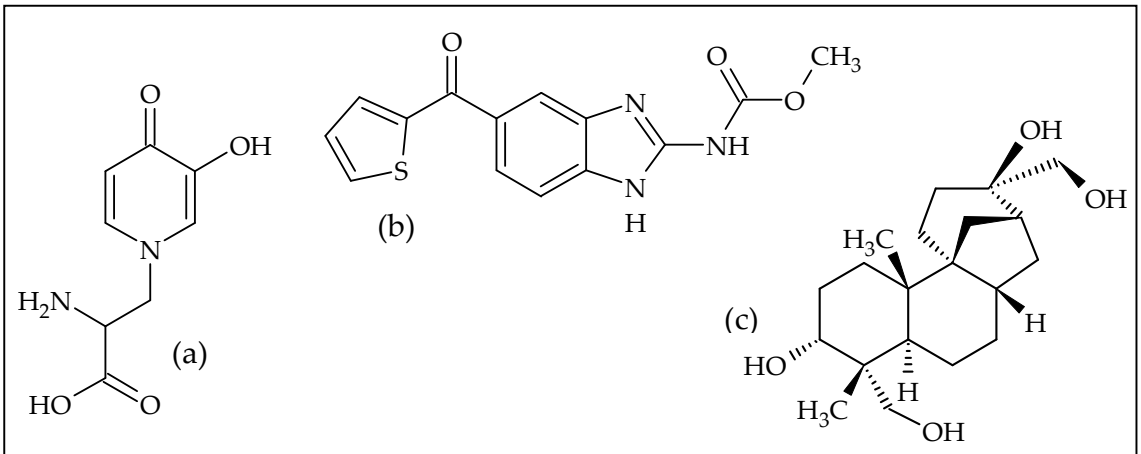

Figure III.3- Structures for blocking agents (a) L-mimosine, (b) nocodazole and (c) aphidicolin.

The four stages of the cell cycle, illustrated in Figure III.4, are the Gap-1 (G_1), synthesis (S), Gap-2 (G_2), mitosis (M) and Gap-0 (G_0) phases. During the first stage, lipid synthesis and degradation are at their highest turnover (Jackowski 1996). It has been shown that the presence of enzymes that hydrolyse the accumulated PtdCho like PtdCho phospholipase C is essential for the progression into the S phase (Xu, Tessner et al. 1993). CTP: Phosphocholine cytidylytransferase (CCT, EC 2.7.7.15), the rate-determining enzyme in PtdCho biosynthesis, shows its maximal activity of the cell cycle during early G_1, while CCT phosphorylation is at its lowest at the same point (Jackowski 1996). L-mimosine (Zink, Sadoni et al. 2003) and

aphidicolin (Jackowski 1994) block cells in the G_1/S barrier. Serum starvation can block cells in the middle of G_1 (Tercé, Brun et al. 1994).

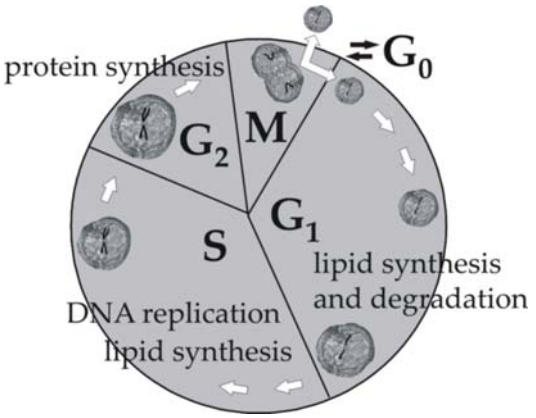

Figure III.4- The eukaryotic cell cycle. Phase contrast image of MDCK cyst courtesy of G. Charras.

During S phase, DNA is replicated into two copies, one for each daughter cell. Phospholipid biosynthesis continues but degradation ceases. Thus, phospholipids accumulate and distribution between the different species remains constant (Jackowski 1996). The most abundant species in the nucleus are phosphatidyl choline (PtdCho), phosphatidyl ethanolamine (PtdEtn) and sphingomyelin (SM) (Boon and Smith 2002). In the S phase, phosphatidyl inositol (PtdIns), a less abundant lipid, is synthesised in the nucleus (Ile, Schaaf et al. 2006). Overall, doubling of the phospholipid mass occurs in the S phase (Figure III.5).

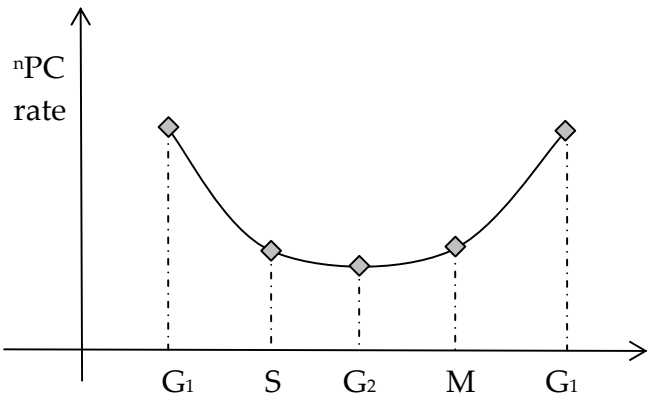

Figure III.5- A rough prediction of the new PC (^{n}PC) synthesis rate during the cell cycle.

In G_2 phase, the cell approximately doubles in size and protein synthesis occurs. A cessation of phospholipid metabolism occurs during G_2 and M phases. Neither synthesis nor degradation of lipids has been significantly observed in these stages, mainly due to the inefficiency of blocking agents to yield pure synchronous cultures because of their short duration. CCT activity is at its lowest when cells enter G_2/M while the highest levels of CCT phosphorylation have been observed here (Jackowski 1996).

Next, M phase takes place: the double membrane surrounding the cell nucleus breaks down; each set of replicated DNA becomes enveloped by a new nuclear membrane; and cytokinesis yields two daughter cells. Phospholipids stop being dynamically transferred through the cell while the nuclear membrane disassembles and reforms. Nocodazole can be used to arrest cells in the M phase (Jackowski 1996).

G_1 phase follows mitosis, and CCT is reactivated by dephosphorylation and then the entire process repeats itself. Alternatively to G_1, cells can post-mitotically enter, temporarily or permanently, a quiescence phase termed as Gap-0 (G_0). Blood lymphocytes, for example, remain in G_0 until antigen stimulation triggers their re-entry into G_1.

Currently, Hague in our research lab is attempting to map the phases of the cell cycle in L-mimosine synchronised HeLa cells by flow cytometry. Preliminary results have showed that L-mimosine achieves approximately 80 percent G_1/S synchronicity in the cells and that the cell cycle in HeLa lasts about 21 hours (Hague 2007). G_1 was mapped occurring in the first three hours post synchronisation, as this blocking agent arrests cells at the G1/S barrier. S phase was observed between six and nine hours, and to a lesser amount at 12 hours post synchronisation. G_2/M was most prominent at 12 hours and G_1 was the most abundant at 21 hours. Based on these results, a cell cycle stage bar has been added as a speculative aid to all the plots of this chapter to indicate where the majority of the cells should be at that particular point post L-mimosine synchronisation.

Unregulated cell division leads to cancer, triggered by defects in the extracellular proteins that stimulate cell division (Collins, Tyler et al. 1997). Cancer cells cannot enter G_0 and repeat the cell cycle indefinitely. Chemotherapeutic anticancer drugs can impede cell division so as to cease or control irregular cell growth.

III.1.1.3. Use of Type I amphiphiles as anticancer agents

HDPC, or miltefosine, is an phospholipid analogue that has been routinely used as the pharmaceutical agent Miltex© (from miltefosine) since 1992 because of its anti-neoplastic properties (Brachwitz and Vollgraf 1995). It belongs to a group of alkyl phosphocholines (APCs) that are characterised by their cytostatic and cytotoxic effects on cancer cells (Berkovic 1998). APCs are part of a wider group of anticancer agents, the alkyl lyso phosphatidyl cholines (ALPs), which includes many structurally unrelated compounds.

The general hypothesis for the mechanism of activity of APCs is that they affect phospholipid metabolism because of chemical structure similarities to membrane lipids such as PtdCho and PhoEth (Wieder, Reutter et al. 1999). HDPC, in particular, can be slowly absorbed into plasma membranes (Breiser, Kim et al. 1987) with no apparent toxic effects in normal cells for up to a concentration of 200 μM and no morphological changes and cell lysis until a concentration of 1 mM (Haase, Wieder et al. 1991).

HDPC inhibited choline incorporation into PtdCho by up to 20 percent and increased PhoEth in cultured kidney cells of canine origin (Geilen, Wieder et al. 1991; Haase, Wieder et al. 1991) and in human cell lines (Berkovic 1998). Geilen et al have suggested that this inhibition is specific to CCT and that is neither due to the detergent properties of HDPC, nor to a decrease of choline uptake and subsequent production of diacyl glycerol, an inhibitor of the enzyme (Geilen, Wieder et al. 1991). HDPC does not directly interact with CCT but prevents the inactive cytoplasmic form of the enzyme to partition into membranes.

HDPC inhibits cell cycle progression by arresting cells at the late S phase/ G_2 phase boundary and neither does it directly interfere with, nor bind to DNA (Brachwitz and Vollgraf 1995). Thus, it can inhibit cancer cell proliferation without mutagenic effects to the general population of normal cells.

Other APCs like lyso phosphatidyl choline (LPC) and 1-O-octadecyl-2-O- methyl-rac –glycero-3-phosphocholine (Et-18-OCH_3) also inhibited choline incorporation into phospholipids (Boggs, Rock et al. 1995). The cytotoxic but not the cytostatic effect of Et-18-OCH_3 was alleviated by the introduction of exogenous LPC in HL60 cells (Boggs, Rock et al. 1995).

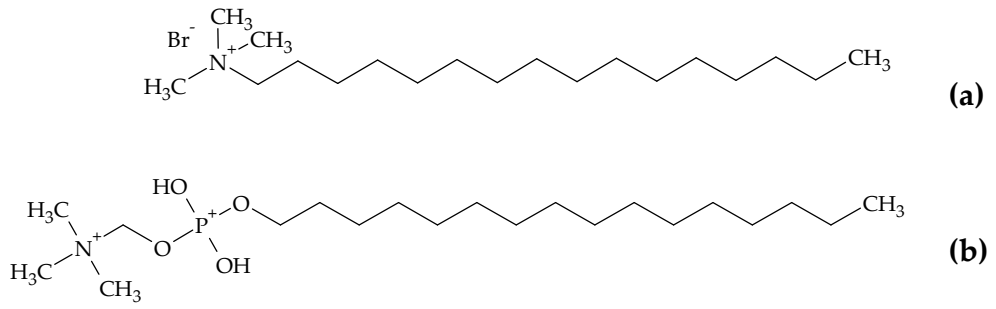

Figure III.6- Chemical structures for Type I amphiphiles (a) CTAB and (b) HDPC.

CTAB is a cationic surfactant with antiseptic properties against bacteria, which is commercially used in cosmetics. Although it has no published anticancer function, its chemical structure is very similar to that of HDPC (Figure III.6). They both preferentially form hexagonal phases as shown from phase studies (Dymond et al 2008, submitted). Thus, according to the stored elastic stress hypothesis (see section II.3.2.2), they should show Type I behaviour and inhibit CCT by decreasing membrane stored elastic stress. Our results (see Section II.4) have in fact also shown that CTAB inhibited *in vitro* CCT activity, as did HDPC. Therefore, the effect of both HDPC and CTAB on the phospholipid metabolism of HeLa was investigated in this chapter.

III.1.2. Regulation of lipid metabolism and membrane stored elastic stress

The cytotoxic effect of a range of ALPs to a different cancer cell line, human leukaemia HL60, and their role in lipid metabolism has been previously investigated in our research group (Dymond 2001). Cationic, anionic, non-ionic and zwitterionic amphiphiles were synthesised and confirmed of Type I behaviour by polarising optical microscopy. Cytotoxicity was then correlated to Type I character of the compounds by investigating their effect on membrane composition of HeLa cells, quantified by ESI-MS. A net decrease of both newly synthesised phosphocholine (PC) and endogenous phosphoethanolamine (PE) species occurred in the presence of compounds with the most pronounced Type I character, in concentrations well below the critical micellar concentration (CMC). This effect was thus not due to detergent action of the amphiphiles. Results were in line with the stored elastic stress hypothesis as Type I amphiphiles should inhibit CCT leading to a decline of PC metabolism. Since PE species are predominantly Type II, cells would enhance PE metabolism in order to equilibrate the effect of Type I compounds.

This line of investigation was further pursued in a preliminary study of the effect of HDPC and CTAB on membrane composition of HL60 cells by ESI-MS (Huth 2006). HDPC inhibited synthesis of new PC while implementation of the cell medium with OA, resulted in larger cell size and marked cell proliferation. Also, relative percentage composition of PC and PE decreased in the presence of OA, whilst PA and PS increased. As OA is a Type II amphiphile, these results further supported the hypothesis that a Type II amphiphile would activate CCT, and in consequence enhance PC biosynthesis.

III.2. Quantitation of lipid species by mass spectrometry

In this chapter, ESI-MS was used to quantify membrane lipids of HeLa cells treated with HDPC and CTAB. As CCT is the rate-determining enzyme of PtdCho biosynthesis, a direct correlation of the effect of Type I amphiphiles to CCT activity in vivo will be attempted as this method can distinguish between endogenous and newly synthesised PC in membranes.

ESI-EMS is an analytical technique that can study molecules in solution after their vaporisation from the liquid to the gas phase (Nelson 2000). The sample is passed through a glass capillary at an electrical potential of approximately 3 KV and thus the solution disperses into a fine mist of charged droplets. A stream of an inert gas is blown to assist microdroplet formation. The solvent then evaporates and charged ions are introduced into the gas phase non-destructively. The ions are then directed into a magnetic and/or an electrical field and their paths through that field are proportional to their mass-to-charge ratio (m/z). A very accurate spectrum of masses for analysed molecules is acquired, in which each peak corresponds to a molecular ion increased by one unit of m/z.

ESI-EMS presents many challenges for the study of large biological molecules like phospholipids mainly due to difficulties with the formation of gas phase ions (Fenn, Mann et al. 1989). However, a quantitative method for detecting phospholipid species by ESI-EMS and stable isotope labelling has been reported and was employed in our experiments (Hunt and Postle 2006). Most importantly, this technique uses non-physiological phospholipids as appropriate internal standards for the quantitation of physiological species. A lipid-dedicated triple quadruple mass spectrometer was used for our experiments (see Section III.6.2.5). A similar method has been reported and employed by the Liebisch Lab to study phospholipid biosynthesis in primary human skin fibroblasts (Binder, Liebisch et al. 2006).

III.3. A novel method of cell sizing by image analysis

Phospholipid biosynthesis and subsequent incorporation of the lipids into membranes are essential to maintaining cell size in dividing cells. Information on cell size can thus aid understanding lipid metabolism during the cell cycle. Consequently, sizing was performed to HeLa cells to complement cell cycle study in addition to lipid quantitation by ESI-MS.

Live cells are typically sized using microscopy images that are statistically analysed by computer software. Alternatively, the principle of light scattering is employed in apparati such as flow cytometers and particle size analysers that can directly provide distribution information from a sample in solution (Givan 2001). Electrical cell counting and sizing of mammalian cells in suspension is also available by means of electrical current passing through a conducting solution (Gregg and Steidley 1965; Adams, Voelker et al. 1967). Also, dead cells can be sized by microscopy images of histological sections (Ashwell, Priest et al. 1976).

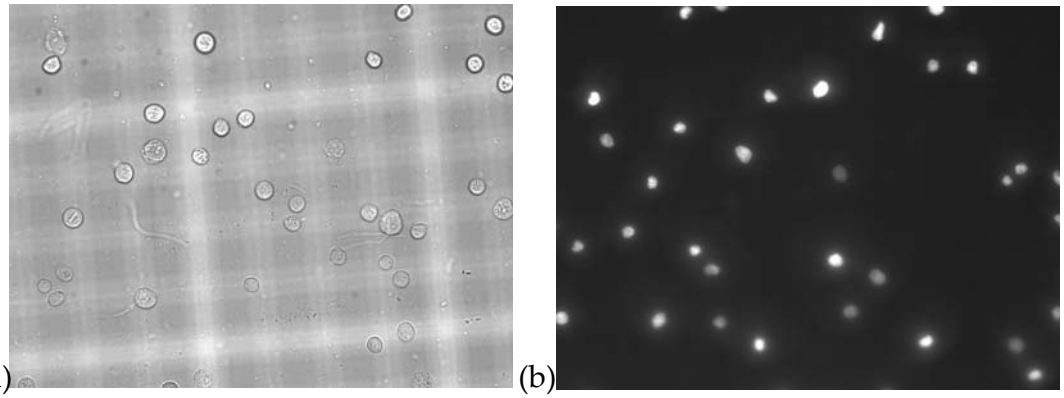

Figure III.7 – Microscopy snapshots of GFP- HeLa cells treated with CTAB by (a) phase contrast and (b) inverse fluorescence microscopy.

Hyperspectral imaging has been recently used to size and determine the cell cycle status of different live cancer cell lines synchronised by serum starvation, aphidicodin or nocodazole (Dicker, Lerner et al. 2007). This method is fairly new; it may well develop to an essential means of identifying cell cycle status of live cells.

In order to satisfy the specific requirements of our experiments and lack of apparatus measuring in our size range, a novel method of sizing live cells using optical microscopy, followed by image and statistical analysis in Matlab© was developed. Software such the open source ImageJ for image analyses could have been used but unfortunately it is not directly suited for large sample populations. Methods based on similar image processing concepts have been used for the sizing of structures as variable as oceanic picoplankton (Viles and Sieracki 1992) and cell cavities in plastic foam (Lewis, Kijak et al. 1996). Sizing latex beads of known size (15±3 μm) by both scanning electron microscopy (SEM) and our method confirmed that the method was reliable. The SEM micrographs (Figure III.8) gave an average diameter of 14.55±1.04 μm while our method resulted in a mean diameter of 18.83±1.5 μm.

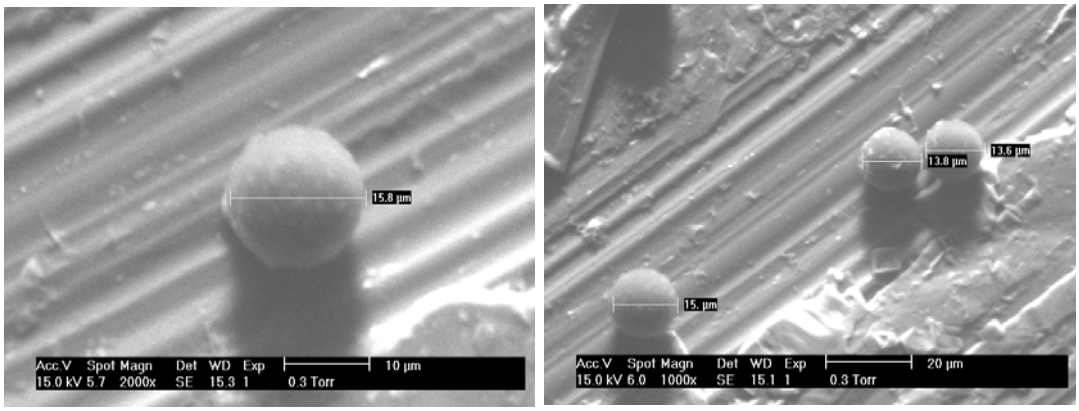

Figure III.8- Scanning electron micrographs of 15 μm diameter latex beads.

Our method was also used to size cell nuclei of HeLa cells. The result was 11.85± 2.18 μm (Figure IV.9). The diameter of CaSki nucleus, another cervical carcinoma cell line, has been sized at approximately 11.5 μm by resinless section electron microscopy (Zink, Fischer et al. 2004).

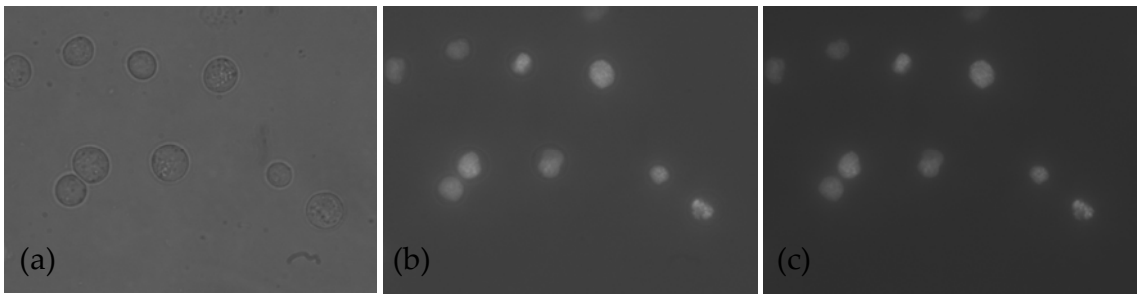

Figure III.9- Microscopy snapshots of HeLa cells used for nuclei sizing by (a) x20x2.5 halogen (b) x20x2.5 halogen and fluo (c) x20x2.5 fluo only.

III.4. Experimental

III.4.1. Materials

D-MEM medium, Hanks' Balanced Salt Solution (HBSS), phosphate buffer saline (PBS), penicillin/streptomycin, foetal bovine serum (South American origin), Virkon and trypsin were purchased from Invitrogen Ltd (Paisley, UK). All solvents, namely water, chloroform, methanol, ammonia, and 1-butanol, were purchased at HPLC grade purity from Sigma Aldrich UK.

The genetically modified HeLa cells containing the GFP gene were kindly provided from the Zink laboratory, Department of Biology, University of Munich, Germany (Zink, Sadoni et al. 2003).

Lipids used for MS standards: 1,2-diarachidoyl-sn-glycero-3-phosphocholine (DAPC) and 1,2-dimyristoyl-sn-glycero-3-phosphoethanolamine (DMPE) were purchased from Avanti Polar Lipids (USA). Choline (d9) chloride N, N, N-trimethyl was from CND isotopes (UK). HDPC, CTAB, myristyl trimethyl ammonium bromide (HDPC MS standard) and tetradecyl trimethyl ammonium bromide (CTAB MS standard) of the highest available purity were from Sigma Aldrich (Dorset, UK).

Sodium chloride (biological grade), 0.4% Trypan blue solution and sodium ferrothiocyanate were from Sigma Aldrich (Dorset, UK). L-mimosine was from Merck (Nottingham, UK). The latex beads were from Polysciences Europe (Germany) and all consumables including serological pipettes, falcon and culture tubes were from Greiner Bio-one LTD (Germany) and Fisher Scientific (UK).

III.4.2. Methods

III.4.2.1. Cell cultures

The cells were grown at 37 °C and 5% CO_2 in standard HeLa medium (50 mL, 4 mM L-glutamine, HEPES buffer, no pyruvate, 5% foetal calf serum and 100 μg/mL of penicillin/streptomycin) in 80 cm^2 culture flasks.

For addition of deuterated choline, the flasks were removed from 37 °C and 5% CO_2 when confluence was no more than 80%. Deuterated phosphocholine (d_9) in HBSS (0.02 mg/mL), and/or CTAB in PBS (3.00, 1.50 and 0.75 μM) or HDPC in PBS (10.50, 5.25 and 2.63 μM) were then added. The flasks were incubated at 37 °C and 5% CO_2 for the required time. The medium was decanted and EDTA-trypsin (5 mL, 0.25%) was added to detach the cells from the flask walls. Additional three minute incubation at 37 °C was allowed. Trypsination was quenched with the addition of HeLa medium (10 mL). The cells were centrifuged for 5 minutes at 1500 xg. The formed pellet was resuspended in HBSS medium (3 mL). The cells were counted by the dye exclusion method using 0.4% Trypan blue solution. The cells were centrifuged for 5 minutes at 1500 xg and the formed pellet was stored at -14 °C.

For cell synchronisation, the flasks were removed from 37 °C when confluence was no more than 70%. L-mimosine in NH_4OH (1 M) was added (200 μM per flask). The cells were incubated for 13 to 16 hours. The medium was decanted and the block was released by washing with PBS (10 mL). The flasks were replenished with fresh HeLa medium. For double synchronisation, the cells were allowed 12 hours at 37 °C and 5% CO_2 and then the synchronisation protocol was repeated.

III.4.2.2. Bligh Dyer total lipid extraction

The original method of total lipid extraction has been adapted for use with our experiments (Bligh and Dyer 1959; Dymond 2001). Each sample of whole cells in aqueous solution was sonicated for one minute. The sample was then made up to one volume (1 mL) with saline (0.9% or 154 mM NaCl). Then, chloroform (1.25 volumes, 1.25 mL). The appropriate amounts of internal standards were added and the sample was thoroughly mixed. Methanol (2.5 volumes, 2.5 mL), chloroform (1.25 volumes, 1.25 mL) and purified water (1.25 volumes, 1.25 mL) were added sequentially and the sample was centrifuged at 3000 xg for 10 minutes. The lower organic phase from each sample was transferred to fresh tubes and heated under a continuous flow of dry nitrogen at 40 °C until dry. Samples were stored at – 20 °C until mass spectrometry was to be performed.

III.4.2.3. Addition of mass spectrometry internal standards

Known amounts of non-physiological lipids 1,2-di-arachidoyl phosphatidyl choline (DAPC) and 1,2-di-myristoyl phosphatidyl choline (DMPE) were used as a measure of quantification of the lipids present in the sample. The amount of standards per sample was adjusted accordingly depending on the cell count and the time passed after synchronisation. Standards were quantified colorimetrically by ferrothiocyanate using the Stewart assay (Stewart 1980).

III.4.2.4. Mass spectrometry

The dried sample, containing the organic phase extracted using the Blight Dyer method, was dissolved in mass spectrometry solvent (600 μL, 20% 1-butanol, 60% methanol, 16% water and 4% concentrated ammonia). An aliquot of at least 150 μL of was loaded into a spray capillary by direct injection with a flow rate of 5 μL/min. The data was collected by ESI-MS on a lipid-dedicated Quatro Ultima triple quadruple mass spectrometer (Micromass, Wytheshaw, UK).

Fragment	Current Energy (eV)	Cone Voltage (V)	Range (m/z)
P184 (184.1)	32	90	450 - 870
P193 (193.0)	25	90	450 - 870
NL141 (141.2)	28	90	400 - 850
P184 HDPC (184.1)	26	71	390 - 450
P61 (60.5)	27	31	250 - 300

Figure III.10- Table of MS scan settings.

Endogenous PtdCho was selectively determined by precursor scans of the PC fragment (m/z 184) while newly synthesised PtdCho was determined by equivalent precursor scans of the PC-d9 fragment (m/z 193). Endogenous PhoEth was selectively determined by the constant neutral loss scans of a protonated PhoEth head group fragment (m/z 141). Incorporated HDPC in the membrane was determined by precursor scans of the PC fragment (m/z 184) at a smaller range, current energy and cone voltage than endogenous PtdCho. Incorporated CTAB in the membrane was determined by precursor scans of the hexadecyl trimethyl ammonium ion fragment (m/z 61). Peak assignment was performed by principle chain assignment for isomers. The drying and collision gas were nitrogen and argon, respectively. MassLynx 4.0 was used for collection and initial analysis of data. Data was subsequently extracted and further analysed in Excel using Visual Basic macros written by Dr. Grielof Koster. Percentage noise was at 1.0 percent for PC and d9 PC and at 1.5 percent for PE.

III.4.2.5. Scanning electron microscopy

Samples (30 μL) of 1% v/v solution of 15 μm latex beads in 0.9% NaCl were evaporated at 50 °C onto a 1.27 mm slotted aluminium head. SEM images of the beads taken in a "wet mode", advantageous for non-conductive samples, with a Gaseous Secondary Electrode (GSE) detector using an environmental scanning electrode microscope (XL30 ESEM, Philips, Electrochemistry Group, University of Southampton) with the assistance of Dr. Clelia Milhano. Optimum combination of accelerating voltage, spot size and vapour pressure were selected for each scanning electron micrograph. Conditions marked on each image.

III.4.2.6. Optical Cell sizing

Pictures were taken using a Zeiss Axiovert 200 inverse fluorescence microscope and Hamamatsu Orca-ER C47-42 95 monochromatic camera (Bioelectronics Group, University of Southampton). For acquiring images under fluorescence conditions, Ph2 and FITC filters were used with gain of 175 and exposure of 0.5 s^{-1}. Under halogen conditions, a Ph1 filter was used with gain of 0 and exposure of 0.018 s^{-1}.

The Matlab© program was written by Daniele Malleo and implemented by the author. First, the "cellcounter3" script was run to each picture in order to provide with size data, which was then exported as a .mat file. An exclusion threshold was applied for all data so all points smaller than 3 pixels were considered as noise. Also, optimum levels of image segmentation were used in each image analysis, which were 82 for all control samples, 62 for the latex beads sample, 133 for 0, 12 and 24 hours post synchronisation samples, 70 for 3, 6, 9 and 144 hours post synchronisation samples, 80 for the 43 hours post synchronisation sample, 109 for HDPC 10.50 μM and 82 for all the other samples with drug present.

Second, the "analyser" script was run to the sum of .mat files for each sample in order to provide with cumulative sizing data, which was then exported as an Excel file.

Third, the "statan2" script was run to the Excel file in order to provide with statistical and distribution analyses, which were then exported as an Excel file. The known distances on a typical haemocytometer were used to calibrate the pixel to μm ratio on the optical images. It must be noted that the "threshold_tool" script must be in the same folder as the images for all three aforementioned scripts to function properly.

III.5. Results and discussion

III.5.1. Control cultures

A complete series of control cultures in triplicate were run for up to 21 hours after synchronisation, where no drug was introduced to the culture medium. Cell viability was measured and then membrane lipid content was quantified by ESI-MS.

III.5.1.1. Cell viability and size during the cell cycle

Assessment of viable cell number is essential in cell culture experiments. It is a measure of how healthy the cultured cells are and whether any implemented compounds in the medium have affected cell division. The most common method of determining cell viability of trypan blue exclusion principle was used in this work. Cells are stained with trypan blue dye and are counted in a haemocytometer. Ability of a cell to exclude the dye is demonstrative of uncompromised membrane integrity, and thus of a healthy living cell.

Results of cell viability in control cultures are shown in Figure III.11. It is quite clear from these data that the error in measuring cell viability using the dye exclusion principle is quite significant as illustrated by error bars for the data points at nine and 21 hours. However, it is useful since it shows the limitations of the cell counting method.

Thus, it can concluded that during the first 21 hours after synchronisation, the number of dead cells has remained approximately constant at about 15 per cent, as far the error of this method allows to infer. The point at nine hours shows high percentage of dead cells at 24.90±4.88 and potentially corresponds to occurrence of apoptosis, which takes place at the end of S phase in human cancer cells (Zhou, Simpson et al. 2003).

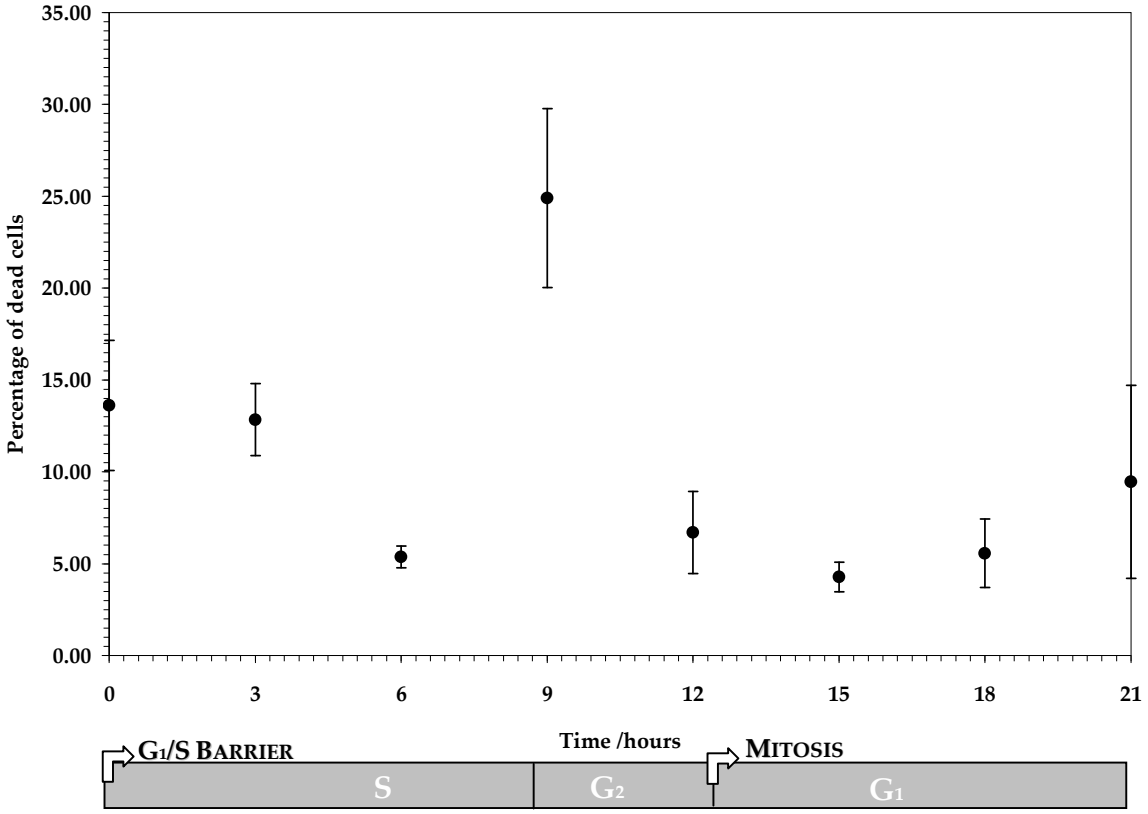

Figure III.11- Plot of percentage dead cells as a function of time in control cultures.

Then, in a separate experiment, the size of HeLa cells in control cultures was measured using our novel method of image analysis over a period of 144 hours post synchronisation. Results are shown in Figure III.12 overleaf.

Overall, cell size did not show significant variation in the first nine hours, ranging between 17 and 20 μm. Maximum size of 19.94±3.03 μm was measured at 12 hours post synchronisation. Finally, cell size decreased considerably to 15.61±1.90 μm at 144 hours post synchronisation as the cells were kept in the same flask, although the growth medium was replenished every 24 hours. However, it could be that the flasks still became overcrowded and cells were under stress due to lack of space for the newly divided cells appearing at the end of each cell cycle. Although error bars are quite significant, it could be postulated that the first and second cell cycles post synchronisation are potentially mapped as shown by the trend line on Figure III.12. Thus, cells show a decreasing mean diameter while becoming asynchronous.

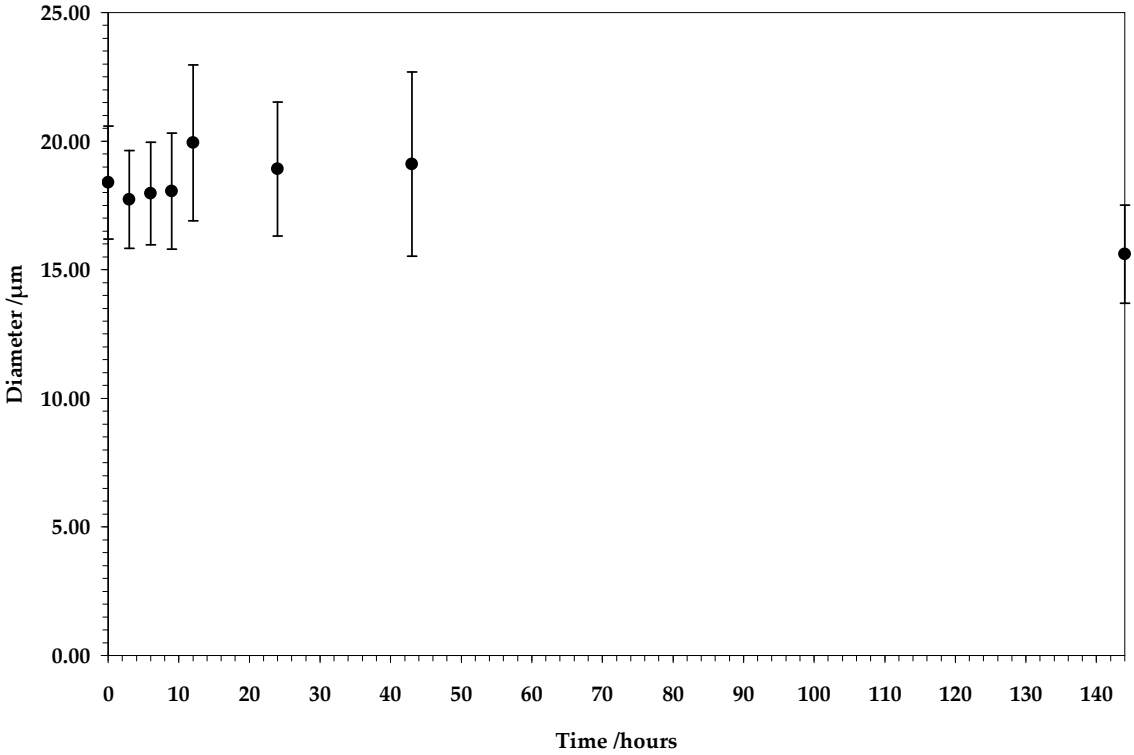

Figure III.12- Plot of mean diameter of cells as a function of time in synchronised control cultures.

Overall, a maximal increase in diameter of 27 percent within error was observed. Since cell volume (V) is expected to double during the cell cycle and the radius of sphere equates to $\left(V \frac{3}{4\pi} \right)^{1/3}$, the radius would increase by 25 percent if the volume doubled. Consequently, our sizing method can be used to monitor cell size with significant accuracy.

Conversely, there is a probability that more pronounced size fluctuations were not observed because they occurred within the error of the sizing method. However, as a significant population of at least 3,000 cells were sized for each time interval, interesting conclusions could be drawn from the distribution of the population.

The two distribution parameters, excess kurtosis and skewness, were thus considered. Kurtosis is a measure of the data outliers in a distribution:

$y = (E (x-\mu)^4)/ \sigma^4$; where μ is the mean, σ is the standard deviation of x and E the expected value of the quantity t.

Excess kurtosis is corrected by subtracting three from kurtosis to make the value of a normal distribution equal to zero. A leptokurtic distribution has large and positive values of excess kurtosis, while the opposite distribution is termed as platykurtic.

Skewness is a measure of the asymmetry of the data around the sample mean in a distribution and is defined for a population x as:

$y = (E (x-\mu)^3)/ \sigma^3$; where μ is the mean, σ is the standard deviation of x and E the expected value of the quantity t.

A normal distribution would have skewness of zero. A left-tail distribution skew with negative values of skewness shows a higher percentage of values smaller than the mean in, while a right-tail distribution shows the opposite effect.

In control cultured cells (Figure III.13), both excess kurtosis and skewness started gradually increasing from nine hours reaching a maximum at 24 hours post synchronisation. Then, both parameters decreased in the interval between 24 and 43 hours. This is in line with the size of the cell population increasing as cells went through the cycle, and then size decreasing when cells divided at some point around 24 hours. Therefore, the distribution was increasingly leptokurtic with more outliers (higher kurtosis) until cell division caused the trend to shift. It must be noted that the distribution of cell sizes remained normal at all intervals passing the Kolmogorof-Smirnof test for normality.

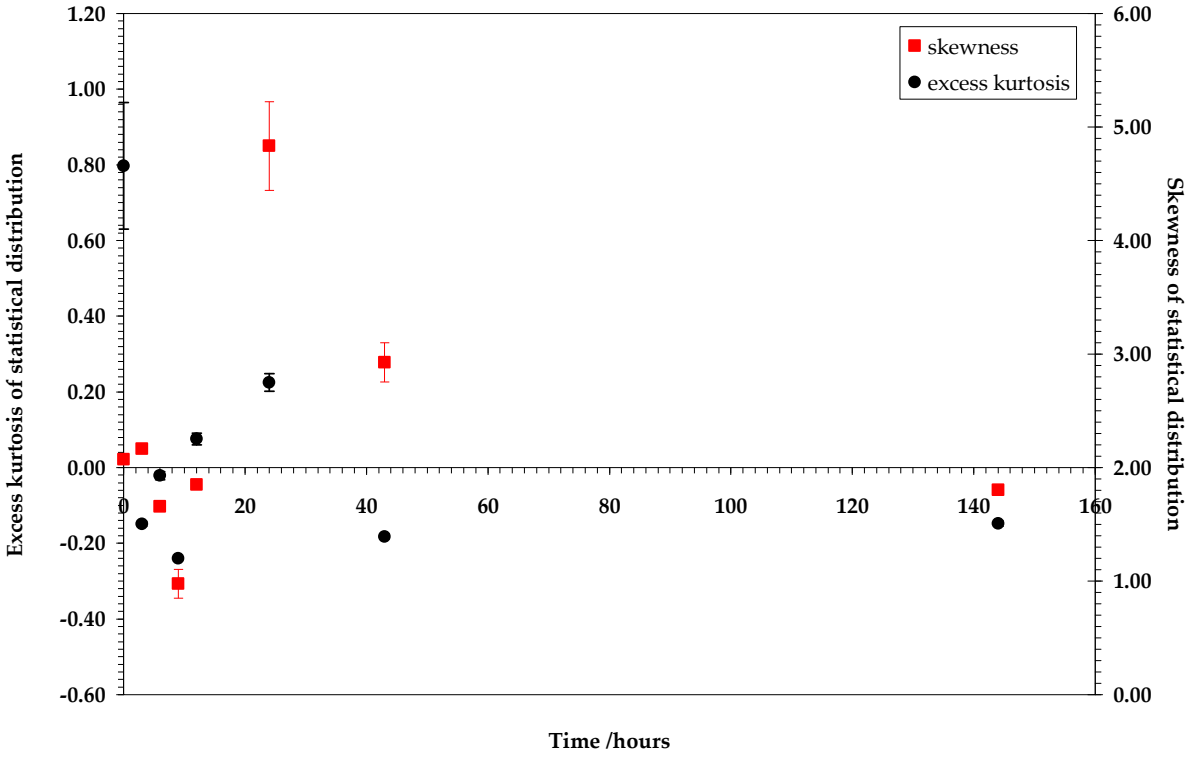

Figure III.13- Plot of distribution parameters, excess kurtosis and skewness, as a function of time in a control cultured population.

Results for parameters of cell size distribution in the presence of HDPC and CTAB are shown in Figure III.14. Data for unsynchronised control cultures showed positive values for both skewness and excess kurtosis. Excess kurtosis is large due to the presence of multiple outliers in the population which is logical for an unsynchronised sample where each would be at a different stage of the cell cycle.

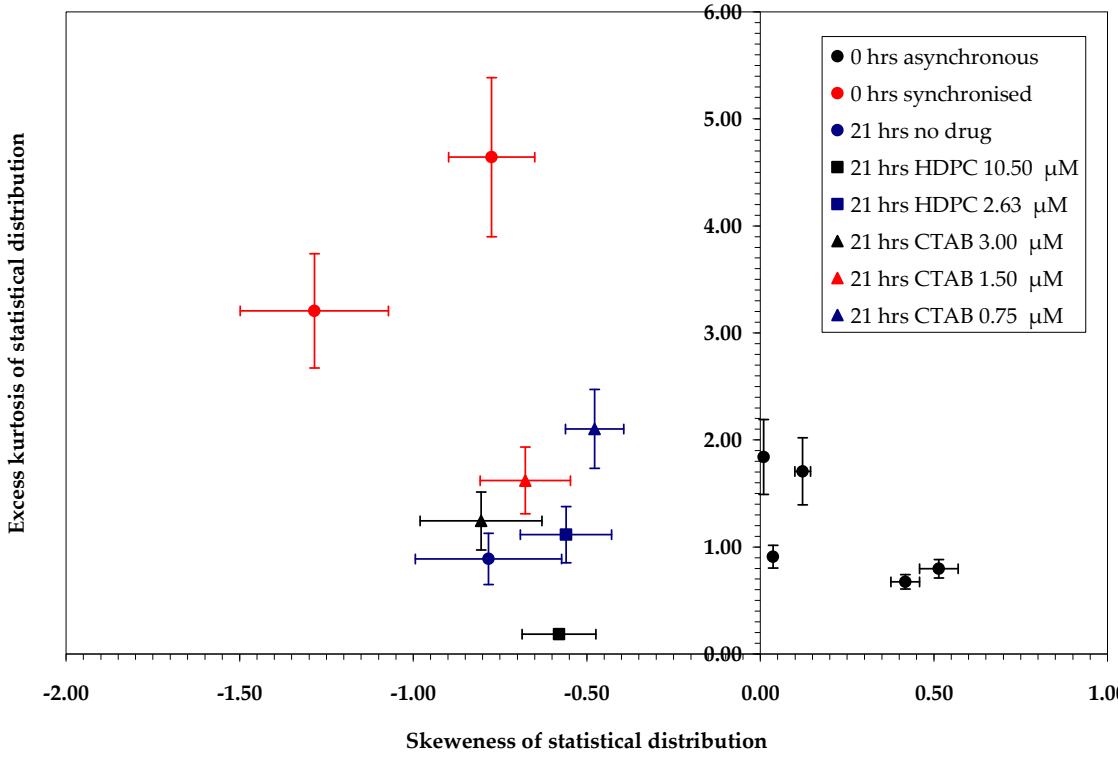

Figure III.14- Plot of distribution skewness as a function of excess kurtosis in control cultures and in the presence of CTAB and HDPC drugs.

In the control with synchronised cells at G_1/S, excess kurtosis was large and positive and skewness negative. Thus, the cell population had many outliers and a high percentage of values smaller than the mean. Results for synchronised cells incubated with no drug were similar; hence solely incubation did not significantly affect diameter distribution. HDPC and CTAB both caused negative values of skewness and excess kurtosis ranging from 0.2 to 2. Thus, cells were predominantly small with less outlier than in the absence of the drugs and both drugs caused cells to shrink slightly.

III.5.1.2. Phospholipid metabolism

III.5.1.2.1. **Total lipid content by mass spectrometry**

The total amount per cell of endogenous PC and PE and newly synthesised PtdCho in the cell membranes of L-mimosine synchronised HeLa cell control cultures was quantified by ESI-MS. For experimental methods, see section III.4. Results are shown in Figure III.15.

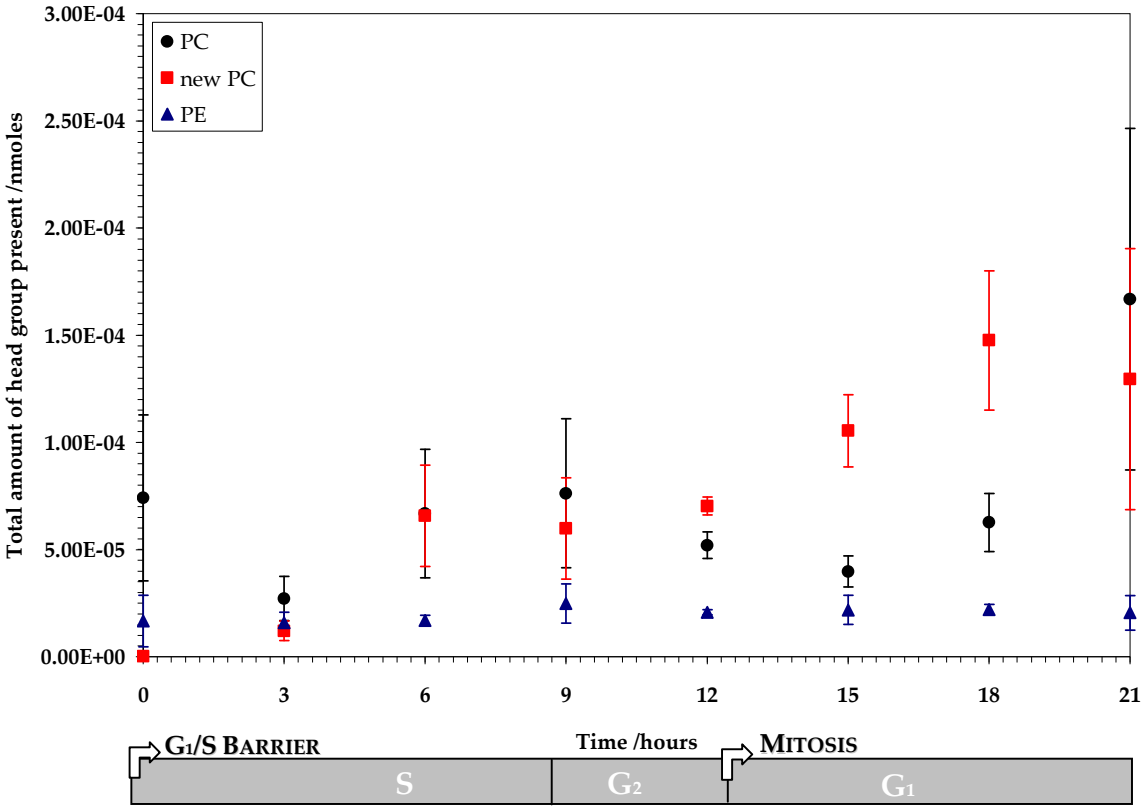

Figure IV.15- Plot of total lipid content per cell for PC, new PC and PE head group classes as a function of time as measured by mass spectrometry in control experiment in the absence of drugs.

Endogenous PtdCho in the cell membrane remained at about 2.00×10^{-5} nmoles/cell, within error, with a sharp increase at the last data point. Newly synthesised PtdCho peaked after 18 hours post synchronisation. This agrees with the literature since new phospholipid mass should double after M phase (Jackowski 1994).

Endogenous PhoEth in the cell membrane remained almost constant, at about 2.00×10^{-5} nmoles per cell throughout the studied period of the first 21 hours.

III.5.1.2.2. **Membrane composition by mass spectrometry**

The data acquired from ESI-MS includes percentages of different acylation patterns for each lipid head group. The advantage of these data is that they are affected by neither cell counting errors nor amounts of non-physiological standards present. Thus, any error originates purely from ESI-MS as an experimental method.

As an exclusion rule, for endogenous and newly synthesised PC, any chains detected at a percentage lower than one percent were omitted as part of the experimental noise. For the PE head group, the threshold was increased at 1.5 percent due to different noise levels in the neutral loss scan mode of ESI-MS, employed in this case. For nomenclature of fatty acid chains, see section I.1.2.

In the following plots (Figures III.16-18), percentages of acylation patterns for fatty acid chains for PC, new PC and PE head groups are presented.

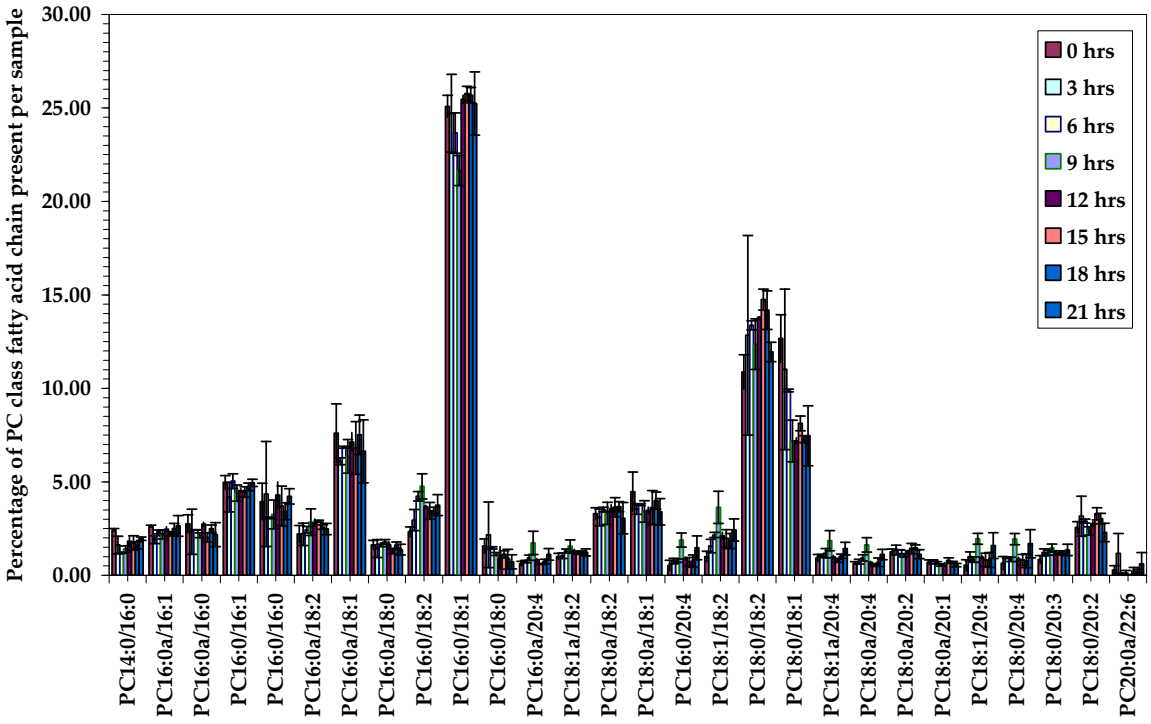

Figure III.16- Plot of fatty acid chains present for PC head group class as a function of time as measured by mass spectrometry in synchronised control cultures.

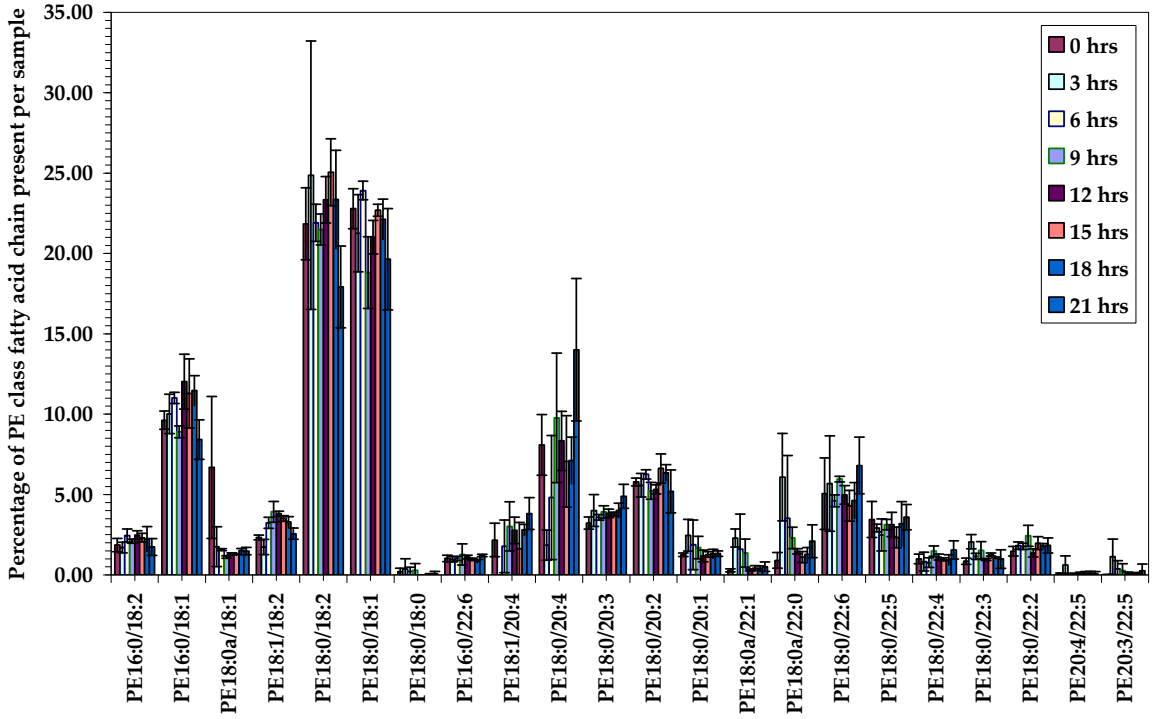

Figure III.17- Plot of fatty acid chains present for PE head group class as a function of time as measured by mass spectrometry in synchronised control cultures.

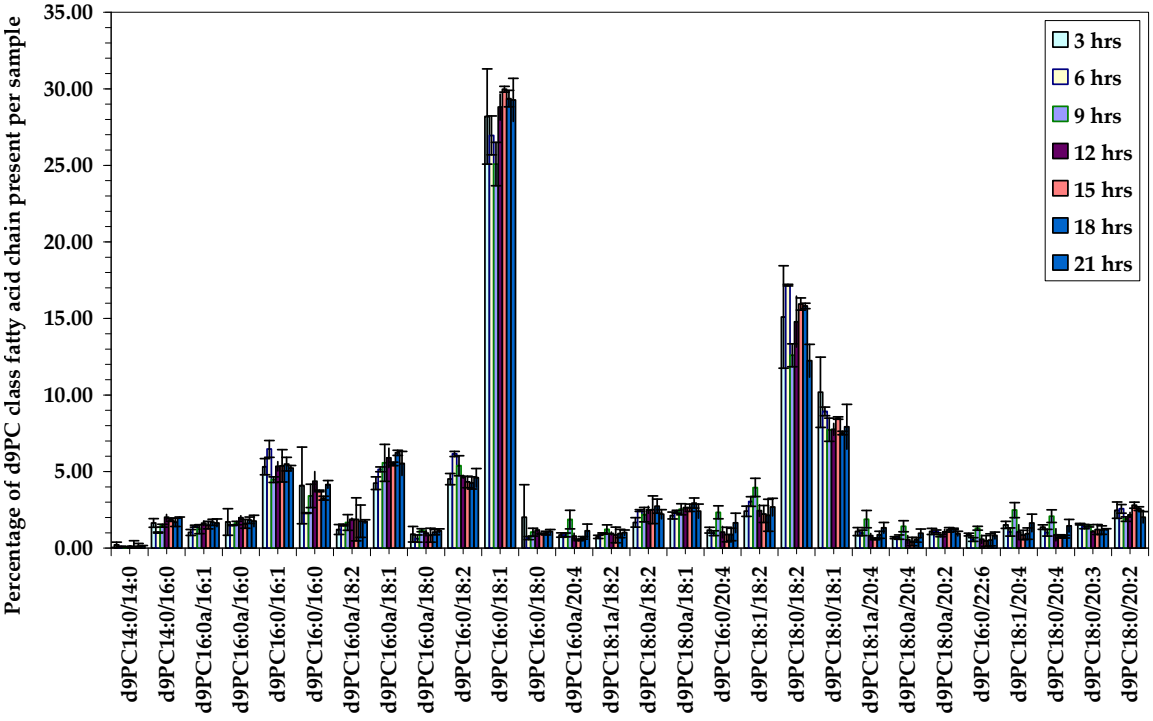

Figure III.18- Plot of fatty acid chains present for new PC head group class as a function of time as measured by mass spectrometry in synchronised control cultures.

Fatty acid species with higher than five percent abundance in at least one time interval are shown in decreasing order of intervals above threshold (Figure III.19).

Endogenous PC			**PE**			**Newly synthesised PC**		
m/z (amu)	Species	Average %	m/z (amu)	Species	Average %	m/z (amu)	Species	Average %
746	PC16:0a /18:1	6.88±0.52	718	PE16:0/ 18:1	10.34±1.30	769	d9PC16:0/ 18:1	25.71±7.30
760	PC16:0/ 18:1	24.65±1.39	744	PE18:0/ 18:2	22.47±2.28	795	d9PC18:0/ 18:2	13.51±4.04
786	PC18:0/ 18:2	13.02±1.27	746	PE18:0/ 18:1	21.53±1.70	797	d9PC18:0/ 18:1	7.71±2.03
788	PC18:0/ 18:1	8.85±2.10	772	PE18:0/ 20:2	5.79±0.56	741	d9PC16:0/ 16:1	5.25±0.67
732	PC16:0/ 16:1	4.65±0.31	768	PE18:0/ 20:4	7.63±3.54	755	d9PC16:0a /18:1	5.26±0.78
			792	PE18:0/ 22:6	5.25±0.43	767	d9PC16:0/ 18:2	4.52±1.10
			790	PE18:0a /22:0	2.35±0.84			
			732	PE18:0a /18:1	2.09±1.87			

Figure III.19- Table of PC head group class fatty acids with a higher than 5% abundance in control cultures. Values and SD are average percentages of all intervals.

The most abundant fatty acid chain present for the PC head group class was found to be PC16:0/18:1. Also, four more species were present at a percentage higher than five percent through the 21 hour studied period: PC18:0/18:2, PC18:0/18:1, PC16:0a/18:1 and PC16:0/16:1. Fluctuations in these five species in both nmoles per cell and percentages are illustrated in Figures III.20 and 21.

Subtle trends were observed during the cell cycle. All five species increased steadily up to nine hours post synchronisation. This is in line with phospholipid synthesis occurring during G_1 and S phases. At G_2/M amounts slowly decreased as lipid metabolism ceases and cells grow bigger on their way to cytokinesis. With cell division occurring some time between 18 and 21 hours, absolute amounts of the abundant species increased again at G_1 phase when lipid synthesis resumes.

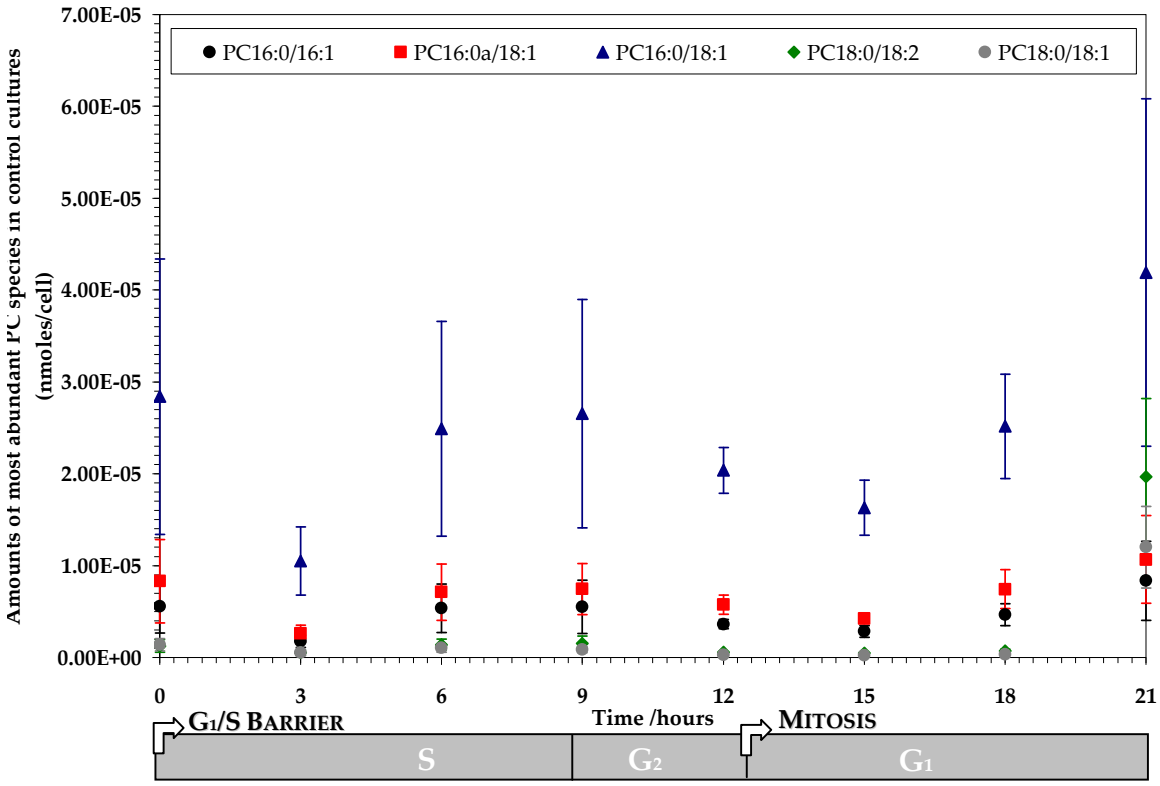

Figure III.20- Plot of amount (nmoles/cell) of most abundant PC head group class fatty species against time (hours) by mass spectrometry in control cultures.

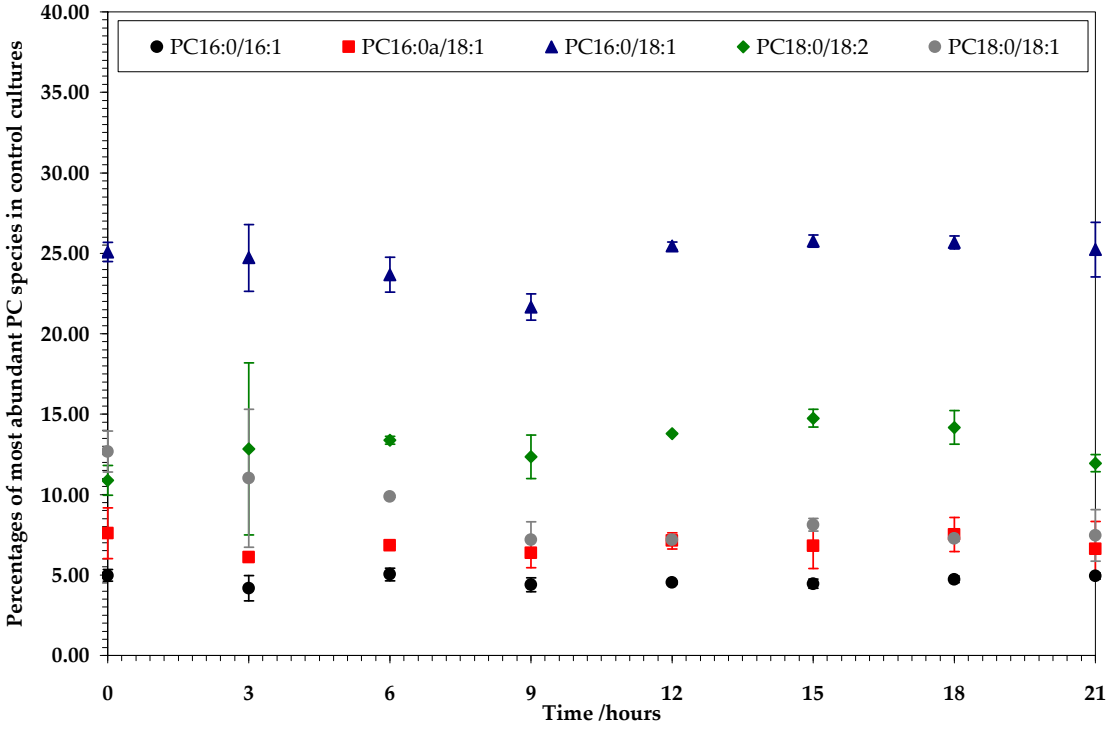

Figure III.21- Plot of percentages of most abundant PC head group class fatty species against time (hours) measured by mass spectrometry in control cultures.

Similarly to PC, the most abundant fatty acid chains for the PE head group class were PE18:0/18:2 and PE18:0/18:1. Six more species showed abundances higher than five percent as seen in Figures III.22 and 23:

- PE16:0/18:1
- PE18:0/20:2
- PE18:0/20:4
- PE18:0/22:6
- PE18:0a/22:0
- PE18:0a/18:1.

Absolute amounts for all eight PE species did not show significant charges throughout the cell cycle. Since PC is a precursor for PE biosynthesis, PC species are synthesised first, mainly through the *de novo* Kennedy pathway, the increase in their PE counterparts will occur a few hours later. For example, the most abundant PC species PC16:0/18:1 shows a local maximum at nine hours at the end of S phase. Conversely, its PE equivalent PE16:0/18:1 peaks three hours later at 12 hours post synchronisation at the G_2/M barrier. Thus, once PC16:0/18:1 becomes metabolically available, some of it is further metabolised to form PE16:0/18:1. It must be also noted that the PE amounts in membranes are lower than for PC, as expected from the literature (Boon and Smith 2002).

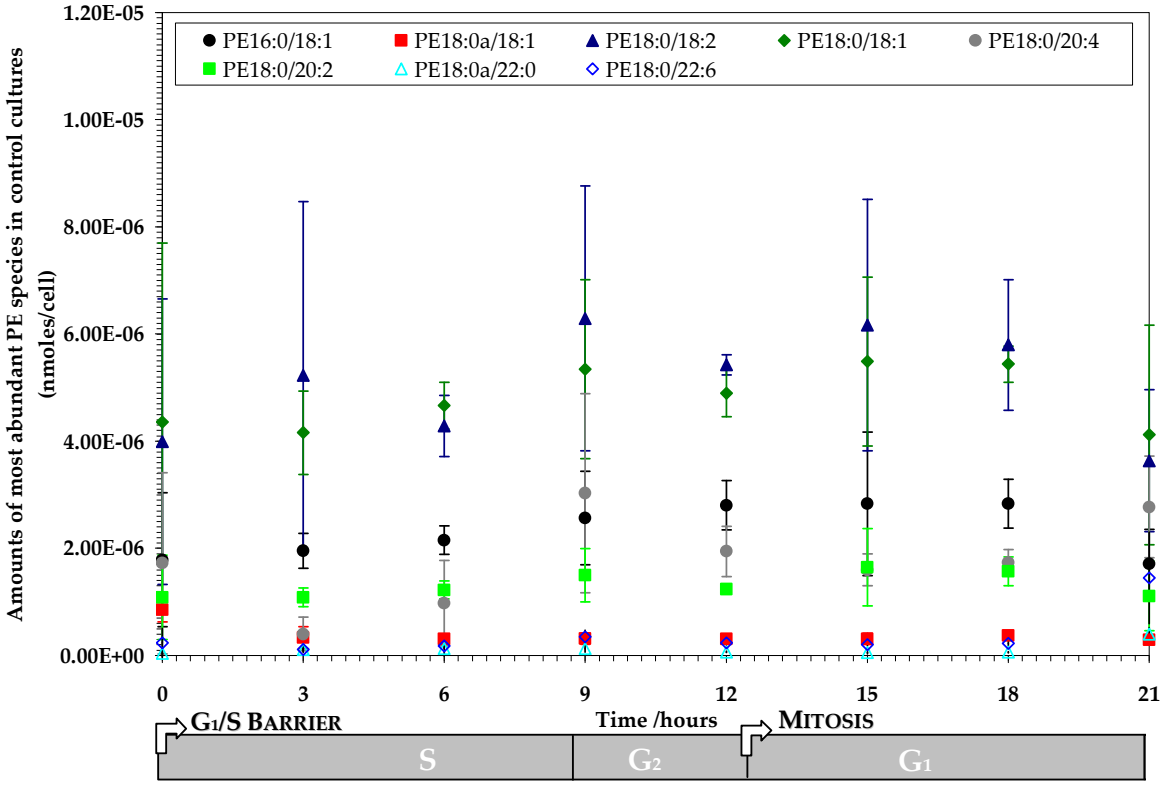

Figure III.22- Plot of amounts (nmoles/cell) of most abundant PE head group class fatty species against time (hours) measured by mass spectrometry in control cultures.

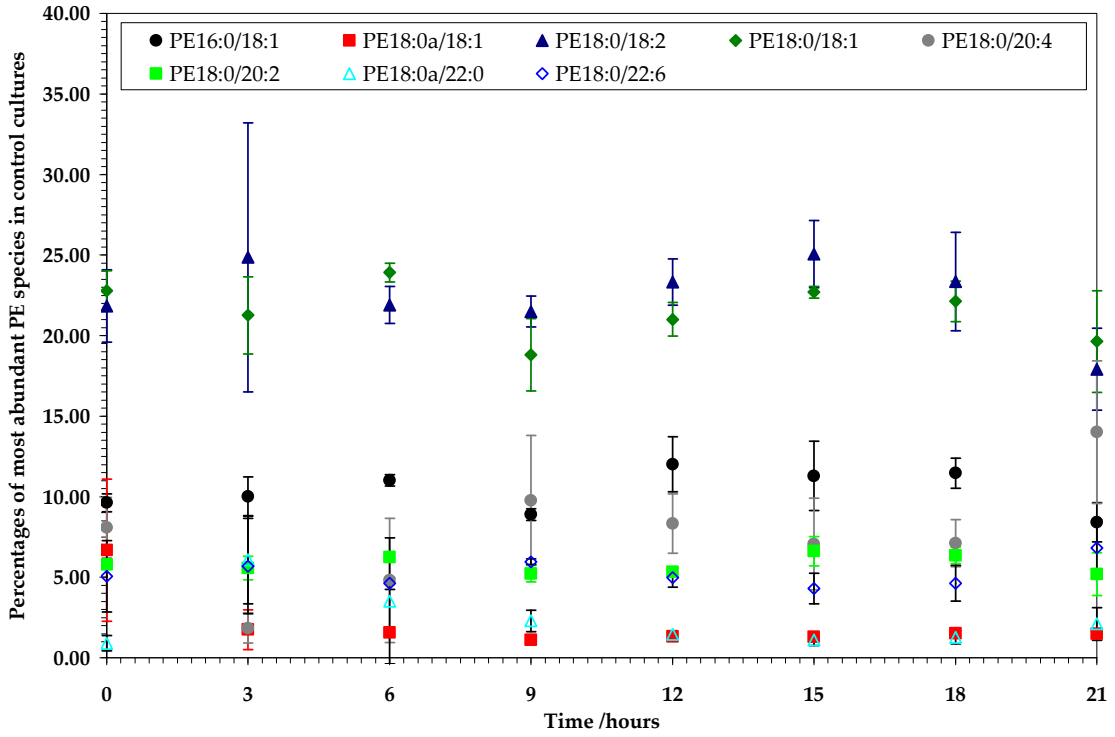

Figure III.23- Plot of percentages of most abundant PE head group class fatty species as a function of time measured by mass spectrometry in control cultures.

For the newly synthesised PC head group class in the membrane, the most abundant fatty acid chain was d9PC16:0/18:1, the same chain length and type as for endogenous PC and PE. Also, five more chains showed abundance higher than five percent as seen in Figures III.24-25.

- d9PC18:0/18:2,
- d9PC18:0/18:1
- d9PC16:0a/18:1
- d9PC16:0/18:2
- d9PC16:0/16:1.

Overall, one additional species was significantly abundant compared for endogenous PC: d9PC16:0/18:2 was at 4.52±1.10 percent compared to 3.58±0.74 percent for PC16:0/18:2.

An increasing trend was observed for all six abundant species up to nine hours post synchronisation, until the end of the S phase when phospholipid metabolism occurs. Then amounts remained constant within error from 12 to 15 hours post synchronisation during G_2/M when no lipid synthesis takes place. Finally, PE species started to increase again at 18 hours when G_1 phase restarted and lipid synthesis resumed

Consequently, the same arguments based on the phases of the cell cycle apply here as for endogenous PC and PE and our results are in line with trends expected from the literature.

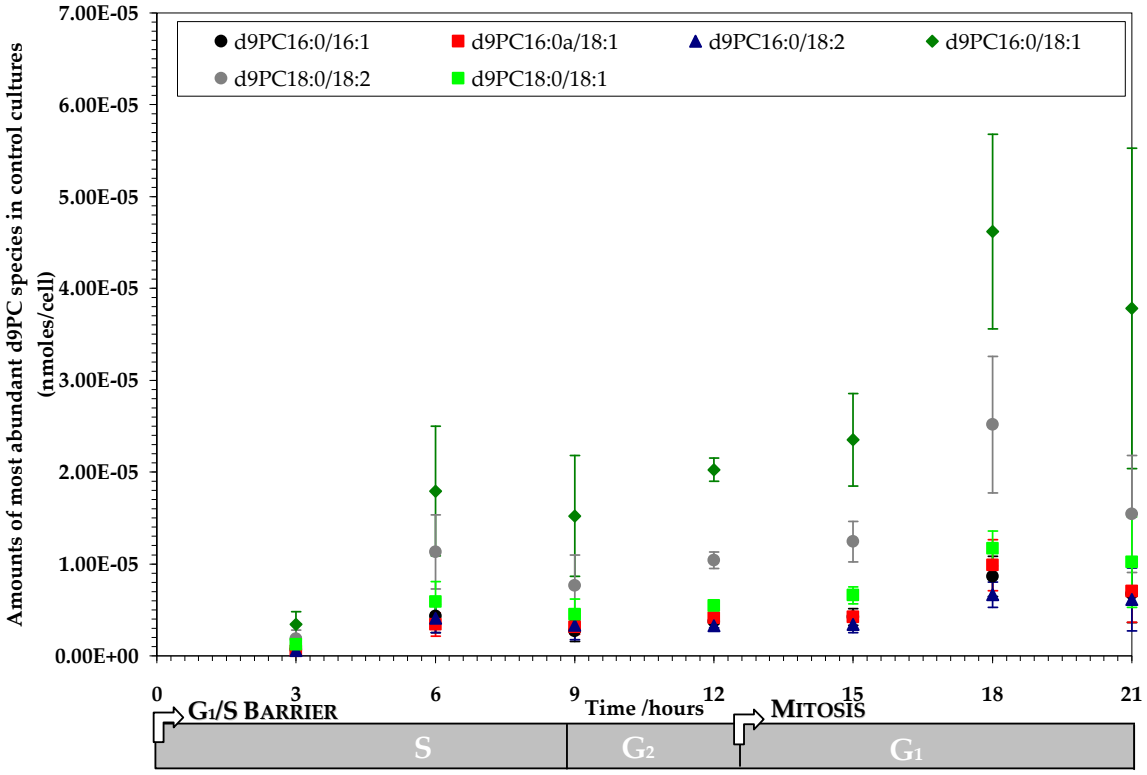

Figure III.24- Plot of amounts (nmoles/cell) of most abundant d9PC head group class fatty species against time by mass spectrometry in control cultures.

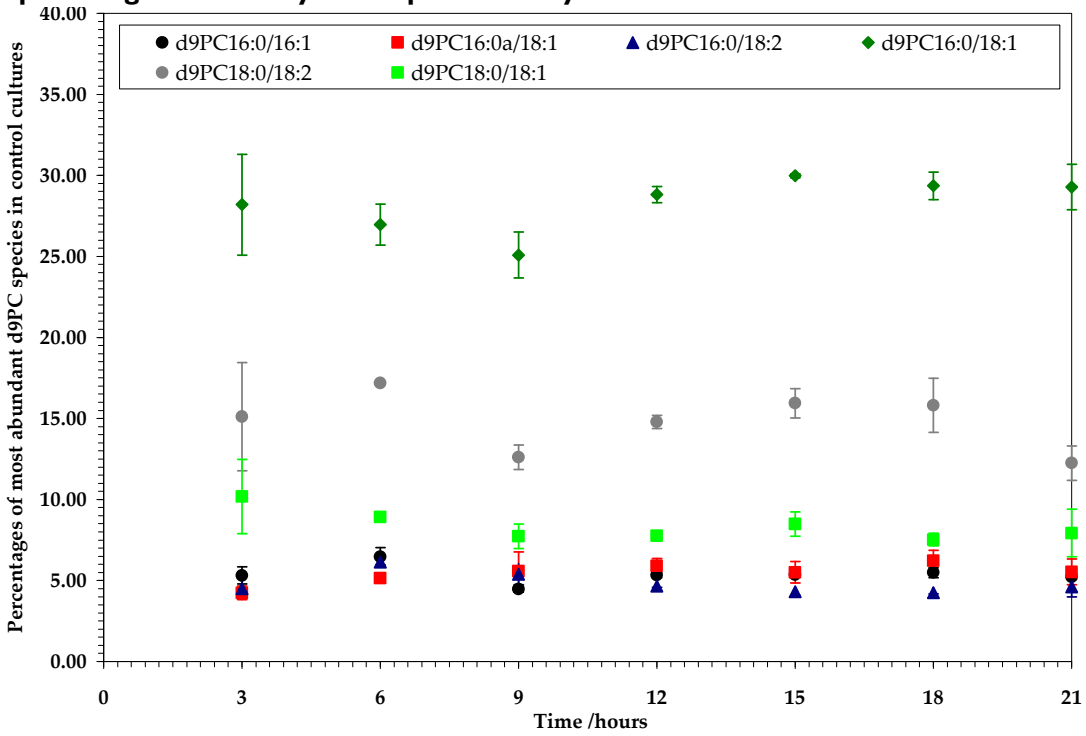

Figure III.25- Plot of percentages of most abundant PC head group class fatty species against time measured by mass spectrometry in control cultures.

III.5.1.2.3. **Rate of new PC synthesis**

The rate of synthesis was calculated as the amount of d9PC in nmoles per cell as a function of time.

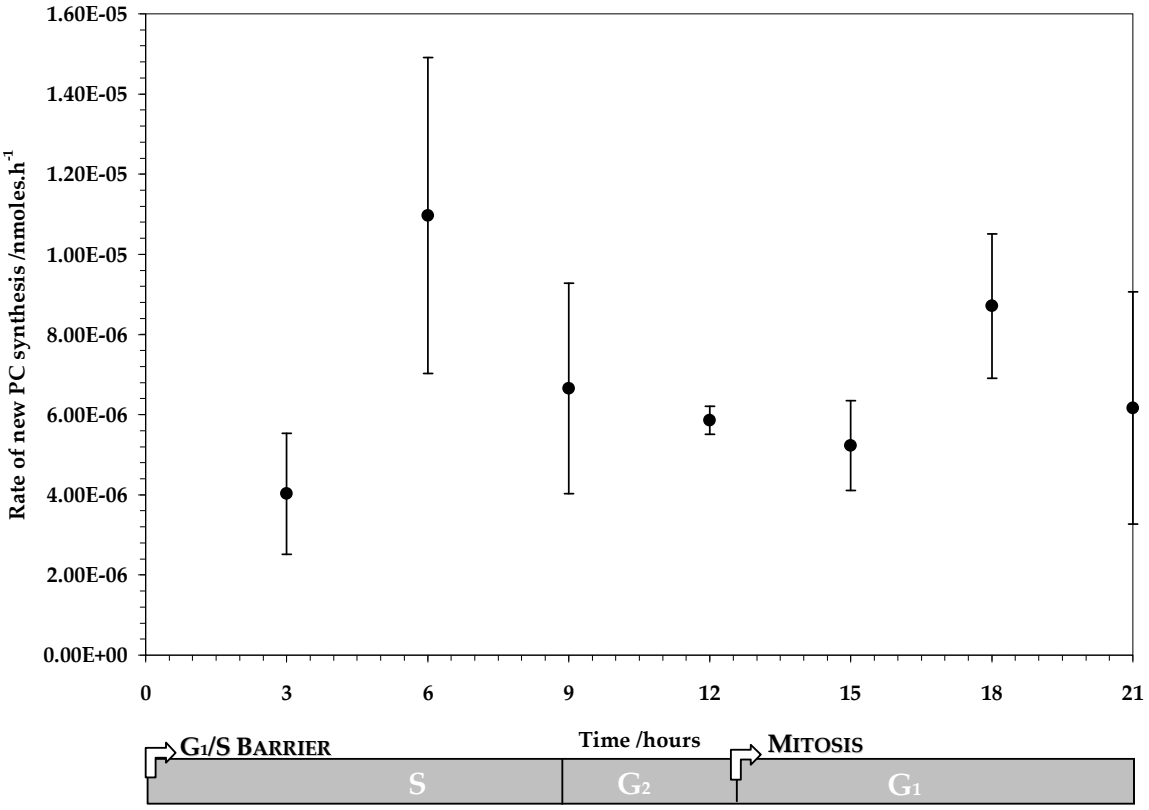

Figure III.26- Plot of rate of new PC synthesis as a function of time as measured by mass spectrometry in control experiment in the absence of drugs.

One significant maximum appears in new PC synthesis in control cultures, at six hours post synchronisation. This interval corresponds to early S phase in HeLa cells synchronised with L-mimosine (Hague 2007). Since the peak of PtdCho biosynthesis occurs at early S phase (Jackowski 1994), then these data follow exactly the expected trend. Then, rate of PtdCho biosynthesis decreased at the end of S phase and during G_2/M. Finally, new PC synthesis restarted when cells entered G1 phase again at about 18 hours post synchronisation.

III.5.2. Cultures in the presence of HDPC

III.5.2.1. Effect of drug on cell viability and size

Three different concentrations of HDPC at 10.50, 5.25 and 2.63 μM were administered on L-mimosine synchronised HeLa cells every three hours for eight time intervals up to 21 hours post synchronisation. Concentrations were chosen based on the ED_{50}[1] value for HDPC HL60 cells at 10.5 μM (Dymond 2001). Results are shown in Figure III.27.

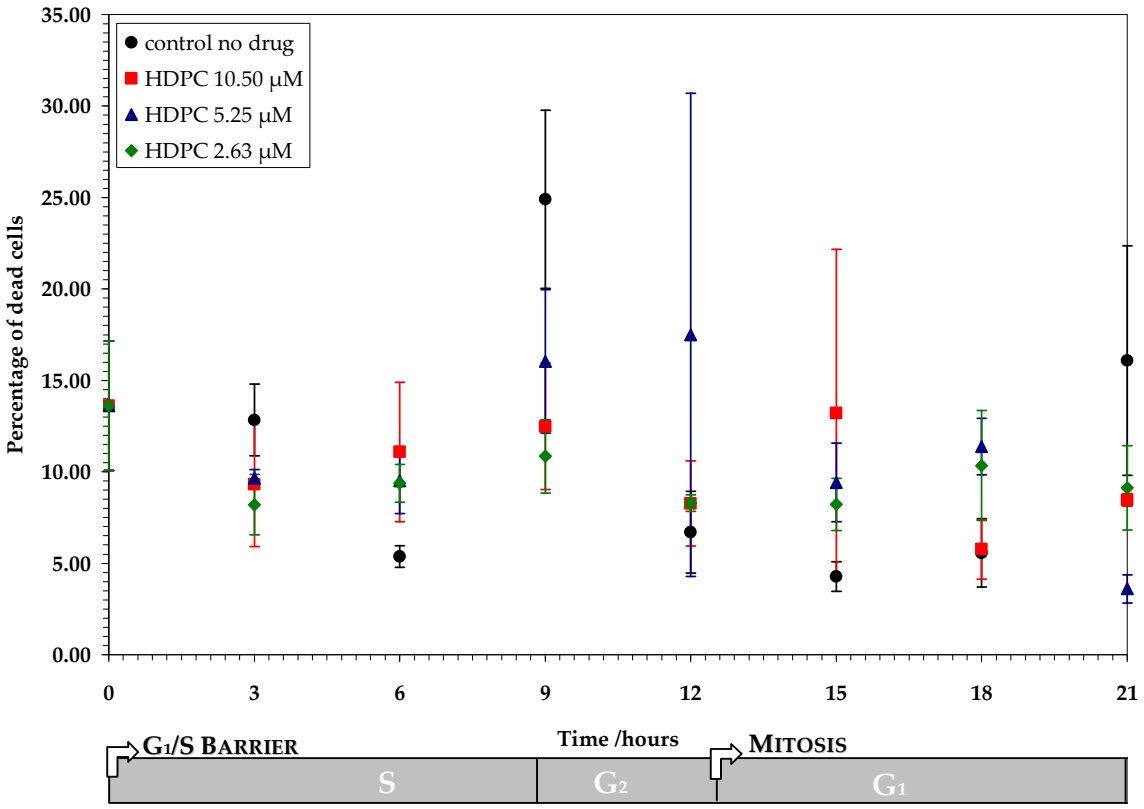

Figure III.27- Plot of percentage dead cells as a function of time in the presence of three different concentrations of HDPC.

[1] The median effective dose (ED_{50}) is the quantity of material needed to cause death to 50 percent of the population.

Distinct trends can be observed in these data, although errors are quite significant due to use of dye exclusion principle for quantifying cell viability. Even the highest concentration of HDPC did not cause marked changes in cell viability. Although HDPC at 10.50 μM corresponds to the ED_{50} value for the HL60 cell line, a higher concentration may be required to cause the same effect in the HeLa line. Also, since ED50 values for a drug are determined over a period of four days, drug effects may not be exhibited as early as the first 21 hours of the cell cycle.

All three HDPC concentrations caused a maximum in the percentage of dead cells at either nine or 12 hours post synchronisation. As explained in section III.4.1.1 for the control cultures, maxima correspond to apoptosis occurring at the end of S phase. However, it appears as if the presence of HDPC decreases the intensity of the maximal peak at nine hours and shifts it towards the next time interval. Overall, less dead cells were present in cultures incubated with HDPC throughout the cell cycle.

III.5.2.2. Effect of drugs on phospholipid metabolism

III.5.2.2.1. **Change in total lipid content**

The effect of HDPC (10.50, 5.25 and 2.63 μM) to the total lipid content per head group class in the membranes of the cultured cells was investigated by ESI-MS. The results for head group classes PC, newly synthesised PC and PE are shown in Figures III.28 to 29. Data for these plots can be found in Appendix II. Experimental methods follow in Section III.4.

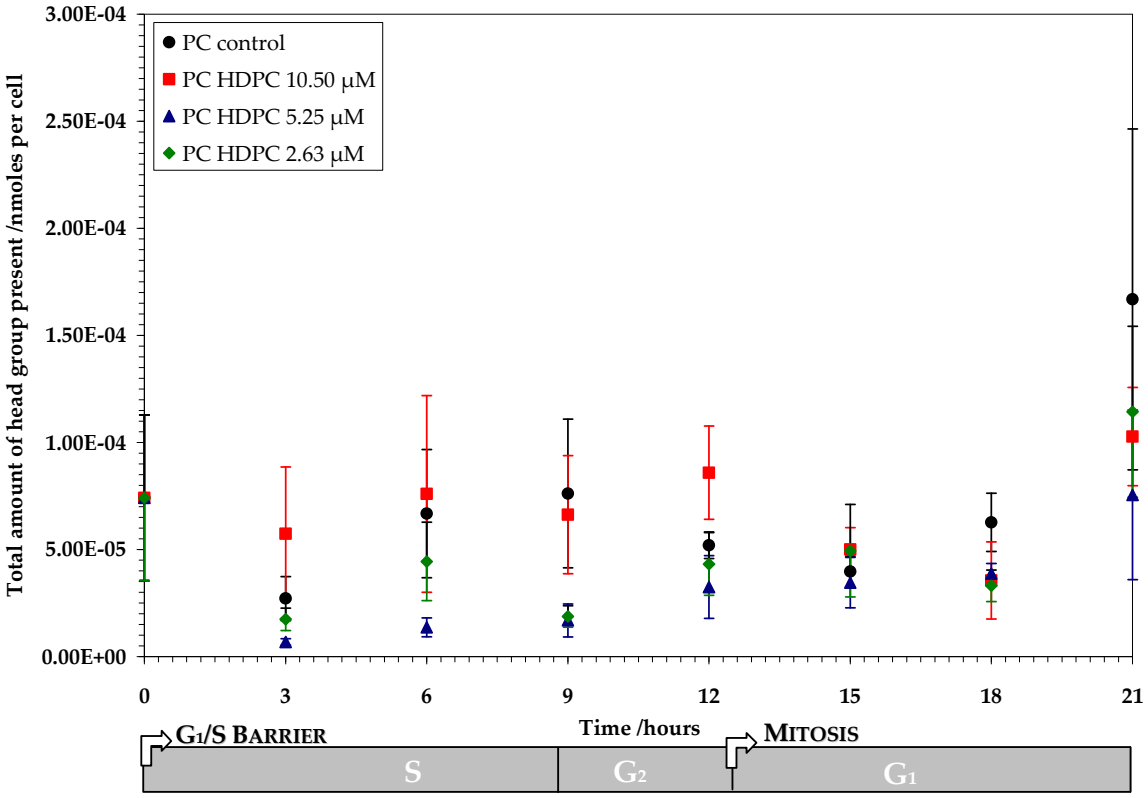

Figure IV.28- Plot of total PC head group class content as a function of time as measured by mass spectrometry in the presence of HDPC.

The two lower concentrations of HDPC at 2.63 and 5.25 μM showed a similar trend of slightly increasing the amount of endogenous PC present in the membranes of HeLa cells. On the contrary, the highest concentration of 10.50 μM had an identical trend to the control cultures, within error. Therefore, it can be concluded that, within error, HDPC did not significantly alter the amount of endogenous PC in the membrane throughout the cell cycle.

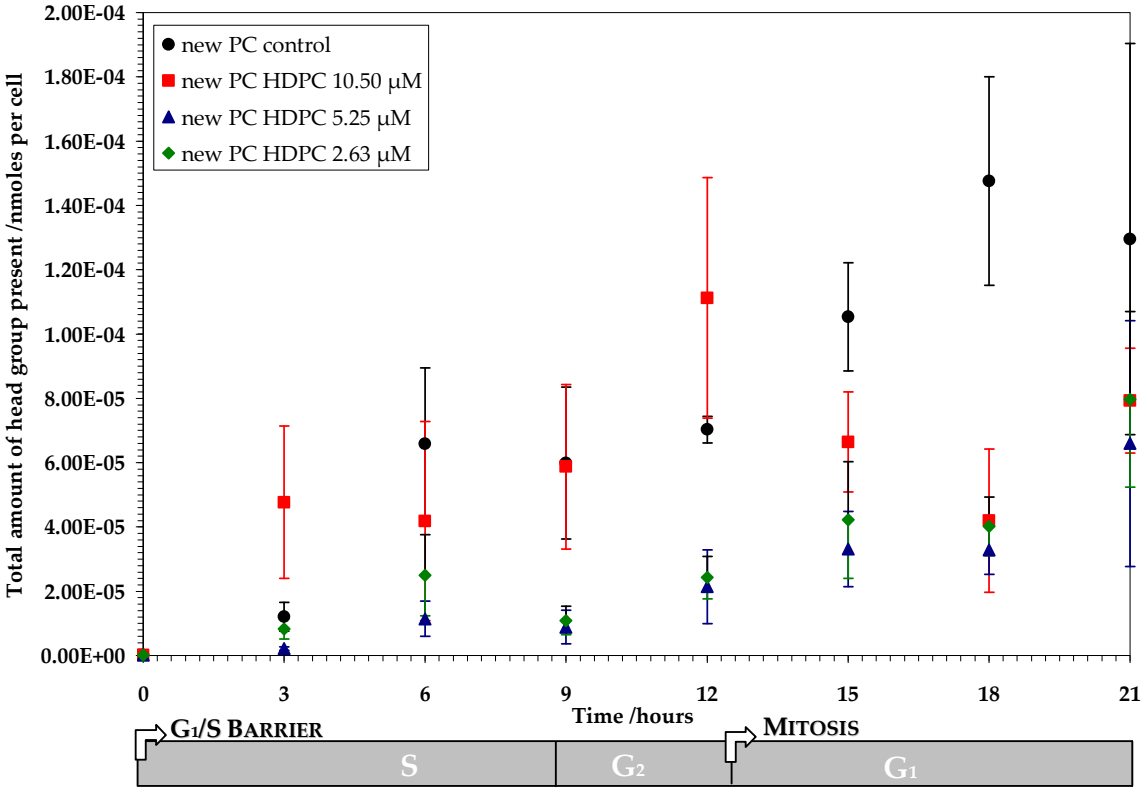

Figure III.29- Plot of total newly synthesised PC head group class content as a function of time as measured by mass spectrometry in the presence of HDPC.

The amount of new PC increases in all three HDPC concentrations, as in the control, and approximately doubles at the end of M phase, as expected from the literature. However, the same trend as for endogenous PC is observed here, with in 2.63 and 5.25 μM HDPC causing an almost identical effect of decrease compared to the control, whilst in 10.50 μM HDPC the total amount of new PC in almost the same as in the control up to 15 hours post synchronisation. After that time interval, all three drug concentrations decreased new PC present in membranes by about four-fold. The trend in the two lower concentrations supports the stored elastic stress hypothesis. HDPC, a Type I amphiphile, inhibited CCT as it partitioned in membranes due to the hydrophobic effect. PC biosynthesis was thus suppressed leading to lower amounts PC produced. It is harder to explain the results for the 10.50 μM HDPC, since new PC levels are slightly higher than for the control.

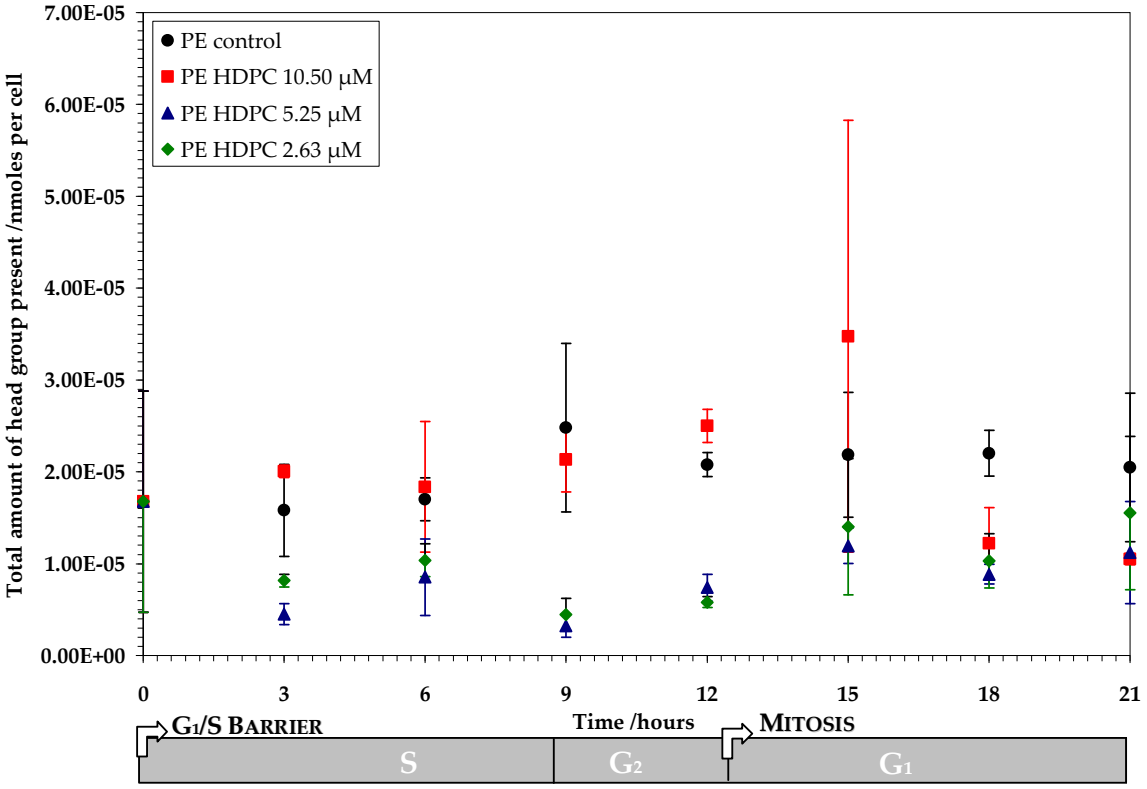

Figure III.30- Plot of total PE head group class content as a function of time as measured by mass spectrometry in the presence of HDPC.

The presence of HDPC caused a similar effect to endogenous PE as to PC. In 10.50 μM HDPC, no significant change was observed within error until 18 hours post synchronisation (Figure III.30). Then, a significant decrease of about 50 percent was observed for the last two time intervals. The two lower concentrations of HDPC showed almost identical trends and amounts of PE in membranes over the cell cycle.

Overall for the three head groups: PC, PE and d9PC the same observation was made in the presence of HDPC. At 2.63 and 5.25 μM HDPC, amounts detected by ESI-MS were significantly lower within error compared to the control. Counter-intuitively, the highest concentration of 10.50 μM HDPC showed no decrease compared to the control until 18 hours post synchronisation at the end of M phase. Then as cells divided and entered G_1, a significant decline within error occurred in the amounts for all three head groups in membranes.

As the appropriate non-physiological lipid standard for HDPC had been included in the standards mix for ESI-MS, it was possible to monitor the amount of the drug that partitioned into membranes of cultured cells. Results for all three drug concentrations are shown in Figure III.31.

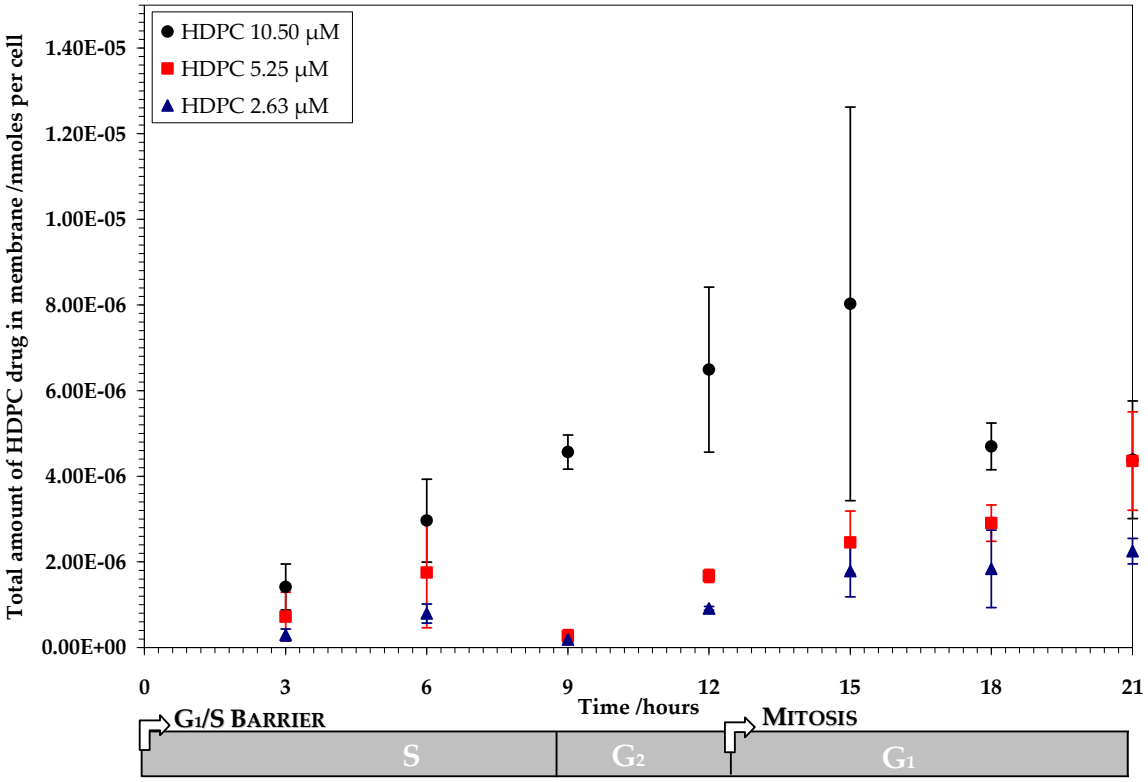

Figure III.31- Plot of HDPC drug in membrane as a function of time as measured by mass spectrometry.

HDPC uptake in the cell membrane was much more pronounced for 10.50 μM HDPC, which showing maximal partitioning at 15 hours post synchronisation during M phase. For 5.25 μM HDPC, the amount of drug in membranes was significantly smaller than for 10.50 μM and only slightly larger than for 2.53 μM. However, at 21 hours post synchronisation, almost the same amount of drug within error had partitioned for all three drug concentrations. Consequently, regardless of the concentration of HDPC, the same amount of drug partitioned in cell membranes after one full cell cycle.

Then, in the plot that follows (Figure III.32), it was attempted to correlate the amount of drug added in the culture medium to the partitioned amount. Thus, a relative measure of the drug partitioning is introduced as a coefficient K, which is the ratio of the drug amount detected in membranes by ESI-MS to the amount added in solution.

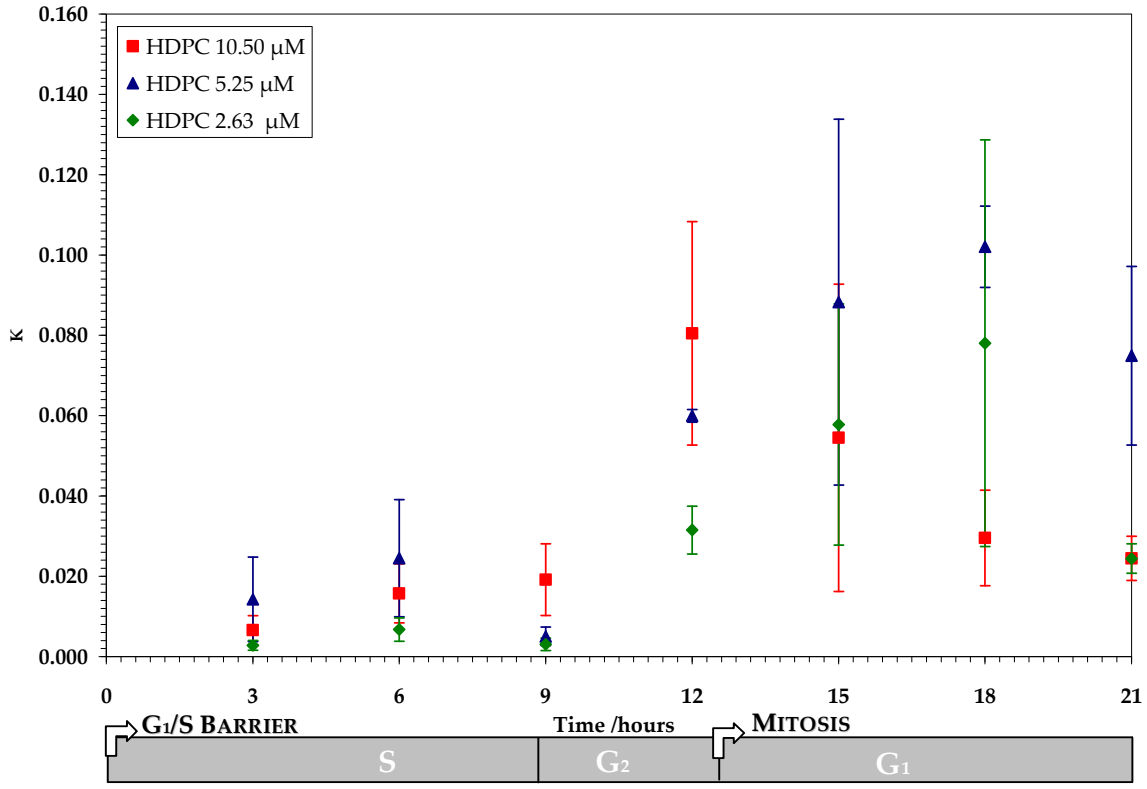

Figure III.32- Plot of partition coefficient K of HDPC drug in membrane as a function of time as measured by mass spectrometry.

The partition coefficient K is very small for the first nine hours post synchronisation but subsequently a maximum K between 0.08 and 1.00 is observed all three drug concentrations. For 10.5 μM HDPC, the maximum occurred at 12 hours whereas for the other two concentrations the effect lagged until 15 and 18 hours after synchronisation.

Consequently, it is deduced that the amount of drug that partitions to membranes after one full cell cycle is not only proportional to the drug concentration present in solution in the culture medium. On the contrary, there is a maximum amount that can potentially partition to membranes and the higher the concentration of the drug in solution, the less the time needed for this upper limit of partitioning to be attained. As seen in Figures IV.31-32, the highest concentration of HDPC reached that maximum earlier than two lower ones. However, all three concentrations partitioned to a maximum k of 0.1 and then equilibrated at a lower value.

III.5.2.2.2. **Membrane composition by mass spectrometry**

As in section III.5.1.2.2.2 for the control cells, data of percentages of the fatty acid chains that composed each of the PC, PE and newly synthesised PC head group classes. The fatty acid species are assigned by their masses to the corresponding m/z amu percentage value detected by ESI-MS. For example, for the m/z value of 788 amu, the peak is assigned to PC18:0/18:1 that has a molecular weight of 788 $g.mol^{-1}$. This has been reported to be present in large amounts in physiological membranes and thus was selected as the most likely (Boon and Smith 2002). Similarly, all peaks within the investigated range are assigned to the most probable species. It must be stressed that many of assignments are putative and not absolute, as for example between 18:0/18:2 and 18:1/18:1 species.

For endogenous PC in the presence of HDPC, the fatty acid chains with abundance higher than five percent in at least one time interval are shown in Figure III.33 in order of decreasing number of intervals above threshold.

HDPC 10.50 μM			**HDPC 5.25 μM**			**HDPC 2.63 μM**		
m/z (amu)	Species	Average %	m/z (amu)	Species	Average %	m/z (amu)	Species	Average %
786	PC18:0/ 18:2	13.35±1.43	786	PC18:0/ 18:2	13.99±1.22	786	PC18:0/ 18:2	12.56±0.72
788	PC18:0/ 18:1	8.76±1.64	788	PC18:0/ 18:1	8.07±0.83	788	PC18:0/ 18:1	8.68±1.09
758*	PC16:0/ 18:2	3.89±0.91	760	PC16:0/ 18:1	25.03±1.82	760	PC16:0/ 18:1	24.48±1.90
760	PC16:0/ 18:1	25.59±1.65	746	PC16:0a /18:1	7.69±0.84	746	PC16:0a /18:1	7.68±1.16
746	PC16:0a /18:1	6.93±0.66	732	PC16:0/ 16:1	4.59±0.45	732	PC16:0/ 16:1	4.59±0.41
732	PC16:0/ 16:1	4.14±0.57				774*	PC18:0a /18:1	4.33±0.75

Figure III.33- Table of PC head group class fatty acids with a higher than 5% abundance in the presence of HDPC drug. Values and SD are average percentages of all intervals. New species, present in less than 5% abundance in control cultures are annotated with an asterisk.

Species with m/z values 786, 788, 760, 746 and 732 are present in high abundance in all three drug concentrations. However, species at 758 amu and 774 amu are only observed at a higher than five percent abundance in HDPC 10.5 and 2.63 μM, respectively, and interestingly were not significantly present in the control cultures.

The fatty acids that showed a change compared to the control were assessed. Only species that showed within error an increment of change compared to the control larger than 10 percent of the measured value in the presence of the drug are considered as changed. For data tables of results, see Appendix II.

Overall, out of the 27 fatty acid species quantified, 13 species changed significantly in the presence of HDPC 10.50 μM, and these can be divided into three groups. Saturated compounds, PC14:0/16:0, PC14:0a/16:1, PC16:0/16:1, PC16:0/16:0 all decreased significantly in at least one time interval after 12 hours post synchronisation. Two compounds, both showing one double bond in one of their chains, PC16:0a/18:2 and PC18:0/18:2, showed an increase in their percentages after 18 hours post synchronisation. And lastly, polyunsaturated species PC16:0a/20:4, PC16:0/20:4, PC18:1a/20:4, PC18:0a/20:4, PC18:0a/20:1, PC18:1/20:4 and PC20:0a/22:6 all decreased in either or both time intervals of three and 12 hours post synchronisation.

In the presence of HDPC 5.25 μM, only PC16:0a/16:0 showed an increase at 15 and 18 hours post synchronisation. Three species, PC14:0/16:0, PC16:0/16:1 and PC16:0/16:0 decreased significantly only at the last interval at 21 hours. Finally, the most considerable trend was observed in nine polyunsaturated species that all showed a steady decrease between nine and 18 hours post synchronisation. Those were PC16:0a/20:4, PC18:1a/18:2, PC16:0/20:4, PC18:1/18:2, PC18:1a/20:4, PC18:0a/20:4, PC18:1/20:4, PC18:0/20:4 and PC18:0/20:3.

In the presence of HDPC 2.63 μM, PC16:0a/16:0 showed the same trend as in 5.25 μM. No species changed only at 21 hours but the same nine species as in 5.25 μM HDPC decreased between nine and 18 hours.

Species with the most pronounced changes are shown individually in plots (Figures III.34 to III.37). First, the most probable species at 774 amu, PC18:0a/18:1, showed considerable increase compared to the control after 12 hours post synchronisation for 2.63 and 5.25 μM HDPC. For 10.50 μM HDPC, percentages for this species are almost the same as for the control.

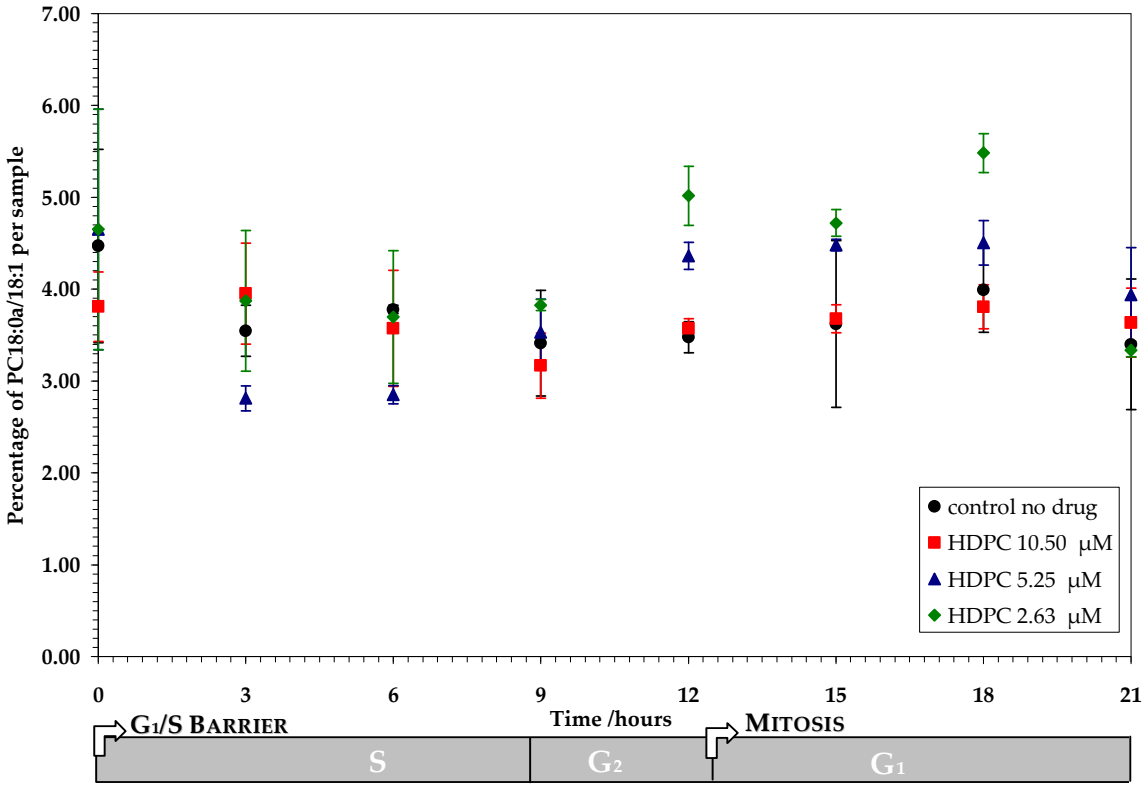

Figure III.34- Plot of percentage abundance of PC18:0a/18:1 species (774 amu) as function of time.

Second, the most likely species at 784 amu, PC18:1/18:2, fluctuated significantly albeit with the same trend compared to the control. For the first six hours post synchronisation, all three drug concentrations caused this species to increase in membranes (Figure III.35). However, after nine hours post synchronisation, the percentage of PC18:1/18:2 in the total species present decrease steadily in the presence of HDPC.

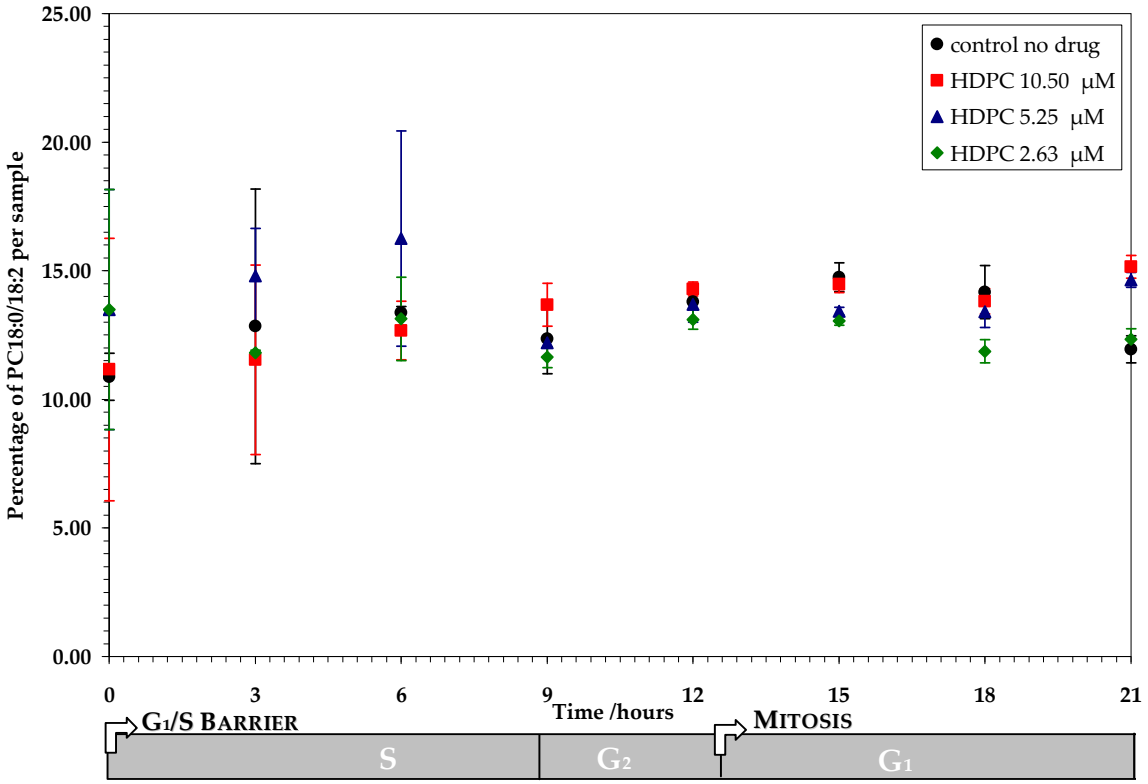

Figure III.35- Plot of percentage abundance of PC18:1/18:2 species (784 amu) as function of time.

Third, a trend for polyunsaturated species of initial increase followed by significant decrease after the nine hours interval was also observed for PC18:1/20:4 and PC18:0/20:4 as shown in Figures III.36 to 37 overleaf.

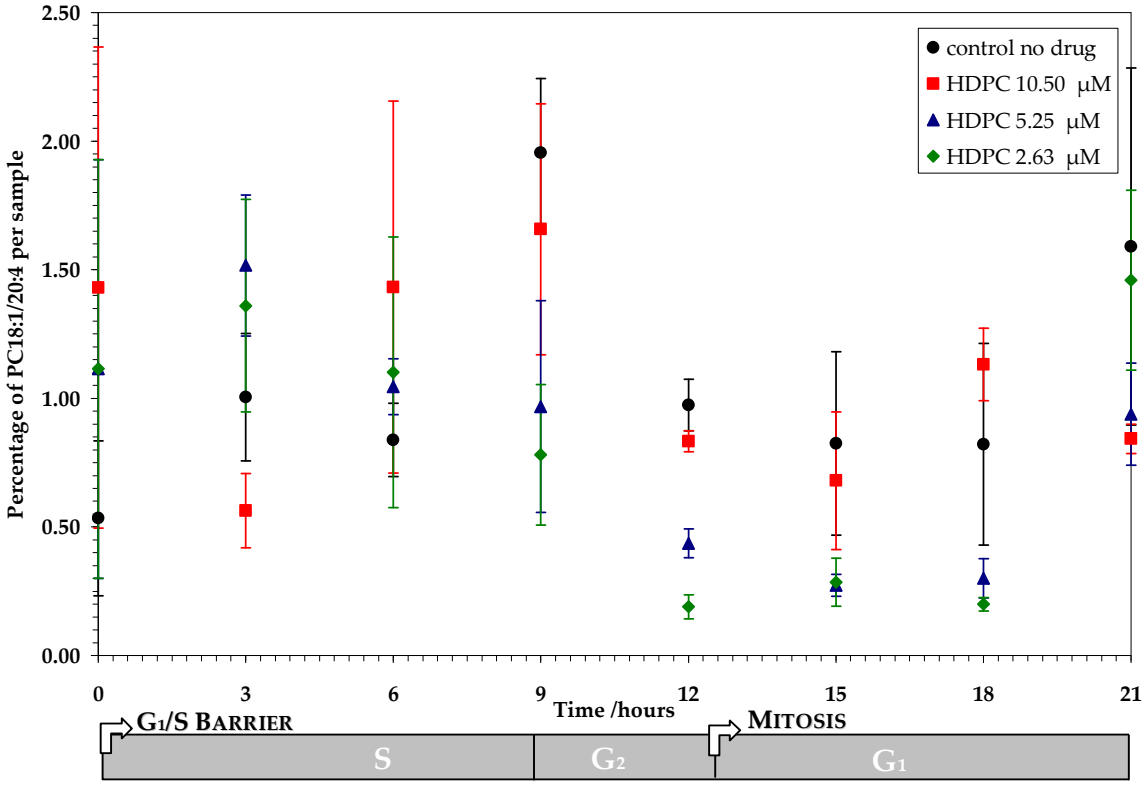

Figure III.36- Plot of percentage abundance of PC18:1/20:4 (808 amu) against time.

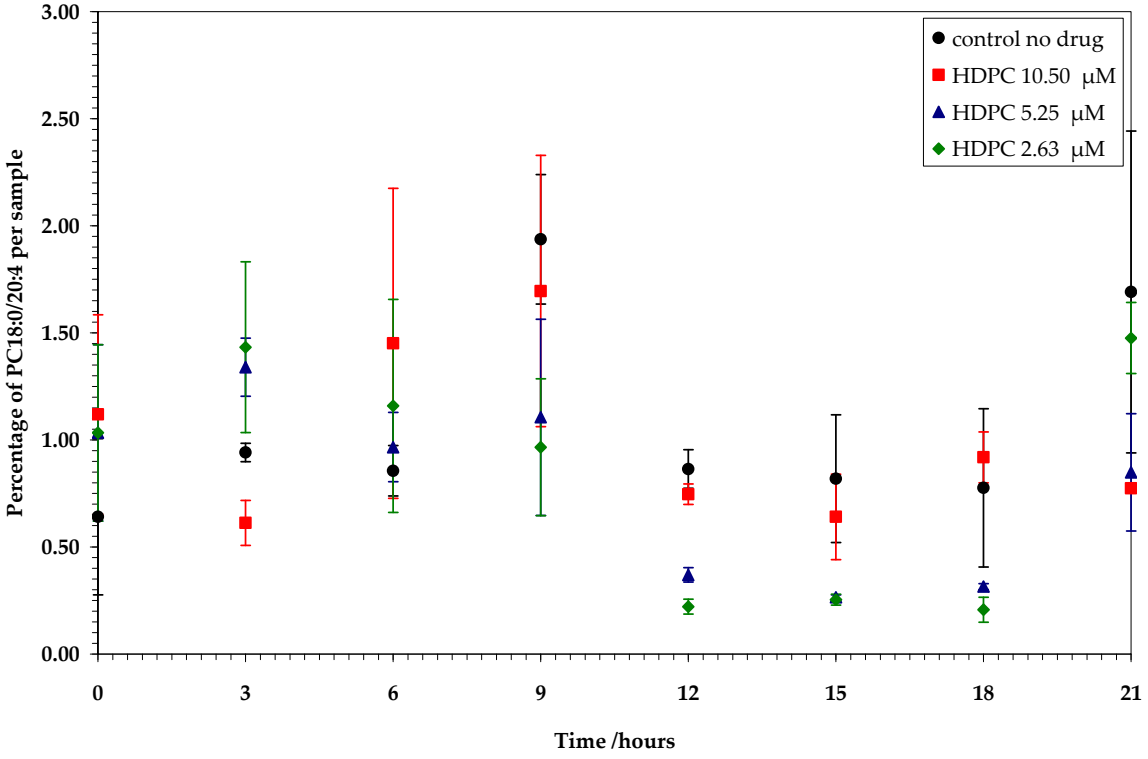

Figure III.37- Plot of percentage abundance of PC18:0/20:4 species (810 amu) against time.

For newly synthesised PC, in the presence of HDPC, the fatty acid chains with abundance higher than five percent in at least one time interval are shown in the table below (Figure III.38).

HDPC 10.50 μM			**HDPC 5.25 μM**			**HDPC 2.63 μM**		
m/z (amu)	Species	Average %	m/z (amu)	Species	Average %	m/z (amu)	Species	Average %
795	d9PC18: 0/18:2	13.72±2.50	795	d9PC18: 0/18:2	10.08±6.65	795	d9PC18: 0/18:2	13.38±2.34
797	d9PC18: 0/18:1	7.77±1.28	797	d9PC18: 0/18:1	5.71±3.76	797	d9PC18: 0/18:1	7.91±1.58
767	d9PC16: 0/18:2	4.75±1.61	767	d9PC16: 0/18:2	3.27±2.29	769	d9PC16: 0/18:1	26.51±7.95
769	d9PC16: 0/18:1	27.22±8.90	769	d9PC16: 0/18:1	20.66±15.17	755	d9PC16: 0a/18:1	6.18±1.27
755	d9PC16: 0a/18:1	5.29±0.70	755	d9PC16: 0a/18:1	4.71±2.97	741	d9PC16: 0/16:1	5.39±1.16
741	d9PC16: 0/16:1	4.73±1.04	741	d9PC16: 0/16:1	4.10±2.18	687*	d9PC14: 0/14:0	1.26±3.12
743*	d9PC16: 0/16:0	3.94±0.80						

Figure III.38- Table of d9PC head group class fatty acids with a higher than 5% abundance in the presence of HDPC drug. Values and SD are average percentages of all intervals. New species, present in less than 5% abundance in control cultures are annotated with an asterisk.

Species with m/z values 795, 797, 769, 755 and 741 are present in high abundance in all three drug concentrations and the control. d9PC16:0/18:2 at 767 amu is present at the 10.50 and 5.25 μM HDPC, and the control but not present in more than five percent in the smaller dug concentration. Also, d9PC16:0/16:0 at 743 amu was not significantly present in control cultures but is in 10.50 μM HDPC.

Then, the fatty acids that showed a change compared to the control were assessed.

In the presence of HDPC 10.50 μM, some but very subtle changes compared to the control were observed. Ten polyunsaturated species decreased in the intervals between 3 and 12 hours post synchronisation: d9PC16:0a/20:4, d9PC16:0/20:4, d9PC18:0/18:2, d9PC18:1a/20:4, d9PC18:0a/20:4, d9PC18:0a/20:2, d9PC16:0/22:6, d9PC18:1/20:4, d9PC18:0/20:4 and d9PC18:0/20:3.

In the presence of HDPC 5.63 μM, ten polyunsaturated species showed a steady decrease between nine and 18 hours post synchronisation: d9PC16:0a/20:4, d9PC18:1a/18:2, d9PC16:0/20:4, d9PC18:1/18:2, d9PC18:1a/20:4, d9PC16:0/22:6, d9PC18:1/20:4, d9PC18:0/20:4 and d9PC18:0/20:3. Also, three species increased between nine and 15 hours: d9PC16:0a/16:0, d9PC16:0/16:1 and d9PC16:0/18:1.

In the presence of HDPC 2.63 μM, the same ten polyunsaturated species decreased as in 5.63 μM. Also, seven saturated and mono-unsaturated species increased their percentage in membranes at various time intervals, not following any trend. For exact values and species, see data tables in Appendix II.

Two plots illustrating the decreasing trend of polyunsaturated species in shown in Figures IV.39 and 40 for d9PC16:0/20:4 and d9PC18:1/18:2, respectively, that had the most pronounced decrease in the presence of HDPC.

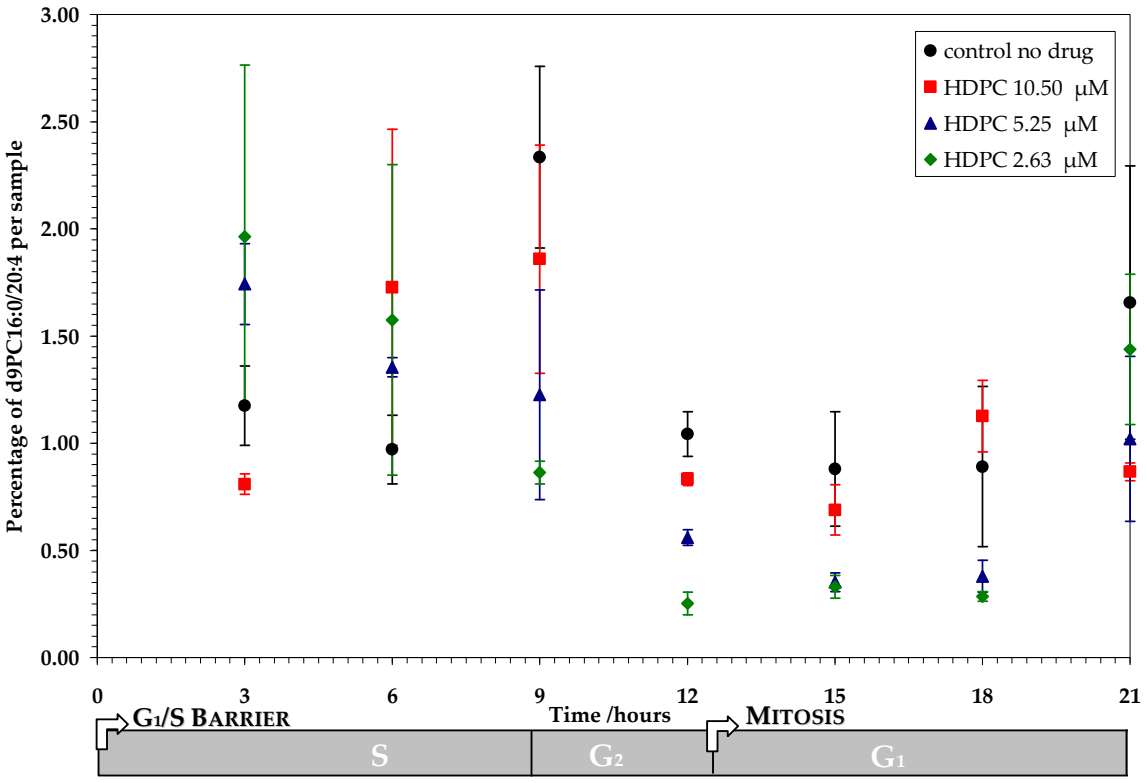

Figure III.39- Plot of percentage abundance of d9PC16:0/20:4 species (791 amu) against time.

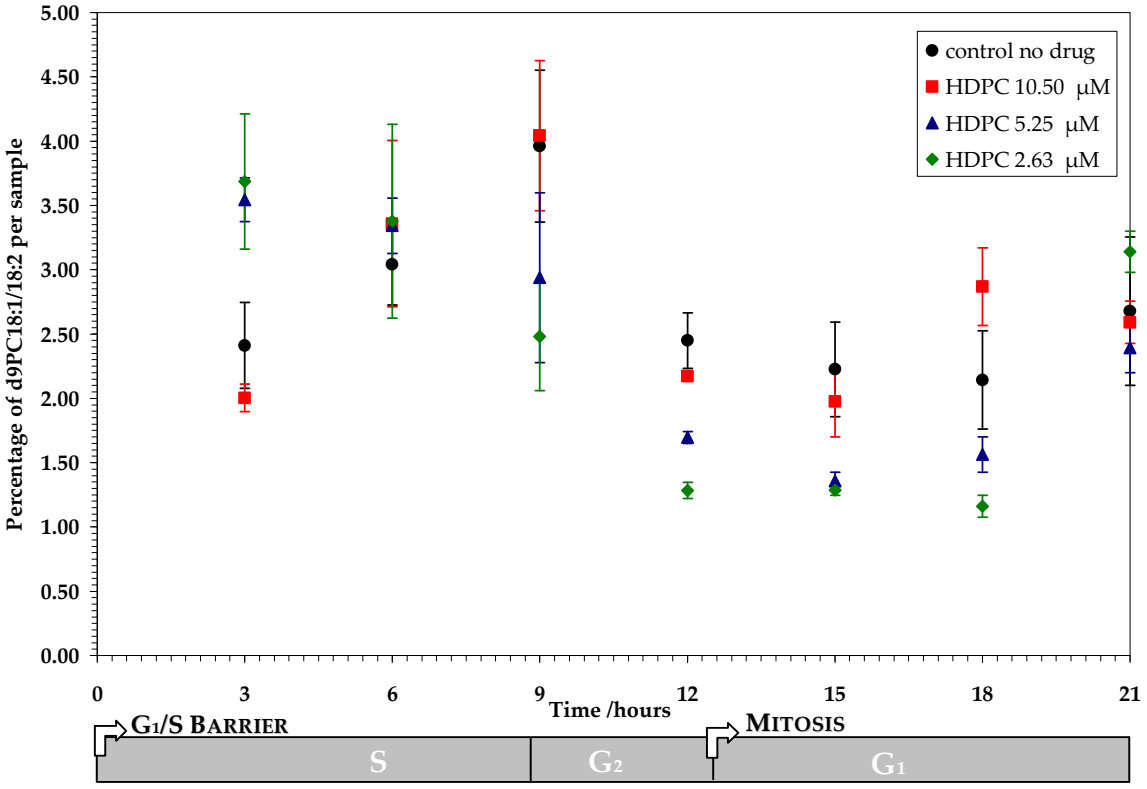

Figure III.40- Plot of percentage abundance of d9PC18:1/18:2 species (793 amu) against time.

For endogenous PE, in the presence of HDPC, the fatty acid chains with abundance higher than five percent in at least one time interval are shown in Figure III.41.

HDPC 10.50 μM			**HDPC 5.25 μM**			**HDPC 2.63 μM**		
m/z (amu)	Species	Average %	m/z (amu)	Species	Average %	m/z (amu)	Species	Average %
718	PE16:0/18:1	11.60±1.45	718	PE16:0/18:1	12.12±3.20	718	PE16:0/18:1	12.08±3.94
744	PE18:0/18:2	22.52±2.43	744	PE18:0/18:2	22.85±1.81	744	PE18:0/18:2	21.37±2.93
746	PE18:0/18:1	22.95±4.10	746	PE18:0/18:1	23.08±5.84	746	PE18:0/18:1	23.16±5.30
766*	PE18:1/20:4	2.55±2.06	766*	PE18:1/20:4	2.90±2.05	766*	PE18:1/20:4	2.49±1.95
768	PE18:0/20:4	6.32±2.66	768	PE18:0/20:4	6.55±3.05	768	PE18:0/20:4	6.97±4.83
772	PE18:0/20:2	5.92±0.77	772	PE18:0/20:2	5.67±1.31	772	PE18:0/20:2	5.55±1.49
792	PE18:0/22:6	4.33±0.62	790	PE18:0a/22:0	1.83±1.68	790	PE18:0a/22:0	2.70±2.41
			792	PE18:0/22:6	4.41±1.76	792	PE18:0/22:6	4.56±1.75

Figure III.41- Table of PE head group class fatty acids with a higher than 5% abundance in the presence of HDPC drug. Values and SD are average percentages of all intervals. New species, present in less than 5% abundance in control cultures are annotated with an asterisk.

PE head group class species with m/z values of 718, 744, 746, 772, 768 and 792 are present in high abundance in all three drug concentrations and the control. PE18:0a/22:0 at 790 amu is present at the 5.25 and 2.63μM HDPC, and the control but not present in more than five percent in the smaller dug concentration. Also, PE18:0a/18:1 at 732 amu was significantly present in control cultures but not in any of HDPC concentrations.

Then, the fatty acids that showed a change compared to the control were assessed. In the presence of HDPC 10.50 μM, PE16:0/18:1 at 718 amu showed a very significant increase of 1.51 percent compared to the control at 21 hours post synchronisation (see Figure III.42). Three polyunsaturated species, PE16:0/22:6,

PE18:0/20:4 and PE18:0/20:3, decreased to a maximum of 3.01 percent in the intervals between 12 and 21 hours.

In the presence of HDPC 5.25 μM, PE16:0/18:1 at 718 amu increased consistently between 12 and 18 hours (see Figure IV.42). PE18:0/18:1 at 746 amu showed an initial decrease for the first six hours, followed by a marked and consistent increase from nine to 15 hours post synchronisation (see Figure IV.43). Five polyunsaturated species, PE18:1/18:2, PE16:0/22:6, PE18:0/20:4, PE18:0/22:6, PE18:0/22:5, showed an increase between three and six hours, followed by significant decrease between 12 and 18 hours post synchronisation. Lastly, six other unsaturated species, PE18:0a/18:1, PE18:0/20:2, PE18:0/20:1, PE18:0a/22:1, PE18:0/22:3, PE18:0/22:2, decreased noticeably between three and six hours post synchronisation but remained unchanged within error for the remainder of the investigated time interval.

In the presence of HDPC 2.63 μM, PE16:0/18:1 at 718 amu showed the same increasing trend as for in the two higher HDPC concentrations (see Figure IV.42). PE18:0/18:1 at 746 amu also fluctuated similarly as in 5.25 μM HDPC. PE16:0/22:6, PE18:0/20:3, PE18:0a/22:0, PE18:0/22:6 and PE18:0/22:3 decreased between 12 and 18 hours. PE18:1/20:4, PE18:0/20:4 and PE18:0/22:5 increased noticeably at 3 hours, and then decreased between 12 and 18 hours. Finally, PE18:0/20:2 decreased by a maximum of 1.43 percent between three and six hours and then remained unchanged.

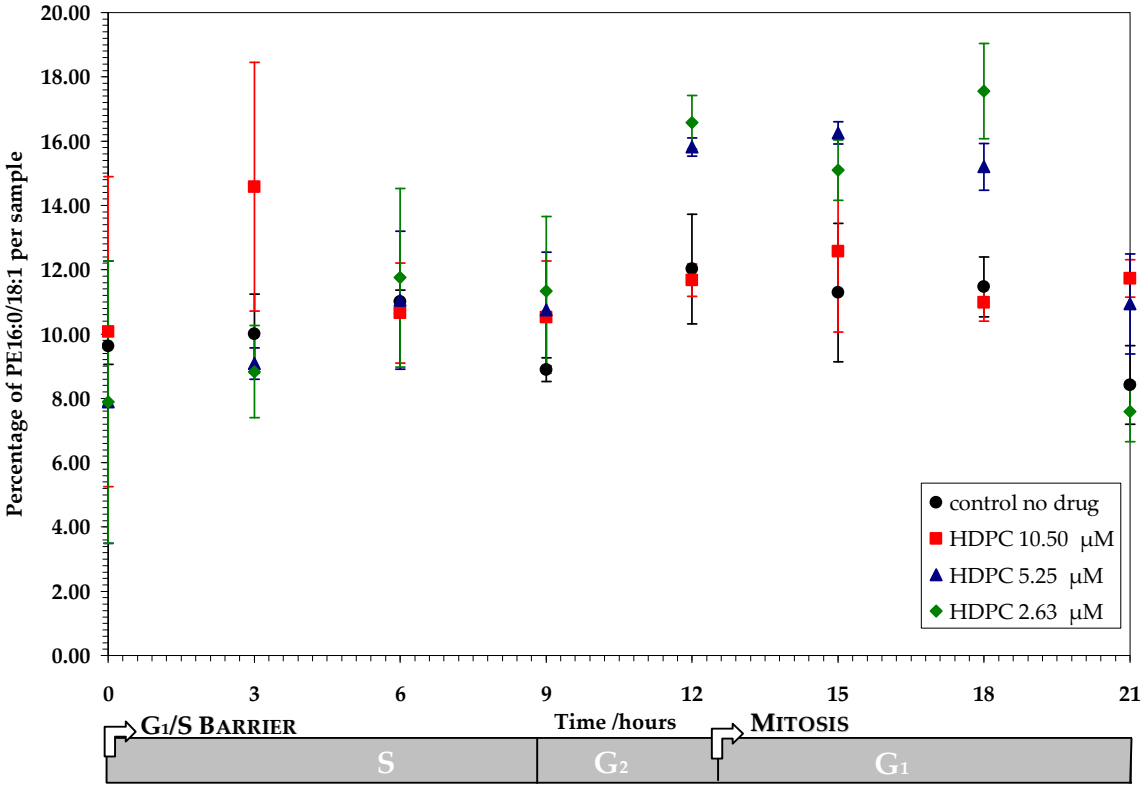

Figure III.42- Plot of percentage abundance of PE16:0/18:1 species (718 amu) against time.

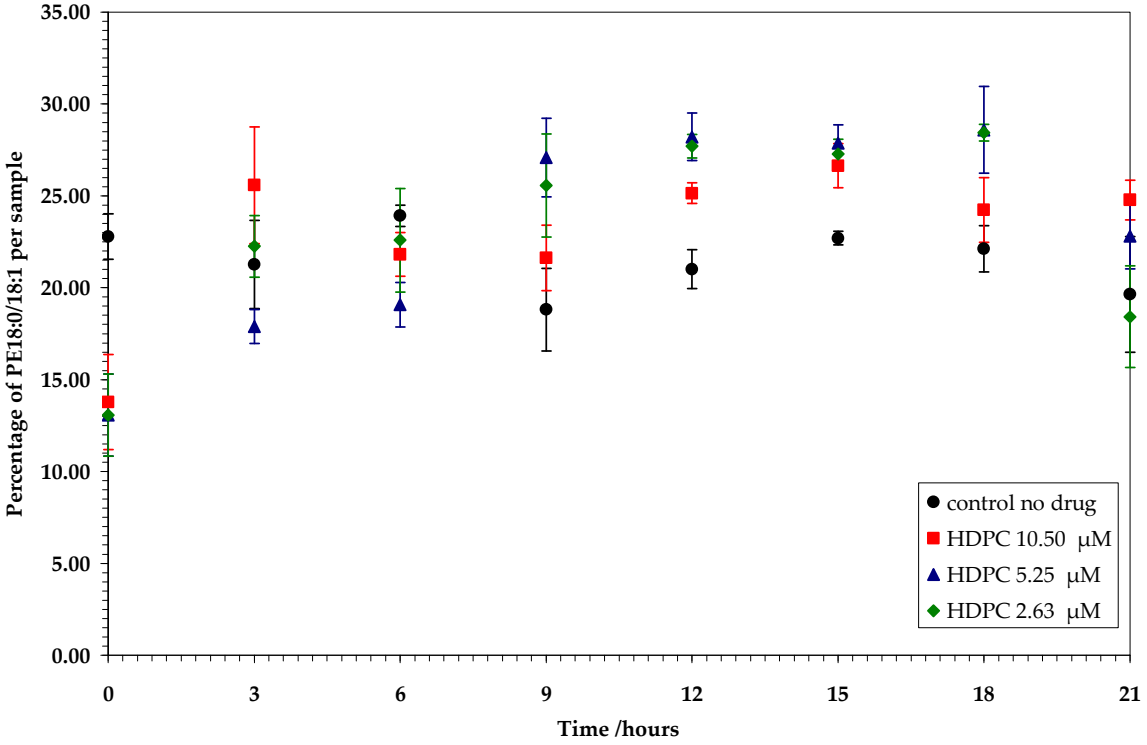

Figure III.43- Plot of percentage abundance of PE18:0/18:1 species (746 amu) against time.

III.5.2.2.3. **Rate of new PC synthesis in the presence of drug**

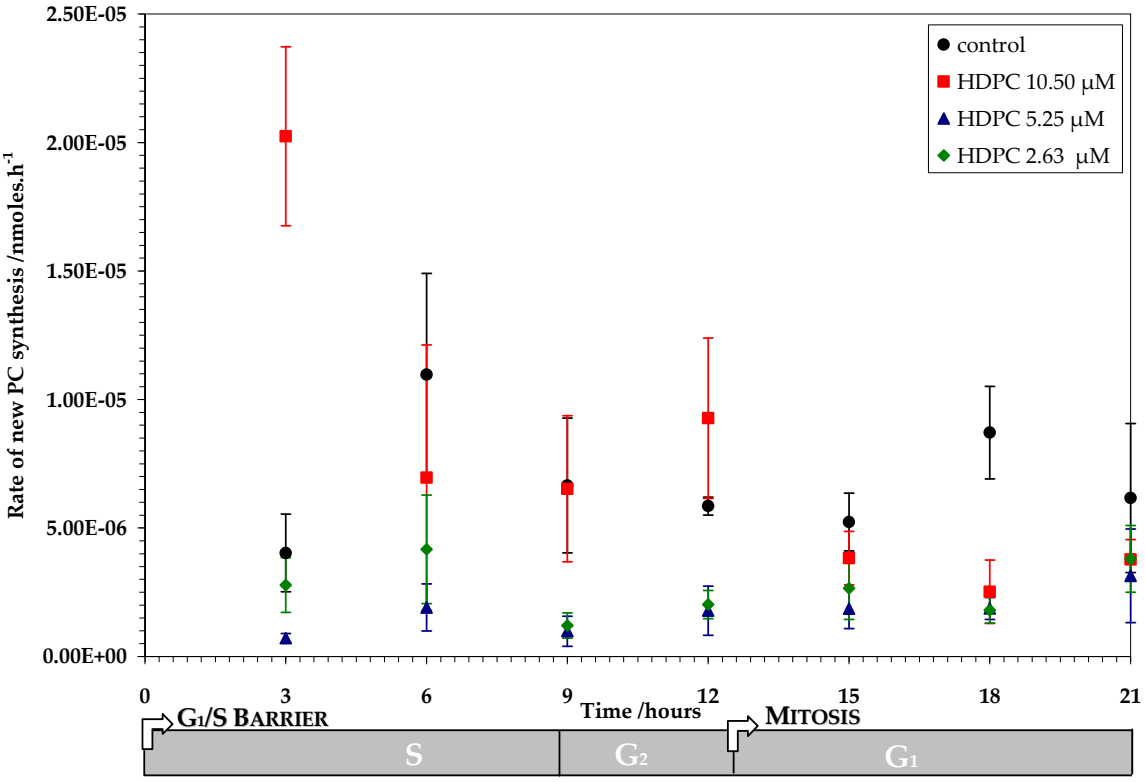

Figure III.44- Plot of rate of new PC synthesis as a function of time as measured by mass spectrometry in control experiment in the presence of HDPC drug.

In Figure III.44, all three drug concentrations appear to have decreased the rate of new PC synthesis present in the membranes of HeLa cells. Although, data for the highest concentration of 10.50 µM have quite significant errors, it can be concluded that our results are in line with the stored elastic stress hypothesis.

Overall, HDPC suppressed synthesis of new PC, which is what would be expected if a Type I amphiphile had integrated into membranes, thereby increasing the stored elastic stress and inhibiting CCT and in consequence PC biosynthesis.

III.5.3. Cultures in the presence of CTAB

III.5.3.1. Effect of drug on cell viability and size

Three different concentrations of CTAB at 3.00, 1.50 and 0.75 μM were administered on L-mimosine synchronised cell lines of HeLa cells every three hours for eight time intervals up to 21 hours post synchronisation. Concentrations were chosen based on the ED_{50} value for CTAB in HL60 cells at 3.00 μM (Dymond 2001). Results are shown in Figure III.45.

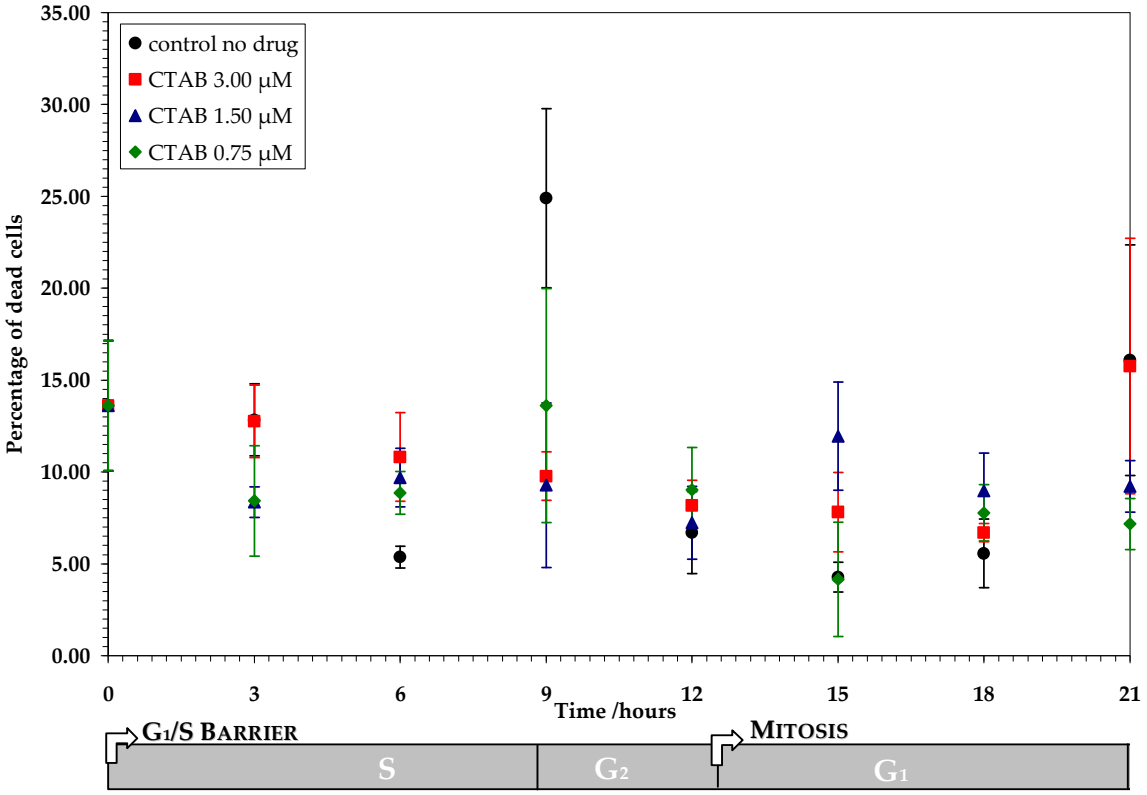

Figure III.45- Plot of percentage dead cells as a function of time in the presence of three different concentrations of CTAB.

Similarly to HDPC, CTAB does not cause any significant changes in cell viability within error in the synchronised HeLa cultures. The reasons, as discussed in section III.5.2.1 for HDPC, may be that the drug concentration is not high enough to cause cell death and that the investigated period of 21 hours is not long enough to see the effects.

III.5.3.2. Effect of drugs on phospholipid metabolism

III.5.3.2.1. **Change in total lipid content by mass spectrometry**

Similarly to HDPC, the effect of CTAB (3.00, 1.5 and 0.75 μM) to the total lipid content per head group class in the membranes of the cultured cells was investigated by ESI-MS. The results for head group classes PC, newly synthesised PC, and PE are shown in Figures III.46 to III.48. Data for these plots can be found in Appendix II. For experimental methods, see section III.4.

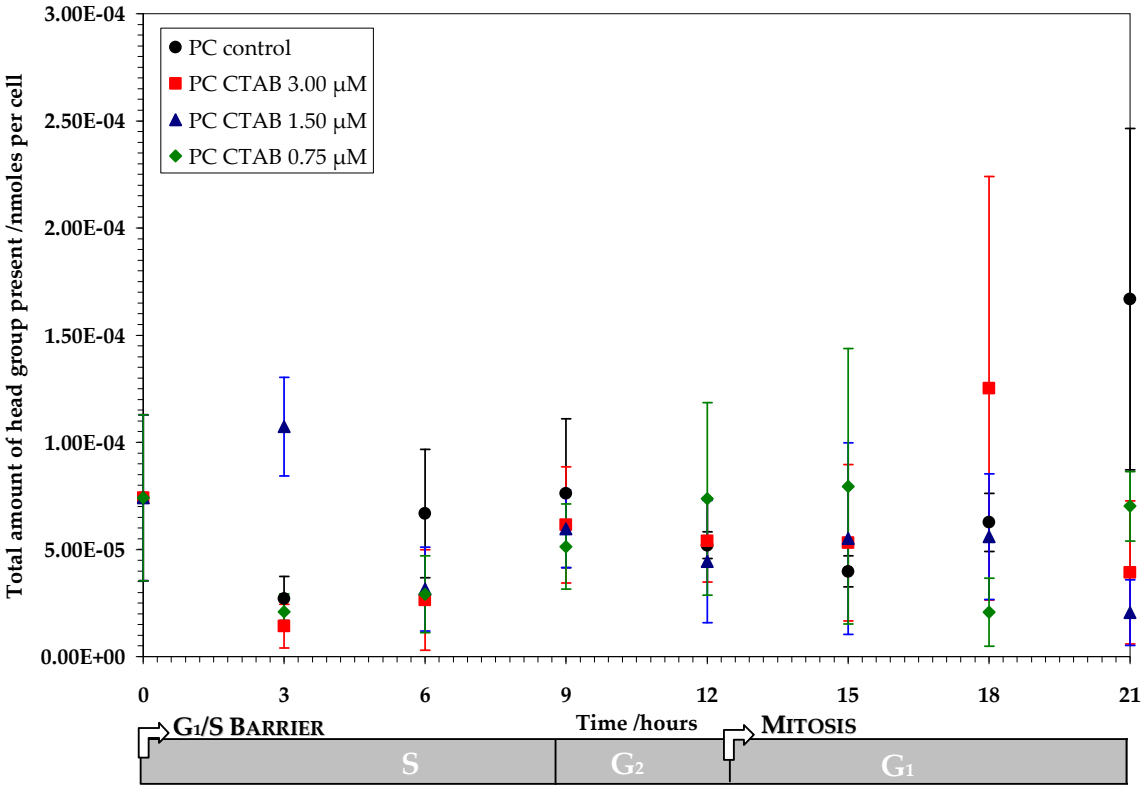

Figure III.46- Plot of total PC head group class content as a function of time as measured by mass spectrometry in the presence of CTAB.

If the point a three hours for 1.50 μM CTAB is considered an outlier, then overall all three concentrations of the drug showed a decrease of total endogenous PC in membranes. It has to be noted that errors are quite significant in these data compared to those acquired for HDPC (Figure III.27), but the same trend of some decrease in the presence of the drug is observed in both.

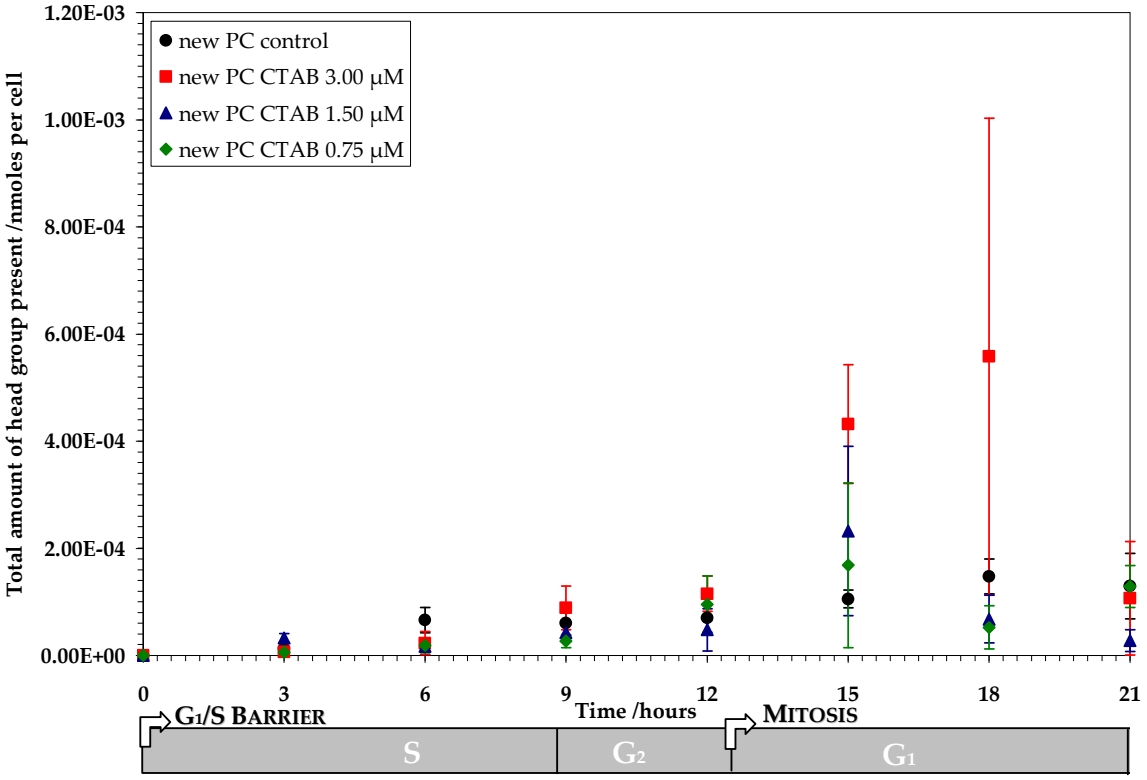

Figure III.47- Plot of total newly synthesised PC head group class content as a function of time as measured by mass spectrometry in the presence of CTAB.

Data points for 3.00 μM CTAB at 15 and 18 hours post synchronisation appear to be outliers with very large errors. As seen previously with endogenous PC, the total amount of newly synthesised PC did not appear to change significantly within error in the presence of CTAB during the cell cycle (Figure III.47). This is an unexpected result since at least some decrease in PC synthesis should appear, similarly to HDPC (Figure III.28). Although both drugs are Type I amphiphiles, they may affect PC biosynthesis by a different mechanism. CTAB may not decrease the total amount of newly synthesised PC, but it could potentially change the composition of the synthesised species in membranes during the cell cycle.

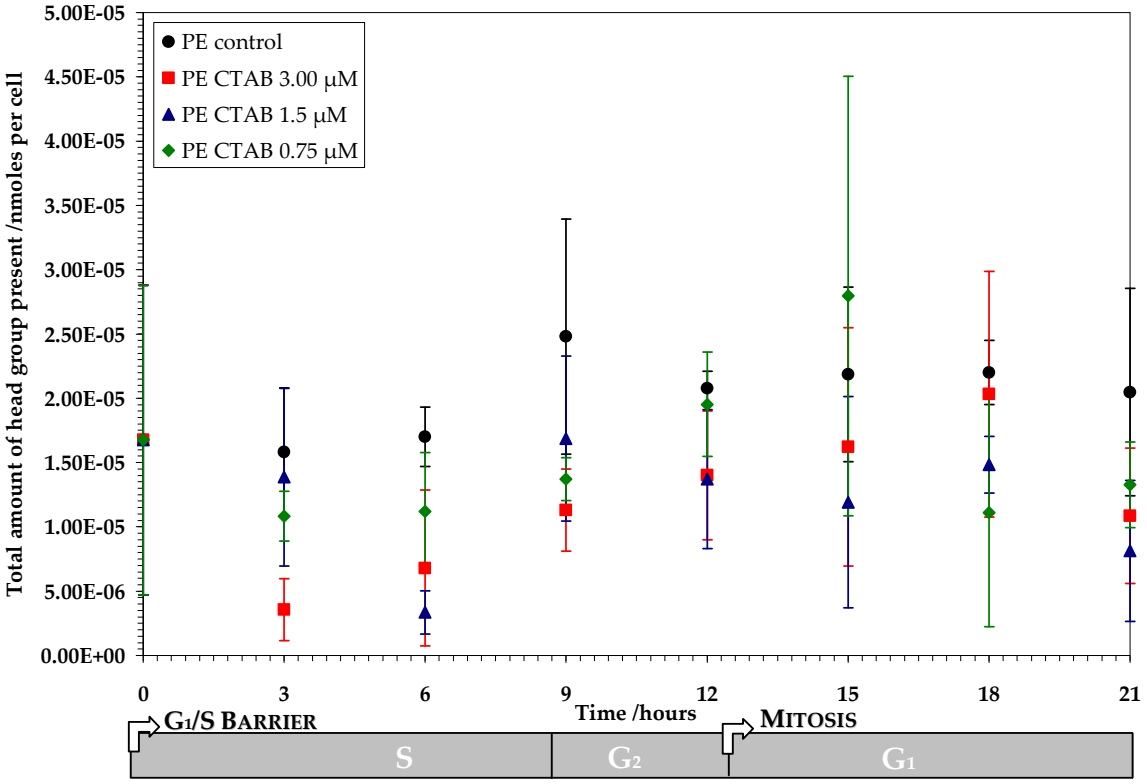

Figure IV.48- Plot of total PE head group class content as a function of time as measured by mass spectrometry in the presence of CTAB.

All three concentrations of CTAB caused a decrease of endogenous PE synthesis (Figure III.48) during the cell cycle. As for PC and d_9PC, errors for these data are quite significantly larger than for HDPC, but the same trend of endogenous PE decrease in membranes is observed in the presence of both drugs.

Overall, for all three head groups PC, d_9PC and PE, CTAB had less pronounced effects compared to HDPC and larger errors in data. However, it can still be concluded that endogenous PC and PE both decreased in the presence of CTAB. Conversely, the latter drug did not affect the synthesis of new PC in membranes within error. The decrease in endogenous PC is in line with PC biosynthesis being suppressed by the presence of a Type I amphiphile increasing the stored elastic stress of membranes and thus inhibiting CCTα. As less PC is being synthesised, PE biosynthesis is also inhibited since PC is the precursor for PE.

The amount of CTAB that partitioned into membranes was also quantified by ESI-MS. Results illustrated in Figure III.49.

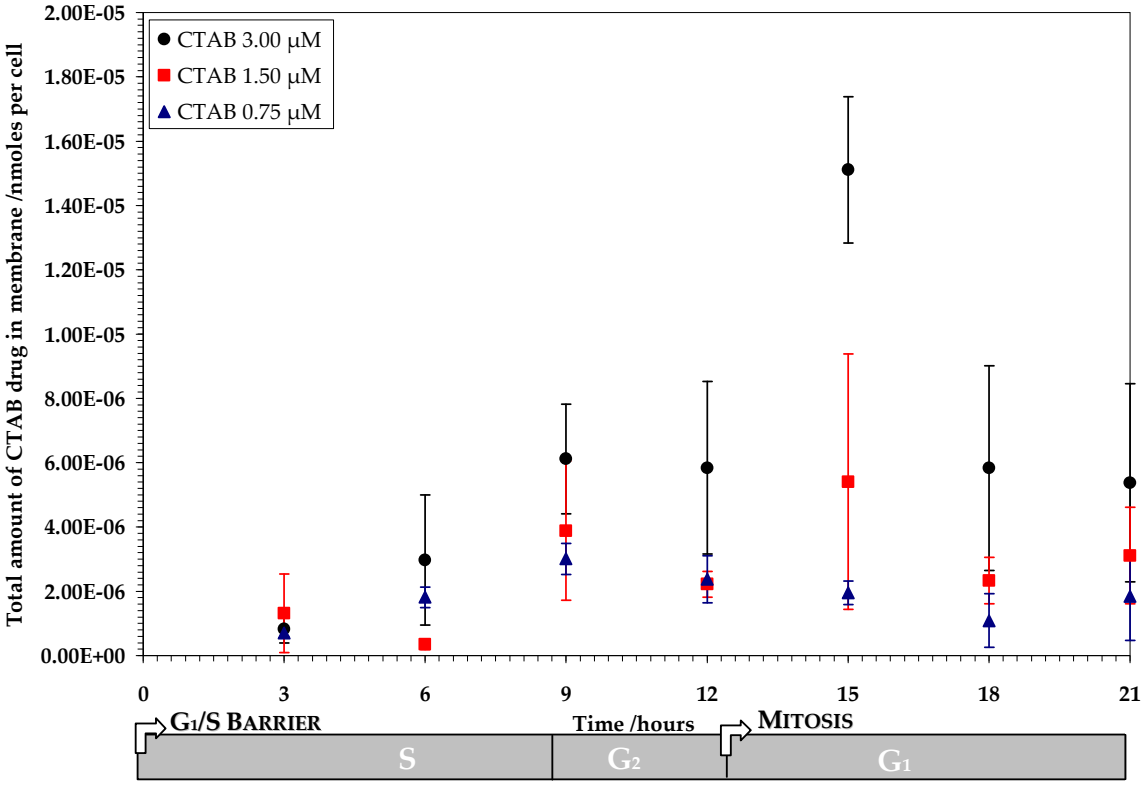

Figure III.49- Plot of CTAB drug in membrane as a function of time as measured by mass spectrometry.

Partitioning of CTAB in membranes followed an identical trend to HDPC (see Figure III.31). In the highest concentration of 3.00 μM, CTAB partitioned the most and peaked at 15 hours, exactly as seen with the highest concentration of HDPC. The two lower concentrations of 1.50 and 0.75 μM CTAB had almost the same amount of drug passing from solution into the membrane. Finally, all three concentrations showed the same amount present in the membrane at 21 hours post synchronisation. Consequently, as for HDPC, the same amount of CTAB drug partitioned in cell membranes after one full cell cycle, regardless of total drug concentration available. All three concentrations tested showed maximal membrane partitioning during M phase.

As for HDPC in Figure IV.32, a plot of the partition coefficient, K, as a function of time is presented (Figure III.50). Partition coefficient defined as for HDPC in section III.5.2.2.1.

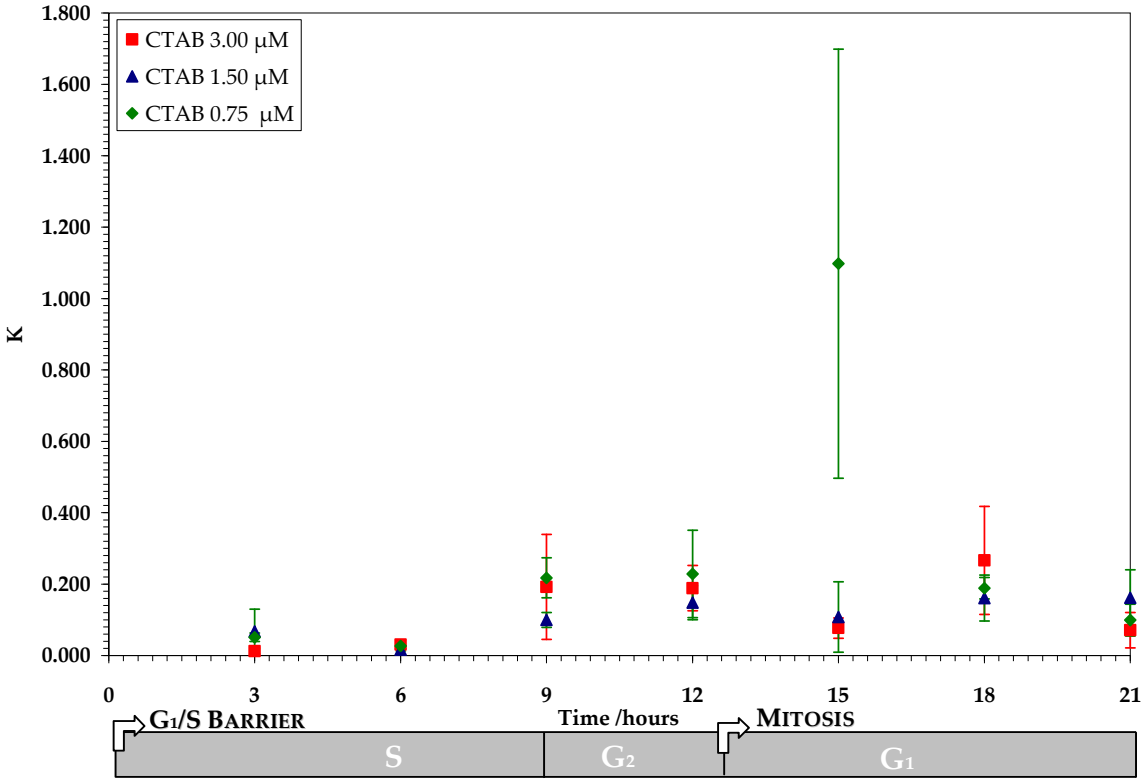

Figure III.50- Plot of partition coefficient K of CTAB drug in membrane as a function of time as measured by mass spectrometry.

In contrast to HDPC that showed a maximum K of 0.1, K for all three CTAB concentrations fluctuated at much higher values. Interestingly, there was not any significant difference between the three concentrations, excluding the point at 15 hours for 0.75 μM CTAB. The latter is probably an outlier, as suggested by the error bar that is noticeably larger to the others acquired for this series of experiments. Our results for K in CTAB further support the argument suggested for k data from HDPC that there is a maximum amount of drug that can partition to membranes, which is not proportional to the concentration of drug in solution, but depends on the drug itself. For further discussion, see conclusions section III.6.

III.5.3.2.2. **Membrane composition by mass spectrometry**

As in Section III.5.1.2.2.2 for control cells and in HDPC, data of percentages of the fatty acid chains that composed each of the PC, PE and newly synthesised PC head group classes. For endogenous PC in the presence of CTAB, the fatty acid chains with abundance higher than five percent in at least one time interval are shown in Figure III.51 in order of decreasing number of intervals above threshold.

CTAB 3.00 μM			**CTAB 1.50 μM**			**CTAB 0.75 μM**		
m/z (amu)	Species	Average %	m/z (amu)	Species	Average %	m/z (amu)	Species	Average %
732	PC16:0/ 16:1	6.03±1.19	732	PC16:0/ 16:1	5.15±0.97	732	PC16:0/ 16:1	4.86±0.37
734	PC16:0/ 16:0	3.87±0.72	746	PC16:0a /18:1	7.27±0.42	746	PC16:0a /18:1	6.34±0.50
746	PC16:0a /18:1	8.21±1.52	760	PC16:0/ 18:1	23.95±2.70	758*	PC16:0/ 18:2	4.10±0.68
758*	PC16:0/ 18:2	4.23±0.73	786	PC18:0/ 18:2	13.24±1.91	760	PC16:0/ 18:1	23.62±1.62
760	PC16:0/ 18:1	23.47±2.34	788	PC16:0/ 16:0	7.11±1.73	786	PC18:0/ 18:2	13.88±2.10
786	PC18:0/ 18:2	12.48±1.22	848*	PC20:0a /22:6	2.25±2.53	788	PC16:0/ 16:0	7.44±0.71
788	PC16:0/ 16:0	6.43±1.90						

Figure III.51- Table of PC head group class fatty acids with a higher than 5% abundance in the presence of CTAB drug. Values and SD are average percentages of all intervals. New species, present in less than 5% abundance in control cultures are annotated with an asterisk.

Species with m/z values 786, 788, 760, 746 and 732 are present in high abundance in all three drug concentrations as were in the control. However, two new species showed significant abundance in the presence of CTAB: PC16:0/18:2 at 758 amu in 3.00 and 0.75 μM, and PC20:0a/22:6 at 774 amu in 1.50 μM.

Then, the fatty acids that showed a change compared to the control were assessed. Only species that showed within error an increment of change compared to the control larger than ten percent of the measured value in the presence of the drug are considered as changed. For data tables of results, see Appendix II.

Overall, 21 species changed significantly in the presence of 3.00 μM CTAB out of the 27 fatty acid species quantified and they can be divided into two groups. First, nine compounds showing no or mono-unsaturation increased mostly in the interval between nine and 18 hours post synchronisation. Those were PC16:0a/16:1, PC16:0a/16:0, PC16:0/16:1, PC16:0/16:0, PC16:0a/18:1, PC16:0a/18:0, PC16:0/18:2, PC18:1a/18:2 and PC18:0a/18:2. The most pronounced increase trend appeared in PC16:0/16:1 shown in Figure IV.52. Second, twelve polyunsaturated compounds decreased in the interval between 12 and 18 hours: PC16:0/20:4, PC18:1/18:2, PC18:0/18:2, PC18:0/18:1, PC18:1a/20:4, PC18:0a/20:4, PC18:0a/20:2, PC18:0a/20:1, PC18:1/20:4, PC18:0/20:4, PC18:0/20:3 and PC18:0/20:2. The most pronounced decrease trend appeared in PC18:0/18:1 (Figure III.53).

In the presence of 1.50 μM CTAB, five saturated and mono-unsaturated species, PC14:0/16:0, PC16:0a/16:0, PC16:0/16:1, PC16:0/16:0, PC18:0a/20:1 increased but in the interval between three and nine hours. However, the increase in percentages was much smaller than in 3.00 μM CTAB. Similarly as in the latter, poly-unsaturated species in 1.50 μM CTAB decreased but to a lesser degree and between three and 15 hours in their majority.

Finally, in 0.75 μM CTAB, the increase in saturated and mono-unsaturated species was less pronounced and its effect further reduced between three and six hours post synchronisation. Interestingly, some polyunsaturated species, PC16:0/20:4, PC18:1/18:2, PC18:1/20:4 and PC18:0/20:4, increased slightly in the intervals between three and six hours. As in the previous higher concentrations of CTAB, a few unsaturated species with longer chains decreased but only between three and six hours.

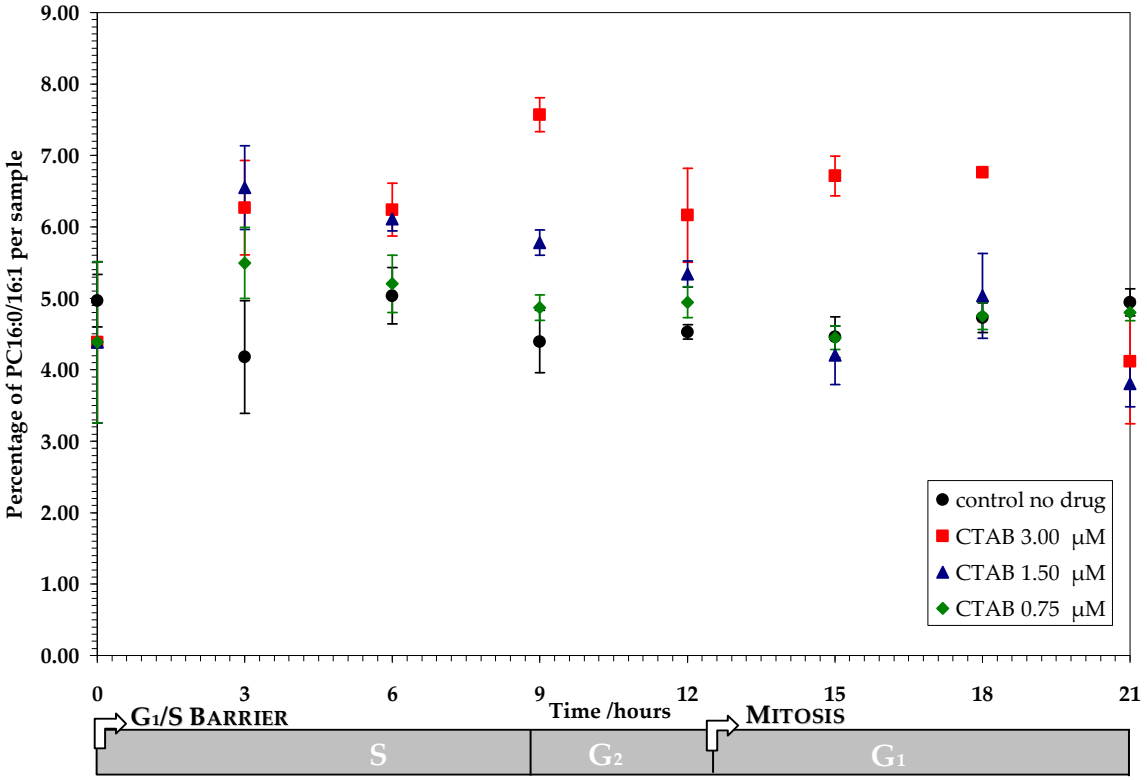

Figure III.52- Plot of percentage abundance of PC16:0/16:1 species (732 amu) against time.

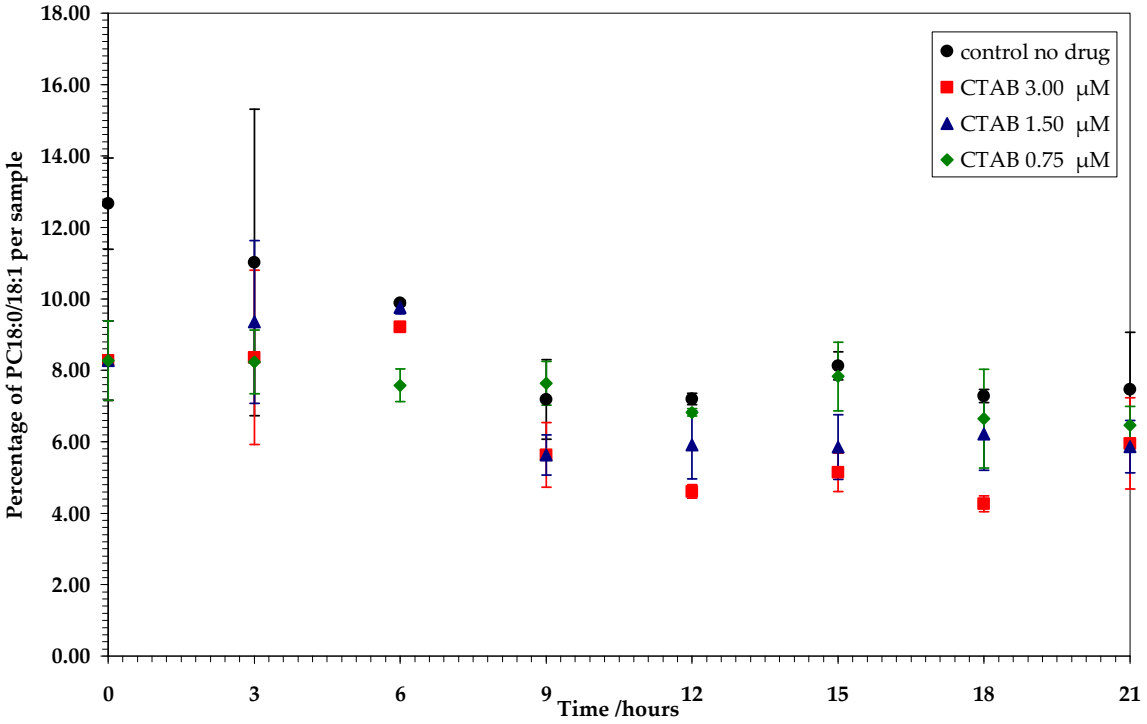

Figure III.53- Plot of percentage abundance of PC18:0/18:1 species (788 amu) against time.

For newly synthesised PC in the presence of HDPC, the fatty acid chains with abundances higher than five percent in at least one time interval are shown in Figure III.54.

CTAB 3.00 μM			**CTAB 1.50 μM**			**CTAB 0.75 μM**		
m/z (amu)	Species	Average %	m/z (amu)	Species	Average %	m/z (amu)	Species	Average %
741	d9PC16: 0/16:1	7.46±2.06	741	d9PC16: 0/16:1	6.06±1.67	741	d9PC16: 0/16:1	5.32±1.05
743*	d9PC16: 0/16:0	3.74±0.99	755	d9PC16: 0a/18:1	6.34±0.93	755	d9PC16: 0a/18:1	5.20±0.54
755	d9PC16: 0a/18:1	6.56±1.83	767	d9PC16: 0/18:2	4.89±1.29	767	d9PC16: 0/18:2	4.99±1.46
767	d9PC16: 0/18:2	5.61±1.61	769	d9PC16: 0/18:1	24.94±6.92	769	d9PC16: 0/18:1	24.45±6.71
769	d9PC16: 0/18:1	24.77±6.93	795	d9PC18: 0/18:2	14.50±2.97	795	d9PC18: 0/18:2	14.67±3.39
795	d9PC18: 0/18:2	13.93±2.69	797	d9PC18: 0/18:1	6.39±1.21	797	d9PC18: 0/18:1	7.20±1.23
797	d9PC18: 0/18:1	5.40±1.15						

Figure III.54- Table of d9PC head group class fatty acids with a higher than 5% abundance in the presence of CTAB drug. Values and SD are average percentages of all intervals. New species, present in less than 5% abundance in control cultures are annotated with an asterisk.

Species with m/z values 795, 797, 769, 755 and 741 are present in high abundance in all three drug concentrations and the control. d9PC16:0/16:0 at 743 amu is a new significantly abundant species in 3.00 μM CTAB compared to the control.

Then, the fatty acids that showed a change compared to the control were assessed. Overall, out of the 28 fatty acid species quantified for d9PC, 20 species changed significantly in the presence of 3.00 μM CTAB. Eight saturated and oligo-unsaturated species increased, mainly after six hours post synchronisation. The most significant and continuous change was demonstrated for d9PC16:0/16:1 (741 amu) that is plotted in Figure IV.55. Another 12 species, polyunsaturated with long chains in their majority, decreased in the intervals between nine and 18 hours. The most consistent decrease was observed for d9PC18:0/18:1 (Figure III.56).

For 1.50 μM CTAB, less saturated species increased and to a lesser percentage. Decrease in the polyunsaturated long species was less distinct and shifted towards earlier time intervals, occurring mainly at three and nine hours. For 0.75 μM CTAB, no significant changes were observed with the exception of d9PC18:0/18:2 (795 amu) that fluctuated between six and nine hours.

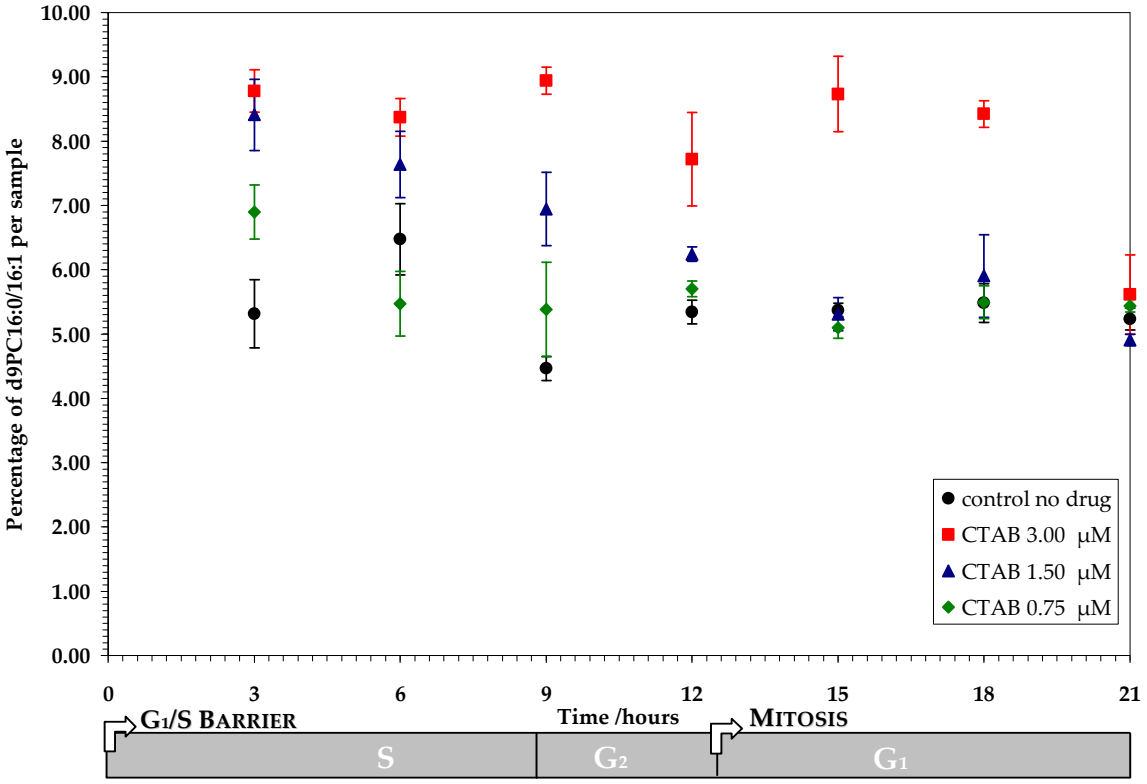

Figure III.55- Plot of percentage abundance of d9PC16:0/16:1 species (741 amu) against time.

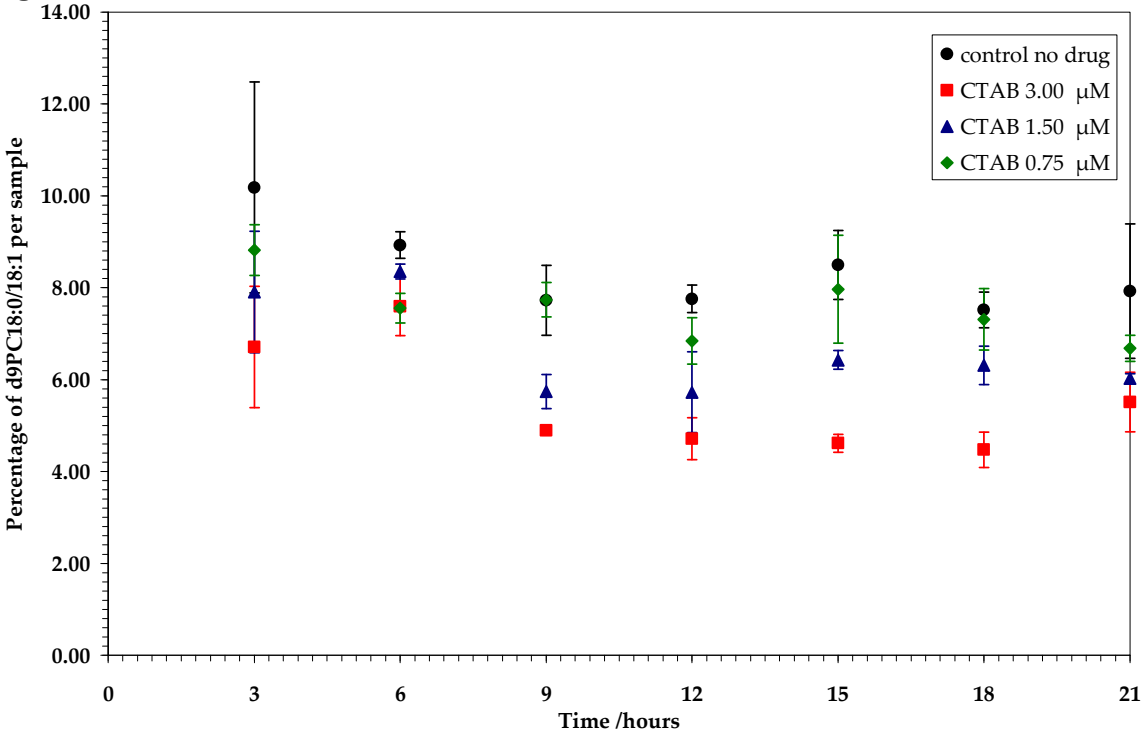

Figure III.56- Plot of percentage abundance of d9PC18:0/18:1 species (797 amu) against time.

For endogenous PE, in the presence of CTAB the fatty acid chains with abundance higher than five percent in at least one time interval are shown in Figure III.57.

CTAB 3.00 μM			**CTAB 1.50 μM**			**CTAB 0.75 μM**		
m/z (amu)	Species	Average %	m/z (amu)	Species	Average %	m/z (amu)	Species	Average %
718	PE16:0/ 18:1	11.79±2.06	718	PE16:0/ 18:1	10.56±2.44	718	PE16:0/ 18:1	8.57± 2.11
744	PE18:0/ 18:2	20.97±3.01	744	PE18:0/ 18:2	19.85±4.22	744	PE18:0/ 18:2	19.81±3.10
746	PE18:0/ 18:1	17.93±2.44	746	PE18:0/ 18:1	19.27±2.66	746	PE18:0/ 18:1	17.58±2.48
766*	PE18:1/ 20:4	3.57±1.35	766*	PE18:1/ 20:4	2.32±1.48	766*	PE18:1/ 20:4	3.16±1.63
768	PE18:0/ 20:4	8.94±2.94	768	PE18:0/ 20:4	6.84±3.38	768	PE18:0/ 20:4	9.01±3.54
772	PE18:0/ 20:2	4.78±1.07	772	PE18:0/ 20:2	5.30±1.01	772	PE18:0/ 20:2	4.72±1.29
790	PE18:0/ 20:4	2.72±1.60	774	PE18:0/ 20:1	2.01±1.17	790	PE18:0 a/22:0	4.53±2.36
792	PE18:0/ 22:6	4.69±1.20	790	PE18:0a /22:0	4.66±2.91	792	PE18:0/ 22:6	5.58±1.33
794	PE18:0/ 22:5	3.12±0.92	792	PE18:0/ 22:6	5.49±2.05	800*	PE18:0/ 22:2	2.34±1.53

Figure III.57- Table of PE head group class fatty acids with a higher than 5% abundance in the presence of CTAB drug. Values and SD are average percentages of all intervals. New species, present in less than 5% abundance in control cultures are annotated with an asterisk.

PE head group class species with m/z values of 718, 744, 746, 772, 768, 790 and 792 were present in high abundance in all three drug concentrations and the control. PE18:0a/18:1 at 732 amu was not significantly present in any of the CTAB concentrations, although it was in the control. PE18:1/20:4 at 766 amu is a new significantly abundant species in CTAB compared to the control.

Then, the fatty acids that showed a change compared to the control were assessed. Overall, out of the 22 fatty acid species quantified for PE, all 22 fluctuated to some extent in the presence of all three concentrations CTAB. No species just showed increase. There were two clear trends of either consistent decrease during the

whole incubation period, or combined increase followed by a decrease occurring in the same species.

In 3.00 μM CTAB, PE16:0/18:1 at 718 amu showed a maximum increase of 3.93 percent compared to the control at nine hours post synchronisation (Figure III.58). A similar trend had been observed in the highest concentration of HDPC, but with smaller increases. Long polyunsaturated species decreased consistently throughout the incubation period, but some of them started with an initial increase in the first six hours and then decreased constantly until the last studied interval of 21 hours post synchronisation. PE18:0/20:4 species (768 amu) is an example of the latter trend (Figure III.59).

In 1.50 μM CTAB, the same trends were observed but with smaller changes in the percentage values. Decreases in the long unsaturated species were less pronounced and shifted towards the earlier studied time intervals of three and six hours. The species showing sharp decreases compared to the control were PE18:0/20:1, PE18:0a/22:1, PE18:0a/22:0 and PE18:0/22:6.

In 0.75 μM CTAB, only two species, PE18:1/20:4 and PE18:0/20:4 fluctuated significantly for the whole first 21 hours post synchronisation. They both increased sharply during the first six hours and then their percentages diminished consistently until the last time interval. The remainder of the long polyunsaturated species that had decreased throughout the 21 hours in the two higher CTAB concentrations, only showed decrease during the first six hours. Finally, PE18:0a/22:1 and PE18:0a/22:0 illustrated an interesting sharp decrease for the first six hours, followed by increases in their percentages between 12 and 21 hours.

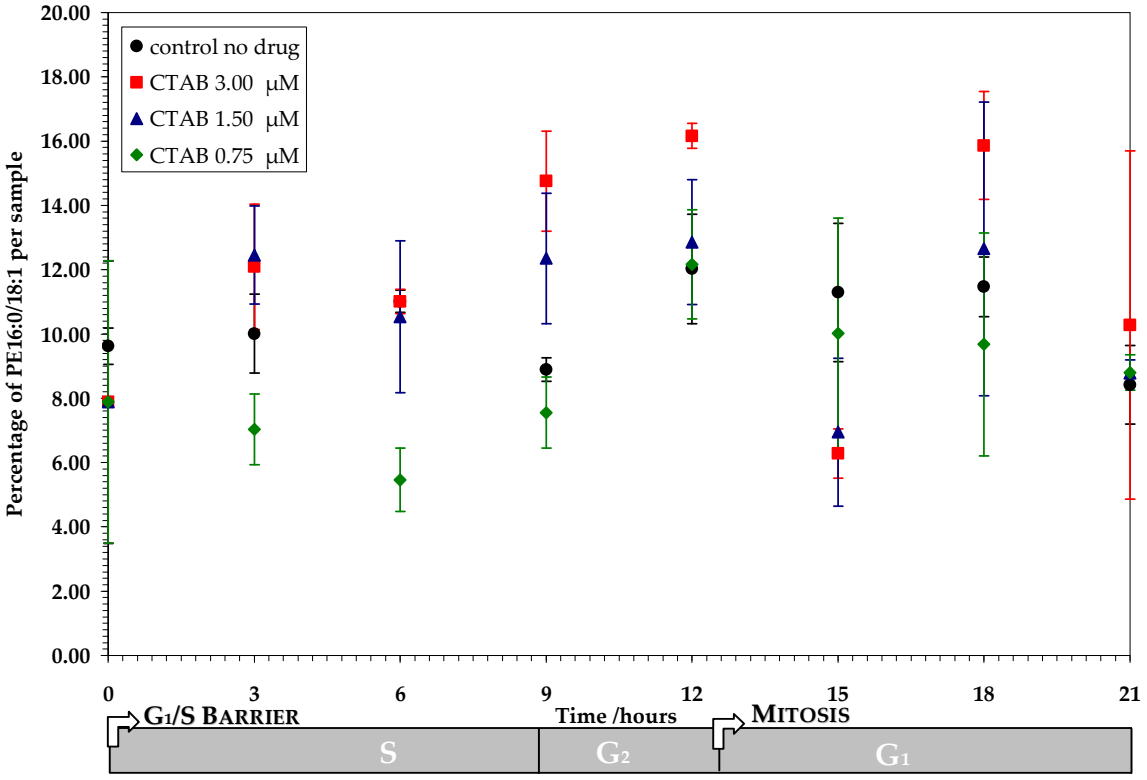

Figure III.58- Plot of percentage abundance of PE16:0/18:1 species (718 amu) against time.

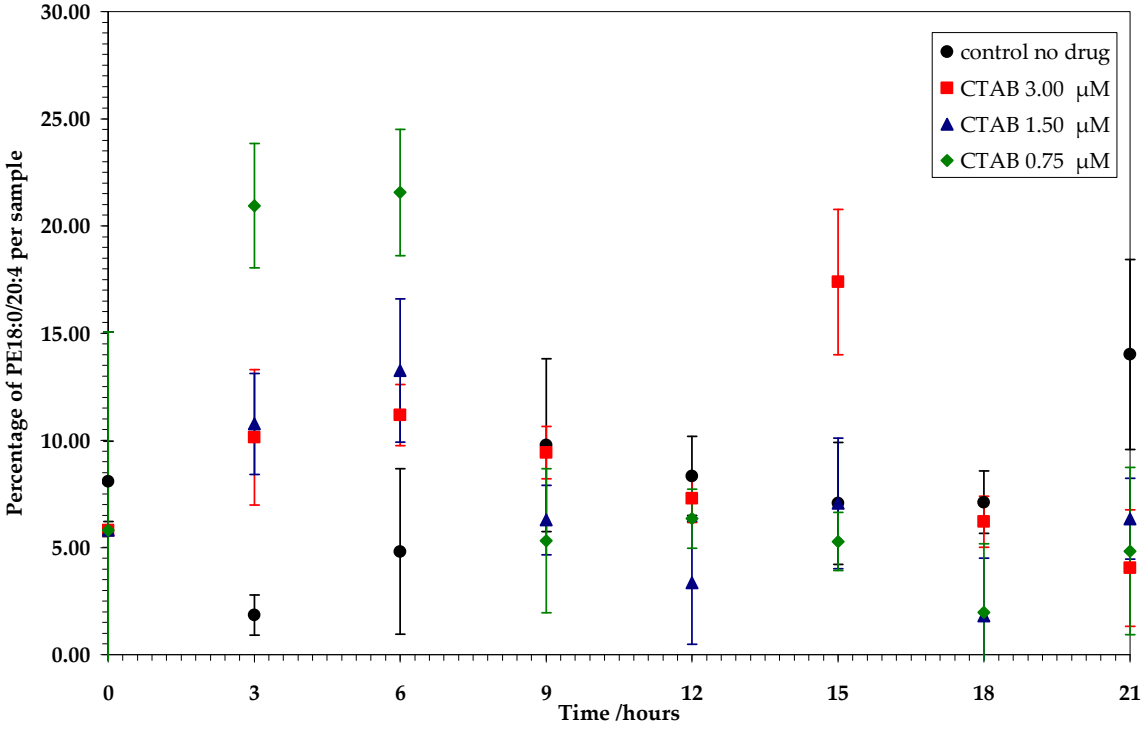

Figure III.59- Plot of percentage abundance of PE18:0/20:4 species (768 amu) against time.

III.5.3.2.3. Rate of new PC synthesis in the presence of drug

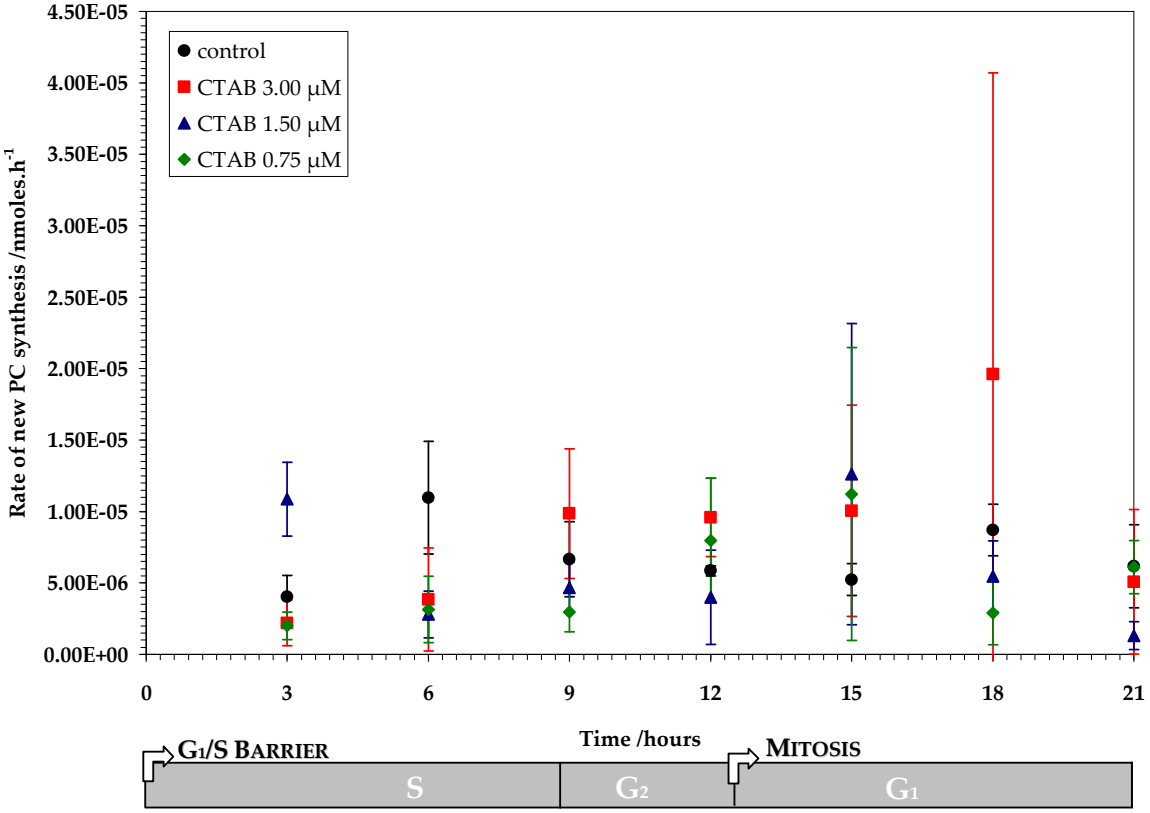

Figure III.60- Plot of rate of new PC synthesis as a function of time as measured by mass spectrometry in control experiment in the presence of CTAB.

CTAB in the culture did not appear to affect the rate of new PC synthesis in HeLa cells during the cell cycle. These data are in contrast to those for HDPC that decreased the rate with maximum decreasing occurring at the end of M phase, 18 hours post synchronisation (see section III.5.2.2.3). This further supports the argument that the two drugs affect PtdCho metabolism in a different fashion.

Overall, the errors are quite large in this particular plot, mainly because of variability in the number of cells in each flask.

III.6. Conclusions and further work

III.6.1. Effect of Type I amphiphiles on CCT

Our *in vitro* studies of CCT (section II.5.1) have shown that both HDPC and CTAB inhibited enzyme activity. HDPC was approximately twice more potent than CTAB. These results deemed essential an *in vivo* investigation of the effect of Type I amphiphiles in phospholipid metabolism, and membranes in particular. Potential changes caused by HDPC and CTAB in the amounts of endogenous and newly synthesised PC and endogenous PE, as well as membrane composition were quantified in HeLa cells by ESI-MS.

HDPC was investigated at three different concentrations at 10.50, 5.25 and 2.63 μM. All three concentrations partitioned to membranes equilibrating at about 5E-06 nmoles per cell after 21 hours incubation with the drug, which corresponds to one full cell cycle. However, in 10.50 μM HDPC, the drug assimilated two-fold more into membranes and showed a maximum at 15 hours. An equivalent trend was observed for the three investigated concentrations of CTAB at 3.00, 1.50 and 0.75 μM. Conversely, the partition coefficient K for CTAB was five-fold larger than for HDPC. This difference could be due to electrostatics. CTAB is positively charged whereas HDPC is zwitterionic and thus neutral (for structures, see Figure IV.5). Membranes are negatively charged at pH 7 due to the hydrophilic head groups of the lipid bilayer (Cevc 1990; Barenholz and Cevc 2000), therefore CTAB partitions more favourably than HDPC because of its positive charge.

Based on our cell viability results, neither drug had a significant cytotoxic effect on HeLa cells. Since concentrations for both HDPC and CTAB were based on the ED_{50} values for a different cell line, it may be that the ED_{50} for HeLa cells is much higher. Therefore, future work should include determination of ED_{50} specifically for the HeLa cell line.

For HDPC, the highest concentration at 10.50 μM did not change the total amount of endogenous PC in membranes during the cell cycle. Counter-intuitively, the two smaller concentrations caused a two-fold decrease. The same trend was observed for both newly synthesised PC and endogenous PE. For CTAB, none of the three concentrations caused a change in the total amount of newly synthesised PC in membranes during the cell cycle. However, all three decreased the total amount of endogenous PC and PE two-fold. In general, it can be concluded that both Type I amphiphiles inhibited PtdCho, and in consequence PtdEth biosyntheses. HDPC was more potent in inhibiting new PC synthesis, causing considerable decrease compared to CTAB. This confirms our *in vitro* results for CCT activity.

HDPC changed membrane composition for endogenous and new PC, as well as endogenous PE head group classes. A large number of polyunsaturated long species decreased by small amounts. In parallel, only a few saturated and oligo-unsaturated species, like PC16:0a/18:2 and PE18:0/18:1, increased significantly. CTAB caused much more significant changes in composition for all three head groups. Nearly all polyunsaturated long species decreased, some by as much as 5 percent. At the same time, quite a lot of saturated and oligo-unsaturated species increased. However, as this type of quantitation has not been done before for Type I amphiphiles, it is hard to assess how much change is significant. Chiefly, it can be inferred that CTAB caused considerably more variation in membrane composition than HDPC, and most changes observed were in the order of less than 1 percent.

Overall, quantitation of lipid molecular species by mass spectrometry is a method that is still being developed for accuracy. Consequently, there is an experimental limit to the conclusions one can draw from these results. However, the observed trends are reliable enough to provide with insight on the effect of Type I amphiphiles, HDPC and CTAB, to PtdCho metabolism in HeLa cells during the

cell cycle. Data from control cultures confirmed characteristic trends known to occur during the cell from the literature:

- An increase in cell death was observed nine hours post synchronisation. This time interval corresponds to the end of S phase, when apoptosis has been reported to occur in human cancer cells (see section III.5.1.1).
- New PC synthesis almost doubled at the end of one full cycle (see section III.5.1.2.1).
- The most abundant fatty acid species in membranes increased steadily during G_1 and S phase as phospholipid synthesis occurred in the first nine hours post synchronisation (see section III.5.1.2.1).
- PE species in membranes were significantly less abundant than PC analogues, since cell membranes consist in markedly more PC than PE (see section III.5.1.2.1).

Cell sizing using our novel method based on optical microscopy imaging was also undertaken. In control cultures, a maximal diameter change of 27 percent was recorded at the end of one full cell cycle, which corresponds to almost doubling of cell volume, as expected from the literature (Wheatley, Inglis et al. 1987). Automated Matlab© statistical analyses provided with interesting information on size distribution which suggested that both HDPC and CTAB potentially decreased cell size and caused cell population distribution changes without disrupting population normality. Thus, afore-mentioned results of decrease in total PC and PE in membranes in the presence of these drugs were further supported.

Our novel sizing method is an efficient way to obtain initial size data on a statistically significant population of a culture, as large as 7,000 cells per experiment. It can provide with insight to changes in cell size by using only as little as 30 μL of the sample. The Matlab© program can readily export statistical analyses of the cell population whilst it can be easily adapted to include features

that suit each individual user. On the other hand, the method would require further developing as it is still crude. Results for latex beads of known size illustrated (see Section IV.3) that SEM can provide with much more accurate results, albeit for a much smaller population of cells. Also, the method is based on a two-dimensional optical image so changes in the volume of the cell cannot be detected. Further implementation to become more user-friendly for users with no programming skills is needed.

As cell culture experiments were very time-consuming and during this study all parameters had to be optimised for the first time, it would be essential for the experiments to be repeated at least once more to ensure reproducibility. Unfortunately, that was not possible within the time constrictions of this investigation and mainly due to very limited availability of the ESI-MS instrument.

Another line of further work could be to use a non-adherent cell line for these studies. Also, the number of analysed species for membrane composition could be reduced by adjusting the culture medium.

Data extraction from MassLynx by Visual Basic macros had many limitations. A custom made program for the purposes of these experiments could improve errors, increase reliability of data, and markedly decrease the time analyses take. A new method that uses an algorithm to process raw spectrometric data has been recently reported (Song, Hsu et al. 2007).

III.6.2. Experimental error consideration

Overall, experimental errors in the results of this chapter are considerably larger comparably to the other two chapters of this thesis. The principal reason for that is the different nature of experiments. Unfortunately, an absolute comparison between analytical MS and kinetic data is not feasible.

It must be also noted that due to the multiple steps of the experimental protocol, error can occur at any stage of the process and propagate until data acquisition. The most significant sources of experimental error can be subdivided to practical and instrumental. Practical errors were the following. First, the biological variability of the cell culture samples. Although the latter is a systematic source of error, it is by no means constant and thus can be neither prevented nor predicted exactly. Second, membranes were extracted using the Bligh Dyer method for each sample individually. Thus, slight variation in the extracted membrane amount per sample was inevitable, regardless the care taken during the process. Third, use of non-physiological lipids as standards also can introduce variability in the sample, from use of different balances and materials when preparing different batches of samples. Fourth, MS instruments have limited availability being part of a shared facility; samples have to be run in tandem during very short time periods.

The instrumental sources of error were the following. First, variability in the experimental method of mass spectrometry data acquisition due to instrumental parameters such as vacuum efficiency, pressure and availability of collision gas. Unfortunately, technical management of the MS instrument was not under our control. Second, inappropriate experimental design of the mass spectrometry protocol as the method was originally for clinical samples and has not been optimised for our samples. Third, the current method of data analysis for mass spectrometry data could result in significant errors that are difficult to detect due to the large amount of data generated.

III.7. References

Adams, R. B., W. H. Voelker, et al. (1967). "Electrical counting and sizing of mammalian cells in suspension: An experimental evaluation." Phys. Med. Biol. **12**(1): 79-82.

Allen, D. D., R. Caviedes, et al. (2005). "Cell lines as in vitro models for drug screening and toxicity studies." Drug Develop. Industr. Pharmacy **31**(8): 757-768.

Ashwell, M., P. Priest, et al. (1976). "Human fat cell sizing- a quick simple method." J. Lipid Res. **17**(190-192).

Barenholz, Y. and G. Cevc (2000). "Structure and properties of membranes." Phys. Chem. Biol. Interfaces: 171-241.

Berkovic, D. (1998). "Cytotoxic etherphospholipid analogues." Gen. Pharmacol. **31**(4): 511-517.

Binder, M., G. Liebisch, et al. (2006). "Metabolic profiling of glycerophospholipid synthesis in fibroblasts loaded with free cholesterol and modified low density lipoproteins." J. Biol. Chem. **281**(31): 21869-21877.

Bligh, E. G. and W. J. Dyer (1959). "A rapid method of total lipid extraction and purification." Can. J. Biochem. Physiol. **37**(8): 911-917.

Boggs, K., C. Rock, et al. (1995). "Lysophosphatidylcholine attenuates the cytotoxic effects of the antineoplastic phospholipid 1-O-octadecyl-2-O-methyl-rac-glycero-3- phosphocholine." J. Biol. Chem. **270**(19): 11612-11618.

Boggs, K. P., C. O. Rock, et al. (1995). "Lysophosphatidylcholine and 1-O-Octadecyl-2-O-Methyl-rac- Glycero-3-phosphocholine inhibit the CDP-choline pathway of phosphatidyl choline synthesis at the CTP:phosphocholine cytidylyltransferase step." J. Biol. Chem. **270**(13): 7757-7764.

Boon, J. M. and B. D. Smith (2002). "Chemical control of phospholipid distribution across bilayer membranes." Med. Res. Rev. **22**(3): 251-281.

Brachwitz, H. and C. Vollgraf (1995). "Analogs of alkyllysophospholipids: chemistry effects on the molecular level and their consequences for normal and malignant cells." Pharmarcol. Therapy **66**: 39-82.

Breiser, A., D.-J. Kim, et al. (1987). "Distribution and metabolism of hexadecyl phosphocholine in mice." Lipids **22**(11): 925-926.

Brown, R. W. and J. H. Henderson (1983). "The mass production and distribution of HeLa cells at Tuskegee Institute, 1953-55." J. Hist. Med. Allied Sci. **38**(4): 415-431.

Cevc, G. (1990). "Membrane Electrostatics." Bioch. Biophys. Acta **1031**(3): 311-382.

Chalfie, M., Y. Tu, et al. (1994). "Green fluorescent protein as a marker for gene expression." Science **263**: 802-805.

Collins, K., J. Tyler, et al. (1997). "The cell cycle and cancer." Proc. Natl. Acad. Sci. USA **94**: 2776–2778.

Dicker, D. T., J. M. Lerner, et al. (2007). "Hyperspectral image analysis of live cells in various cell cycle stages." Cell Cycle **6**(20): 2563-2570.

Dymond, M. K. (2001). An investigation into the mechanism of action of amphiphiles with antineoplastic properties. School of Chemistry, University of Southampton.

Fenn, J. B., M. Mann, et al. (1989). "Electrospray ionization for mass spectrometry of large biomolecules." Science **246**(4926): 64.

Gartler, S. M. (1967). Genetic markers as tracers in cell culture. N. C. I. Monograph. **26:** 167-195.

Gartler, S. M. (1968). "Apparent HeLa contamination of human heteroploid cell lines." Nature **217**: 750-751.

Geilen, C. C., T. Wieder, et al. (1991). "Hexadecylphosphocholine inhibits translocation of CTP:choline-phosphate cytidylyltransferase in Madin-Derby canine kidney cells." J. Biol. Chem. **267**: 6719-6724.

Gey, G. O., W. D. Coffman, et al. (1952). "Tissue culture studies of the proliferative capacity of cervical carcinoma and normal epithelium." Cancer Res. **12**: 264-265.

Givan, A. L. (2001). Flow cytometry: First principles, Wiley-Liss.

Gregg, E. C. and K. D. Steidley (1965). "Electrical counting and sizing of mammalian cells in suspension." Biophys. J. **5**: 393-405.

Haase, R., T. Wieder, et al. (1991). "The phospholipid analogue hexadecylphosphocholine inhibits phosphatidylcholine biosynthesis in Madin-Darby canine kidney cells." FEBS **288**(1-2): 129-132.

Hague, C. (2007). FACS study of L-mimosine synchronised HeLa cultures.

Hunt, A. N. and A. D. Postle (2006). "Mass spectrometry determination of endonuclear phospholipid composition and dynamics." Methods **39**: 104-111.

Huth, S. L. (2006). Investigation of the effect of Type I and II amphiphiles on the membrane lipid composition in HL60 cells, University of Southampton.

Ile, K. E., G. Schaaf, et al. (2006). "Phosphatidylinositol transfer proteins and cellular nanoreactors for lipid signalling." Nature Chem. Biol. **2**(11): 576-583.

Jackowski, S. (1994). "Coordination of membrane phospholipid synthesis with the cell cycle." J. Biol. Chem. **269**(5): 3858-3867.

Jackowski, S. (1996). "Cell cycle regulation of membrane phospholipid metabolism." J. Biol. Chem. **271**(34): 20219–20222.

Kanda, T., K. F. Sullivan, et al. (1998). "Histone–GFP fusion protein enables sensitive analysis of chromosome dynamics in living mammalian cells." Curr. Biol. **8**(7): 377-385.

Lewis, K. M., I. Kijak, et al. (1996). "An image analysis method for cell-size and cell-size distribution measurement in rigid foams." J. Cell. Plastics **32**(3): 235-259.

Masters, J. R. (2002). "HeLa cells 50 years on: the good, the bad and the ugly." Nature Rev. Cancer **2**(4): 315-319.

Nelson-Rees, W. A., D. W. Daniels, et al. (1981). "Cross-contamination in cells in culture." Science **212**(4493): 446-452.

Nelson-Rees, W. A. and R. R. Flandermeyer (1976). "HeLa cultures defined." Science **191**(4222): 96-98.

Nelson, D. L., Cox, M.M. (2000). Lehninger Principles of Biochemistry, 3rd edition. New York, Worth Publishers.

Song, H., F.-F. Hsu, et al. (2007). "Algorithm for processing raw mass spectrometric data to identify and quantitate complex lipid molecular species in mixtures by data-dependent scanning and fragment ion database searching." J. Am. Soc. Mass. Spectrom. **18**: 1848-1858.

Stewart, J. C. M. (1980). "Colorimetric determination of phospholipids with ammonium ferrothiocyanate." Analyt. Biochem. **104**(1): 10-14.

Tercé, F., H. Brun, et al. (1994). "Requirement of phosphatidyl choline for normal progression through the cell cycle in C3H/10T1/2 fibroblasts." J. Lipid Res. **35**: 2130-2142.

Viles, C. L. and M. E. Sieracki (1992). "Measurement of marine picoplankton cell size by using a cooled,charge-coupled device camera with image-analyzed fluorescence microscopy." Appl. Envir. Microbiol. **58**(2): 584-592.

Wheatley, D. N., M. S. Inglis, et al. (1987). "Hydration, volume changes and nuclear magnetic resonance proton relaxation times of HeLa S3 cells in M phase and the subsequent cell cycle." J. Cell Sci. **88**: 13-23.

Wieder, T., W. Reutter, et al. (1999). "Mechanisms of action of phospholipid analogs as anticancer compounds." Progr. Lipid Res. **38**: 249-259.

Xu, X., T. Tessner, et al. (1993). "Phosphatidylcholine hydrolysis and c-myc expression are in collaborating mitogenic pathways activated by colony-stimulating factor." Mol. Cell. Biol. **13**(3): 1552-1533.

Zhou, W., P. J. Simpson, et al. (2003). "Fatty acid synthase triggers apoptosis during S phase in human cancer cells." Cancer Res. **63**: 7330-7337.

Zink, D., A. H. Fischer, et al. (2004). "Nuclear structure in cancer cells." Nature Rev. Cancer **4**: 677-687.

Zink, D., N. Sadoni, et al. (2003). "Visualizing chromatin and chromosomes in living cells." Methods **29**: 42-50.

Chapter IV

Regulation of PFK-1 by membrane lipid composition

Table of Contents

IV.1. Introduction

IV.1.1. Glycolysis

Glycolysis, from the Hellenic γλυκός and λύσις, for sweet and breakdown, also known as the Embden-Meyerhoff pathway, involves the anaerobic degradation of one mole of glucose to two moles of pyruvate with a net gain of two moles of adenosine triphosphate (ATP), the energy storage molecule in cells (Stryer 1999; Nelson 2000). This was the first metabolic pathway to be clearly recognised as early as the 1940s and since then it has been the subject of innumerable biochemical studies, conferences and reviews (Phillips, Blake et al. 1981).

Glycolysis can occur in the absence or presence of oxygen in nearly all organisms, both eukaryotic and prokaryotic. Interestingly, the majority of cancer cells have increased glycolytic rates in a phenomenon known as the Warburg effect (Warburg 1956). The latter is considered as one of the most significant metabolic changes during malignant transformation (DeBerardinis, Lum et al. 2008) and tumour suppressor protein p53 has been shown to regulate glycolysis (Ma, Sung et al. 2007). Thus glycolytic enzymes are potential targets of anti-cancer agents (Pelicano, Martin et al. 2006).

There are ten distinct steps in the glycolytic pathway, each catalysed by a different enzyme. A summary of all reactions occurring during the pathway follows in Figure IV.1 overleaf. However, this discussion will be limited to the third step of glycolysis, on which our investigation focused on. Phosphofructokinase or ATP: D-fructose 6-phosphate 1-phosphotransferase (PFK, EC 2.7.1.1.l) catalyses the third step of glycolysis, during which D-fructose 6-phosphate (F6P) is phosphorylated by ATP to yield D-fructose-1,6-bisphosphate (F16BP). This reaction is both rate-determining and regulatory for the whole biosynthetic route. Consequently, PFK is the key enzyme in the degradation of glucose and generation of ATP in cells.

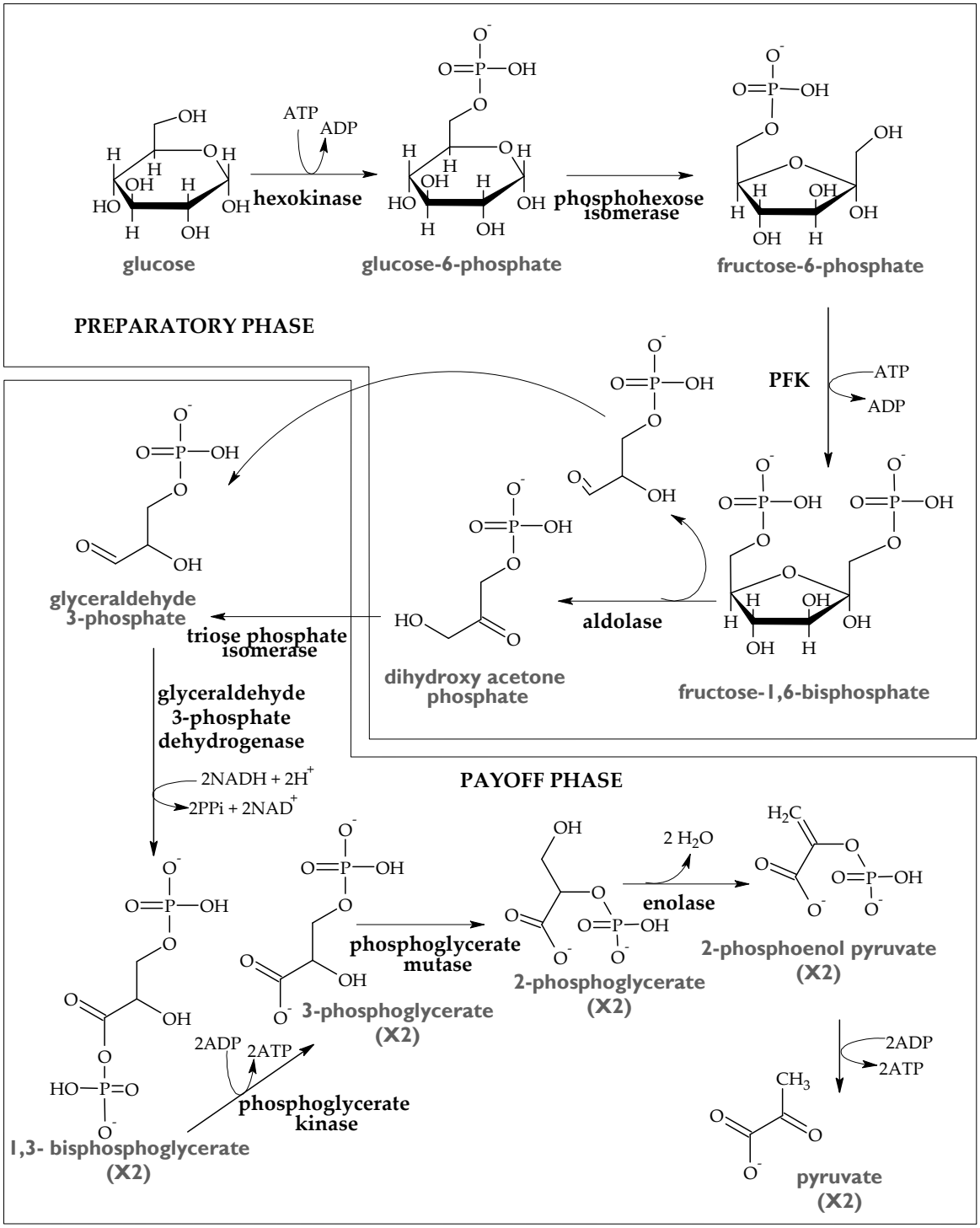

Figure IV.1- Summary of the glycolytic pathway, where phosphofructokinase (PFK) is our enzyme of interest. The preparatory and payoff phases are illustrated. The whole process yields two moles of pyruvate, two moles of ATP, and two moles of NADH.

IV.1.2. Phosphofructokinase-1

IV.1.2.1. PFK-1 structure and function

Two isoforms of phosphofructokinase have been recognised thus far, PFK-1 and PFK-2. The former is the classically studied enzyme found in all organisms whereas the latter has only been shown in *E. coli* (Babul 1978). Both isoforms catalyse the same reaction, but are structurally (Cabrera, Caniuguir et al. 2006) and kinetically unrelated (Caniuguir, Cabrera et al. 2005). In humans, PFK-1 is localised in muscle, liver and platelet cells and is thus termed as PFK-M, PFK-L and PFK-P, respectively (Vora 1983).

PFK-1 can be further classified into three groups depending on the source organism (Hoffman 1976). First, mammalian enzymes are the largest, forming homotetramers that can further aggregate, with each subunit at about 85 kDa. Second, yeast PFK-1 is a $\alpha_4\beta_4$ hetero-octamer with each monomer at approximately 115 kDa. Third, bacterial enzymes are the smallest of the three groups, showing homotetramers with 35 kDa subunits.

Genes pfk1 and pfk2 encode the α and β subunits of PFK-1, respectively (Heinisch 1986). The subunits of eukaryotes and prokaryotes show significant homology and the protein sequence is conserved throughout all organisms despite their differences in oligomerisation (Poorman, Randolph et al. 1984; Heinisch 1989).

The first crystal structure for PFK-1 was resolved in 1991 at 2.4 Å from bacterium *Escherichia coli* (Shirakihara and Evans 1988). A structure at 2.5 Å for another bacterial PFK-1 from *B. stearothermophilus* followed a few years later in a publication in Nature journal (Schirmer and Evans 1990). These two enzymes are often mentioned interchangeably in the literature because of their many structural and kinetic similarities (French and Chang 1987). The first eukaryotic structure was resolved in 2007 (Martinez-Oyanedel, McNae et al. 2007).

B. stearothermophilus PFK-1 is a homo-tetramer, arranged as a dimer of dimers, where each subunit has 319 amino acids and a molecular weight of 33.9 kDa (Evans and Hudson 1979). Each monomer forms interactions with only two of the other subunits in the tetramer, which assembles into two three-layered αβα sandwich structured domains (Figure IV.2). The ATP substrate binds to the larger of the two domains, while co-substrate F6P to the smaller one. There are four identical active sites and four identical effector sites, each situated along dimer-dimer interfaces on the homo-tetramer. Hence, oligomerisation is a prerequisite for the formation of the eight binding sites.

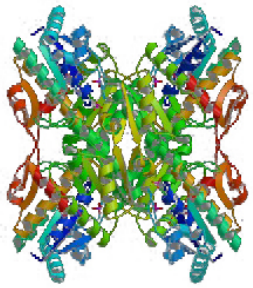

Figure IV.2- PFK-1 of *B. stearothermophilus* (Evans, Farrants et al. 1981).

Effectors are regulatory molecules for enzyme activity that bind in sites other than the active site, which are termed allosteric, and are structurally different to the substrates (Fersht 2002). PFK-1 from *B. stearothermophilus* and *E.coli* is allosterically inhibited by phosphoenol pyruvate (PEP) and activated by adenosine diphosphate (ADP) (Blangy, Buc et al. 1968; Kimmel 2001). All effectors bind on the same sites on PFK-1 (Evans, Farrants et al. 1986).

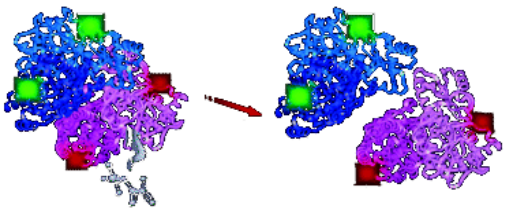

Figure IV.3- PFK-1 tetrameric form illustrating allosteric inhibition by PEP (Quinlan and Reinhart 2006).

PFK-1 is associated with diseases such as diabetes, ischemia and renal failure (Vats, Yadav et al. 2004; Vannucci, Brucklacher et al. 2005). In particular, Tarui or phosphofructokinase deficiency disease is a rare condition that occurs when mammalian PFK-M is completely absent leading to complete inhibition of the glycolysis pathway in muscle tissue (Nakajima, Hamaguchi et al. 1995; Exantus, Ranchin et al. 2004).

IV.1.2.2. PFK-1 regulation

PFK-1 is regulated by allosteric effectors, phosphorylation, macromolecular interaction and binding to membranes.

IV.1.2.2.1. **Inhibition and allostery models**

Steady state kinetics are used in dynamic systems such metabolic reactions catalysed by enzymes in cells. The steady state is an approximation in which the rate of product formation is equal to the rate of substrate depletion. The Michaelis-Menten equation is the basic equation for steady state kinetics which assumes a negligible concentration of enzyme compared to that of substrate (Michaelis and Menten 1913). According to Michaelis-Menten kinetics, the rate of the reaction, v, is directly proportional to the concentration of enzyme, $[E]_0$, but follows saturation kinetics with respect to the concentration of substrate, [S], as illustrated in Figure IV.4.

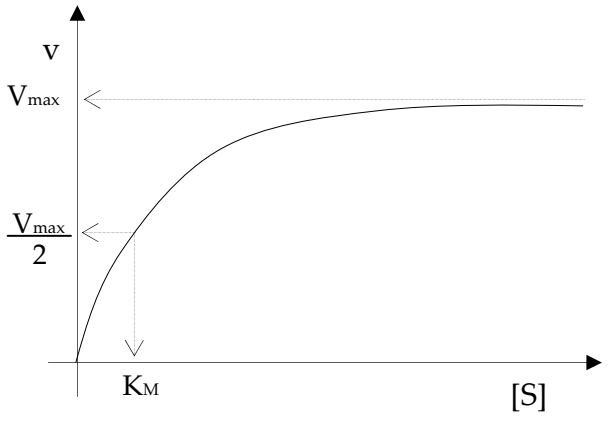

Figure IV.5- Typical Michaelis- Menten kinetics.

At low [S], v increases linearly but levels off at a limiting value V_{max} as expressed in the equation, where K_M is the Michaelis constant and K_{cat} the turnover number:

$$v = \frac{[E]_0 [S] k_{cat}}{K_M + [S]} .$$

Data analysis is easier when the Michaelis-Menten is transformed to a linear form in the double reciprocal equation (Lineweaver and Burk 1934):

$$\frac{1}{v} = \frac{1}{V_{max}} + \frac{K_M}{V_{max}[S]} .$$

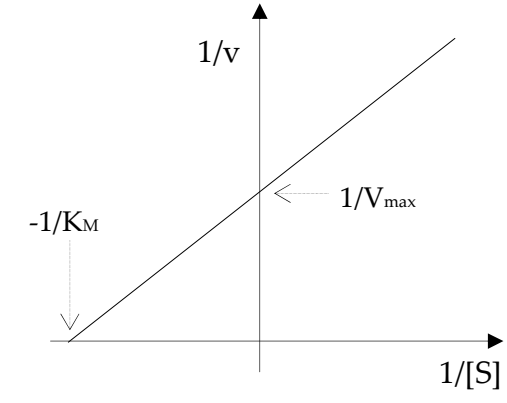

Figure IV.4- The Lineweaver-Burk plot.

Enzymes can be reversibly inhibited by the non-covalent binding of inhibitors in four main types of inhibition summarised in Figure IV.6.

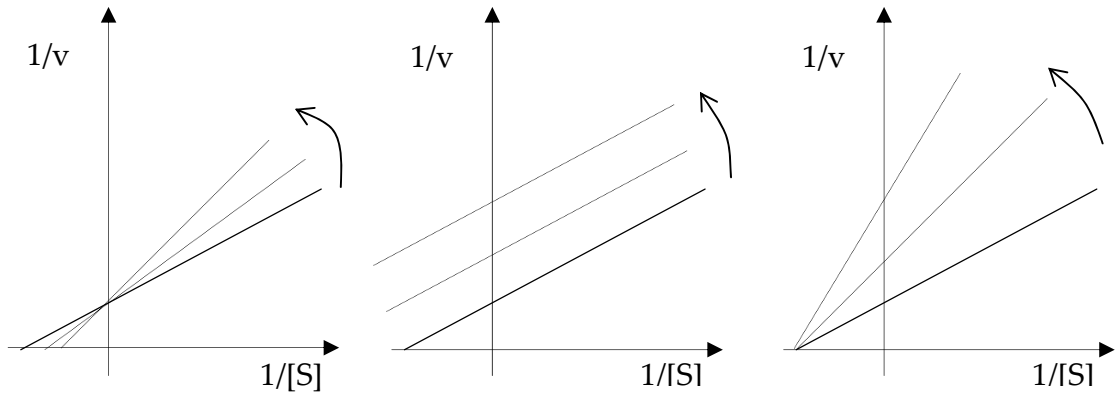

(a) competitive (b) uncompetitive (b) non- competitive

Figure IV.6- Lineweaver-Burk plots of different types of inhibition where the darker line is the reaction in the absence of inhibitor and the arrow indicates increasing inhibition. In (a), competitive inhibition occurs when an inhibitor binds reversibly to the active site, competing with the substrate and affecting K_M only. In (b), an uncompetitive inhibitor binds simultaneously with the substrate but only with the enzyme-substrate complex. In (c), non-competitive inhibition solely decreases k_{cat}. Diagram based on textbook figure (Fersht 2002).

However, in the presence of allosteric effectors and cooperativity, Michaelis-Menten kinetics can no longer be applied. Allosteric cooperativity can be either homotropic, when regulated by binding of substrates, or heterotropic, when controlled by binding of allosteric effectors (Fersht 2002). The Monod-Wyman-Changeux (MWC) model for allosteric kinetics is the most eminent mechanism for allosteric regulation of enzymes (Monod, Wyman et al. 1965) and PFK-1 was one of the first to be applied to (Blangy, Buc et al. 1968).

The model predicts that an enzyme controlled by allosteric kinetics has two states which exist in equilibrium. An inactive tense (T) state has a low affinity for both substrates and effectors, and is thus the predominant form of the unligated protein. On the contrary, the relaxed (R) state is catalytically active, has a high affinity for ligands and is less constrained than the T state.

The model can be applied if a protein is an oligomer that exists in two conformational states with different ligand affinity and that all binding sites in each state are equivalent. A sigmoidal binding curve can be then constructed for every allosteric protein based on the dissociation constants, K_T and K_R, for the T and R states, respectively, and the allosteric constant, L, which is equal to the ratio of the enzyme concentration in the tight state to that of the relaxed state.

Tetrameric bacterial PFK-1 has one allosteric site per subunit, where inhibitor PEP binds and closes the effector site causing repacking of the subunit interface (Evans 1991). An arginine residue (Arg^{252}), that stabilises F6P in the active site, twists and limits access to the substrate (Evans, Farrants et al. 1986). This leads to a relative rotation of 7° of dimers in the tetramer and induces a conformational shift from the R to the T state of the enzyme. The latter is triggered by a decreasing active site affinity for substrate F6P (Schirmer and Evans 1990). Although the larger substrate binding domain of the enzyme remains essentially rigid during the allosteric conformational change, the low affinity T state can only occur in the presence of PEP, which promotes protein stability (Quinlan and Reinhart 2006).

Affinities of sites for substrates and effectors depend on the interactions among the sites (Lipscomb 1998). Negative cooperativity of the binding ligands was introduced by Koshland into allostery with the sequential model (Koshland, Nemethy et al. 1966). Binding of the first ligand is suggested to decrease enzyme affinity for a second ligand, which is a concept that clashes with the MWC model of equivalent affinity symmetrical sites (Koshland 1996). The sequential model is a development of the induced fit idea that substrate binding triggers enzyme conformational changes that position the active site to its active configuration.

Eigen received the 1967 Chemistry Nobel Prize in Chemistry proposing the general model, which combines MWC and sequential models but considers all possible combinations of binding, similarly to a chessboard (Eigen 1967).

The allosteric transition triggered by effector binding does not disrupt the subunit interface, which was verified by time resolved fluorescence of a tryptophan residue ($Tryp^{179}$) buried in the interface (Kim, Chowdhury et al. 1993). PFK-1 activity has been shown to be regulated by a large range of allosteric effectors, both inhibitors and activators.

Both *B. stearothermophilus* and *E. coli* PFK-1 (BsPFK-1 and EcPFK-1) are inhibited by PEP. F6P kinetics in PEP are sigmoidal and cooperative, while in its absence follow hyperbolic Michaelis-Menten kinetics (Blangy, Buc et al. 1968; Valdez, French et al. 1989). Residue 161, a glutamate in BsPFK-1 and a glutamine in EcPFK-1, provides essential hydrogen bonding with PEP (Auzat, Byrnes et al. 1995) while Gly^{212} acts a pivot on which a loop hinges upon effector binding (Zhu, Byrnes et al. 1995).

In EcPFK-1, although PEP inhibition and F6P cooperativity are mediated via structural changes in the active site (Auzat, Bras et al. 1994), the two processes are not related to the same structural transition (Auzat, Byrnes et al. 1995). EcPFK-1 is an example of how local changes in the tertiary protein structure triggered by effector binding, can lead to global changes in the quaternary structure modifying enzyme properties (Auzat, Le Bras et al. 1995). A satisfactory mechanism of how exactly local changes occur which satisfies both experimental evidence and thermodynamic parameters has not been yet proposed (Kimmel and Reinhart 2000).

Activators ADP and guanosine diphosphate (GDP) can alleviate PEP inhibition. However, GDP is a strong activator for EcPFK-1 whilst only a weak one for BsPFK-1 (Byrnes, Hu et al. 1995). Mg.ADP can bind in both allosteric and active sites (Riley-Lovingshimer and Reinhart 2005).

Saturation by F6P substrate is markedly different in BsPFK-1 and EcPFK-1. In the former, it shows hyperbolic Michaelis-Menten kinetics (Valdez, French et al. 1989) while in the latter it is cooperative (Blangy, Buc et al. 1968).

There is binding antagonism between Mg.ATP and F6P in BsPFK-1 for binding to the active sites (Byrnes, Zhu et al. 1994). A high concentration of Mg.ATP converts Michaelis-Mentel hyperbolic F6P kinetics to sigmoidal but the inhibition can be reversed by AMP and is non-allosteric. That is either because Mg.ATP forms an abortive complex with the active site (Byrnes, Zhu et al. 1994), or Mg.ATP is rate-limiting in an alternative kinetically unfavourable mechanism (Wang and Kemp 2001; Riley-Lovingshimer and Reinhart 2005). Conversely, Mg.ATP inhibition is allosteric in EcPFK-1(Berger and Evans 1991), with one Mg.ATP molecule bound in one active site behaving as an allosteric inhibitor for F6P affinity in a second active site (Fenton and Reinhart 2003). Overall, PFK-1 catalysis, and, in consequence, glycolysis are activated when the ratio of ATP/AMP and energy levels fall in cells.

In both BsPFK-1 and EcPFK-1, there are four active and four allosteric sites (Shirakihara and Evans 1988; Schirmer and Evans 1990). As all the sites can interact with each other, the total possible interactions are three homotropic for F6P, three homotropic for Mg.ATP and four heterotropic. Each heterotropic interaction contributes uniquely to the overall allosteric effect in free energy when an allosteric effect binds to the enzyme (Fenton, Parichartanakul et al. 2004; Ortigosa, Kimmel et al. 2004). However, cooperativity has been shown for EcPFK-1 in the absence of heterotropic regulation (Byrnes, Hu et al. 1995). Experiments with hybrid BsPFK-1 with only one active and one allosteric site have shown that the free energy of PEP inhibition for the hybrid is approximately three-fold than for the native protein (Kimmel and Reinhart 2001), further illustrating the complexity of heterotropic interactions. Residues 156 to 160 of EcPFK-1 are particularly important in the mediation of heterotropic interactions (Kundrot and Evans 1991).

BsPFK-1 has also been shown to be allosterically inhibited by non-physiological compound 2-phosphoglycolate that increases K_M for F6P without changing V_{max} of the reaction, similarly to PEP but with a smaller effect (Tlapak-Simmons and Reinhart 1994).

Most of the experimental evidence in the literature on PFK-1 kinetics is on the two bacteria, *B. stearothermophilus* and *E. coli*, as discussed above. The enzyme isolated from the archaebacterium *Desulfurococcus amylolyticus* is not controlled by allosteric effectors and shows hyperbolic Michaelis-Menten kinetics (Hansen and Schonheit 2000). Similarly, *Lactobacillus bulgaricus* PFK-1 is only affected by allosteric ligands, Mg.ADP and PEP, when they are present at much higher concentrations compared to BsPFK-1 and EcPFK-1 (Paricharttanakul, Ye et al. 2005).

For yeast *Schizosaccharomyces cerevisiæ*, PFK-1 shows cooperativity for substrate F6P while AMP and fructose-2,6-bisphosphate are allosteric effectors (Nissler, Otto et al. 1983). Conversely, the enzyme for *Kluyveromuces lactis* does not show cooperativity for F6P but is still affected in a less pronounced fashion by allosteric effectors (Bar, Schellenberger et al. 1997). Another yeast, simple unicellular eukaryote *Schizosaccharomyces pombe* has a single subunit PFK-1 which has lower cooperativity for F6P than *S. cerevisiae* but is as sensitive to effectors (Reuter, Naumann et al. 2000).

Eukaryote *Austromegabalanus psittacus* PFK-1 shows cooperative binding for F6P, as well as allosteric activation by AMP and fructose-2,6-bisphosphate, and inhibition by ATP and citric acid (Simpfendorfer, Oelckers et al. 2006). It must be noted that citric acid is an effector, which binds synergistically with Mg.ATP, but not an allosteric one (Goldhammer and Paradies 1979). However, the kinetic behaviour for mammalian PFK-1 is far more complex than that exhibited by either bacterial or yeast because the enzyme shows an association–dissociation reaction (Uyeda 1979).

Human PFKM-1 and PFKL-1 of erythrocytes have were found susceptible to inhibition by excess Mg.ATP and citric acid even before complete enzyme purification was achieved (Layzer, Rowland et al. 1969). Then, fructose-2,6-bisphosphate was shown to increase affinity for F6P and alleviates ATP inhibitory effect in isolated rat hepatocytes (Schaftingen, Hue et al. 1980).

Mammalian skeletal muscle PFK-1 shows hyperbolic Michaelis-Menten kinetics with respect to both substrates F6P and Mg.ATP at pH 8.0 (Kemp and Foe 1983). However, at pH values lower than 7.5, enzyme kinetics become cooperative and sigmoidal for F6P and excess Mg.ATP causes inhibition. Allosteric activators AMP and ADP antagonise ATP inhibition, while inhibitors citric acid, PEP and 3-phosphoglycerate act synergistically with Mg.ATP (Uyeda 1979; Bosca, Aragon et al. 1985). Studies at physiological PFKM-1 concentration have suggested a concentration dependency for the animal enzyme because diluted amounts used in *in vitro* assays significantly modify enzyme allostery (Bosca, Aragon et al. 1985).

Residue 161, that regulates hydrogen bonding of the active site in bacterial PFK-1, has changed roles and become essential in Mg.ATP allosteric inhibition through evolution from bacteria to mammals (Poorman, Randolph et al. 1984). Experiments with rabbit PFKM-1 have recently shown that allosteric inhibition by Mg.ATP and fructose-2,6-bisphosphate occurs through the same mechanism of forming an active tetramer from inactive dimeric enzyme form (Zancan, Almeida et al. 2007).

Allostery models and kinetic mechanisms for PFK-1 are still debated to this day. The biggest criticism against the MWC mechanism is its assumption of binding site symmetry, whereas the sequential model assumes the conformational change as a sequential process. A kinetic mechanism that can support fully the available experimental evidence is yet to be suggested. The complexity of PFK-1 kinetics exasperated Charles Cori, one of its first investigators in the 1950s, into characterising it as an "*all-hysteric enzyme*" (Sols 1979).

IV.1.2.2.2. **Phosphorylation**

PFK-1 regulation is also subject to phosphorylation. Protein kinases can transfer phosphate group from Mg.ATP to a specific site on the enzyme, resulting to stabilisation of the active conformation (Stryer 1999).

Brand and co-workers first showed that rat liver PFK-1 was activated through phosphorylation by an AMP-dependent kinase and deactivated by a phosphatase catalysed phosphorylation (Brand and Soeling 1975).

There is controversy on the exact mechanism because of the discrepancy between *in vitro* and *in vivo* experimental data. The latter show inhibition by phosphorylation through covalent modification of hydroxyl groups on PFK-1, while the former consistently demonstrate enzyme activation by exogenous or endogenous purified kinases (Simpfendorfer, Oelckers et al. 2006). Over-expression of kinases in the glycolytic pathway of *E.coli* through genetic modification increased glycolytic fluxes (Emmerling, Bailey et al. 1999; Emmerling, Bailey et al. 2000).

Conversely, PFK-2 the less abundant isoform of phosphofructokinase is solely controlled by activation by phosphorylation of a single serine residue (Stryer 1999).

Overall, regulation by phosphorylation has been observed for PFK-1 in different species, but the exact mechanism is still unclear. However, it does not appear that phosphorylation makes a significant contribution to PFK-1 regulation compared to allostery, especially for mammalian proteins (Kemp and Foe 1983).

IV.1.2.2.3. **Transcriptional control**

PFK-1 transciptional control occurs at an earlier level than afore-mentioned allostery and phosphorylation mechanisms. It has been shown that the promoter of human PFKM-1 controls expression of phosphofructokinase in different tissues (Johnson and McLachlan 1994).

IV.1.2.2.4. **Binding to membranes**

Mammalian liver PFK-1 was first shown to be inactivated by fatty acids in 1976 (Ramadoss, Uyeda et al. 1976). Palmitic and oleic acids decreased enzyme activity, but fatty acid inhibition could be prevented by the presence of allosteric effectors F6P, AMP, Mg.ATP and F16BP. Binding studies suggested that there are three binding site for lipids, the first binding two to four moles of oleic acid (OA) per mole of enzyme without affecting enzyme activity, whilst the second bound five to 15 moles of OA that completely and irreversibly inactivate the enzyme.

Human erythrocyte PFK-1 was subsequently shown to bind reversibly to the inner side of human and rabbit erythrocyte membranes altering enzyme kinetics (Karadsheh and Uyeda 1977). In more detail, the saturation kinetics for F6P switched from sigmoidal cooperative for the free PFK-1 to hyperbolic Michaelis-Menten in the presence of membranes. Also, the membrane bound enzyme no longer showed allosteric inhibition by 2,3-diphosphoglycerate and excess Mg.ATP. Further binding studies on human PFKM-1 showed that erythrocyte membrane binding depends on pH, potassium chloride concentration but is completely reversible (Higashi, Richards et al. 1979). Allosteric effectors ADP and Mg.ATP were found very potent in eluting rabbit liver PFK-1 from erythrocyte membranes (Jenkins, Madden et al. 1984).

Two other glycolytic enzyme, aldolase (Strapazon and Steck 1977) and glyceraldehyde 3-phosphate dehydrogenase (G3DP) (Yu and Steck 1975) were also shown to bind to erythrocyte membranes, three-fold more tightly than PFK-1 (Higashi, Richards et al. 1979). *In vitro* assays where all three enzymes were present resulted in reduced erythrocyte binding of PFK-1, and addition of aldolase and G3DP displaced PFK-1 from membranes (Higashi, Richards et al. 1979). Also, phosphorylated and dephosphorylated PFK-1 bind with the same affinity to erythrocyte membranes (Higashi, Richards et al. 1979).

Aldolase and G3DP associate with membranes by both forming a complex with the cytoplasmic surface domain of Band 3 protein(Yu and Steck 1975; Strapazon and Steck 1977). The latter is a well-characterised integral glycoprotein that is most predominant in human erythrocyte membranes (Yu and Steck 1975).

Rabbit muscle aldolase binds to membranes with negative cooperativity (Strapazon and Steck 1976). Binding can be alleviated by increasing the ionic strength or the pH in the assay (Strapazon and Steck 1977). Conversely, G3DP binds to erythrocyte membranes with positive cooperativity (Yu and Steck 1975). The enzyme complex with Band 3 is held together by electrostatic interactions between basic residues on the active sites of aldolase and G3DP, and the highly acidic amino terminus of Band 3 (Kliman and Steck 1980; Murthy, Liu et al. 1981). PFK-1 was also suggested to associate through its poly-basic adenine nucleotide allosteric site with the amino-terminal of Band 3 (Jenkins, Kezdy et al. 1985). Dissociation of tetramers in solution, which then bind to membranes as dimers was the suggested mechanism. Also, it has been shown that during myocardial ischemia PFK-1 reversibly translocates to myocardial membranes, where it is catalytically inactive (Hazen, Wolf et al. 1994).

Recently, it was suggested that all three enzymes form a common complex with Band 3 on the human erythrocyte membrane through a poly-acidic amino acid sequence (Campanella, Chu et al. 2005). This argument was supported a year later with an attempt at mapping the exact enzyme binding sites on Band 3 (Chu and Low 2006).

Phosphorylation of tyrosine residues on the acidic terminus of Band 3 by a protein kinase in human erythrocytes prevented the binding of all three glycolytic enzymes, and thus stimulated glycolysis (Harrison, Rathinavelu et al. 1991). On the contrary, rabbit muscle PFK-1 binding to myofibril membranes was also shown to be independent of membrane phosphorylation (Andres, Carreras et al. 1996).

As summarised in this section, experimental evidence has unequivocally shown mammalian PFK-1 to bind to the inner leaflet of human erythrocyte membranes with allostery inhibition, despite this enzyme being classically considered cytoplasmic. Also, it has been suggested that most of the active PFK-1 in the cell is membrane-bound (Jenkins, Madden et al. 1984). Consequently, many questions arise about the mechanism of enzymatic control of glycolysis through binding to membranes.

IV.1.2.2.5. **Other types of control**

Calmodulin, which regulates CTP: phosphocholine cytidylytransferase (CCTα) by interacting with it protectively against calpains (see section II.1.3.3), also binds to rabbit PFKM-1 (Mayr and Heilmeyer 1983). Binding of calmodulin to the latter induces a conformational dissociation of the enzyme tetramer to a dimer without seriously compromising catalytic activity (Marinho-Carvalho, Zancan et al. 2006). Clotrimazole, a calmodulin antagonist, has been shown to inhibit PFK-1 both indirectly by inhibiting calmodulin and directly by detaching the enzyme from the cytoskeleton (Zancan, Rosas et al. 2007). Sola-Penna and co-workers had previously reported that PFK-1 interacts with actin in the cytoskeleton (El-Bacha, Freitas et al. 2003).

Also, insulin has been shown to bind to rabbit PFKM-1 through a specific receptor with stimulatory effects to glycolysis (Zancan and Sola-Penna 2005). Insulin stimulation increases intracellular calcium cation levels by boosting calcium influx in erythrocytes, which do not contain any organelles (Zancan and Sola-Penna 2005). A synergistic effect between insulin and calmodulin has been suggested, but the exact mechanism is still unclear (Zancan and Sola-Penna 2005).

IV.1.2.3. Why PFK-1?

There were three main reasons behind the choice of this particular enzyme. First, BsPFK-1 has 13 amphipathic α-helices in each monomeric subunit, although only four of them in total for the whole tetramer are exposed when the dimer of dimers is assembled (Evans and Hudson 1979).

Second, mammalian PFK-1 has been shown to bind to erythrocyte membranes with strong experimental evidence, as summarised in a previous section (see section IV.1.2.2.4). Therefore, BsPFK-1 could also potentially bind to membranes.

Third, PFK-1 is rate-determining for the whole biosynthetic pathway of glycolysis (Goldhammer and Paradies 1979; Corredor and Bosca 1985; Zhang, Gao et al. 2007). This enzyme is also regulatory since the reaction is virtually irreversible. PFK-1 only catalyses the forward direction, whilst fructose biphosphatase (EC 3.1.3.11) catalyses the backward dephosphorylation of F16BP to F6P.

Other secondary reasons contributed to our choice of this enzyme. It has been suggested that glycolysis, sugar metabolism, and phospholipolysis, lipid degradation are coupled as mammalian myocardial phosphosholipase A2 (PLA2) directly and specifically interacts with PFK-1 (Hazen and Gross 1993). Also, PFK-1 is regulated by calmodulin like CCTα (see sections II.1.3.3 for CCTα and IV.1.2.2.4 for PFK-1).

PFK-1 from *B. stearothermophilus* in particular was studied because of its commercial cost-effective availability in high purity. Most importantly, this enzyme provides a convenient model system of PFK-1 allosteric behaviour without the complexity of *E. coli* and eukaryotic enzymes. BsPFK-1 shows hyperbolic kinetics in the absence of effectors that can be simply explained by the Michaelis-Menten and Monod models without enlisting use of more complicated kinetic models required for the cooperative kinetics of EcPFK-1 and eukaryotic PFK-1.

Also, being a homotetramer, any conclusions drawn for BsPFK-1 would apply to larger aggregates forming in other organisms.

Consequently, although PFK-1 is not classified as an amphitropic protein like CCTα, it is a cytoplasmically active enzyme that can still function efficiently when bound to membranes, has multiple amphipathic α-helices and is regulatory for a major metabolic pathway. This study was thus conducted to find whether PFK-1 activity depends on membrane lipid composition and whether PFK-1 is regulated via membrane stored elastic stress, in an analogous manner to CCTα (see chapter II).

IV.2. Development a new radiochemical PFK-1 assay

IV.2.1. Available PFK-1 assays

There are several different assays available in the literature that can be used to *in vitro* monitor PFK-1 activity (Uyeda 1979):

- A coupled spectrophotometric or fluorometric NADH decrease assay where F16BP is coupled to aldolase, G3DP and triose phosphate isomerase reactions where two moles of NADH are oxidised for every one mole of F-1,6-BP formed.
- A coupled spectrophotometric or fluorometric ADP production assay using pyruvate kinase and lactate dehydrogenase.
- An assay using continuous measurement of protons production using a pH stat.
- A radiochemical assay using [γ-^{32}P] ATP to form ^{32}P-F-1,6-BP with and F6P, originally used for ATPase activity measurements, has been reported as a successful way to assay PFK-1 activity (Sola-Penna, dos Santos et al. 2002).

The radiochemical method was preferred for our experiments mainly because it does not involve membrane binding enzymes. Enzymes aldolase and G3DP, that are used in the first type of coupled assays, have been shown to bind to membranes (Yu and Steck 1975; Strapazon and Steck 1977) and modulate catalytic activity as described in section IV.1.2.2.4. Similarly, the kinase used in the second type of coupled assays would also regulate enzyme activity through phosphorylation (see section IV.1.2.2.2). Finally, changes in pH have been shown to affect PFKM-1 activity (Kemp and Foe 1983). Therefore, an exclusive study of the effect of membranes on PFK-1 is not possible when using any of the non-radiochemical assays.

Another advantage of the radiochemical assay is that it has already been used to investigate PFK-1 in the presence of cellular components such as insulin and calmodulin (Zancan and Sola-Penna 2005; Zancan and Sola-Penna 2005). Thus, introduction of large unilamellar vesicles (LUVs) in the assay as a viable model of membranes will potentially not disrupt assay conditions.

IV.2.2. A novel radiochemical PFK-1 assay

As part of this investigation, it was attempted to adapt the already available ^{32}P radiochemical PFK-1 assay for use with the less hazardous isotope ^{33}P. Preliminary experiments by Li in our research lab, also confirmed by initial experiments for this thesis, showed that the protocol was not reproducible using ^{33}P. Therefore, the need to develop a novel ^{33}P PFK-1 radiochemical assay arose.

First, non-radioactive experiments were undertaken in order to establish optimal thin layer chromatography (TLC) conditions, including type of TLC plates, eluent and elution duration, as well as spot visualisation techniques.

Then, radioactive controls and assays were ran so as to adjust the amount of ^{33}P radioactivity for optimal results while keeping the amounts as small as possible, following the rule of best practical means for radiochemical work.

Subsequently, the relative amounts of ATP, F6P, lipid and PFK-1 were implemented for a 50 μL assay and an appropriate incubation time was established. The most challenging task was to find an effective way to quench enzyme activity. BsPFK-1 is extremely potent catalytically and the method used in the ^{32}P PFK-1 assay could not stop the reaction.

Different quenching agents were thus investigated in order to find which one stopped enzyme activity without hindering either catalysis or visualisation. Copper(II) previously found to inhibit BsPFK-1 activity of PFK-1 (Gebhard, Ronimus et al. 2001) could not quench the reaction. Immersion in liquid nitrogen

appeared to stop catalytic activity intermittently but not effectively. Finally, based on observations that urea completely unfolds EcPFK-1 (Bras, Teschner et al. 1989; Cowan and Storey 2002), a combination of addition of 66.7 μM urea followed by a ten minute immersion in liquid nitrogen effectively quenched BsPFK-1 catalytic activity.

The key differences between the two ^{32}P and ^{33}P PFK-1 radiochemical assays are summarised in Figure IV.7.

	^{32}P radiochemical assay	**^{33}P radiochemical assay**
Buffer	50 mM Tris- HCl, 5 mM $MgCl_2$, 5 mM $(NH_4)_2SO_4$ pH 7.4 at RT	50 mM Tris- HCl, 5 mM $MgCl_2$, 5 mM $(NH_4)_2SO_4$ pH 7.4 at RT
Assay	400 μL for 30 seconds at 37°C	50 μL for ten minutes at 37°C
Assay conditions	1 mM F6P, 1mM [γ-32P] ATP at 4 μCi/μmol and 2 μg of purified rabbit PFKM-1.	100 μM F6P, 10 μM [γ-32P] ATP at 292 μCi/μmol and 5.83 mu/mL of purified BsPFK-1
Quenching agent	Quenched with 0.1 H HCl. Centrifuged at 1500xg at 4 C for 15 minutes. Supernatant frozen in liquid nitrogen and lyophilised overnight. Lyophilised residue re-dissolved in distilled water and spotted.	Quenched with 66.7 μM urea. Immersed in liquid nitrogen for ten minutes.
TLC elution conditions	3.5 h in 4:1:4 isopropanol: acetone:(10 mM lactate/ 5mM H_3PO_4)	8 h in 4:1:6 isopropanol: acetone:(28 mM lactate/ 19 mM H_3PO_4)
Visualisation	Sugars revealed by spraying with 0.02% (w/v) orcinol in 2 M H_2S0_4, then incubated at 100 °C for 10 minutes. Radioactive spots detected by autoradiography for 24 h at RT.	Sugars revealed by spraying with 0.02% (w/v) orcinol in 2 M H_2S0_4, then incubated at 200 °C for 30 minutes. Radioactive spots detected by autoradiography for 48 h at -10 °C.

Figure IV.7- Comparative table of optimised experimental conditions for ^{32}P and ^{33}P radiochemical assays

Overall, there are both similarities and differences between the two assays. On the one hand, the same buffer is used in both since magnesium sulphate has been shown to enhance PFK-1 binding to membranes (Higashi, Richards et al. 1979).

Also, the component solvents of the TLC eluent are the same but at different concentrations.

On the other hand, our ^{33}P PFK-1 assay combines the benefits of the previously available ^{32}P assay with the advantages of markedly smaller decay energy, a smaller assay volume, use of a cheap commercial source of enzyme while ^{33}P is a cheaper and less hazardous radiochemical. Finally, this assay allows the study of the effect of membranes to PFK-1 activity by means of introduction of large unilamellar vesicles (LUVs). The latter are particularly efficient models of the cell membrane as discussed in section I.I.4.

Consequently, we first used the ^{33}P PFK-1 radiochemical assay to undertake kinetic studies, which we compared to results from the spectrophotometric and ^{32}P radiochemical methods. Since our results were comparable to the literature, we then investigated the effect of membranes and membrane composition on the catalytic activity of BsPFK-1.

IV.3. Experimental

IV.3.1. Materials

All chemicals were of highest possible grade. DOPC, OA, $MgCl_2$, Tris buffer, urea, ATP, F6P, $(NH_4)_2SO_4$, lactic acid, and H_3PO_4 were from Sigma Aldrich (Dorset, UK). PFK-1, Type VII, from *Bacillus stearothermophilus* was also acquired from Sigma. Pre-coated F_{254} 60 Å silica gel Merck TLC plates on plastic support were from VWR (Leicestershire, UK). Purified water, acetone and isopropanol of HPLC grade were acquired from Fisher Scientific (Leicestershire, UK). ACS Scintillation Cocktail and adenosine 5'-[μ-33P] triphosphate triethylammonium salt (9.25 MBq, 25 μCi) were purchased by GE Healthcare, formerly Amersham Biosciences (Buckinghamshire, UK). Polypropylene scintillation vials and FujiFilm RX NIF medical film was purchased from Fisher Scientific (Leicestershire, UK).

During the development of the radiochemical assay the following types of TLC plates were tested but did yield satisfactory results: Merck Cellulose F matrix, Polyester support, 0.1 mm; Macherey-Nagel Polygram Sil G/UV_{254}, polyester support, 0.20 mm, 60 Å pores; Macherey-Nagel Alugram Sil U V_{254} matrix, aluminium support, 0.20 mm, 60 Å pores; Whatman DEAE cellulose 300 Flexible matrix, DEAE support; and Whatman Polyester Flexible plates.

IV.3.2. Methods

IV.3.2.1. Preparation of LUVs

The appropriate volumes of lipid for each composition were decanted into 3 mL brown HLPC vials to a total lipid amount of 2.54 μmoles. Pure water (200 μL) was added to each vial and the samples were lyophilised to dryness. Standard buffer (169.3 μL, 150 mM Bis Tris, 10 mM $MgCl_2$ of pH 7.0 at 37 °C) was pipetted into the vials, which were then vortexed for 10 minutes and rested for 20 minutes. The samples were subsequently sonicated for 20 minutes and allowed to rest for a further 20 minutes. Four freeze-thaw cycles were carried out. Before use in the assay, the vesicles were sized using a Coulter N4 PLUS Particle Sizer (Attard Group) using a 10 μM amphiphile sample.

IV.3.2.2. Radiochemical Assay

Reaction in a 50 μL assay volume (0.10 mM F6P, 5.83 munits/mL PFK-1) was initiated with the addition of ATP (0.01 mM) and incubated at 37 °C for 10 minutes. Buffer used contained 50 mM Tris, 5 mM $MgCl_2$, 5 mM $(NH_4)_2SO_4$ and pH 7.4 at 37 °C. Activity of ^{33}P is 50 nCi per 50 μL assay. The reaction was quenched with immersion into liquid nitrogen for 10 minutes and addition of 10 μL 0.4 M urea. The whole assay was spotted onto silica gel TLC plates and eluted in 4:1:6 isopropanol: acetone: (28 mM lactic acid /19 mM phosphoric acid) mixture for 8 hours. The plate was then visualised using autoradiography by exposing films to decay for at least 24 hours at -20 °C as illustrated in Figure IV.8.

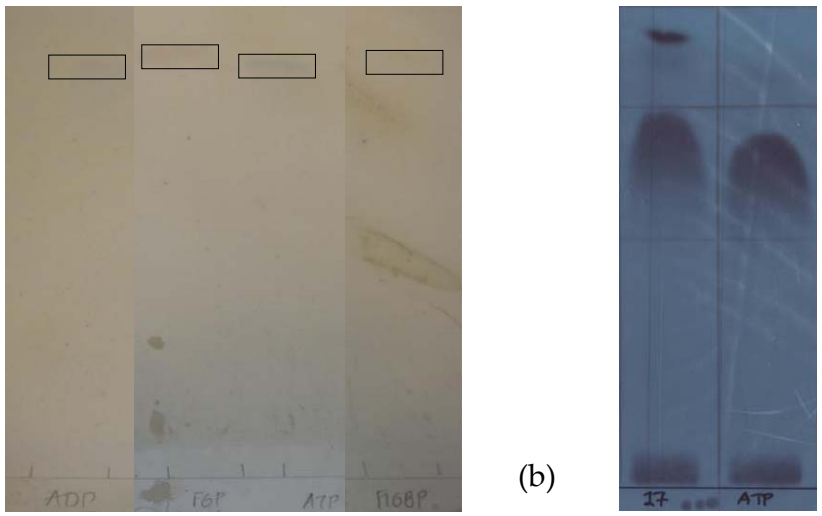

Figure IV.8- TLC plates from PFK-1 ^{33}P assay. In (a), reference spots for substrates F6P and ATP, and products F16BP and ADP have been visualised with orcinol. In (b), autoradiographies of the reaction mixture and an ATP reference spot are shown.

Each spot was cut out separately for each fraction and inserted into liquid scintillation vials with the addition of ACS Scintillation Cocktail (4 mL). Radioactive decay was measured using the LS6500 Beckman Liquid Scintillation Counter (School of Chemistry, Radiochemical Lab). After the end of the assay the radionuclide content was disposed following the local rules of the School of Chemistry, University of Southampton under the Radiation Protection Act.

IV.4. Kinetic investigation of PFK-1

IV.4.1. BsPFK-1 kinetics as a function of time

A time variable kinetics assay was run in order to establish an incubation time for BsPFK-1 under the conditions of our novel ^{33}P radiochemical assay (Figure IV.9).

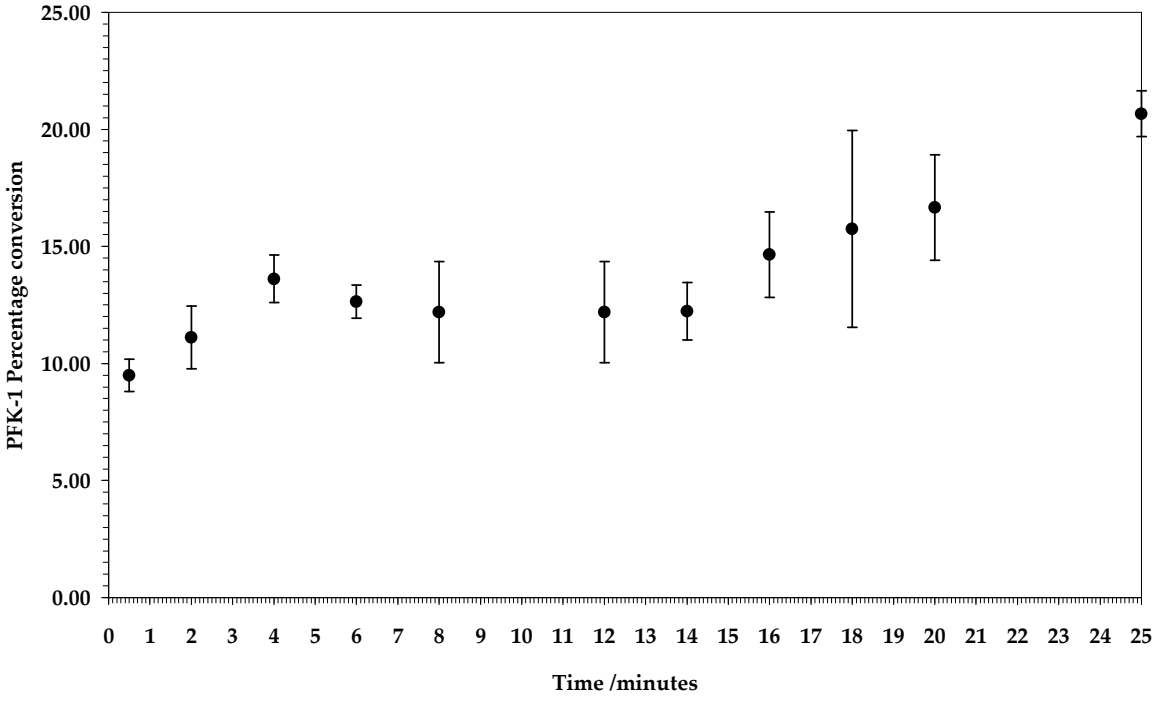

Figure IV.9- Plot of PFK-1 percentage conversion as a function of time for a 100 μM F6P, 10 μM ATP and 5.83 mU/mL PFK-1 assay (Assay 68).

BsPFK-1 activity reached a plateau at approximately 15 minutes. Thus, a ten minute incubation time was selected as it was on the plateau of the saturation curve. This is an experimentally manageable time that improves on the 30 seconds used in the ^{33}P radiochemical assay (Sola-Penna, dos Santos et al. 2002). It must be noted that the enzyme does not show a typical saturation curve, as exhibited for CCTα (see section II.3) since a nine percent conversion was observed at an incubation time as short as 30 seconds. It could be that the linear increase of reaction had already occurred even before the 30 second data point, which is the minimum that can be feasibly measured.

IV.4.2. BsPFK-1 kinetics as a function of enzyme concentration

A variable BsPFK-1 concentration assay was run in order to find the appropriate enzyme amount required for the conditions of our novel ^{33}P radiochemical assay (Figure IV.10). The experiment was also repeated in the presence of binary LUVs containing DOPC and DOPC/OA (50:50).

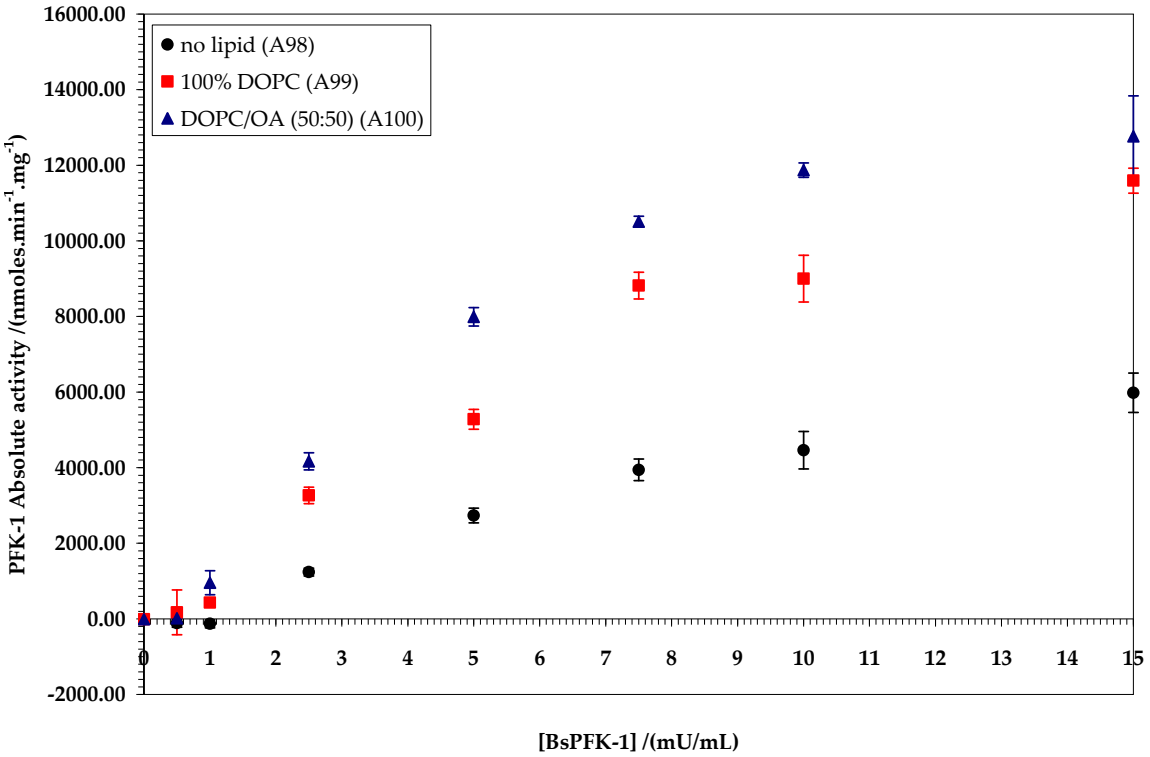

Figure IV.10- Plot of PFK-1 absolute activity against enzyme concentration for 100 μM F6P and 10 μM ATP assays in the presence of 25 μM LUVs.

PFK-1 absolute activity showed an exponential trend in both absence and presence of membranes. The DOPC/OA (50:50) binary system was about two-fold more activating compared to no lipid present. DOPC was also activating, but to a lesser degree than when OA was present in the binary LUVs. All three experiments reached a plateau at the higher concentrations of enzyme.

An optimal enzyme concentration of 5.00 mU/mL of solid was chosen for the conditions of our assay for the assay was chosen as since it is in the linear range of the observed trends. This corresponds to a 5.83 mU/mL pure protein concentration.

IV.4.3. BsPFK-1 kinetics as a function of lipid concentration

Variable total lipid concentration assays were run in order to find the appropriate lipid amount required for the conditions of our novel ^{33}P radiochemical assay (Figure IV.11).

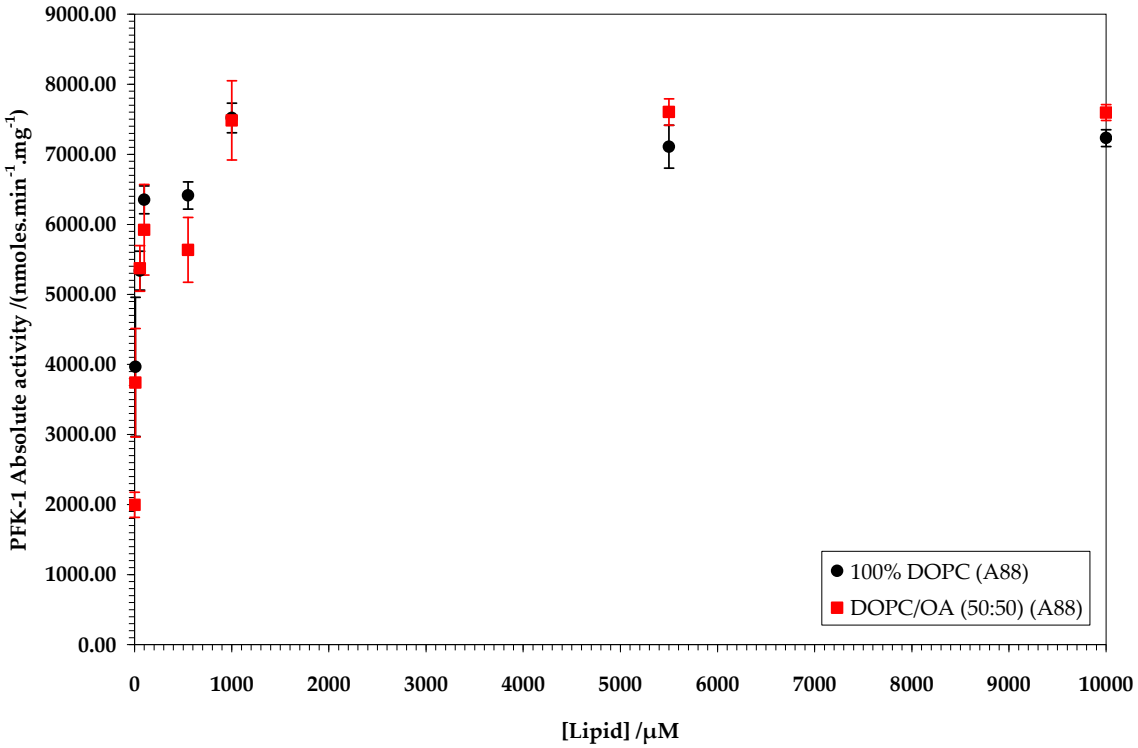

Figure IV.11- Plot of PFK-1 absolute activity against lipid concentration for 100 μM F6P, 10 μM ATP and 5.83 mU/mL assays in the presence of LUVs.

The DOPC/OA (50:50) binary system was more activating than 100% DOPC, but at very high lipid concentrations both systems showed saturation.

The same experiment was repeated with the acquisition of a higher density of data points plotted on a logarithmic scale (Figure IV.12). As in Figure IV.11, DOPC/OA (50:50) was more activating than 100% DOPC throughout the range. Saturation of enzyme activity occurred at approximately 1 mM of total lipid. Interestingly, OA and sodium dodecyl sulphate (SDS) have been shown to both deactivate rat liver PFK-1 as fatty acid monomers in solution, not in LUVs as in our experiment (Ramadoss, Uyeda et al. 1976).

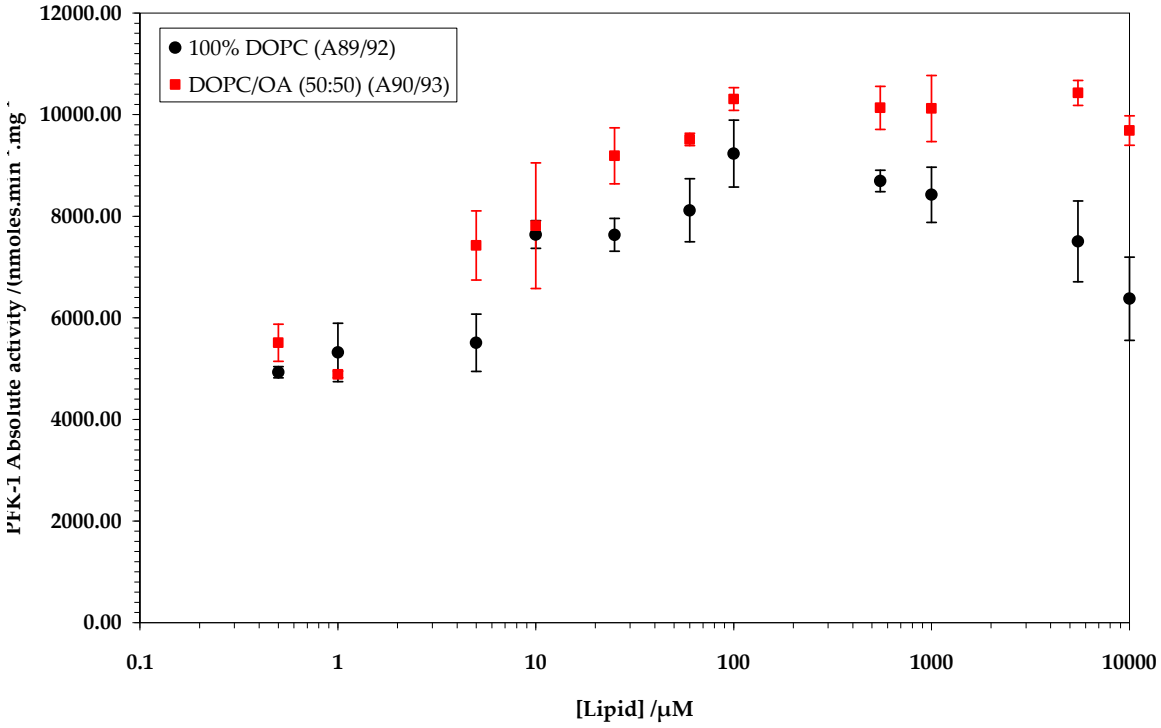

Figure IV.12- Plot of PFK-1 absolute activity against lipid concentration for 100 μM F6P, 10 μM ATP and 5.83 mU/mL assays in the presence of LUVs.

Comparing PFK-1 and CCTα, CCTα activity saturated at 0.2 mM of total lipid compared to 1 mM for PFK-1 (Fagone 2003). Also, PFK-1 maximum saturation occurred with a five-fold smaller amount of enzyme (94.6 fmoles) compared to 11.2 nmoles for CCTα.

Enzyme	Lipid amount at saturation point of lipid variable plot	Lipid amount in 50 μL assay	Enzyme amount in 50 μL assay	Enzyme : Lipid ratio in 50 μL assay
PFK-1	50 nmoles	1.25 nmoles	9.46 E-06 nmoles (94.6 fmoles)	7.75 E-06
CCTα	10 nmoles	50 nmoles	11.2 nmoles	0.23

Figure IV.13- Table of lipid and enzyme amounts in PFK-1 and CCTα assays.

Consequently, a much larger excess of total lipid is required for CCTα maximal activation compared to PFK-1 (Figure IV.13).

As a result, a 25 μM concentration of total lipid was decided as the total lipid amount to be used in our ^{33}P radiochemical BsPFK-1 assay. That value corresponds to the concentration of DOPC/OA (50:50) which caused a 50 percent change in enzyme activity. It was chosen since OA has been reported as the most potent lipid effector of PFK-1 and hence it would allow investigating the effects of less activating systems. Also, the value is in very close agreement to the 35 μM OA that caused a 50 percent change in rat liver PFK-1 activity in a spectrophotometric assay (Ramadoss, Uyeda et al. 1976).

IV.4.4. BsPFK-1 kinetics as a function of ATP concentration

ATP BsPFK-1 kinetics were investigated in order to establish our assay conditions and to assess the accuracy of our novel ^{33}P radiochemical assay in comparison to results acquired by spectrophotometric assays from the literature. Our results are shown in Figure IV.14.

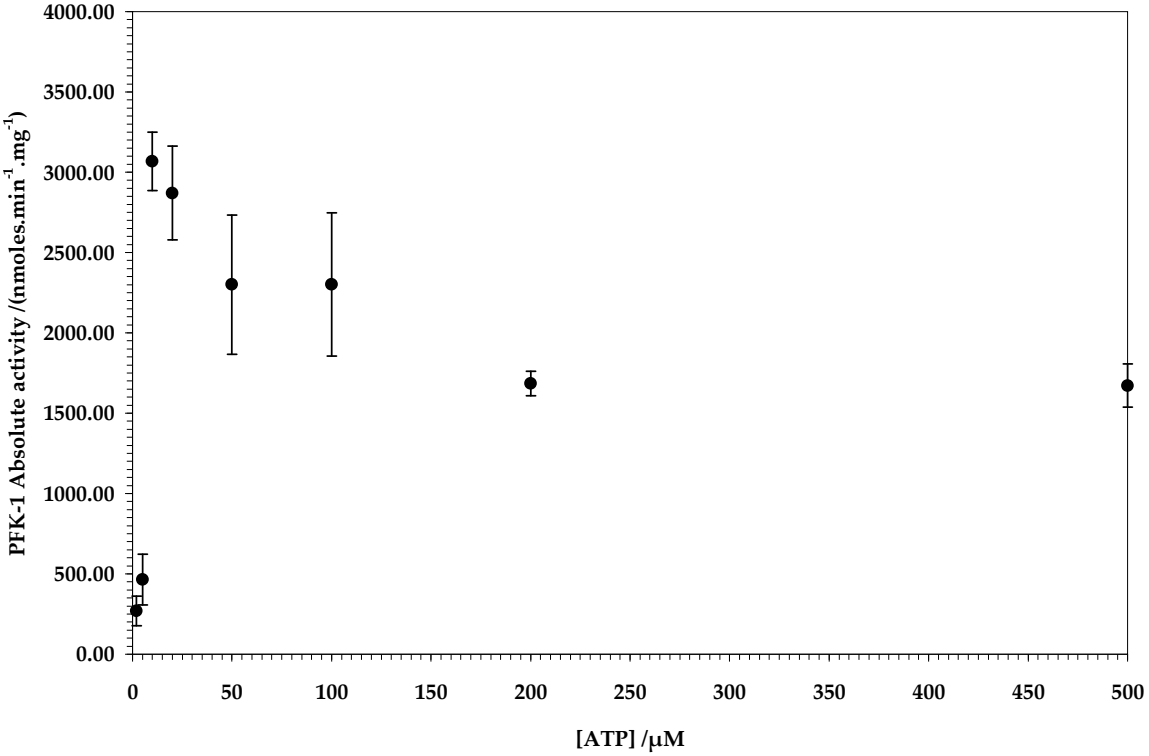

Figure IV.14- Plot of PFK-1 absolute activity against ATP concentration for a 100 μM F6P and 5.83 mU/mL assay (Assay 66).

A 25 μM ATP gave the maximal absolute activity for the enzyme. Further increase of the co-substrate ATP started to decrease catalytic activity with reached a plateau at approximately 1700 nmoles.min^{-1}.mg^{-1}. This trend is in line with results shown in the literature (Byrnes, Zhu et al. 1994) since ATP non-allosterically inhibits F6P.

In a separate experiment, the effect of four different ATP assay concentrations of 10, 25, 50 and 100 μM, to the variable time kinetics for BsPFK-1 was investigated (Figure IV.15). Results for 100 μM ATP are not shown since the reaction was completely inhibited and percentage conversion remained close to zero throughout the assay. A 10 μM ATP concentration was thus decided for our assay conditions.

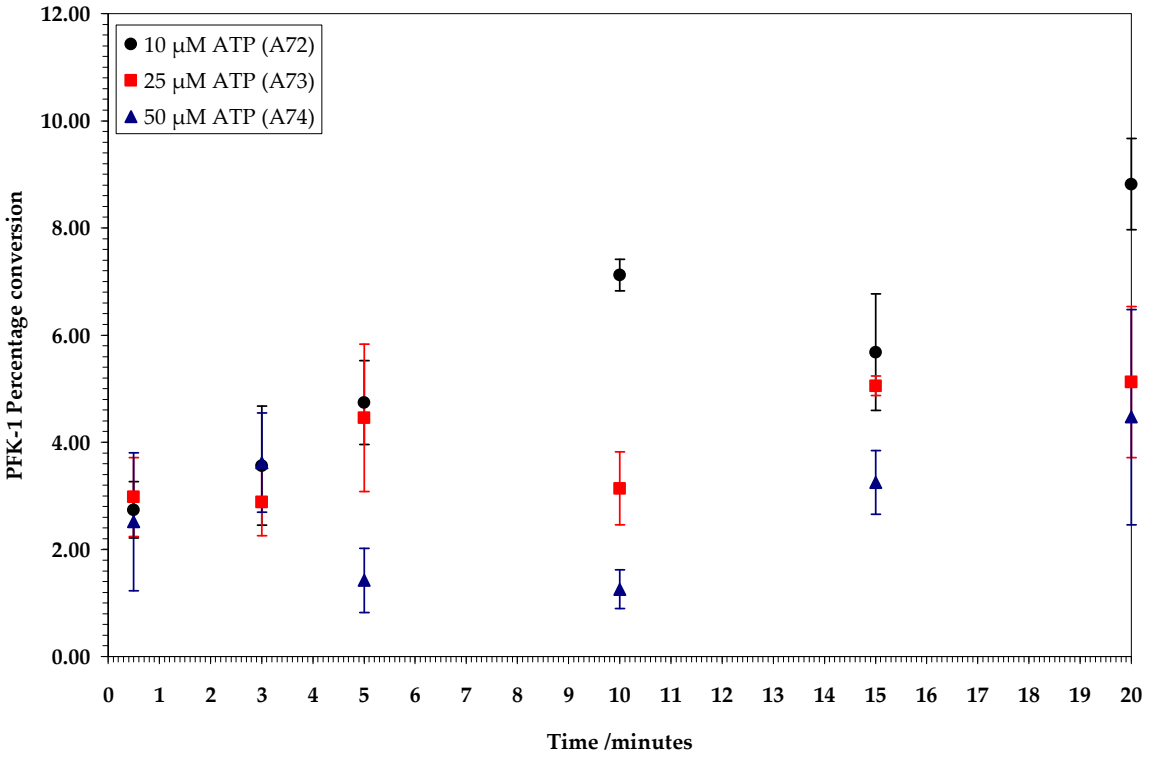

Figure IV.15- Plot of PFK-1 absolute activity as a function of time for 100 μM F6P and 5.83 mU/mL assays in 10, 25 and 50 μM ATP in the presence of LUVs.

Maximal conversion rates were observed at 10 μM ATP. The two higher ATP concentrations at 25 and 50 μM significantly decreased BsPFK-1 catalytic activity. These results support the ATP kinetics data (Figure IV.14) and again illustrate the how ATP inhibits enzyme activity at high concentrations.

IV.4.5. BsPFK-1 kinetics as a function of F6P concentration

As for the other assay components, F6P BsPFK-1 kinetics were investigated in order to establish assay conditions and to compare with results from spectrophotometric assays in the literature. Our results are shown in Figure IV.16.

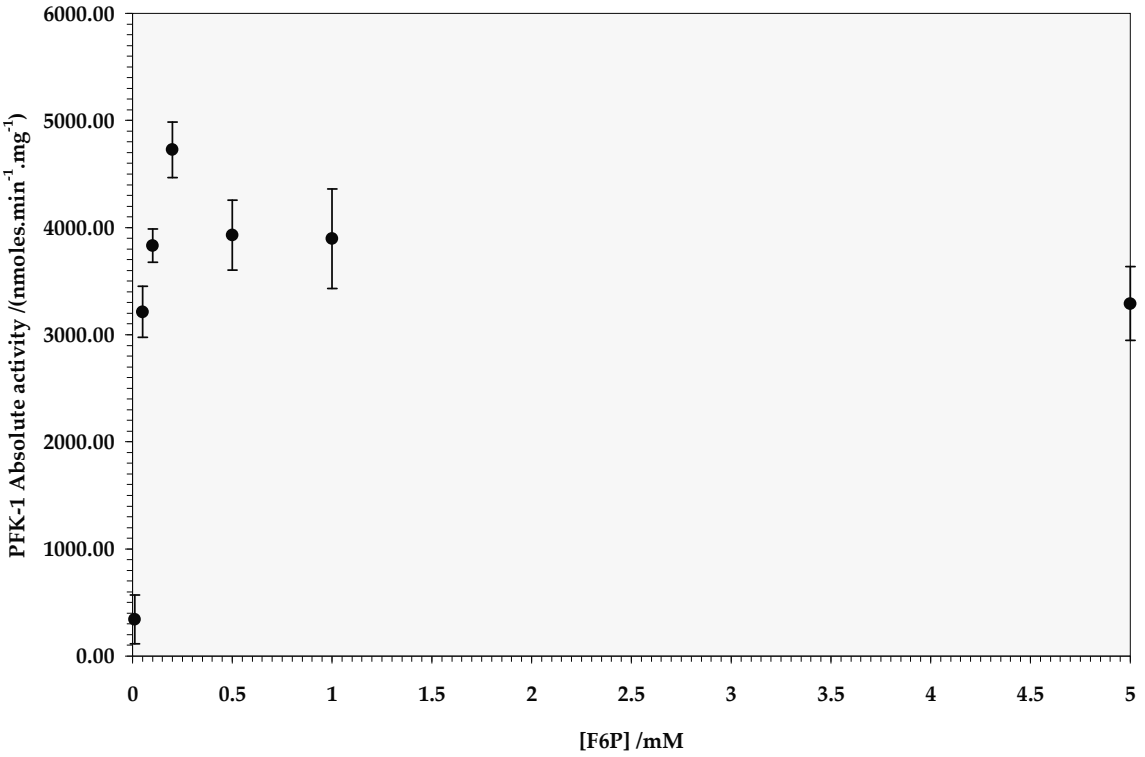

Figure IV.16- Plot of PFK-1 absolute activity against F6P concentration for a 10 μM ATP and 5.83 mU/mL assay (Assay 94).

Enzyme activity increased exponentially reaching a maximum at a 0.2 mM F6P. Then, saturation occurs and enzyme activity slowly decreased. These results illustrate hyperbolic Michaelis-Menten kinetics as expected for BsPFK-1 (Valdez, French et al. 1989). From these data, V_{max} and K_M were estimated at 4726.79±260.16 nmoles.min^{-1}.mg^{-1} and 35.00± 3.85 μM respectively.

F6P saturation plots were also acquired in the presence of binary LUVs consisting in either 100% DOPC or DOPC/OA (50:50), as shown in Figure IV.17.

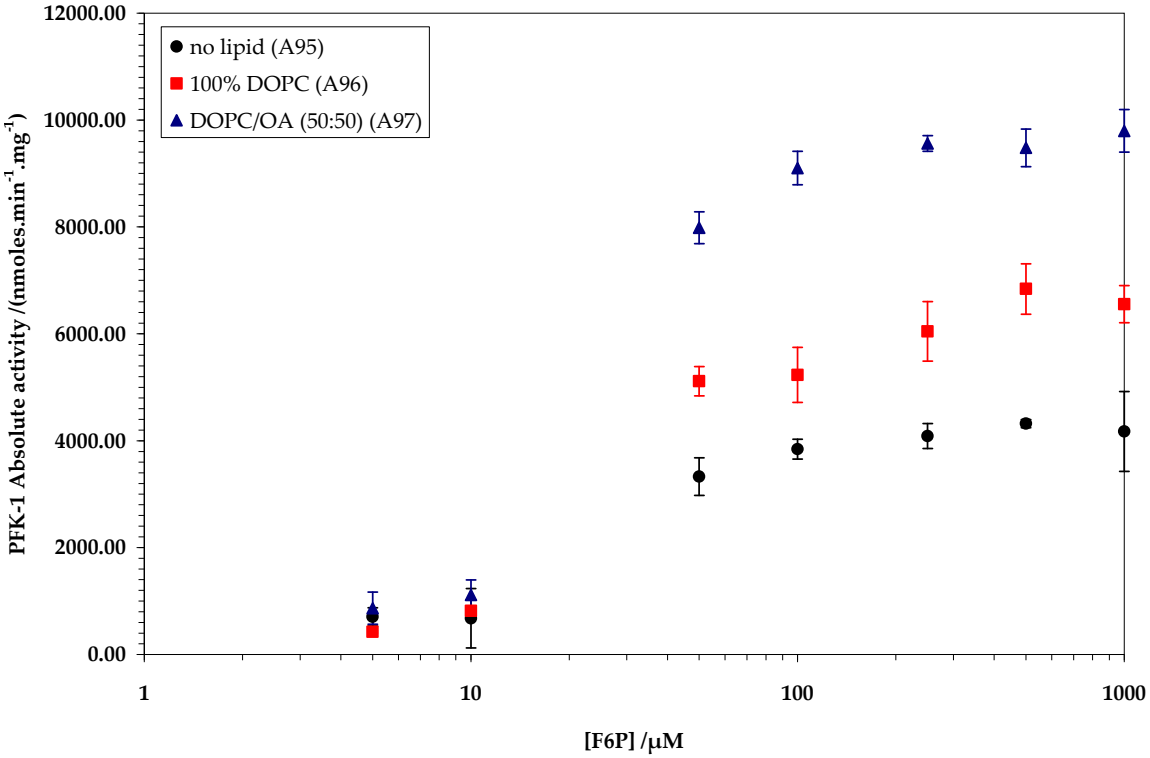

Figure IV.17- Plot of PFK-1 absolute activity against F6P concentration for 10 μM ATP and 5.83 mU/mL PFK-1 assays in the presence of 25 μM LUVs.

A maximal two-fold activation was observed in the presence of 100% DOPC LUVs, whilst the DOPC/OA (50:50) binary system caused a three-fold activation compared to no lipid present. However, kinetics remained non-allosteric Michaelis-Menten in the presence of both lipidic systems.

Results for BsPFK-1 in the presence of LUVs are in line with those for membrane bound human PFK-1. The latter also shows hyperbolic kinetics when membrane bound, although its F6P kinetics are cooperative and allosteric in the absence of membranes (see section IV.1.2.2.4).

System	V_{max} /nmoles.min-1.mg-1	K_M /μM
no lipid	4285.01±574.33	32.0±4.3
100% DOPC	6571.40±373.72	34.0±2.0
DOPC/OA (50:50)	9759.78±306.54	32.0±1.0

Figure IV.18- V_{max} and K_M values in the presence and absence of lipids.

As shown in Figure IV.18, the presence of lipids in the assay increased V_{max} and but did not affect K_M. This suggests that BsPFK-1 binding to membranes is uncompetitive with respect to the substrate F6P and that membranes bind simultaneously to F6P without inhibiting the formation of the enzyme-substrate complex. Lineweaver-Burk plots for these kinetic data can be used for further analyses (see section IV.1.2.2.1).

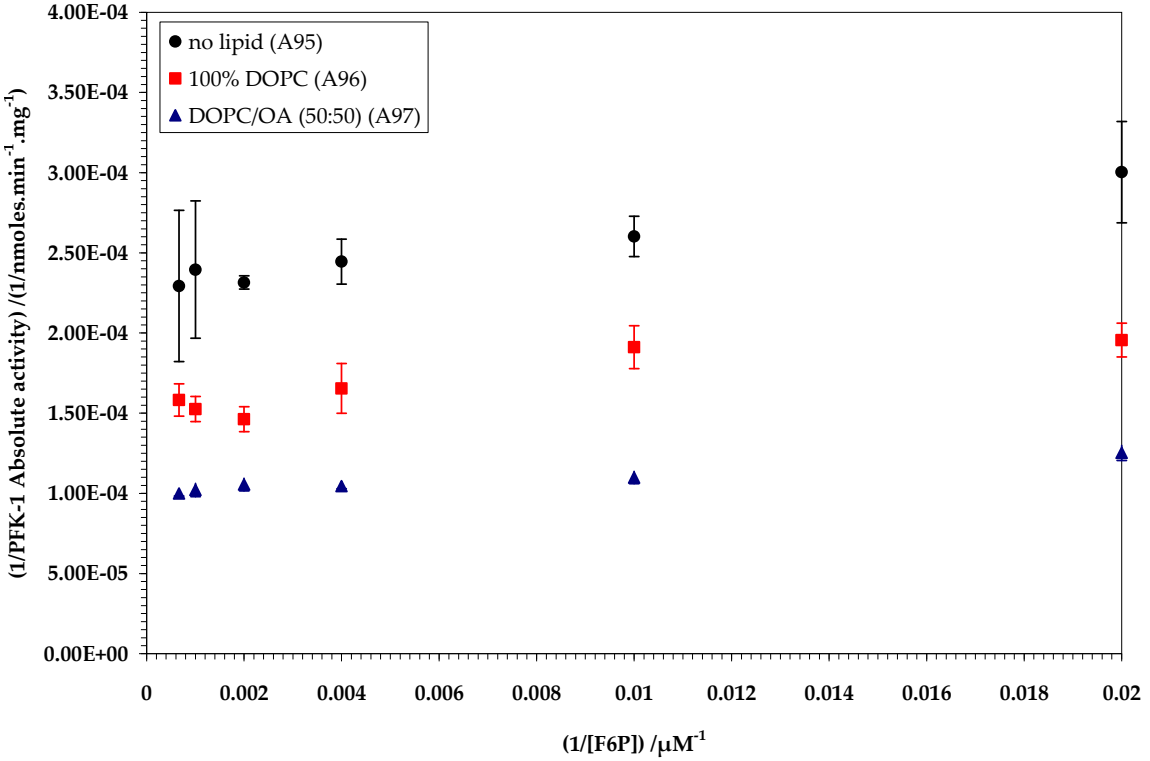

Figure IV.19- Lineweaver-Burke plot for BsPFK-1 for 10 μM ATP and 5.83 mU/mL PFK-1 assays in the presence of 25 μM LUVs.

As seen in Figure IV.19, Lineweaver-Burke plots showed characteristics of uncompetitive effectors with curves having same slope but different y-intercept.

However, since Michaelis-Menten kinetics do not strictly apply to membrane bound enzymes, there are limitations to the conclusions drawn using V_{max} and K_M comparisons as calculated from Michaelis-Menten equations. An interesting new kinetic model has been suggested, termed as surface dilutions kinetics, which takes into account the surface interactions of enzymes involved associated with lipids. Surface dilutions equations can be applied to all lipid interfaces including micelles, vesicles, liposomes and membranes. For cobra venom PLA2 in mixed micelles consisting in DOPC and detergent Triton X-100, the soluble enzyme (E) associates with micelles (A) forming an enzyme-mixed micelle complex (EA) during the first and bulk step of the surface dilutions kinetics model (Carman, Deems et al. 1995):

$$E + A \underset{k_{-1}}{\overset{k_1}{\rightleftharpoons}} EA$$

The enzyme can either bind to the micelle surface non-specifically (surface binding model), or it can interact with a particular phospholipid molecule on the micelle surface (phospholipid binding model). Subsequently to both scenarios, PLA2 hydrolyses a phospholipid molecule (B) of the micelle to a fatty acid and a lysophospholipid. Thus, an EAB complex forms in the catalytic site during this surface step:

$$EA + B \underset{k_{-2}}{\overset{k_2}{\rightleftharpoons}} EAB$$

In the final step, the EAB complex dissociates to the product/s (Q) and the enzyme-mixed micelle complex:

$$EAB \underset{k_{-3}}{\overset{k_3}{\rightleftharpoons}} Q + EA$$

Overall, the kinetic rate equation for surface dilutions kinetics is:

$$V = \frac{V_{max}(A)(B)}{K_s{}^A K_M{}^B + K_M{}^B(A) + (A)(B)},$$

where $K_s{}^A = k_{-1}/k_1$ and $K_M{}^B = (k_{-2} + k_3)/ k_2$.

Consequently, surface dilutions kinetics could potentially be applied to PFK-1 for modelling enzyme association with membranes, in a fashion similar to PLA2.

IV.5. Effect of allosteric effectors on BsPFK-1

IV.5.1. Inhibition by PEP in the presence of lipids

PEP inhibits BsPFK-1 activity and switches F6P kinetics from Michaelis-Menten to cooperative, as discussed in section IV.1.2.2.1. Therefore, F6P BsPFK-1 kinetics were studied for 5, 25 and 100 μM PEP as shown in Figures IV.20-21.

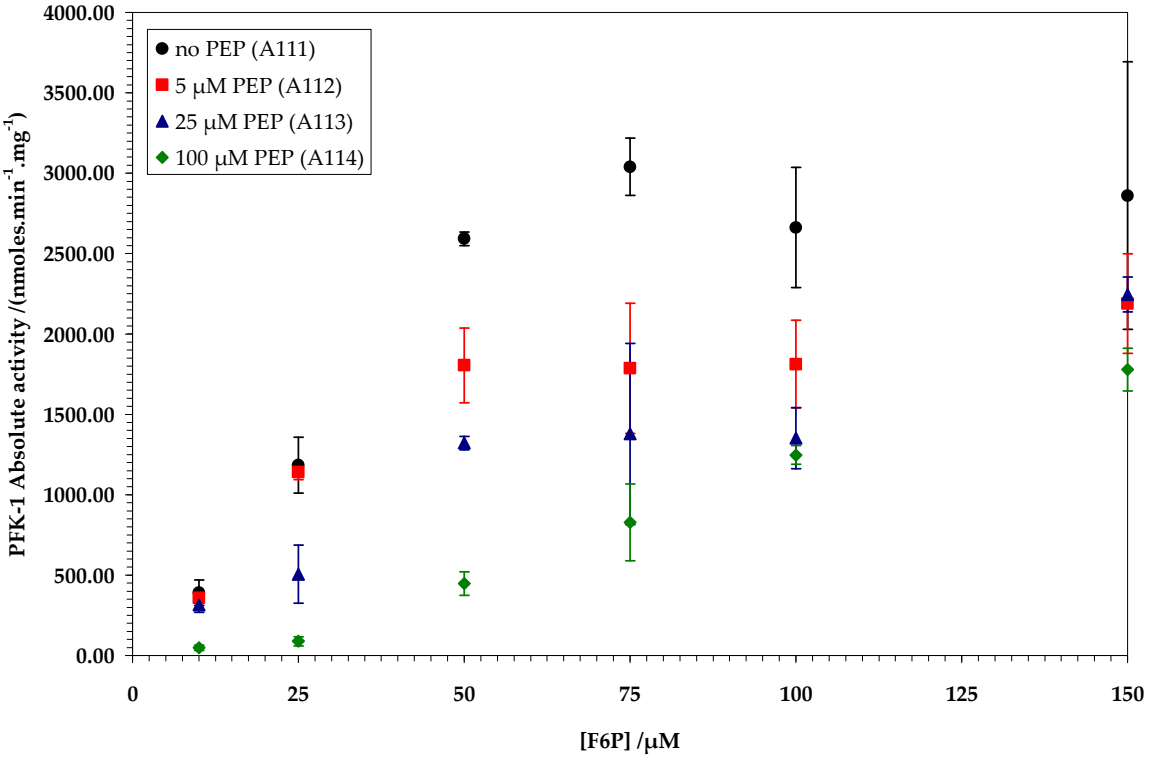

Figure IV.20- Plot of PFK-1 absolute activity against F6P concentration for 10 μM ATP and 5.83 mU/mL PFK-1 assays in the presence of PEP.

As seen more clearly in the small F6P range experiment in Figure IV.20, an increasing concentration of PEP changed the F6P saturation plot from hyperbolic to sigmoidal. At higher F6P concentrations, all saturation plots converged towards the same absolute activity, showing than an excess of F6P alleviated PEP inhibition (Figure IV.21). In the latter figure, V_{max} is considerably smaller than values observed for previous assays. Since the same batch of enzyme was used for up to Assay 109; this suggests that the enzyme degrades quickly even stored at -20 °C.

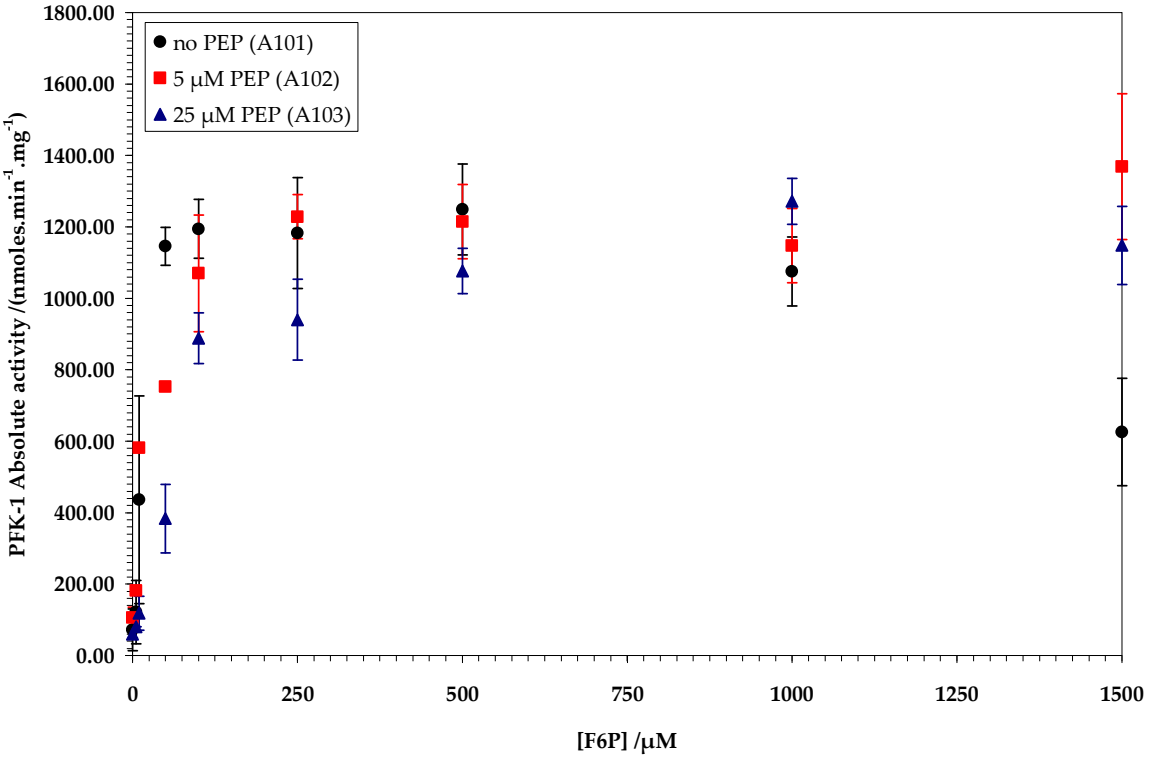

Figure IV.21- Plot of PFK-1 absolute activity against F6P concentration for 10 μM ATP and 5.83 mU/mL PFK-1 assays in the presence of PEP.

PEP inhibition was also investigated in the presence of binary LUVs consisting in either 100% DOPC or DOPC/OA (50:50). Results for 5 μM PEP are shown in Figures IV.22-23. Addition of both lipid systems alleviated PEP inhibition and switched F6P saturation plots from cooperative back to hyperbolic Michaelis-Menten. There are no equivalent experiments in the literature for BsPFK-1, but a similar trend has been reported for human erythrocyte PFK-1 (Karadsheh and Uyeda 1977).

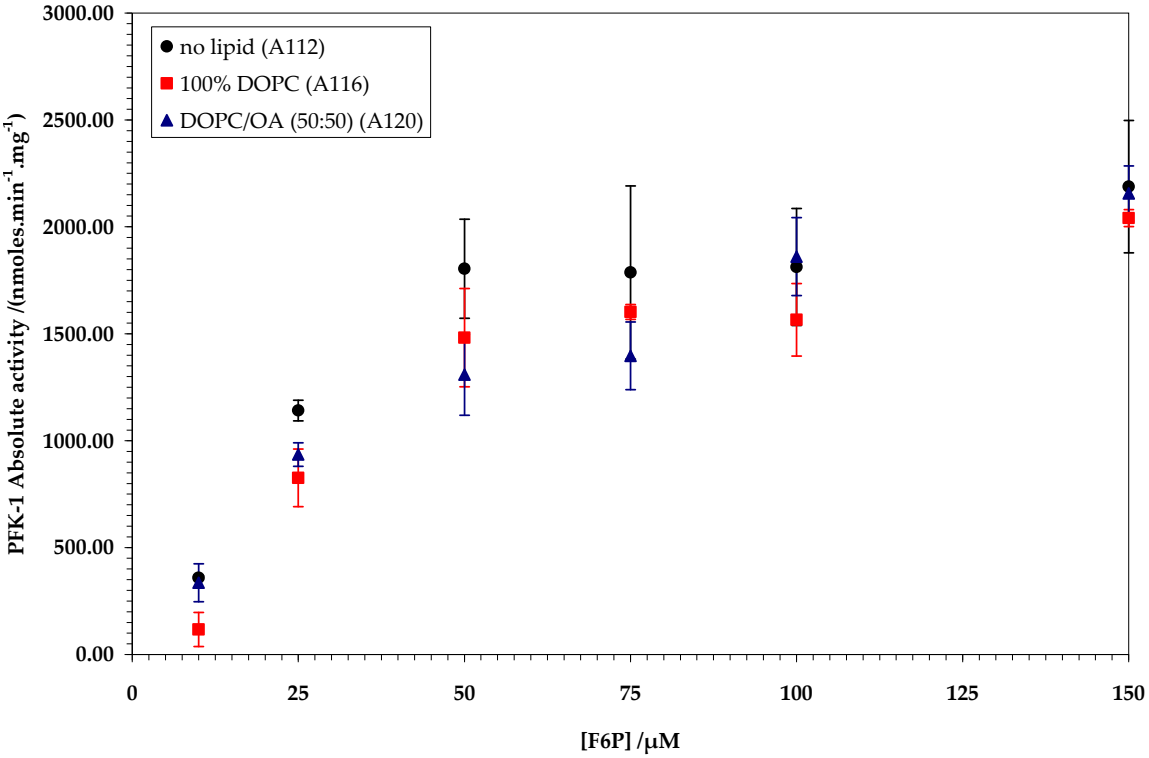

Figure IV.22- Plot of PFK-1 absolute activity against F6P concentration for 10 µM ATP and 5.83 mU/mL PFK-1 assays in 5 µM PEP and 25 µM LUVs.

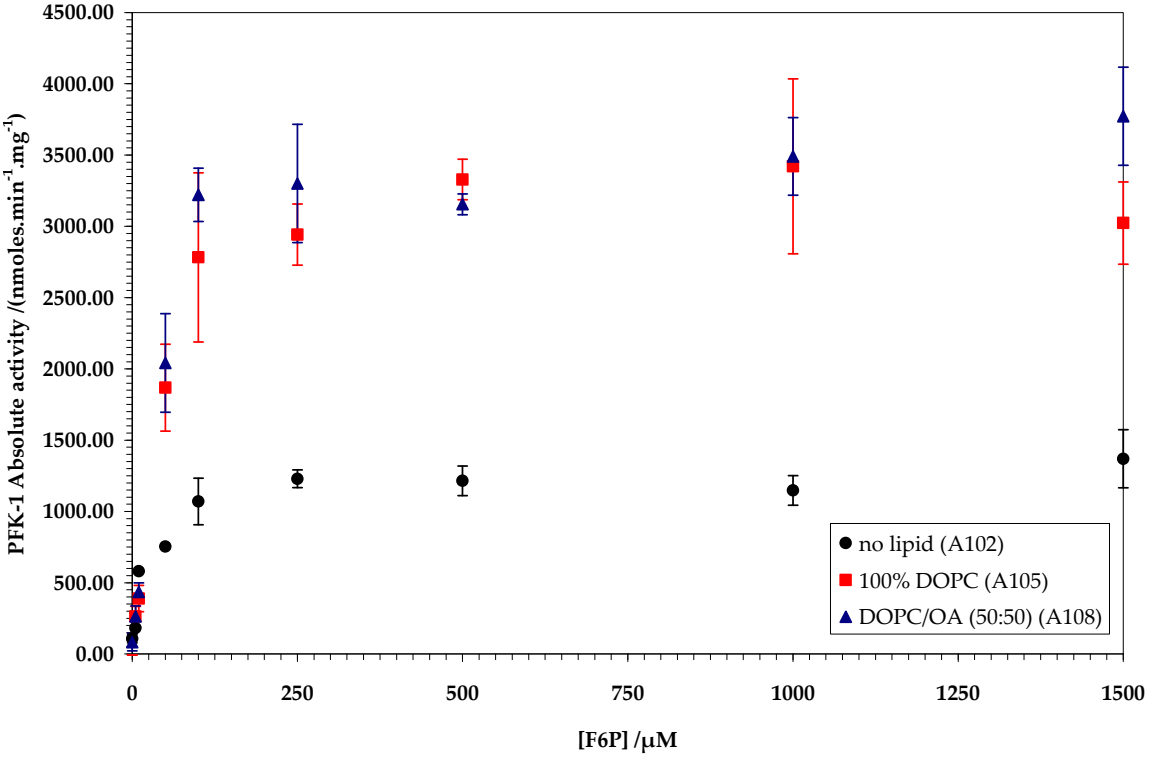

Figure IV.23- Plot of PFK-1 absolute activity against F6P concentration for 10 µM ATP and 5.83 mU/mL PFK-1 assays in 5 µM PEP and 25 µM LUVs.

F6P saturation plots in the presence of 25 and 100 μM PEP and binary LUVs are shown overleaf in Figures IV.25-26. In these higher concentrations of PEP, activation by lipids is less pronounced than in 5 μM PEP. Also, the presence of lipids does not appear to alleviate the cooperative effect of PEP as markedly as in the smaller PEP concentration. F6P kinetics remained sigmoidal and levelled off at concentrations of F6P higher than 500 μM in the presence of 25 μM PEP. Consequently, a ratio of lipid to PEP larger than 1 is required for lipids to reverse the inhibitory effect of PEP.

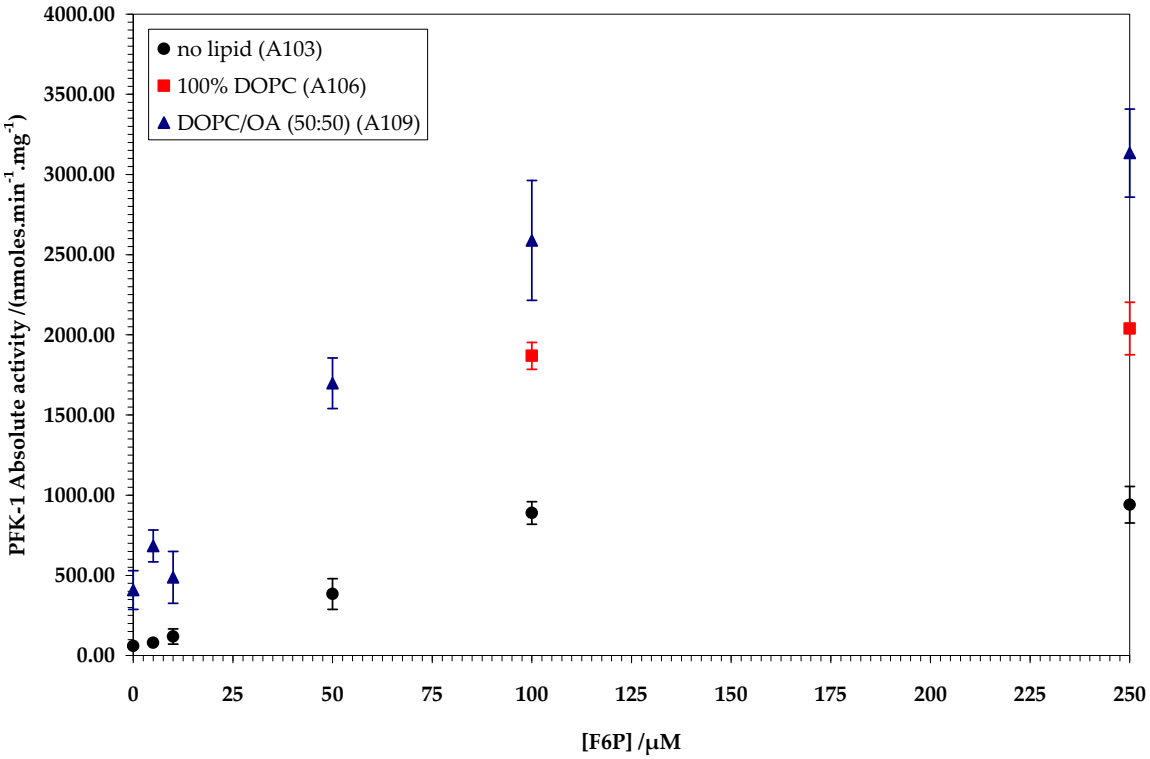

Figure IV.24- Plot of PFK-1 absolute activity against F6P concentration for 10 μM ATP and 5.83 mU/mL PFK-1 assays in 25 μM PEP and 25 μM LUVs.

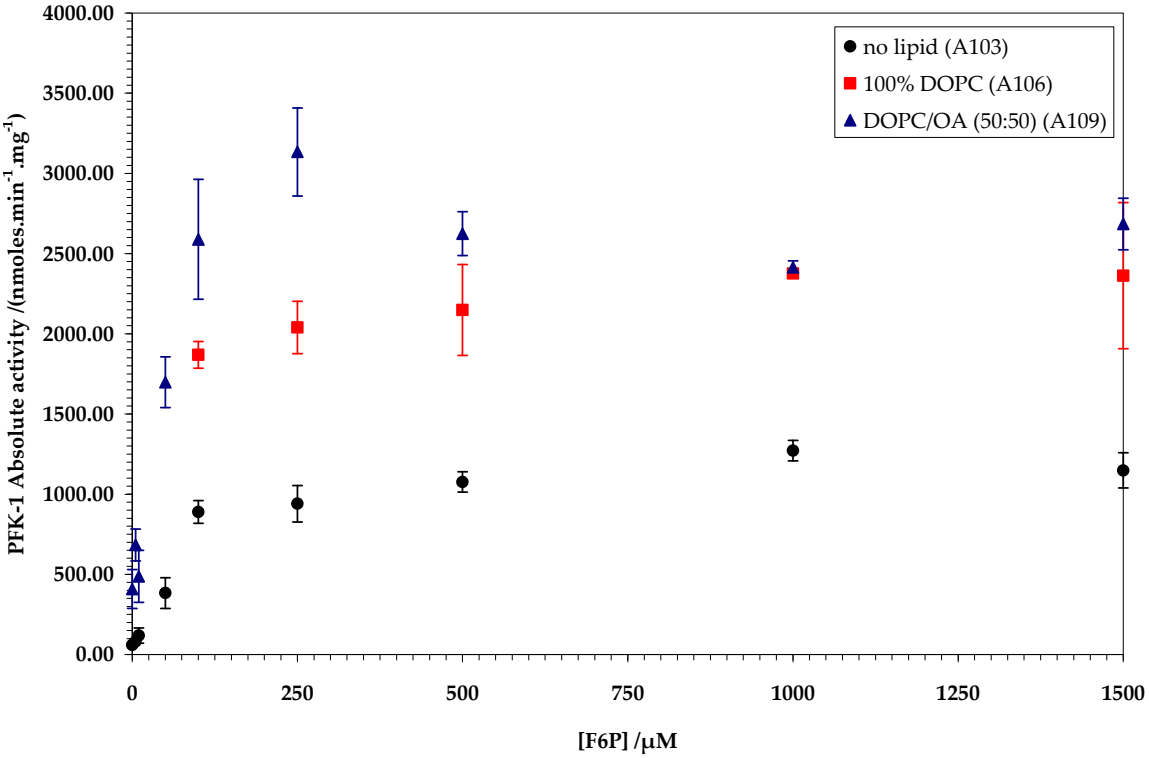

Figure IV.25- Plot of PFK-1 absolute activity against F6P concentration for 10 µM ATP and 5.83 mU/mL PFK-1 assays in 25 µM PEP and 25 µM LUVs.

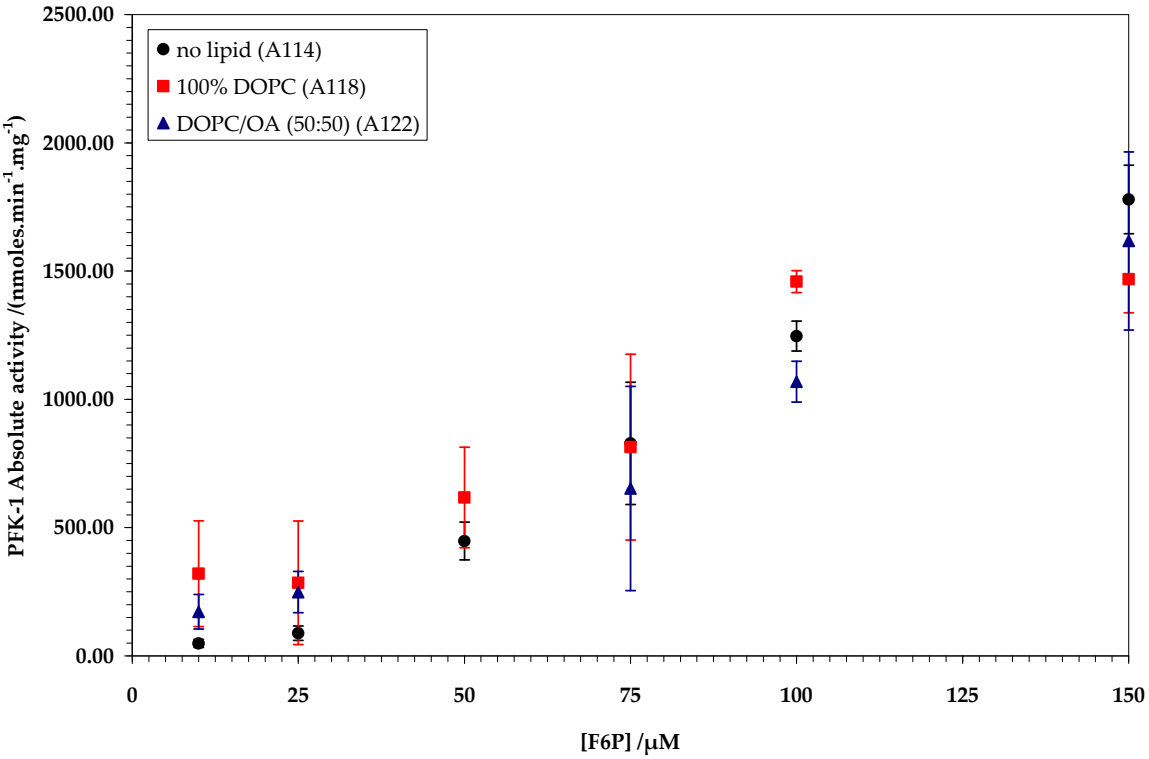

Figure IV.26- Plot of PFK-1 absolute activity against F6P concentration for 10 µM ATP and 5.83 mU/mL PFK-1 assays in 100 µM PEP and 25 µM LUVs.

Estimated values for V_{max} and K_M in the presence of LUVs and PEP are summarised in Figure IV.27.

System	PEP /μM	V_{max} /nmoles.min^{-1}.mg^{-1}	K_M /μM
no lipid	0	1169.05±125.69	18.75±2.02
	5	1243.13±134.83	17.50±1.90
	25	1165.40±79.69	18.75±1.28
100% DOPC	0	2291.39±621.54	22.00±5.97
	5	3257.56±344.97	43.75±4.63
	25	2295.54±251.35	60.00±6.57
DOPC/OA (50:50)	0	3265.51±382.68	29.00±3.40
	5	3472.79±222.82	42.50±2.73
	25	2574.51±110.36	35.00±1.50

Figure IV.27- V_{max} and K_M values in the presence of PEP.

In the absence of lipid, increasing PEP concentration causes K_M to increase as the curve becomes sigmoidal, while V_{max} remains the same within error. In the presence of 100% DOPC, V_{max} was 55 percent higher compared no lipid, but K_M followed the same trend of increasing with increasing PEP concentration in the assay. Finally, in the presence of DOPC/OA (50:50), V_{max} increased by 61 percent in average compared to no lipid whilst K_M did not significantly change within error. Lineweaver-Burke plots for F6P in the presence of PEP and lipidic systems confirmed these conclusions (Figures IV.28-31).

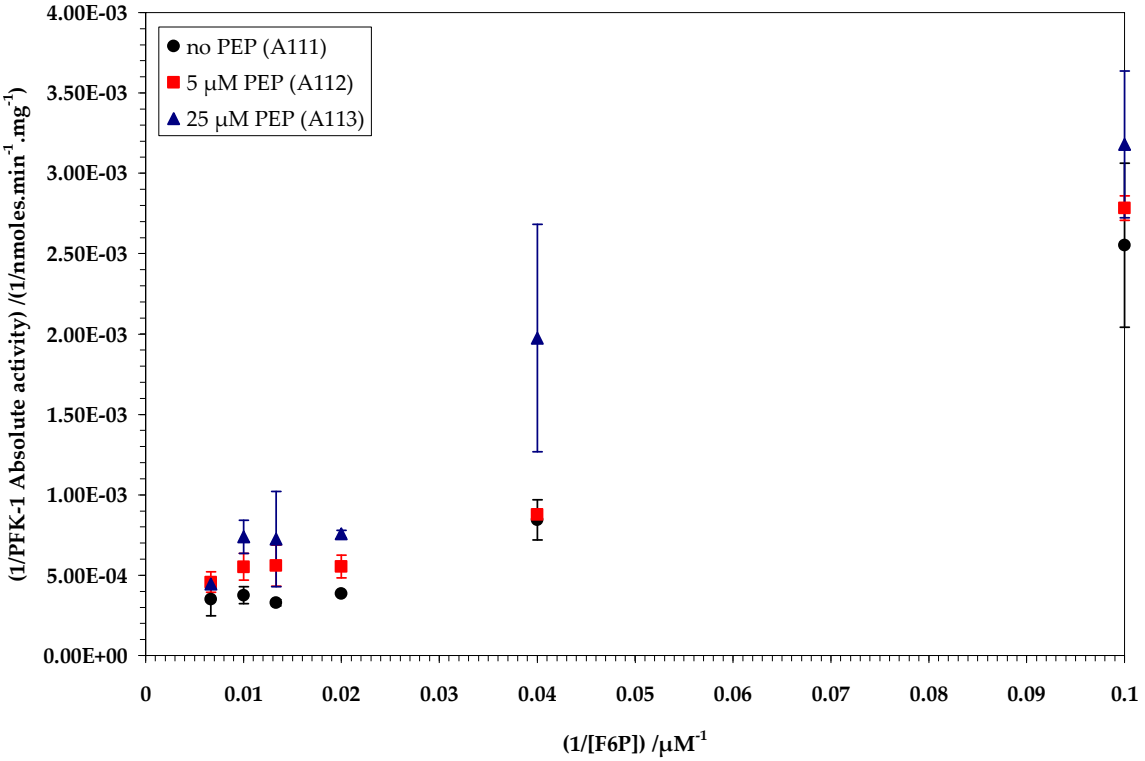

Figure IV.28- Lineweaver-Burke plot for BsPFK-1 for 10 μM ATP and 5.83 mU/mL PFK-1 assays in the presence of PEP and no lipid.

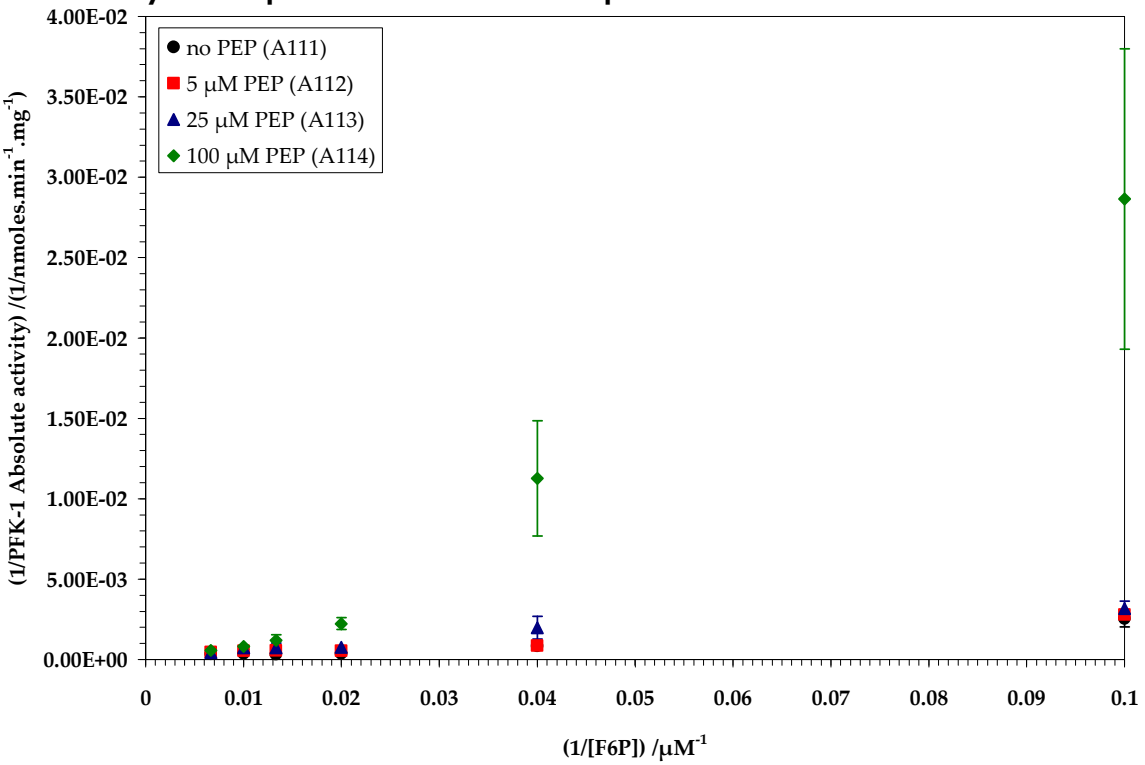

Figure IV.29- Lineweaver-Burke plot for BsPFK-1 for 10 μM ATP and 5.83 mU/mL PFK-1 assays in the presence of PEP and no lipid.

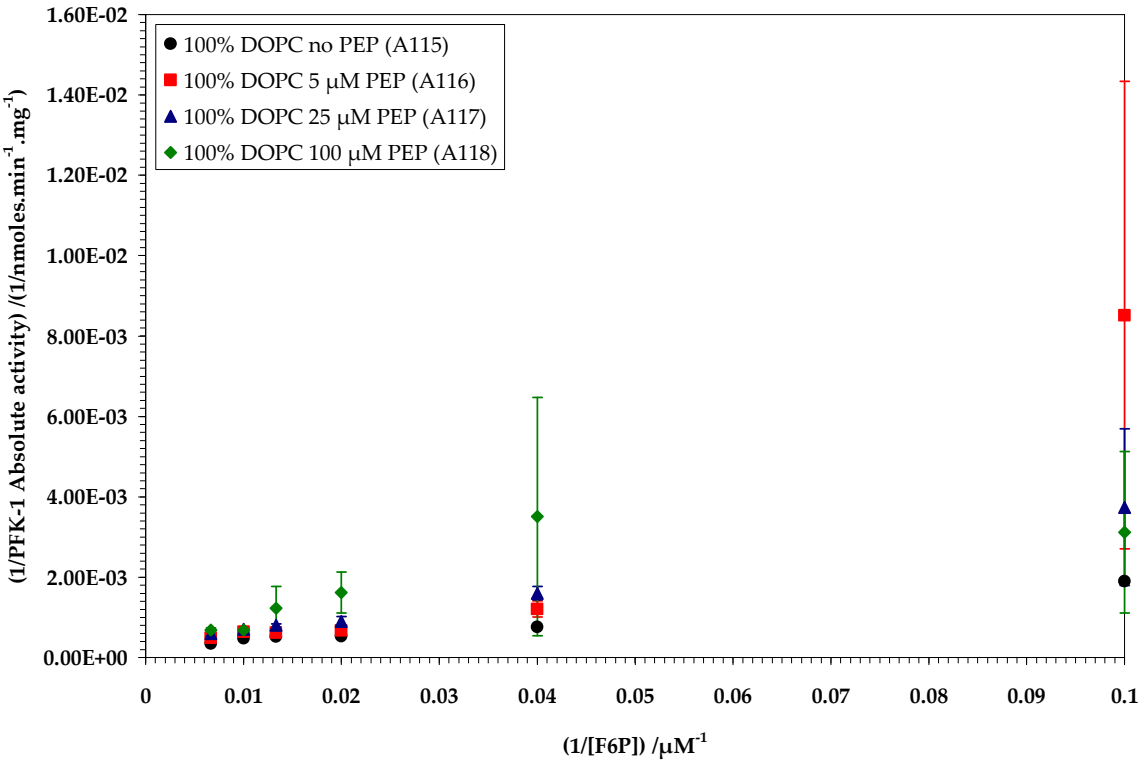

Figure IV.30- Lineweaver-Burke plot for BsPFK-1 for 10 µM ATP and 5.83 mU/mL PFK-1 assays in the presence of PEP and 25 µM LUVs.

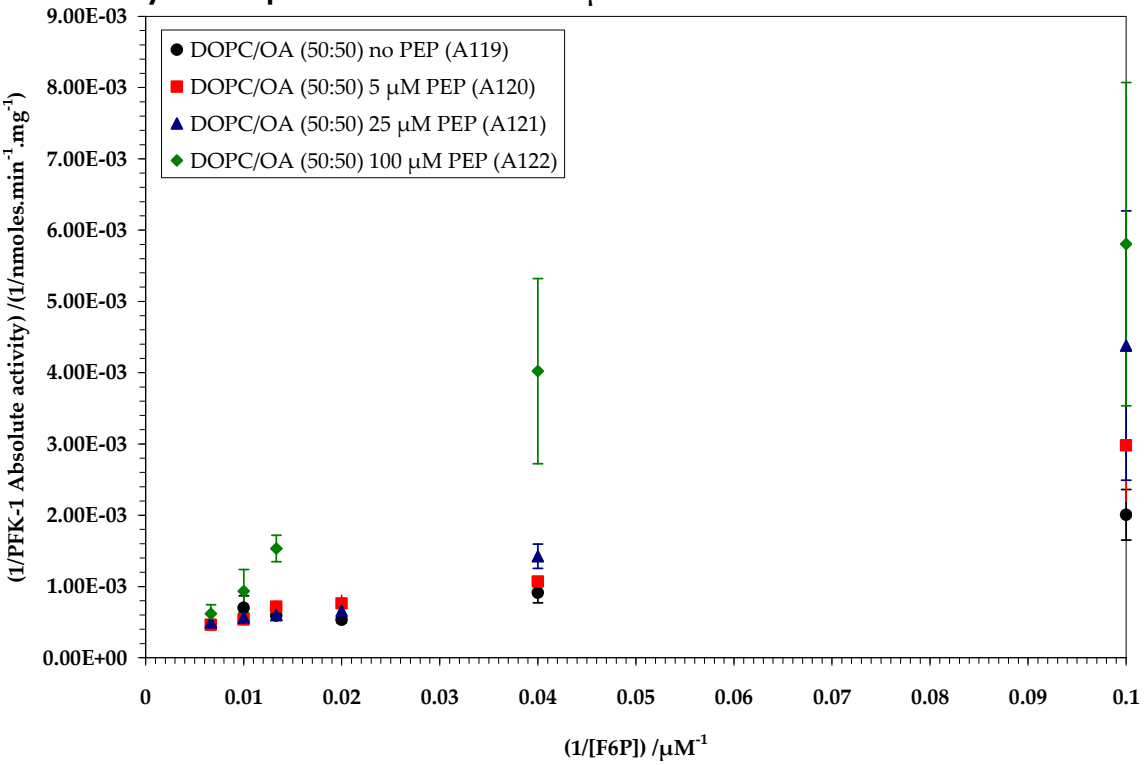

Figure IV.31- Lineweaver-Burke plot for BsPFK-1 for 10 µM ATP and 5.83 mU/mL PFK-1 assays in the presence of PEP and 25 µM LUVs.

IV.5.2. Activation by ADP in the presence of lipids

ADP increases BsPFK-1 activity, as discussed in section IV.1.2.2.1. Therefore, F6P BsPFK-1 kinetics were studied for 5, 25 and 100 μM ADP as shown in Figures IV.32-34. All three concentrations of ADP activated the enzyme to the same V_{max} within error, but the F6P saturation plot became more sigmoidal in the presence of the highest ADP concentration and K_M increased.

In 5 μM ADP and 25 μM binary LUVs, V_{max} increased 61 and 71 percent for DOPC and OA, respectively, compared to no lipid. K_M did not change significantly. The same trend was observed in the presence of 25 and 100 μM ADP. In the highest ADP concentration, a very marked increase of about 90 percent in V_{max} occurred in the presence of both lipids. Consequently, a coordinate or non-competitive activation effect of ADP and lipids is suggested. It has definitely been shown that ADP and lipid do not compete for the same binding site during BsPFK-1 activation. Estimated values for V_{max} and K_M in the presence of LUVs and ADP are summarised in Figure IV.32. Lineweaver-Burke plots for these data are shown in Figures IV.37-40.

System	ADP /μM	V_{max} /nmoles.min^{-1}.mg^{-1}	K_M /μM
no lipid	0	625.67±84.62	12.5±1.70
	5	713.87±140.53	17.5±3.45
	25	807.75±103.47	17.5±2.24
	100	571.94±171.21	23.75±7.11
100% DOPC	0	1907.99±179.50	11.00±1.04
	5	1823.48±236.83	18.75±2.44
	25	1965.59±158.35	15.00±1.21
	100	9491.29±374.46	32.5±1.28
DOPC/OA (50:50)	0	2310.74±263.39	19.00±2.17
	5	2442.55±265.77	17.5±1.90
	25	2696.95±296.31	18.75±2.06
	100	6091.82±4333.7	27.5±19.56

Figure IV.32- V_{max} and K_M values in the presence of ADP.

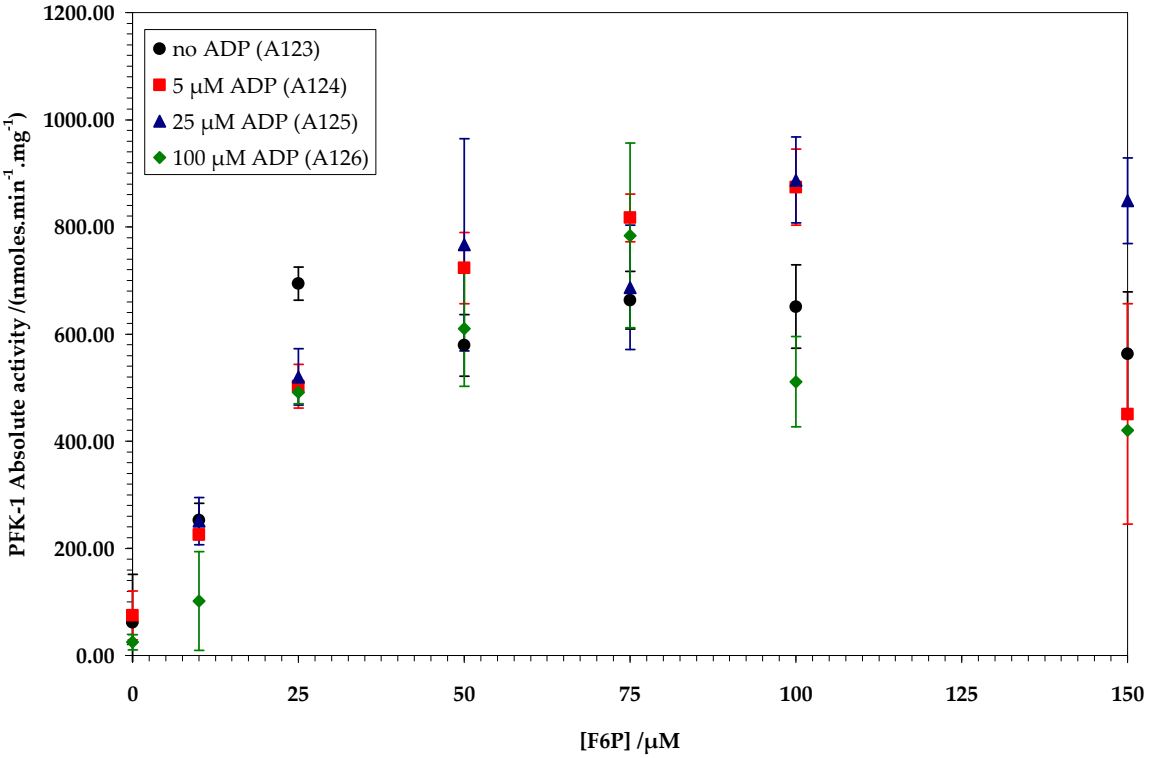

Figure IV.33- Plot of PFK-1 absolute activity against F6P concentration for 10 µM ATP and 5.83 mU/mL PFK-1 assays in the presence of ADP and no lipid.

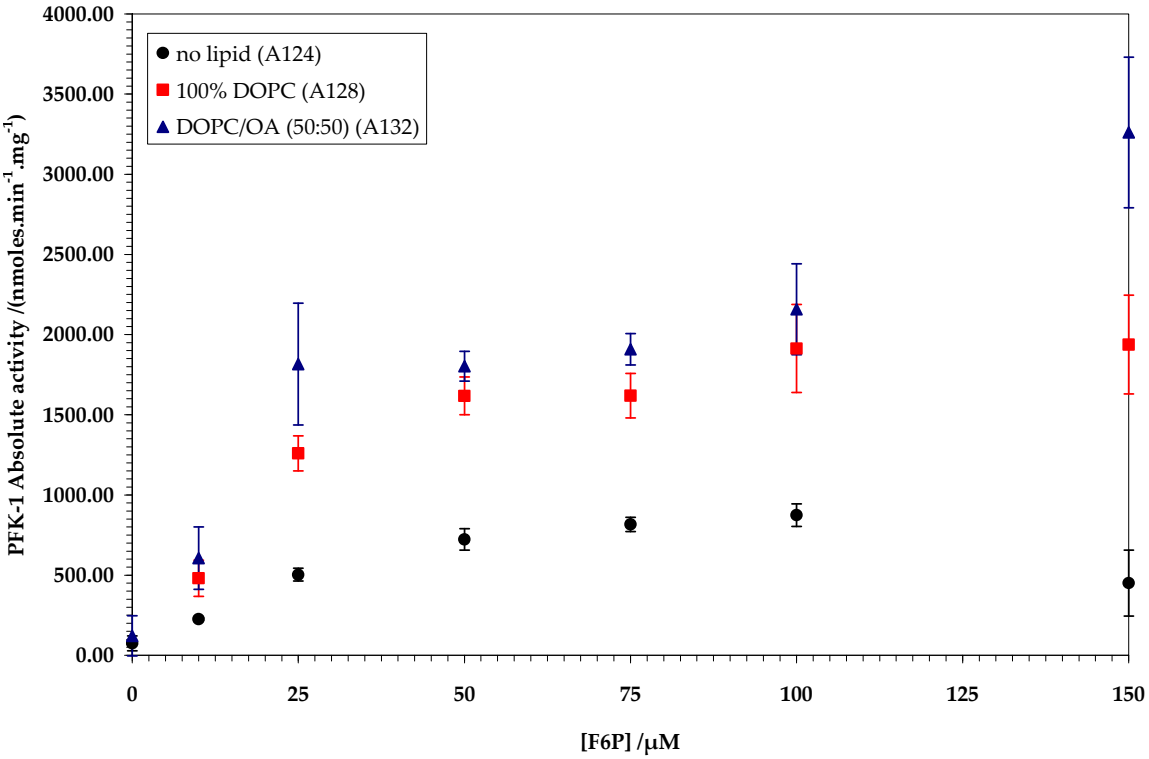

Figure IV.34- Plot of PFK-1 absolute activity against F6P concentration for 10 µM ATP and 5.83 mU/mL PFK-1 assays in the presence of 5 µM ADP and 25 µM LUVs.

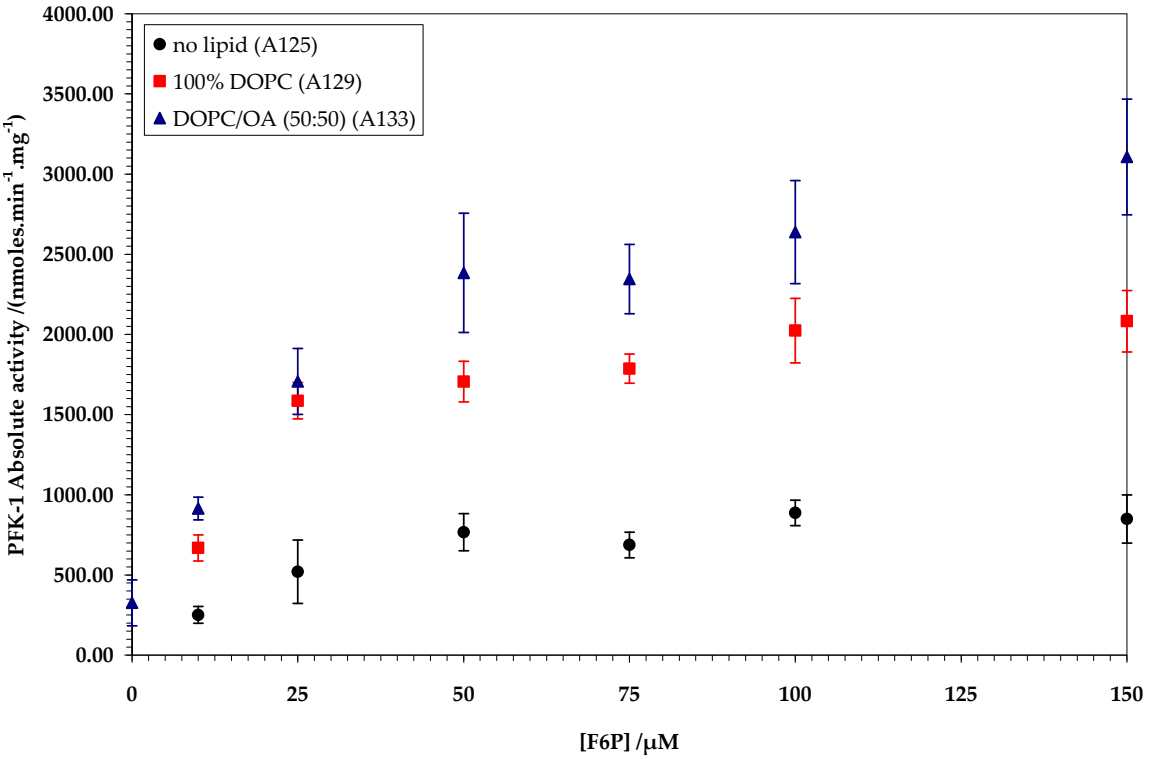

Figure IV.35- Plot of PFK-1 absolute activity against F6P concentration for 10 µM ATP and 5.83 mU/mL PFK-1 assays in the presence of 25 µM ADP and 25 µM LUVs.

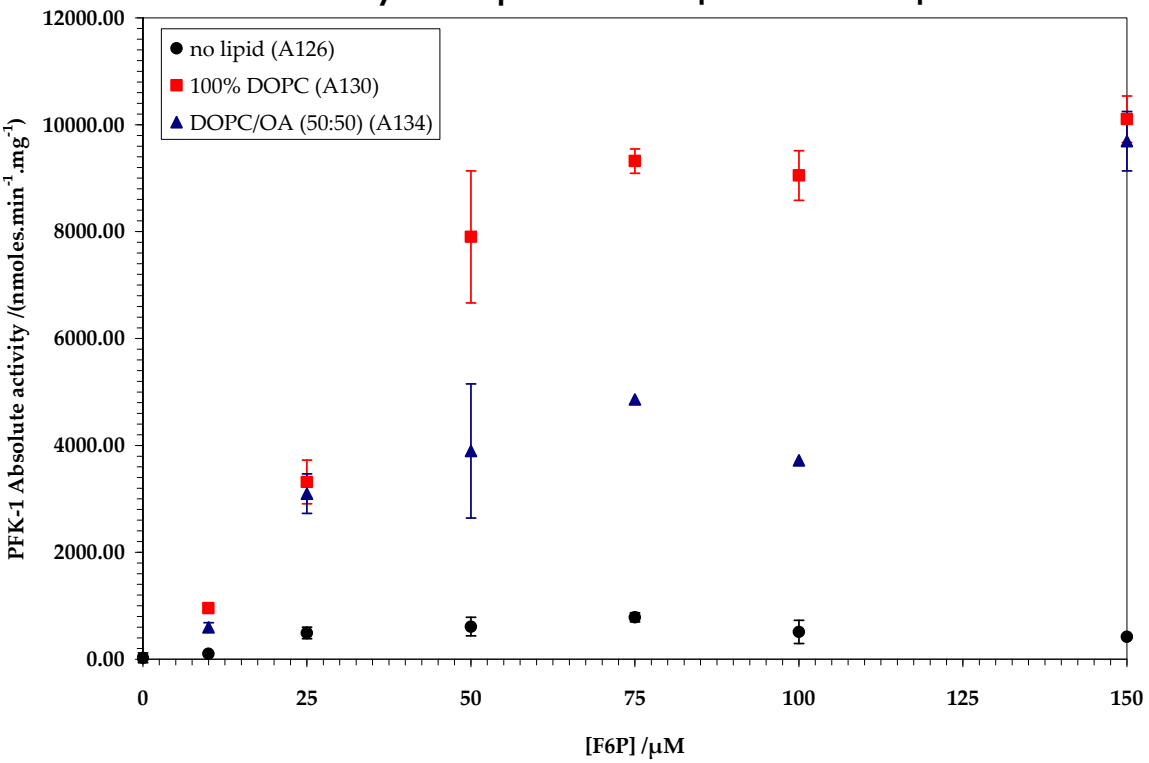

Figure IV.36- Plot of PFK-1 absolute activity against F6P concentration for 10 µM ATP and 5.83 mU/mL PFK-1 assays in the presence of 100 µM ADP and 25 µM LUVs.

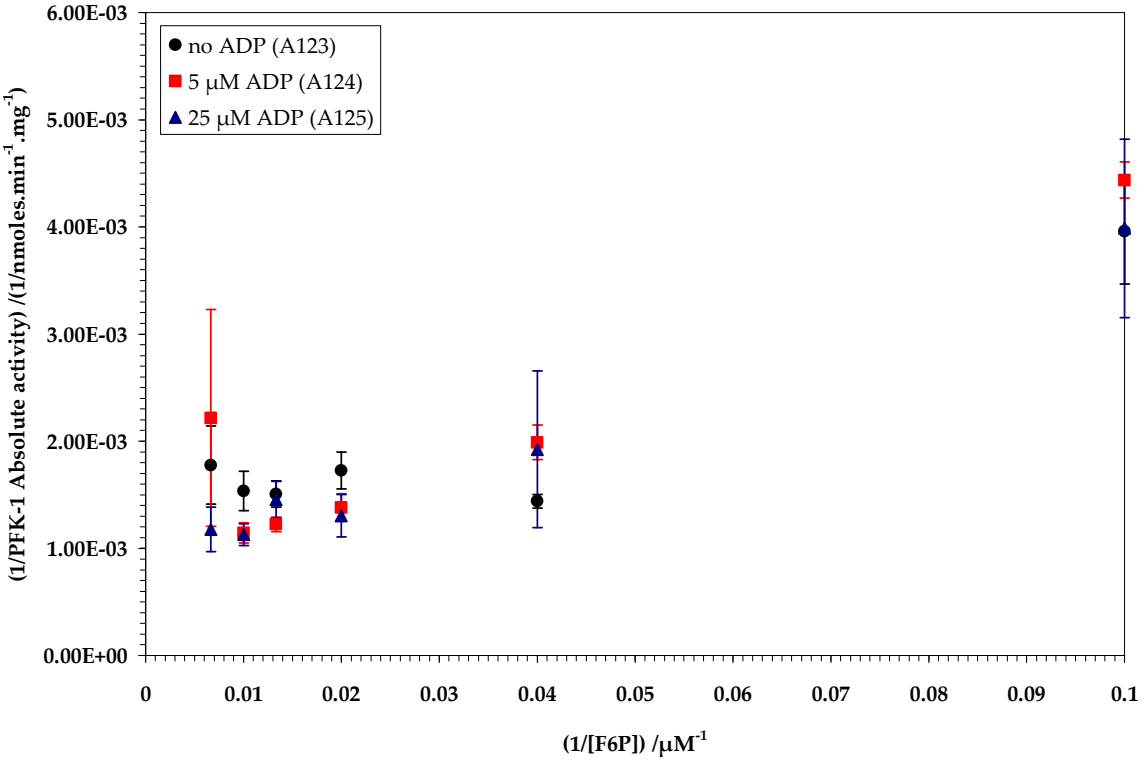

Figure IV.37- Lineweaver-Burke plot for BsPFK-1 for 10 μM ATP and 5.83 mU/mL PFK-1 assays in the presence of ADP and no lipid.

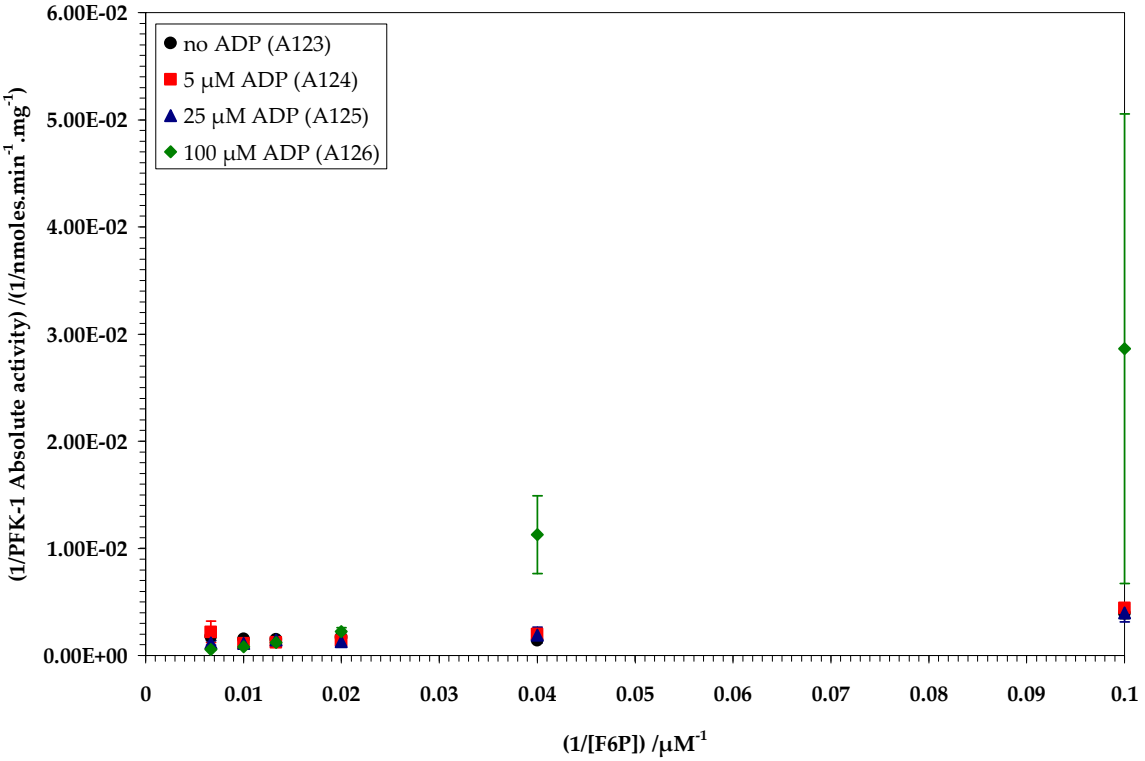

Figure IV.38- Lineweaver-Burke plot for BsPFK-1 for 10 μM ATP and 5.83 mU/mL PFK-1 assays in the presence of ADP and no lipid.

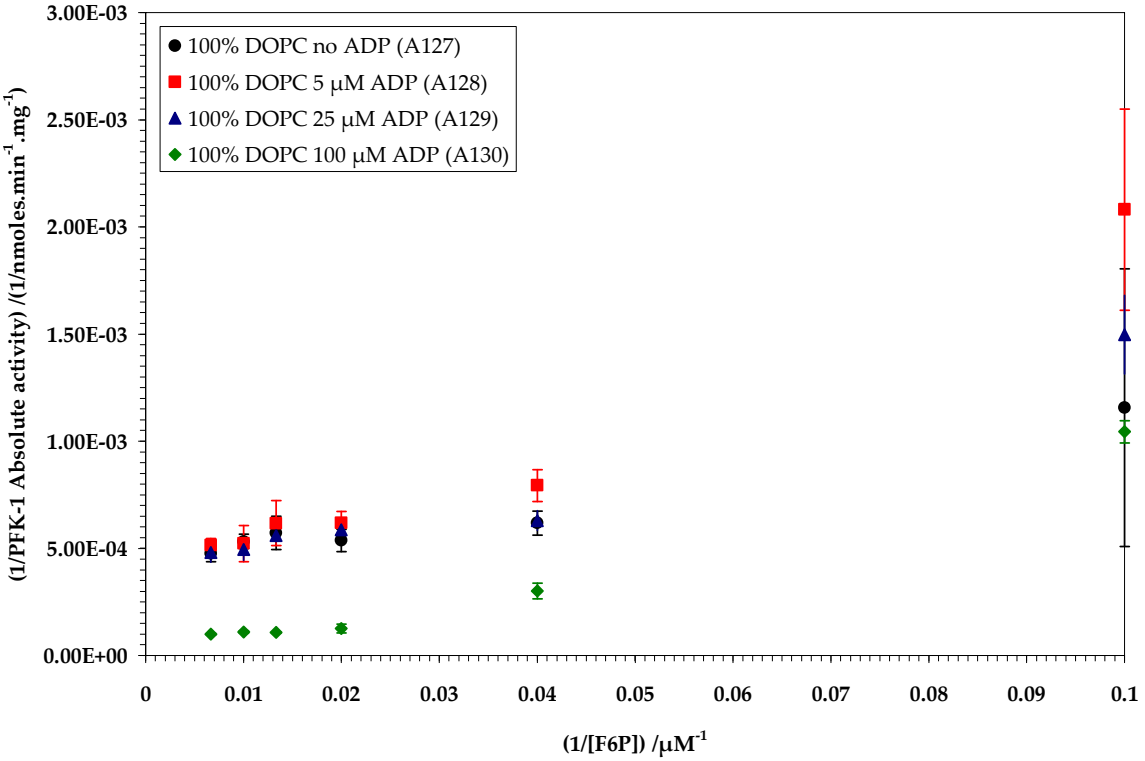

Figure IV.39- Lineweaver-Burke plot for BsPFK-1 for 10 μM ATP and 5.83 mU/mL PFK-1 assays in the presence of ADP and 25 μM LUVs.

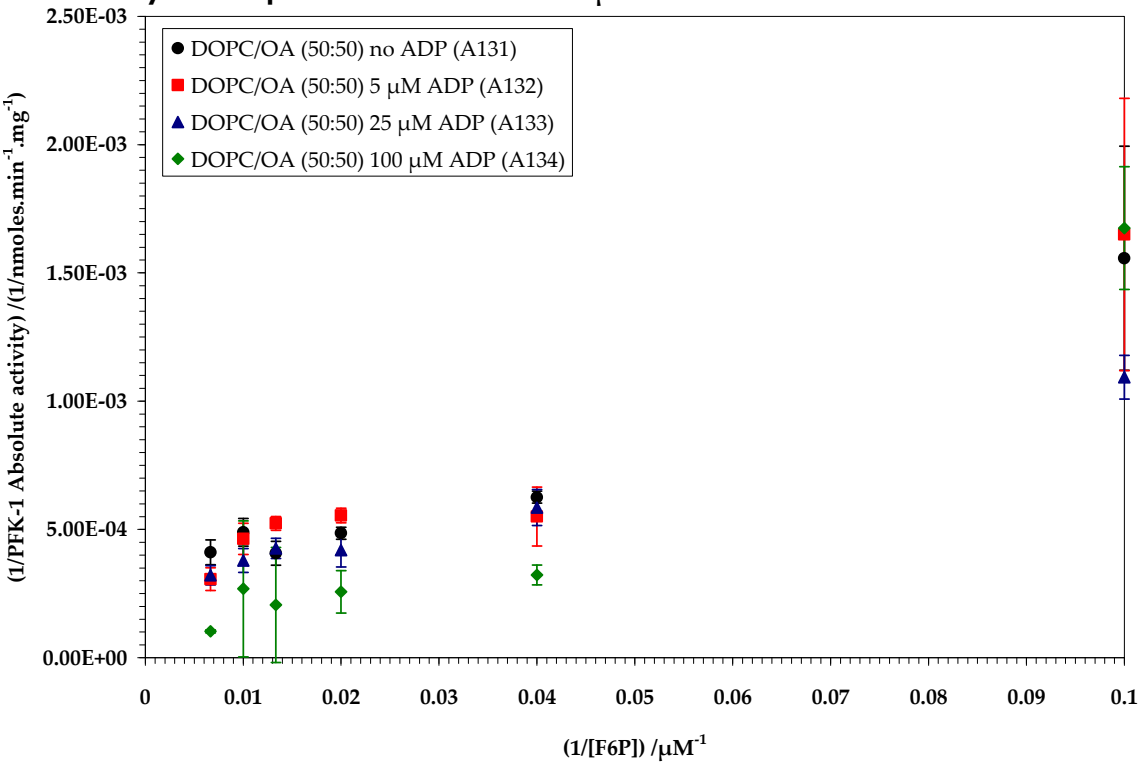

Figure IV.40- Lineweaver-Burke plot for BsPFK-1 for 10 μM ATP and 5.83 mU/mL PFK-1 assays in the presence of ADP and 25 μM LUVs.

IV.6. Conclusions

First, a novel ^{33}P radiochemical assay was developed for BsPFK-1. Its accuracy was compared in a kinetic investigation of F6P, ATP, enzyme and time saturation plots and effectors ADP and PEP. Results were in line with data from spectrophotometric assays in the literature with the added advantage of very small error.

Second, the effect of vesicles composed of DOPC and OA on BsPFK-1 was then studied using our ^{33}P radiochemical assay. The binary mixture DOPC/OA (50:50) was found to increase catalytic activity two-fold and three-fold compared to DOPC and no lipid present, respectively. In the presence of inhibitor PEP, lipids alleviated the inhibitory effect when their concentration was at least equal to that of PEP. Also, the activator ADP was about 95 percent more effective in the presence of lipids. Consequently, the activating effect of membranes to the catalytic activity of PFK-1 reported in the literature for mammalian and rabbit erythrocyte PFK-1 was confirmed from our results. The effect of membranes on BsPFK-1 kinetics has not been, to our knowledge, previously investigated for *B. stearothermophilus*.

It could be speculated that BsPFK-1 forms a transient complex with LUVs, but not through binding at the effector allosteric sites, since the effectors ADP and PEP can both bind as per normal in the presence of lipids. However, formation of this BsPFK-1/LUVs complex must change the conformation of the enzymatic tetramer since affinity for the effector was modulated in the presence of membranes. Since our results indicated that membrane composition affects PFK-1 activity and in consequence glycolysis, then the most essential further work would be to obtain experimental evidence that PFK-1 associates with lipids through a physical interaction. Binding information can be acquired either by a radiochemical binding assay or by isothermal titration calorimetry. If direct binding was sufficiently

proved, then a direct correlation of PFK-1 enzyme membrane binding and glycolysis would be established. Consequently, lipids could be potential agents for the treatment of glycolytic diseases.

Since DOPC/OA mixtures have been shown to form inverse hexagonal phases (Seddon 1990), this system is classified a Type II amphiphile. Therefore, our results are in line with the stored elastic stress hypothesis, which predicts that DOPC/OA should activate the enzyme. While these data suggest that stored curvature elastic energy may play a role in modulating enzyme activity, they are significantly different from the results obtained with CCTα. Further work is required for the stored elastic stress hypothesis to be clearly supported. First, the effect of a variety of LUVs binary systems need to be investigated including Type II, 0 and I, as well as anionic, cationic, zwitterionic and neutral amphiphiles. Due to the complexity and hazards of radiochemical assays, a spectrophotometric assay could be used to screen the systems initially and then successful candidate systems to be further investigated radiochemically.

Overall, results in this chapter raise interesting questions about the fundamental mechanisms that underlie the effect of membrane lipid composition on PFK-1 activity.

IV.7. References

Andres, V., J. Carreras, et al. (1996). "Myofibril-bound muscle phosphofructokinase is less sensitive to inhibition by ATP than the free enzyme, but retains its sensitivity to stimulation by bisphosphorylated hexoses." Intern. J. Biochem. Cell. Biol. **28**(10): 1179-1184.

Auzat, I., G. L. Bras, et al. (1994). "The cooperativity and allosteric inhibition of *Escherichia coli* phosphofructokinase depend on the interaction between threonine-125 and ATP." Proc. Natl. Acad. Sci. U. S. A. **91**(12): 5242-5246.

Auzat, I., W. M. Byrnes, et al. (1995). "Role of residue 161 in the allosteric transitions of two bacterial phosphofructokinases." Biochemistry **34**(21): 7062-7068.

Auzat, I., G. Le Bras, et al. (1995). "Hypercooperativity induced by interface mutations in the phosphofructokinase from *Escherichia coli*." J. Mol. Biol. **246**(2): 248-243.

Babul, J. (1978). "Phosphofructokinases from *Escherichia coli*: Purification and characterization of the nonallosteric isozyme." J. Biol. Chem. **253**(12): 4350-4355.

Bar, J., W. Schellenberger, et al. (1997). "Purification and characterisation of phosphofructokinase from yeast *Kluyveromuces lactis*." Yeast **13**: 1309-1317.

Berger, S. A. and P. R. Evans (1991). "Steady-state fluorescence of *Escherichia coli* phosphofructokinase reveals a regulatory role for ATP." Biochemistry **30**(34): 8477-8480.

Blangy, D., H. Buc, et al. (1968). "Kinetics of the allosteric interactions of phosphofructokinase from *Escherichia coli*." J. Mol. Biol. **31**(1): 13-35.

Bosca, L., J. J. Aragon, et al. (1985). "Modulation of muscle phosphofructokinase at physiological concentration of enzyme." J. Biol. Chem. **260**(4): 2100-2107.

Brand, I. A. and H. D. Soeling (1975). "Activation and inactivation of rat liver phosphofructokinase by phosphorylation-dephosphorylation." FEBS Letters **57**(2): 163-168.

Bras, G. L., W. Teschner, et al. (1989). "Urea-induced inactivation, dissociation, and unfolding of the allosteric phosphofructokinase from *Escherichia coli*." Biochemistry **28**(17): 6836-6841.

Byrnes, M., X. Zhu, et al. (1994). "Kinetic characteristics of phosphofructokinase from *Bacillus stearothermophilus*: MgATP nonallosterically inhibits the enzyme." Biochemistry **33**(11): 3424-3431.

Byrnes, W. M., W. Hu, et al. (1995). "A chimeric bacterial phosphofructokinase exhibits cooperativity in the absence of heterotropic regulation." J. Biol. Chem. **270**(8): 3828-3835.

Cabrera, R., A. Caniuguir, et al. (2006). "Crystallization and preliminary crystallographic analysis of the tetrameric form of phosphofructokinase-2 from *Escherichia coli*, a member of the ribokinase family." Acta Crystallographica, F: Struct. Biol. Cryst. Comm. **F62**(9): 935-937.

Campanella, M. E., H. Y. Chu, et al. (2005). "Assembly and regulation of a glycolytic enzyme complex on the human erythrocyte membrane." Proc. Natl. Acad. Sci. U. S. A. **102**(7): 2402-2407.

Caniuguir, A., R. Cabrera, et al. (2005). "Role of Cys-295 on subunit interactions and allosteric regulation of phosphofructokinase-2 from *Escherichia coli*." FEBS Letters **579**(11): 2313-2318.

Carman, G. M., R. A. Deems, et al. (1995). "Lipid signaling enzymes and surface dilution kinetics." J. Biol. Chem. **270**(32): 18711-18714.

Chu, H. Y. and P. S. Low (2006). "Mapping of glycolytic enzyme-binding sites on human erythrocyte band 3." Biochem. J. **400**: 143-151.

Corredor, C. and L. Bosca (1985). "A problematic enzyme. Comments." TIBS **10**(2): 62.

Cowan, K. J. and K. B. Storey (2002). "Urea and KCl have differential effects on enzyme activities in liver and muscle of estivating versus nonestivating species." Biochem. Cell Biol. **80**(6): 745-755.

DeBerardinis, R. J., J. J. Lum, et al. (2008). "The biology of cancer: Metabolic reprogramming fuels cell growth and proliferation." Cell Metabol. Rev. **7**(1): 11-20.

Eigen, M. (1967). Kinetics of reaction control and information transfer in enzyme acids. The 5th Nobel Symposium: Fast reactions and primary processes in chemical kinetics, Lindigo, Sweden.

El-Bacha, T., M. S. Freitas, et al. (2003). "Cellular distribution of phosphofructokinase activity and implications to metabolic regulation in human breast cancer " Mol. Genet. Metab. **79**: 294-299.

Emmerling, M., J. E. Bailey, et al. (1999). "Glucose catabolism of *Escherichia coli* strains with increased activity and altered regulation of key glycolytic enzymes." Metab. Engin. **1**(2): 117-127.

Emmerling, M., J. E. Bailey, et al. (2000). "Altered regulation of pyruvate kinase or co-overexpression of phosphofructokinase increases glycolytic fluxes in resting *Escherichia coli*." Biotechnology and Bioengineering **67**(5): 623-627.

Evans, P. R. (1991). "Structural aspects of allostery." Curr. Op. Struct. Biol. **1**(5): 773-779.

Evans, P. R., G. W. Farrants, et al. (1981). "Phosphofructokinase: structure and control." Philos. Trans. R. Soc. Lond. [Biol] **293**: 53-62.

Evans, P. R., G. W. Farrants, et al. (1986). "Crystallographic structure of allosterically inhibited phosphofructokinase at 7 Å resolution." J. Mol. Biol. **191**(4): 713-720.

Evans, P. R. and P. J. Hudson (1979). "Structure and control of phosphofructokinase from *Bacillus stearothermophilus*." Nature **279**(5713): 500-504.

Exantus, J., B. Ranchin, et al. (2004). Report: Acute renal failure in a patient with phosphofructokinase deficiency. Germany, Departement de Pediatrie, Hopital Edouard-Herriot, Universite Claude-Bernard, Lyon, France**:** 111-3.

Fagone, P. (2003). Modulation of CCTa by membrane biophysics, PhD Thesis. School of Chemistry. University of Southampton.

Fenton, A. W., N. M. Paricharttanakul, et al. (2004). "Disentangling the web of allosteric communication in a homotetramer: Heterotropic activation in phosphofructokinase from *Escherichia coli*." Biochemistry **43**(44): 14104-14110.

Fenton, A. W. and G. D. Reinhart (2003). "Mechanism of substrate inhibition in *Escherichia coli* phosphofructokinase." Biochemistry **42**(43): 12676-12681.

Fersht, A. (2002). Structure and mechanism in protein science, Freeman.

French, B. A. and S. H. Chang (1987). "Nucleotide sequence of the phosphofructokinase gene from *Bacillus stearothermophilus* and comparison with the homologous *Escherichia coli* gene." Gene **54**(1): 65-71.

Gebhard, S., R. S. Ronimus, et al. (2001). "Inhibition of phosphofructokinases by copper(II)." FEMS Microbiology Letters **197**(1): 105-109.

Goldhammer, A. R. and H. H. Paradies (1979). "Phosphofructokinase: structure and function." Curr. Top. Cell. Reg. **15**: 109-141.

Hansen, T. and P. Schonheit (2000). "Purification and properties of the first-identified, archaeal, ATP-dependent 6-phosphofructokinase, an extremely thermophilic non-allosteric enzyme, from the hyperthermophile *Desulfurococcus amylolyticus*." Arch. Microbiol. **173**(2): 103-109.

Harrison, M. L., P. Rathinavelu, et al. (1991). "Role of band 3 tyrosine phosphorylation in the regulation of erythrocyte glycolysis." J. Biol. Chem. **266**(7): 4106-4111.

Hazen, S. L. and R. W. Gross (1993). "The specific association of a phosphofructokinase isoform with myocardial calcium-independent phospholipase A2. Implications for the coordinated regulation of phospholipolysis and glycolysis." J. Biol. Chem. **268**(13): 9892-9900.

Hazen, S. L., M. J. Wolf, et al. (1994). "The rapid and reversible association of phosphofructokinase with myocardial membranes during myocardial ischemia." FEBS Letters **339**(3): 213-216.

Heinisch, J. J. (1986). "Isolation and characterisation of the two structural genes coding for phosphofructokinase in yeast." Mol. Gen. Genet. **202**: 75-82.

Heinisch, J. J. (1989). "The phosphofructokinase genes of yeast evolved from two duplication events." Gene **78**: 309-321.

Higashi, T., C. S. Richards, et al. (1979). "The interaction of phosphofructokinase with erythrocyte membranes." J. Biol. Chem. **254**(19): 9542-9550.

Hoffman, E. (1976). "The significance of Phosphofructokinase in the Regulation of Carbohydrate Metabolism." Rev. Physiol. Biochem. Pharmacol. **75**: 1-68.

Jenkins, J. D., F. J. Kezdy, et al. (1985). "Mode of Interaction of phosphofructokinase with the erythrocyte membrane." J. Biol. Chem. **260**(19): 10426-10433.

Jenkins, J. D., D. P. Madden, et al. (1984). "Association of phosphofructokinase and aldolase with the membrane of the intact erythrocyte." J. Biol. Chem. **259**(15): 9374-9378.

Johnson, J. L. and A. McLachlan (1994). "Novel clustering of Sp1 transcription factor binding sites at the transcription initiation site of the human muscle phosphofructokinase p1 promoter." Nucl. Acids Res. **22**(23): 5085-5092.

Karadsheh, N. S. and K. Uyeda (1977). "Changes in allosteric properties of phosphofructokinase bound to erythrocyte membranes." J. Biol. Chem. **252**(21): 7418-7420.

Kemp, R. G. and L. G. Foe (1983). "Allosteric regulatory properties of muscle phosphofructokinase." Mol. Cell. Biochem. **57**(2): 147-154.

Kim, S. J., F. N. Chowdhury, et al. (1993). "Time-resolved fluorescence of the single tryptophan of *Bacillus stearothermophilus* phosphofructokinase." Biophys. J. **65**(1): 215-226.

Kimmel, J. L. (2001). Texas A and M Univ. U.S.A. Thesis: Investigation into the molecular basis for the allosteric regulation of phosphofructokinase from *Bacillus stearothermophilus*.

Kimmel, J. L. and G. D. Reinhart (2000). "Reevaluation of the accepted allosteric mechanism of phosphofructokinase from *Bacillus stearothermophilus*." Proc. Natl. Acad. Sci. U. S. A. **97**(8): 3844-3849.

Kimmel, J. L. and G. D. Reinhart (2001). "Isolation of an individual allosteric interaction in tetrameric phosphofructokinase from *Bacillus stearothermophilus*." Biochemistry **40**(38): 11623-11629.

Kliman, H. J. and T. L. Steck (1980). "Association of glyceraldehyde-3-phosphate dehydrogenase with the human red cell membrane. A kinetic analysis." J. Biol. Chem. **255**(13): 6314-6321.

Koshland, J., D.E. (1996). "The structural basis of negative cooperativity: receptors and enzymes." Curr.Op. Struct. Biol. **6**(6): 757-761.

Koshland, J., D.E., G. Nemethy, et al. (1966). "Comparison of experimental binding data and theoretical models in proteins containing subunits." Biochemistry **5**(1): 365-385.

Kundrot, C. E. and P. R. Evans (1991). "Designing an allosterically locked phosphofructokinase." Biochemistry **30**(6): 1478-1484.

Layzer, R. B., L. P. Rowland, et al. (1969). "Physical and kinetic properties of human phosphofructokinase from skeletal muscle and erythrocytes." J. Biol. Chem. **244**(14): 3823-3831.

Lineweaver, H. and D. Burk (1934). "The determination of enzyme dissociation constants." J. Am. Chem. Soc. **56**: 658-666.

Lipscomb, W. N. (1998). "Multisubunit allosteric proteins." NATO ASI Series, Series A: Life Sciences **301**(Protein Dynamics, Function, and Design): 27-35.

Ma, W., H. J. Sung, et al. (2007). "A pivotal role for p53: balancing aerobic respiration and glycolysis." J. Bioenerg. Biomemb. **39**: 243-246.

Marinho-Carvalho, M. M., P. Zancan, et al. (2006). "Modulation of 6-phosphofructo-1-kinase oligomeric equilibrium by calmodulin: Formation of active dimers." Mol. Genet. Metab. **87**(3): 253-261.

Martinez-Oyanedel, J., I. W. McNae, et al. (2007). "The first crystal structure of phosphofructokinase from a eukaryote: *Trypanosoma brucei*." J. Mol. Biol. **366**: 1185-1198.

Mayr, G. W. and L. M. G. Heilmeyer (1983). "Phosphofructokinase is a calmodulin binding protein." FEBS **159**(1-2): 51-57.

Michaelis, L. and M. L. Menten (1913). "The kinetics of invertin action." Biochem. Z. **49**: 333-369.

Monod, J., J. Wyman, et al. (1965). "On the nature of allosteric transitions: A plausible model." J. Mol. Biol. **12**: 88-118.

Murthy, S. N., T. Liu, et al. (1981). "The aldolase-binding site of the human erythrocyte membrane is at the NH2 terminus of band 3." J. Biol. Chem. **256**(21): 11203-11208.

Nakajima, H., T. Hamaguchi, et al. (1995). "Phosphofructokinase deficiency: recent advances in molecular biology." Muscle Nerve **3**: S28-34.

Nelson, D. L., Cox, M.M. (2000). Lehninger Principles of Biochemistry, 3rd edition. New York, Worth Publishers.

Nissler, K., A. Otto, et al. (1983). "Similarity of activation of yeast phosphofructokinase by AMP abd fructose-2,6-bisphosphate." Biochem. Biophys. Res. Comm. **111**(1): 294-300.

Ortigosa, A. D., J. L. Kimmel, et al. (2004). "Disentangling the web of allosteric communication in a homotetramer:Heterotropic inhibition of phosphofructokinase from *Bacillus stearothermophilus*." Biochemistry **43**: 577-586.

Paricharttanakul, N. M., S. Ye, et al. (2005). "Kinetic and structural characterization of phosphofructokinase from *Lactobacillus bulgaricus*." Biochemistry **44**(46): 15280-15286.

Pelicano, H., D. S. Martin, et al. (2006). "Glycolysis inhibition for anticancer treatment." Oncogene **25**: 4633-4646.

Phillips, D., C. C. F. Blake, et al. (1981). "The enzymes of glycolysis: Structure, activity and evolution." Philos. Trans. R. Soc. Lond. [Biol] **293**: 1-214.

Poorman, R. A., A. Randolph, et al. (1984). "Evolution of phosphofructokinase - gene duplication and creation of new effector sites." Nature **309**(5967): 467-469.

Quinlan, R. J. and G. D. Reinhart (2006). "Effects of protein-ligand associations on the subunit interactions of phosphofructokinase from *B. stearothermophilus*." Biochemistry **45**(38): 11333-11341.

Ramadoss, C. S., K. Uyeda, et al. (1976). "Studies on the fatty acid inactivation of phosphofructokinase." J. Biol. Chem. **251**(1): 98-107.

Reuter, R., M. Naumann, et al. (2000). "Purification, molecular and kinetic characterization of phosphofructokinase-1 from the yeast *Schizosaccharomyces pombe*: evidence for an unusual subunit composition." Yeast **16**(14): 1273-1285.

Riley-Lovingshimer, M. R. and G. D. Reinhart (2005). "Examination of MgATP binding in a tryptophan-shift mutant of phosphofructokinase from *Bacillus stearothermophilus*." Arch. Biochem. Biophys. **436**(1): 178-186.

Schaftingen, E. V., L. Hue, et al. (1980). "Control of the fructose 6-phosphate/fructose 1,6-bisphosphate cycle in isolated hepatocytes by glucose and glucagon." Biochem. J. **192**: 887-895.

Schirmer, T. and P. R. Evans (1990). "Structural basis of the allosteric behavior of phosphofructokinase." Nature **343**(6254): 140-145.

Seddon, J. M. (1990). "Structure of the inverted hexagonal (HII) phase, and non-lamellar phase transitions of lipids." Biochim. Biophys. Acta **1031**(1): 1-69.

Shirakihara, Y. and P. R. Evans (1988). "Crystal structure of the complex of phosphofructokinase from *Escherichia coli* with its reaction products." J. Mol. Biol. **204**(4): 973-994.

Simpfendorfer, R. W., K. B. Oelckers, et al. (2006). "Phosphofructokinase from muscle of the marine giant barnacle *Austromegabalanus psittacus*: kinetic characterization and effect of in vitro phosphorylation." Comp. Biochem. Physiol. **142**(3-4): 382-389.

Sola-Penna, M., A. C. dos Santos, et al. (2002). "A radioassay for phosphofructokinase-1 activity in cell extracts and purified enzyme." J. Biochem. Biophys. Meth. **50**(2-3): 129-140.

Sols, A. (1979). "Multimodulation of enzyme activity. Physiological significance and evolutionary origin." ICN-UCLA Symposia on Molecular & Cellular Biology **13**(Modulation Protein Funct.): 27-45.

Strapazon, E. and T. L. Steck (1976). "Binding of rabbit muscle aldolase to band 3, the predominant polypeptide of the human erythrocyte membrane." Biochemistry **15**(7): 1421-1424.

Strapazon, E. and T. L. Steck (1977). "Interaction of the aldolase and the membrane of human erythrocytes." Biochemistry **16**(13): 2966-2971.

Stryer, L. (1999). Biochemistry, 4th edition. New York, W.H. Freeman and Company.

Tlapak-Simmons, V. L. and G. D. Reinhart (1994). "Comparison of the inhibition by phospho(enol)pyruvate and phosphoglycolate of phosphofructokinase from *B. stearothermophilus*." Arch. Biochem. Biophys. **308**(1): 226-30.

Uyeda, K. (1979). "Phosphofructokinase." Advances in Enzymology and Related Areas of Molecular Biology **48**: 193-244.

Valdez, B. C., B. A. French, et al. (1989). "Site-directed mutagenesis in *Bacillus stearothermophilus* fructose-6- phosphate 1-kinase. Mutation at the substrate-binding site affects allosteric behavior." J. Biol. Chem. **264**(1): 131-135.

Vannucci, R. C., R. M. Brucklacher, et al. (2005). "Glycolysis and perinatal hypoxic-ischemic brain damage." Devel. Neurosc. **27**(2-4): 185-190.

Vats, V., S. P. Yadav, et al. (2004). "Ethanolic extract of *Ocimum sanctum* leaves partially attenuates streptozotocin-induced alterations in glycogen content and carbohydrate metabolism in rats." J. Ethnopharmac. **90**(1): 155-160.

Vora, S. (1983). "Isozyme of human phosphofructokinase: biochemical and genetic aspects." Isozymes: Current Topics in Biological and Medical Research **11**: 3-23.

Wang, X. and R. G. Kemp (2001). "Reaction path of phosphofructo-1-kinase is altered by mutagenesis and alternative substrates." Biochemistry **40**(13): 3938-3942.

Warburg, O. (1956). "On the origin of cancer cells." Science **123**: 309-314.

Yu, J. and T. L. Steck (1975). "Associations of Band 3, predominant polypeptide of human erythrocyte membrane." J. Biol. Chem. **250**(23): 9176-9184.

Yu, J. and T. L. Steck (1975). "Isolation and characterization of band 3, the predominant polypeptide of the human erythrocyte membrane." J. Biol. Chem. **250**(23): 9170-9175.

Zancan, P., F. V. R. Almeida, et al. (2007). "Fructose-2,6-bisphosphate counteracts guanidinium chloride-, thermal-, and ATP-induced dissociation of skeletal muscle key glycolytic enzyme 6-phosphofructo-1-kinase: A structural mechanism for PFK allosteric regulation " Arch. Biochem. Biophys. **467**(2): 275-282.

Zancan, P., A. O. Rosas, et al. (2007). "Clotrimazole inhibits and modulates heterologous association of the key glycolytic enzyme 6-phosphofructokinase." Biochem. Pharmacol. **73**: 1520-1527.

Zancan, P. and M. Sola-Penna (2005). "Calcium influx: A possible role for insulin modulation of intracellular distribution and activity of 6-phosphofructo-1-kinase in human erythrocytes." Mol. Genet. Metab. **86**(3): 392-400.

Zancan, P. and M. Sola-Penna (2005). "Regulation of human erythrocyte metabolism by insulin: Cellular distribution of 6-phosphofructo-1-kinase and its implication for red blood cell function." Mol. Genet. Metab. **86**(3): 401-411.

Zhang, L., Q. Gao, et al. (2007). "Simple and complex spatiotemporal structures in a glycolytic allosteric enzyme model." Biophys. Chem. **125**(1): 112-116.

Zhu, X., M. Byrnes, et al. (1995). "Role of glycine 212 in the allosteric behavior of phosphofructokinase from *Bacillus stearothermophilus*." Biochemistry **34**(8): 2560-2565.

Chapter V

Conclusions

Table of Contents

V.1. Conclusions

V.1.1. CCTα

In vitro studies of CCTα by means of a ^{14}C radiochemical assay led to results that supported the stored elastic stress hypothesis as a regulatory mechanism of the enzyme. Application of an alternative lipid-dependent hypothesis of CCTα regulation, the electrostatics theory, could not explain the majority of data.

In vivo investigation of the phosphatidyl choline biosynthesis was also undertaken using a transfected GFP-HeLa cell line. Hexadecyl phosphocholine (HDPC) was considerably more potent than hexadecyl ammonium bromide (CTAB) in inhibiting new phosphocholine (PC) synthesis. Both drugs changed the acylation patterns for endogenous and new PC, as well as endogenous phosphoethanolamine head group classes. Also, cell sizing data suggested that the presence of both drugs in the culture could potentially shift the cell population distribution towards smaller cell diameters. Overall, phosphatidyl choline metabolism was inhibited by the presence of these two Type I amphiphiles, as predicted by the stored elastic stress hypothesis.

V.1.2. PFK-1

As part of this investigation, we developed a novel ^{33}P radiochemical assay for PFK-1. Kinetic studies on substrates ATP and F6P, and allosteric effectors PEP and ADP were undertaken for PFK-1 of *Bacillus stearothermophilus* in the presence of dioleoyl phosphocholine (DOPC) and DOPC/oleic acid (OA) (50:50). OA was found to increase catalytic activity twofold and threefold compared to DOPC and no lipid present, respectively. However, the activation was much smaller than for CCTα. While these results suggest that stored curvature elastic energy may play a role in modulating enzyme activity, they are significantly different from the results obtained with CCT. Also, it is much harder to apply the hypothesis to an enzyme

like PFK-1 which has been classically considered a cytoplasmic enzyme, and which exhibits very complicated allosteric kinetics. Therefore, interesting questions arise about the fundamental mechanisms that underlie the effect of membrane lipid composition on PFK-1 activity.

V.2. Further work

V.2.1. *In vitro* CCTα studies

The most important further work related to the *in vitro* investigation of CCTα would be to conduct phase studies on the 28 lipidic systems studied under physiological conditions and also under our assay conditions, most importantly in the presence of the assay buffer which contains divalent cations. This is way is would be possible to draw more confident conclusions with regards to phase behaviour, and in consequence, typology of the systems.

If this line of CCTα work is further studied, it would also be beneficial to develop a less hazardous alternative to the ^{14}C radiochemical assay for effectively assaying enzyme activity in the presence of membranes. One potential route could be the use of atomic force microscopy (AFM), which has been used successfully and accurately to study lipid vesicles adsorbed on substrates under liquid (Shibata-Seki, Masai et al. 1996) and to characterise liposomes in general (Ruozi, Tosi et al. 2005).

Another interesting experiment would be to assay all three enzymes involved in the Kennedy pathway collectively in the same experiment by providing radiochemically labelled choline as the only substrate. This would allow the investigation of the effect of membranes to the whole pathway, although chromatographic separation of products may prove challenging.

Finally, the lateral stress diagrams for some of the investigated binary systems could be theoretically predicted and compared to our experimental results. Lateral

stress diagrams for systems containing di-palmitoyl phosphatidyl choline (Ollila, Hyvoenen et al. 2007).

V.2.2. *In vivo* studies of lipid metabolism

In reference to the *in vivo* studies, the experiments should be repeated at least once to confirm reproducibility. It would be interesting to also monitor phosphatidyl ethanolamine biosynthesis by addition of deuterated ethanolamine. Unfortunately, this has not been previously attempted, thus new mass spectrometry protocols would have to be developed. Potentially, use of a non-adherent cell line would render the cell culture experiments easier and allow more continuous studies of the same cell line. Finally, should this mass spectrometry work is continued, it is pivotal to develop a more user-friendly and less time consuming method for data analysis of mass spectrometry data.

V.2.3. *In vitro* PFK-1 studies and other work

A few more experiments on PFK-1 kinetics would further our current findings, such as PFK-1 ATP saturation plots in the presence of membranes and with different concentrations of F6P. Additionally, it would be beneficial to prove that lipids physically bind to PFK-1 by means of binding assays or isothermal calorimetry. Kinetics of PFK-1 of an organism showing more complicated allostery could be investigated using our novel ^{33}P radiochemical assay in the presence of membranes. Finally, enzymes aldolase and glyceraldehyde 3-phosphate dehydrogenase of glycolysis which have also been shown to bind to membranes with a regulatory effect could also be assayed.

In light of the results presented in this thesis, the study of the effect membrane composition and of the stored elastic energy on another amphipathic enzymes arise as an interesting new direction for research. Since it has been suggested that glycolysis, sugar metabolism, and phospholipolysis are coupled through a direct

physical interaction between PFK-1 and mammalian myocardial PLA2 (Hazen and Gross 1993), a potential candidate might be phospholipase A2 (PLA2), for which a radiochemical assay is already available. The biological significance of this reaction is that produces lipid-derived mediators of inflammation, allergy and tumorigenesis, examples of which are the bioactive molecules of eicosanoids and platelet-activating factor (Ghosh, Tucker et al. 2006). Interestingly, PLA2 also bears a structural similarity to CCTα, as it possesses an N-terminal amphipathic α- helix with hydrophobic strips which regulates membrane binding and enzyme activity (Qin, Pande et al. 2005). PLA2 is activated by binding onto membranes, as is CCTα, and its hydrolytic ability is increased by the presence of Type II lipids, as predicted by the stored elastic stress hypothesis (Gabriel, Agman et al. 1987; Sen, Isac et al. 1991; Zidovetzki, Laptalo et al. 1992). Consequently, interesting correlation to conclusions of this thesis may arise from studies of PLA2.

V.3. References

Gabriel, N. E., N. V. Agman, et al. (1987). "Enzymatic-hydrolysis of short-chain lecithin long-chain phospholipid unilamellar vesicles - sensitivity of phospholipases to matrix phase state." Biochemistry **26**(23): 7409-7418.

Ghosh, M., D. E. Tucker, et al. (2006). "Properties of the group IV phospholipase A2 family." Progr. Lip. Res. **45**(6): 487-510.

Hazen, S. L. and R. W. Gross (1993). "The specific association of a phosphofructokinase isoform with myocardial calcium-independent phospholipase A2. Implications for the coordinated regulation of phospholipolysis and glycolysis." J. Biol. Chem. **268**(13): 9892-9900.

Ollila, S., M. T. Hyvoenen, et al. (2007). "Polyunsaturation in lipid membranes: Dynamic properties and lateral pressure profiles." J. Phys. Chem. B **111**(12): 3139-3150.

Qin, S., A. H. Pande, et al. (2005). "Evidence for the regulatory role of the N-terminal helix of secretory phospholipase A2 from studies on native and chimeric proteins." J. Biol. Chem. **280**(44): 36773-36783.

Ruozi, B., G. Tosi, et al. (2005). "Atomic force microscopy and photon correlation spectroscopy: Two techniques for rapid characterization of liposomes." Eur. J. Pharmaceut. Sci. **25**(1): 81-89.

Sen, A., T. V. Isac, et al. (1991). "Bilayer packing stress and defects in mixed di-linoleoyl phosphatidyl ethanolamine and palmitoyl-oleoyl phosphatidyl choline and their susceptibility to phospholipase-A2." Biochemistry **30**(18): 4516-4521.

Shibata-Seki, T., J. Masai, et al. (1996). "In-situ atomic force microscopy study of lipid vesicles adsorbed on a substrate." Thin Solid Films **273**(1-2): 297-303.

Zidovetzki, R., L. Laptalo, et al. (1992). "Effect of diacylglycerols on the activity of cobra venom, bee venom and pig pancreatic phospholipases-A2." Biochemistry **31**(33): 7683-7681.

Appendix I

Abbreviations

Abbreviation	Term
2D	Two dimensional
A	Amphiphile cross-sectional area.
ADP	Adenosine diphosphate
ALPs	alkyl lyso phosphatidyl cholines
APCs	alkyl phosphocholines
Arg	Arginine amino acid
ATP	Adenosine triphosphate
BsPFK-1	Phosphofructokinase of *B. stearothermophilus*
c_1	Maximum principal curvature
C16EO8	Octaethylene glycol monohexadecyl ether
C18:0 CER	N-Stearoyl-D-erythro-Sphingosine
C18:1 CER	N-Oleoyl-D-erythro-Sphingosine
c_2	Minimum principal curvature
C6:0 PG	1,2-Dihexanoyl-sn-Glycero-3-[Phospho-rac-(1-glycerol)]
C8:0 DG	1,2-Dioctanoyl-sn-Glycerol
CCP	CTP-choline diacylglycerol phosphocholine transferase
CCT	CTP:phosphocholine cytidylytransferase
CCTα	Protein isoform α of CCT
CCTβ_1	Protein isoform β_1 of CCT
CCTβ_2	Protein isoform β_2 of CCT
CDP	Cytidyl diphosphate
CET	CTP: phosphoethanolamine cytidylytransferase
CHOL	Cholesterol
CK	Choline kinase
CMC	Critical micellar concentration
C_o	Spontaneous curvature of monolayer
CTAB	Hexadecyl-trimethyl ammonium bromide
CTP	Cytidyl triphosphate
d_9PC	Deuterated choline
DAG	Diacyl glycerol
DAPI	4,6-diamidino-2-phenyl-indole
DES	D-erythro-sphingosine
DESP	D-erythro-sphingosine-phosphate
DHDMAB	Di-hexadecyl-di-methyl ammonium bromide
DMPC	1,2-di-myristoyl- phosphatidyl choline (PC14:0/14:0)
DNA	Deoxyribonucleic acid
DOG	1,2-di-oleoyl-sn-glycerol (18:1/18:1)
DOPA	Di-oleoyl-phosphatidate or 1,2-di-oleoyl-sn-glycero-3-phosphate (PA18:1/18:1)
DOPC	Di-oleoyl-phosphatidyl choline or 1,2-di-oleoyl-sn-glycero-3-phosphatidyl-choline (PC18:1/18:1)

DOPE	Di-oleoyl-phosphatidyl ethanolamine or 1,2-di-oleoyl-sn-glycero-3-phosphatidyl-ethanolamine (PE18:1/18:1)
DOPS	1,2-di-oleoyl-sn-glycero-3-phosphatidyl-serine (PS18:1/18:1)
DPHPC	1,2-di-O-phytanyl-sn-glycero-3-phosphocholine
DPHPE	1,2-di-O-phytanyl-sn-glycero-3-phosphatidyl-ethanolamine
DPPA	1,2-dipalmitoyl-sn-glycero-3-phosphate (PA16:0/16:0)
DPPC	1,2-dipalmitoyl-sn-glycero-3 phosphocholine (PC16:0/16:0)
DPPS	1,2-dipalmitoyl-sn-glycero-3-phosphatidyl-serine (PS16:0/16:0)
DSPA	Di-stearoyl-phosphatidate (PA18:0/18:0)
DTT	Dithiothreitol
EcPFK-1	Phosphofructokinase of *E. coli*
ED_{50}	Median effective dose for a chemical compound
ESI-MS	Electrospray ionisation mass spectrometry
Et-18-OCH_3	1-O-octadecyl-2-O- methyl-rac –glycero-3-phosphocholine
F16BP	D-fructose 1,6-bisphosphate
F6P	D-fructose 6-phosphate
G3DP	Glyceraldehyde-3-phosphate dehydrogenase
g_c	Membrane curvature elastic energy
GDP	Guanosine diphosphate
GDP	Guanosine diphosphate
GFP	Green fluorescence protein
Gly	Glycine amino acid
H	Mean curvature of a monolayer
H_0	Spontaneous curvature of a monolayer
HDPC	Hexadecyl phosphatidylcholine
HeLa	Henrietta Lacks human negroid cervix epitheloid carcinoma cell line
K	Membrane/water partition coefficient
K_B	Boltzmann constant
K_M	Michaelis constant for enzymes kinetics
K_R	Dissociation constant for R state
K_T	Dissociation constant for T state
l_c	Maximum length of hydrocarbon chains for a lipid
LPC	Lysophosphatidyl choline
LUVs	Large unilamellar vesicles
MD	Molecular dynamics
MWC	Monod-Wyman-Changeux
NADH	Nicotinamide adenine dinucleotide
O COA	Oleoyl coenzyme A
OA	Oleic acid (18:1)
OPA	1-oleoyl-sn-glucero-3-phosphate (PA18:1)
OPS	1-oleoyl-sn-glycero-3-phosphatidyl-serine (PS18:1)
PA	Phosphatidic acid

PC	Phosphocholine
PE	Phosphoethanolamine
PEMT1	Phosphatidyl ethanolamine N-methyltransferase
PEMT1 or CHO2	Phosphatidyl ethanolamine N-methyltransferase
PEMT2	Phosphatidyl N-methylethanolamine N-methyltransferase
PEMT2 or OPI3	Phosphatidyl N-methylethanolamine N-methyltransferase
PEP	Phosphoenol pyruvate
PEP	Phosphoenol pyruvate
PFK-1	Phosphofructokinase-1
PFK-2	Phosphofructokinase-2
PFK-L	Liver phosphofructokinase
PFK-M	Muscle phosphofructokinase
PFK-P	Platelet phosphofructokinase
PLA_2	Phospholipase A_2
POG	1-palmitoyl-2-oleoyl-sn-glycerol (16:0/18:1)
PS	Phosphoserine
PtdCho	Phosphatidyl choline
PtdEth	Phosphatidyl ethanolamine
PtdGro	Phosphatidyl glycerol
PtdIns	Phosphatidyl inositol
PtdSer	Phosphatidyl serine
R	Relaxed acive enzyme state of allosteric model
R_1	Maximum normal of a monolayer
R_2	Minimum normal of a monolayer
S	Relative activity of the enzyme
SAG	1-stearoyl-2-arachidonoyl-sn-glycerol (18:0/20:4)
SAM	S-adenosyl-methionine
SDS	Sodium dodecyl sulphate
SEM	Scanning electron microscope
SM	Sphingomyelin or N-Stearoyl-D-erythro-Sphingosylphosphorylcholine
SUVs	Small unilamellar vesicles
T	Temperature
T	Tense inactive enzyme state of allosteric model
TLC	Thin layer chromatography
V_{max}	Maximal rate of enzyme
ΔG	Gibbs free energy
ΔH	Enthalpy
ΔS	Entropy
ζ	Critical packing parameter for a lipid
κ_G	Gaussian curvature

κ_M	Mean curvature bending modulus for stored elastic stress hypothesis
$\pi(z)$	Lateral pressure of a monolayer
τ	Total stored elastic stressof the bilayer, aka torque tension
$\tau(z)$	Lateral stress of a monolayer
υ	Cylindrical volume of chains for a lipid

Appendix II

Data Tables

Table of Contents

AII.1. Data tables for CCTα results (Chapter II)

AII.1.1. LUV sizing by light scattering

For reasons of brevity, sizing data for all experiments is not shown for all radiochemical assays mentioned in this thesis. One A typical example of vesicle sizing results is shown for DOPC/OA vesicles used in Assay 19. Assay data shown in Table AII.3 and plots in Figure II.11 and II.12 of Chapter II. Vesicles were sized before each radiochemical assay using a at Coulter N4 PLUS Particle Sizer at a 90 ° angle. In all experiments, it was ensured that the majority of the vesicles were at least 1000 nm in diameter. See overleaf for intensity plots as exported by the particle sizing instrument.

Molar % of OA in DOPC/OA	Percentage of vesicles with a diameter larger than 1000nm	Exact diameter/nm
0	97.8	2000.0 ± 137.0
10	100.0	2000.0 ± 137.0
20	100.0	2000.0 ± 137.0
30	100.0	2000.0 ± 137.0
40	92.3	1780.0 ± 293.1
50	93.5	2000.0 ± 137.0
60	85.7 14.3	175.7 ± 283.3 251.0 ± 46.3

Table AII.1- Sizing data for Assay 19.

DOPC/OA (100:0)

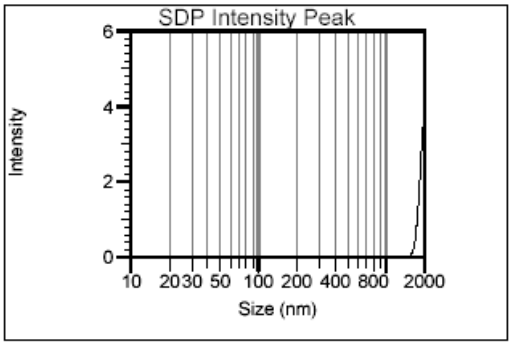

DOPC/OA (90:10)

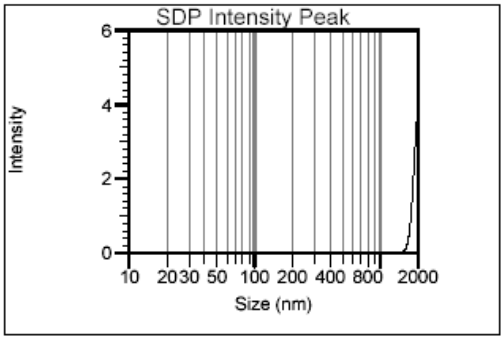

DOPC/OA (80:20)

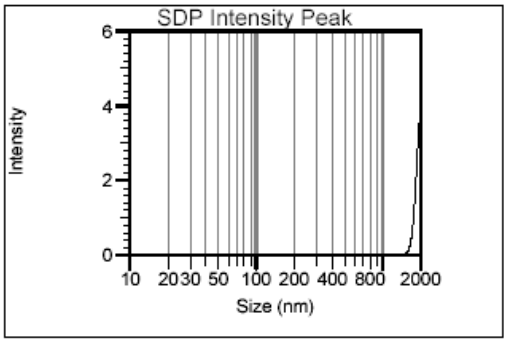

DOPC/OA(70:30)

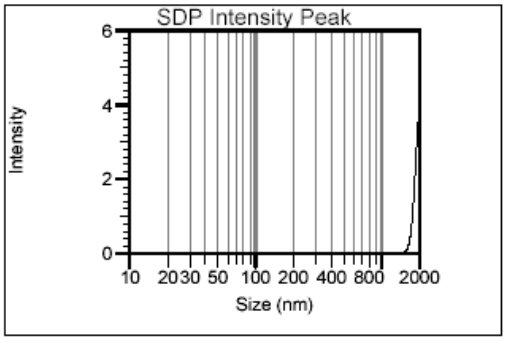

DOPC/OA (60:40)

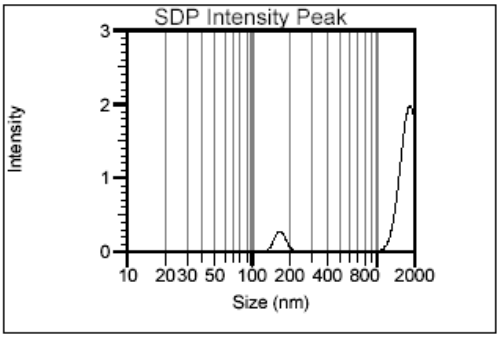

DOPC/OA (50:50)

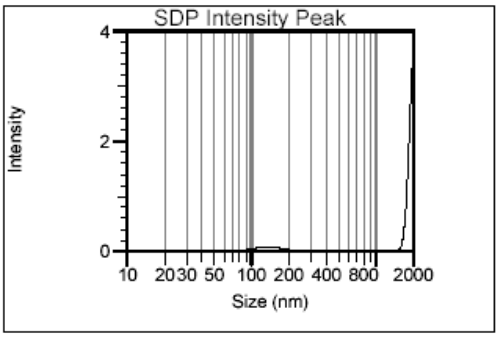

DOPC/OA (40:60)

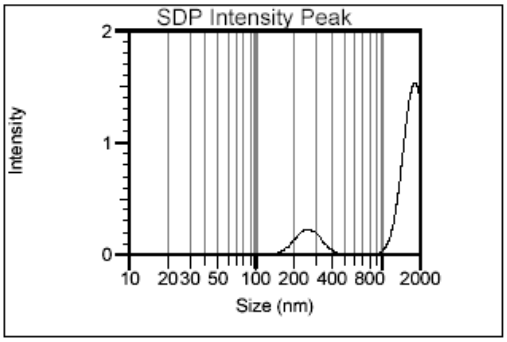

AII.1.2. Results for CCTα radiochemical assays

AII.1.2.1. CCTα kinetics

Time /minutes	Percentage conversion	Standard deviation
0	1.34	0.22
3	7.36	0.73
6	11.44	1.26
9	14.56	0.93
12	20.55	0.58
15	21.39	1.23
17	23.12	1.57
19	22.63	2.07
20	21.95	1.00

Table AII.2- Assay 7 data used in Figures II.9.

AII.1.2.2. DOPC/OA

Molar % of OA in DOPC/OA	Absolute activity /mol.min^{-1}.mg^{-1}	Standard deviation	CCT relative activity to 100% DOPC	Standard deviation
0	822.59	156.03	1.00	0.19
10	2058.57	272.74	2.50	0.33
20	4138.20	223.74	5.03	0.27
30	5824.87	384.27	7.08	0.47
40	6538.26	421.87	7.95	0.51
50	6819.76	161.56	8.29	0.20
60	6678.34	262.12	8.12	0.32

Table AII.3- Assay 19 data used in Figures II.11 and II.12.

AII.1.2.3. DOPC/DOPA

Molar % of DOPA in DOPC/DOPA	Absolute activity /mol.min^{-1}.mg^{-1}	Standard deviation	CCT relative activity to 100% DOPC	Standard deviation
0	741.85	47.98	1.00	0.06
10	3933.44	169.67	5.30	0.23
20	5722.04	27.70	7.71	0.04
30	5941.99	404.90	8.01	0.55
40	6753.21	119.66	9.10	0.16
50	6454.43	81.70	8.70	0.11
60	5063.28	768.22	6.83	1.04

Table AII.4- Assay 20 data used in Figures II.11 and II.12.

AII.1.2.4. DOPC/OPA

Molar % of OPA in DOPC/OPA	Absolute activity /mol.min^{-1}.mg^{-1}	Standard deviation	CCT relative activity to 100% DOPC	Standard deviation
0	477.63	100.58	1.00	0.21
10	614.68	56.27	1.29	0.12
20	865.35	76.30	1.81	0.16
30	1342.48	97.44	2.81	0.20
40	2087.16	132.02	4.37	0.28
50	2420.25	62.87	5.07	0.13
60	2551.48	155.32	5.34	0.33

Table AII.5- Assay 15 data used in Figures II.11 and II.12.

AII.1.2.5. DOPC/DPPA

Molar % of DPPA in DOPC/DPPA	Absolute activity /mol.min^{-1}.mg^{-1}	Standard deviation	CCT relative activity to 100% DOPC	Standard deviation
0	1755.50	688.40	1.00	0.39
5	2015.65	311.45	1.15	0.18
10	2306.69	216.93	1.31	0.12
15	3473.19	252.35	1.98	0.14
20	2542.92	295.03	1.45	0.17
25	3679.82	321.44	2.10	0.18
30	3486.41	89.29	1.99	0.05
40	3936.21	286.14	2.24	0.16

Table AII.6- Assay 51 data used in Figures II.11 and II.12.

AII.1.2.6. DOPC/OPS

Molar % of OPS in DOPC/OPS	Absolute activity /mol.min^{-1}.mg^{-1}	Standard deviation	CCT relative activity to 100% DOPC	Standard deviation
0	647.36	212.79	1.00	0.33
10	408.59	320.05	0.63	0.09
20	822.48	324.65	1.27	0.50
30	1265.44	181.49	1.95	0.28
40	1567.08	305.31	2.42	0.47
50	1388.06	438.43	2.14	0.68
60	1472.41	177.85	2.27	0.27

Table AII.7- Assay 13 data used in Figures II.14 and II.15.

AII.1.2.7. DOPC/DOPS

Molar % of DOPS in DOPC/DOPS	Absolute activity /mol.min^{-1}.mg^{-1}	Standard deviation	CCT relative activity to 100% DOPC	Standard deviation
0	1539.89	11.08	1.00	0.01
10	1616.07	105.07	1.05	0.07
20	2106.59	246.52	1.37	0.16
30	3225.08	103.23	2.09	0.07
40	4547.26	100.76	2.95	0.07
50	6416.09	125.78	4.17	0.08
60	6947.78	105.99	4.51	0.07

Table AII.8- Assay 44 data used in Figures II.14 and II.15.

AII.1.2.8. DOPC/DPPS

Molar % of DPPS in DOPC/DPPS	Absolute activity /mol.min^{-1}.mg^{-1}	Standard deviation	CCT relative activity to 100% DOPC	Standard deviation
0	1766.35	691.42	1.00	0.39
5	1733.43	181.73	0.98	0.10
10	2950.02	156.34	1.67	0.09
15	3223.32	113.53	1.82	0.06
20	4841.98	169.85	2.74	0.10
25	5624.81	177.34	3.18	0.10
30	4923.04	855.15	2.79	0.48
40	4078.97	93.82	2.31	0.05

Table AII.9- Assay 50 data used in Figures II.14 and II.15.

AII.1.2.9. DOPC/DOPE

Molar % of DOPE in DOPC/DOPE	Absolute activity /mol.min^{-1}.mg^{-1}	Standard deviation	CCT relative activity to 100% DOPC	Standard deviation
0	763.54	110.30	1.00	0.14
10	1150.15	237.02	1.51	0.31
20	1366.33	47.19	1.79	0.06
30	1775.47	150.92	2.33	0.20
40	2722.07	242.61	3.57	0.32
50	3466.51	140.68	4.54	0.18
60	3073.42	243.29	4.03	0.32

Table AII.10- Dymond assay data used in Figures II.17 and II.18.

AII.1.2.10. DOPC/DPHPE

Molar % of DPHPE in DOPC/DPHPE	Absolute activity /mol.min^{-1}.mg^{-1}	Standard deviation	CCT relative activity to 100% DOPC	Standard deviation
0	651.08	227.16	1.00	0.35
5	823.49	216.82	1.26	0.33
10	1792.19	176.77	2.75	0.27
15	2552.57	178.89	3.92	0.27
20	3083.56	205.93	4.74	0.32
25	3916.11	192.27	6.01	0.30
30	5976.35	171.14	9.18	0.26
40	5649.41	75.26	8.68	0.12

Table AII.11- Assay 61 data used in Figures II.17 and II.18.

AII.1.2.11. DOPC/POG

Molar % of POG in DOPC/POG	Absolute activity /mol.min^{-1}.mg^{-1}	Standard deviation	CCT relative activity to 100% DOPC	Standard deviation
0	1230.08	952.07	1.00	0.48
1	644.39	281.03	0.52	0.06
3	871.57	363.66	0.71	0.27
5	959.51	672.23	0.78	0.28
7	704.86	70.39	0.57	0.27
9	784.64	260.89	0.64	0.12
10	815.26	376.33	0.66	0.32
15	1003.41	266.78	0.82	0.22

Table AII.12- Assays 54 and 58 data used in Figures II.21 and II.22.

AII.1.2.12. DOPC/SAG

Molar % of SAG in DOPC/SAG	Absolute activity /mol.min^{-1}.mg^{-1}	Standard deviation	CCT relative activity to 100% DOPC	Standard deviation
0	566.94	55.13	1.00	0.10
1	735.65	212.06	1.30	0.37
3	998.88	147.32	1.76	0.26
5	971.16	136.18	1.71	0.24
7	939.11	104.20	1.66	0.18
9	1011.82	171.51	1.78	0.30
10	1745.54	26.94	3.08	0.05

Table AII.13- Assay 57 data used in Figures II.21 and II.22.

AII.1.2.13. DOPC/DOG

Molar % of DOG in DOPC/DOG	Absolute activity /mol.min^{-1}.mg^{-1}	Standard deviation	CCT relative activity to 100% DOPC	Standard deviation
0	607.16	306.38	1.00	0.50
2	5829.44	507.46	9.60	0.84
4	2201.47	395.30	3.63	0.65
6	741.04	125.00	1.22	0.21
8	202.92	31.98	0.33	0.05
10	175.02	5.40	0.29	0.01

Table AII.14- Assay 17 data used in Figures II.21 and II.22.

AII.1.2.14. DOPC/SM

Molar % of SM in DOPC/SM	Absolute activity /mol.min^{-1}.mg^{-1}	Standard deviation	CCT relative activity to 100% DOPC	Standard deviation
0	831.96	79.25	1.00	0.10
1	887.17	74.73	1.07	0.09
3	889.09	157.52	1.07	0.19
5	788.98	135.58	0.95	0.16
7	617.66	47.50	0.74	0.06
9	983.12	251.55	1.18	0.30
10	889.04	169.08	1.07	0.20

Table AII.15- Assay 24 data used in Figures II.24 and II.25.

AII.1.2.15. DOPC/DPHPC

Molar % of DPHPC in DOPC/DPHPC	Absolute activity /mol.min^{-1}.mg^{-1}	Standard deviation	CCT relative activity to 100% DOPC	Standard deviation
0	595.29	56.87	1.00	0.10
5	612.20	67.58	1.03	0.11
10	717.19	66.58	1.20	0.11
15	1040.05	140.29	1.75	0.24
20	955.30	117.10	1.60	0.20
25	1225.93	35.48	2.06	0.06
30	1599.39	182.40	2.69	0.31
40	2060.88	83.40	3.46	0.14

Table AII.16- Assay 39 data used in Figures II.24 and II.25.

AII.1.2.16. DOPC/C18:0 CER

Molar % of C18:0 CER in DOPC/C18:0 CER	Absolute activity /mol.min^{-1}.mg^{-1}	Standard deviation	CCT relative activity to 100% DOPC	Standard deviation
0	570.09	44.33	1.00	0.08
5	1093.88	100.69	1.92	0.18
10	904.22	84.64	1.59	0.15
15	954.46	31.67	1.67	0.06
20	1017.00	39.84	1.78	0.07
25	1289.21	122.53	2.26	0.21
30	1014.93	219.30	1.78	0.38
40	1704.81	257.12	2.99	0.45

Table AII.17- Assay 41 data used in Figures II.27 and II.28.

AII.1.2.17. DOPC/C18:1 CER

Molar % of C18:1 CER in DOPC/C18:1 CER	Absolute activity /mol.min^{-1}.mg^{-1}	Standard deviation	CCT relative activity to 100% DOPC	Standard deviation
0	729.34	94.57	1.00	0.13
5	1055.29	146.62	1.45	0.20
10	1265.34	73.50	1.73	0.10
15	1409.89	227.27	1.93	0.31
20	2295.06	431.26	3.15	0.59
25	3248.49	140.04	4.45	0.19
30	2168.25	100.09	2.97	0.14
40	3858.57	48.10	5.29	0.07

Table AII.18- Assay 42 data used in Figures II.27 and II.28.

AII.1.2.18. DOPC/DES

Molar % of DES in DOPC/DES	Absolute activity /mol.min^{-1}.mg^{-1}	Standard deviation	CCT relative activity to 100% DOPC	Standard deviation
0	1783.73	291.99	1.00	0.16
1	1918.14	266.61	1.08	0.15
3	2032.75	119.80	1.14	0.07
5	2306.37	143.43	1.29	0.08
7	2463.85	138.36	1.38	0.08
9	1806.87	327.68	1.01	0.18
10	2747.69	207.20	1.54	0.12

Table AII.19- Assay 26 data used in Figures II.35 and II.36.

AII.1.2.19. DOPC/DESP

Molar % of DESP in DOPC/DESP	Absolute activity /mol.min^{-1}.mg^{-1}	Standard deviation	CCT relative activity to 100% DOPC	Standard deviation
0	1656.51	273.55	1.00	0.17
1	2187.39	126.59	1.32	0.08
3	2162.76	122.33	1.31	0.07
5	1867.71	71.02	1.13	0.04
7	2078.85	136.16	1.25	0.08
9	1995.62	196.96	1.20	0.12
10	1763.79	343.32	1.06	0.21

Table AII.20- Assay 27 data used in Figures II.35 and II.36.

AII.1.2.20. DOPC/CHOL

Molar % of CHOL in DOPC/CHOL	Absolute activity /mol.min^{-1}.mg^{-1}	Standard deviation	CCT relative activity to 100% DOPC	Standard deviation
0	528.20	40.07	1.00	0.08
1	757.38	50.96	1.43	0.10
3	621.90	11.26	1.18	0.02
5	967.28	6.80	1.83	0.01
7	1100.44	122.15	2.08	0.23
9	1090.06	18.57	2.06	0.04
10	1051.17	189.57	1.99	0.36

Table AII.21- Assay 46 data used in Figures II.39 and II.40.

AII.1.2.21. DOPC/C6:0 PG

Molar % of C6:0 PG in DOPC/C6:0 PG	Absolute activity /mol.min^{-1}.mg^{-1}	Standard deviation	CCT relative activity to 100% DOPC	Standard deviation
0	599.93	102.45	1.00	0.17
2	699.67	135.19	1.17	0.23
4	712.75	124.53	1.19	0.21
6	708.99	129.12	1.18	0.22
8	866.12	56.79	1.44	0.09
10	1107.08	30.18	1.85	0.05
12	1870.22	187.39	3.12	0.31

Table AII.22- Assay 18 data used in Figures II.39 and II.40.

AII.1.2.22. DOPC/C8:0 DG

Molar % of C8:0 DG in DOPC/C8:0 DG	Absolute activity /mol.min^{-1}.mg^{-1}	Standard deviation	CCT relative activity to 100% DOPC	Standard deviation
0	434.49	16.20	1.00	0.04
1	426.92	9.86	0.98	0.02
3	695.95	144.23	1.60	0.33
5	750.39	292.55	1.73	0.67
7	869.49	34.83	2.00	0.08
9	789.41	98.79	1.82	0.23
10	1261.76	174.91	2.90	0.40

Table AII.23- Assay 60 data used in Figures II.39 and II.40.

AII.1.2.23. DOPC/O COA

Molar % of O COA in DOPC/O COA	Absolute activity /mol.min^{-1}.mg^{-1}	Standard deviation	CCT relative activity to 100% DOPC	Standard deviation
0	1103.39	260.90	1.00	0.21
1	820.21	185.33	0.74	0.17
3	911.15	183.88	0.83	0.17
5	739.59	235.48	0.67	0.21
7	950.57	343.11	0.86	0.31
9	838.86	256.75	0.76	0.23
10	983.04	347.65	0.89	0.32
15	873.42	225.00	0.79	0.19

Table AII.24- Assays 38 and 47 data used in Figures II.39 and II.40.

AII.1.2.24. DOPC/DOPE/CTAB

Molar % of CTAB in DOPC/DOPE/CTAB (80:20:X)	Absolute activity /mol.min^{-1}.mg^{-1}	Standard deviation	CCT relative activity to 100% DOPC	Standard deviation
0	1411.56	204.02	1.00	0.14
5	1569.82	135.94	1.11	0.10
10	986.45	134.24	0.70	0.10
15	475.49	16.65	0.34	0.01
20	482.14	8.29	0.34	0.01
25	240.86	189.26	0.17	0.01

Table AII.25- Assay 69 data used in Figures II.42 and II.43.

AII.1.2.25. DOPC/DOPE/SDS

Molar % of SDS in DOPC/DOPE/SDS (80:20:X)	Absolute activity /mol.min^{-1}.mg^{-1}	Standard deviation	CCT relative activity to 100% DOPC	Standard deviation
0	1570.37	424.96	1.00	0.27
2.5	1128.02	100.14	0.72	0.06
5	1910.20	468.72	1.22	0.30
10	1595.81	343.63	1.02	0.22
15	3890.53	455.19	2.48	0.29
20	4126.60	352.40	2.63	0.22

Table AII.26- Assay 75 data used in Figures II.42 and II.43.

AII.1.2.26. DOPC/DOPE/HDPC

Molar % of HDPC in DOPC/DOPE/HDPC (80:20:X)	Absolute activity /mol.min^{-1}.mg^{-1}	Standard deviation	CCT relative activity to 100% DOPC	Standard deviation
0	1403.00	204.51	1.00	0.15
5	372.11	29.40	0.27	0.02
10	264.97	60.93	0.19	0.04
15	294.10	29.32	0.21	0.02
20	127.07	27.43	0.09	0.02
25	111.82	105.82	0.08	0.08

Table AII.27- Assay 70 data used in Figures II.42 and II.43.

AII.1.2.27. DOPC/DOPE/DHDMAB

Molar % of DHDMAB in DOPC/DOPE/ DHDMAB (80:20:X)	Absolute activity /mol.min^{-1}.mg^{-1}	Standard deviation	CCT relative activity to 100% DOPC	Standard deviation
0	2305.63	53.02	1.00	0.02
3	2208.00	590.17	0.96	0.26
5	1799.34	244.39	0.78	0.11
10	1087.00	273.85	0.47	0.12
15	550.52	109.88	0.24	0.05
20	422.89	14.95	0.18	0.01

Table AII.28- Assay 78 data used in Figures II.42 and II.43.

AII.1.2.28. DOPC/DOPE/C16EO8

Molar % of C16EO8 in DOPC/DOPE/ C16EO8 (80:20:X)	Absolute activity /mol.min^{-1}.mg^{-1}	Standard deviation	CCT relative activity to 100% DOPC	Standard deviation
0	2548.08	1092.62	1.00	0.43
2.5	3341.98	223.28	1.31	0.09
5	3345.14	294.39	1.31	0.12
10	2146.35	73.00	0.84	0.03
15	1710.30	270.81	0.67	0.11
20	1727.31	67.94	0.68	0.03

Table AII.29- Assay 76 data used in Figures II.42 and II.43.

AII.1.2.29. Micellar SDS

Concentration /mM	Absolute activity /mol.min^{-1}.mg^{-1}	Standard deviation
0	146.03	170.23
0.005	56.07	11.35
0.010	67.37	16.69
0.050	191.31	13.15
0.100	434.33	41.61
1.000	364.33	558.86
8.000	70.45	71.51
20.000	65.58	66.84
50.000	68.11	22.89

Table AII.30- Assay 77 data used in Figure II.46.

AII.1.2.30. Micellar CTAB

Concentration /mM	Absolute activity /mol.min^{-1}.mg^{-1}	Standard deviation
0	145.59	168.34
0.005	45.76	8.50
0.010	56.05	3.41
0.050	37.09	2.06
0.100	55.62	3.37
1.000	105.62	60.96
10.000	119.53	40.14
20.000	56.73	27.92
50.000	32.31	4.34
100.00	34.40	31.08

Table AII.31- Assay 74 data used in Figure II.46.

AII.2. Data tables for cell cultures results (Chapter III)

AII.2.1. Cell sizing

AII.2.1.1. Control cultures

Time /hours	Diameter /μm	SD	Skewness	SD	Excess kurtosis	SD
0	18.39	2.20	0.02	2.65E-03	4.66	5.58E-01
3	17.73	1.90	0.05	5.36E-03	1.51	2.27E-02
6	17.97	2.00	-0.10	-1.15E-02	1.93	3.72E-02
9	18.06	2.26	-0.31	-3.84E-02	1.20	1.44E-02
12	19.94	3.03	-0.04	-6.82E-03	2.25	5.07E-02
24	18.92	2.60	0.85	1.17E-01	2.75	7.57E-02
43	19.11	3.59	0.28	5.22E-02	1.39	1.94E-02
144	15.61	1.90	-0.06	-7.19E-03	1.51	2.27E-02

Table AII.32- Data used in Figures III.11 to III.13.

AII.2.1.2. HDPC after 21 hours incubation

Concentration /μM	Diameter /μm	SD	Skewness	SD	Excess kurtosis	SD
10.50	18.33	3.36	-0.58	-1.06E-01	0.19	3.48E-04
5.25	17.93	4.22	-0.84	-1.97E-01	0.28	8.06E-04
2.63	18.13	4.27	-0.56	-1.32E-01	1.12	1.24E-02

Table AII.33- Data used in Figures III.11 to III.13.

AII.2.1.3. CTAB after 21 hours incubation

Concentration /μM	Diameter /μm	SD	Skewness	SD	Excess kurtosis	SD
3.00	19.07	4.16	-0.80	-1.75E-01	1.24	1.55E-02
1.50	18.25	3.51	-0.68	-1.30E-01	1.62	2.63E-02
0.75	18.77	3.29	-0.48	-8.38E-02	2.10	4.43E-02

Table AII.34- Data used in Figures III.11 to III.13.

AII.2.2. Control cultures

AII.2.2.1. Cell viability

Time /hours	Percentage of dead cells	Standard deviation
0	13.61	3.54
3	12.84	1.97
6	5.36	0.60
9	24.90	4.88
12	6.70	2.24
15	4.27	0.81
18	5.57	1.87
21	16.08	6.28

Table AII.35- Data used in Figure III.10.

AII.2.2.2. Total lipid content by ESI-MS

Time /hours	PC /nmoles	SD	PE /nmoles	SD	d9PC /nmoles	SD
0	7.42E-05	3.86E-05	1.68E-05	1.20E-05	1.53E-07	8.36E-08
3	2.71E-05	1.03E-05	1.58E-05	5.01E-06	1.21E-05	4.53E-06
6	6.68E-05	2.99E-05	1.70E-05	2.32E-06	6.58E-05	2.37E-05
9	7.62E-05	3.47E-05	2.48E-05	9.15E-06	5.99E-05	2.36E-05
12	5.20E-05	6.18E-06	2.08E-05	1.30E-06	7.03E-05	4.17E-06
15	3.98E-05	7.22E-06	2.19E-05	6.78E-06	1.05E-04	1.68E-05
18	6.27E-05	1.36E-05	2.20E-05	2.49E-06	1.48E-04	3.25E-05
21	1.67E-04	7.96E-05	2.05E-05	8.07E-06	1.29E-04	6.08E-05

Table AII.36- Data used in Figure III.14.

AII.2.2.3. Fatty acid membrane composition by ESI-MS

AII.2.2.3.1. **Endogenous PC**

		Time/hours							
MW /amu	**Fatty acid species**	**0**	**3**	**6**	**9**	**12**	**15**	**18**	**21**
706	**PC14:0/16:0**	2.42	1.62	1.18	1.41	1.83	1.74	1.61	1.96
718	**PC16:0a/16:1**	2.62	1.91	2.32	2.18	2.46	2.21	2.49	2.65
720	**PC16:0a/16:0**	2.76	2.33	2.43	2.14	2.73	2.02	2.49	2.18
732	**PC16:0/16:1**	4.97	4.18	5.04	4.40	4.53	4.46	4.73	4.94
734	**PC16:0/16:0**	3.94	4.35	3.07	3.25	4.29	3.71	3.43	4.22
744	**PC16:0a/18:2**	2.20	2.19	2.44	2.84	2.81	2.90	2.58	2.48
746	**PC16:0a/18:1**	7.60	6.10	6.85	6.37	7.14	6.81	7.52	6.63
748	**PC16:0a/18:0**	1.63	1.43	1.60	1.81	1.62	1.27	1.62	1.37
758	**PC16:0/18:2**	2.33	2.95	4.23	4.75	3.67	3.45	3.47	3.75
760	**PC16:0/18:1**	25.08	24.71	23.66	21.65	25.46	25.76	25.67	25.23
762	**PC16:0/18:0**	1.57	2.17	1.46	1.14	0.92	1.12	0.86	0.72
768	**PC16:0a/20:4**	0.62	0.73	0.93	1.73	0.83	0.60	0.73	1.12
770	**PC18:1a/18:2**	1.01	1.04	1.29	1.57	1.31	1.20	1.21	1.23
772	**PC18:0a/18:2**	3.30	3.09	3.51	3.32	3.56	3.63	3.67	3.06
774	**PC18:0a/18:1**	4.47	3.55	3.78	3.41	3.48	3.62	3.99	3.40
782	**PC16:0/20:4**	0.53	0.77	0.78	1.88	0.89	0.72	0.76	1.47
784	**PC18:1/18:2**	1.01	1.57	2.16	3.64	2.11	1.97	1.83	2.43
786	**PC18:0/18:2**	10.88	12.84	13.37	12.36	13.80	14.75	14.18	11.95
788	**PC18:0/18:1**	12.67	11.02	9.89	7.18	7.20	8.12	7.28	7.46
794	**PC18:1a/20:4**	0.93	1.06	1.18	1.85	0.99	0.77	1.02	1.42
796	**PC18:0a/20:4**	0.65	0.72	0.93	1.62	0.70	0.55	0.69	1.11
800	**PC18:0a/20:2**	1.26	1.35	1.36	1.08	1.30	1.43	1.48	1.13
802	**PC18:0a/20:1**	0.70	0.80	0.67	0.55	0.61	0.79	0.70	0.55
808	**PC18:1/20:4**	0.53	1.00	0.84	1.95	0.97	0.82	0.82	1.59
810	**PC18:0/20:4**	0.64	0.94	0.86	1.94	0.86	0.82	0.78	1.69
812	**PC18:0/20:3**	0.84	1.23	1.21	1.46	1.14	1.21	1.16	1.36
814	**PC18:0/20:2**	2.56	3.16	2.90	2.37	2.76	3.29	3.02	2.29
848	**PC20:0a/22:6**	0.28	1.18	0.06	0.14	0.04	0.22	0.21	0.60

Table AII.37- Percentage data of endogenous PC class fatty acid chains per sample for control cultures used in Figure III.15.

		Time/hours							
MW /amu	**Fatty acid species**	**0**	**3**	**6**	**9**	**12**	**15**	**18**	**21**
706	**PC14:0/16:0**	0.08	0.47	0.01	0.17	0.29	0.38	0.19	0.09
718	**PC16:0a/16:1**	0.05	0.21	0.10	0.23	0.13	0.11	0.28	0.55
720	**PC16:0a/16:0**	0.48	1.20	0.02	0.13	0.10	0.24	0.20	0.64
732	**PC16:0/16:1**	0.37	0.79	0.39	0.43	0.10	0.28	0.21	0.19
734	**PC16:0/16:0**	0.98	2.81	0.04	0.77	0.71	1.06	0.45	0.41
744	**PC16:0a/18:2**	0.46	0.60	0.18	0.71	0.20	0.05	0.12	0.30
746	**PC16:0a/18:1**	1.57	0.18	0.05	0.90	0.50	1.41	1.05	1.69
748	**PC16:0a/18:0**	0.23	0.48	0.07	0.09	0.17	0.12	0.17	0.29
758	**PC16:0/18:2**	0.25	0.57	0.25	0.67	0.06	0.45	0.17	0.56
760	**PC16:0/18:1**	0.59	2.08	1.08	0.81	0.23	0.38	0.40	1.69
762	**PC16:0/18:0**	0.37	1.75	0.06	0.07	0.60	0.19	0.54	0.38
768	**PC16:0a/20:4**	0.12	0.07	0.14	0.63	0.07	0.03	0.12	0.31
770	**PC18:1a/18:2**	0.16	0.15	0.11	0.32	0.07	0.05	0.09	0.19
772	**PC18:0a/18:2**	0.32	0.45	0.12	0.59	0.22	0.51	0.27	0.84
774	**PC18:0a/18:1**	1.05	0.28	0.04	0.58	0.17	0.91	0.46	0.71
782	**PC16:0/20:4**	0.29	0.14	0.09	0.38	0.08	0.23	0.33	0.64
784	**PC18:1/18:2**	0.28	0.37	0.14	0.86	0.19	0.47	0.41	0.59
786	**PC18:0/18:2**	0.92	5.34	0.24	1.36	0.02	0.56	1.04	0.52
788	**PC18:0/18:1**	1.27	4.29	0.07	1.11	0.16	0.40	0.18	1.60
794	**PC18:1a/20:4**	0.18	0.05	0.25	0.54	0.08	0.08	0.11	0.34
796	**PC18:0a/20:4**	0.07	0.13	0.17	0.38	0.05	0.06	0.23	0.28
800	**PC18:0a/20:2**	0.15	0.27	0.00	0.09	0.04	0.27	0.15	0.24
802	**PC18:0a/20:1**	0.11	0.02	0.06	0.05	0.06	0.15	0.05	0.09
808	**PC18:1/20:4**	0.30	0.25	0.14	0.29	0.10	0.36	0.39	0.69
810	**PC18:0/20:4**	0.36	0.04	0.12	0.30	0.09	0.30	0.37	0.75
812	**PC18:0/20:3**	0.21	0.18	0.13	0.21	0.07	0.10	0.09	0.30
814	**PC18:0/20:2**	0.30	1.07	0.10	0.22	0.11	0.33	0.28	0.50
848	**PC20:0a/22:6**	0.23	1.06	0.04	0.11	0.00	0.20	0.12	0.61

Table AII.38- Standard deviation for percentage data of endogenous PC class fatty acid chains per sample for control cultures used in Figure III.15.

		Time/hours							
MW /amu	**Fatty acid species**	**0**	**3**	**6**	**9**	**12**	**15**	**18**	**21**
732	**PC16:0/16:1**	5.5E-06	1.8E-06	5.4E-06	5.5E-06	3.6E-06	2.8E-06	4.7E-06	8.3E-06
746	**PC16:0a/18:1**	8.3E-06	2.6E-06	7.1E-06	7.4E-06	5.7E-06	4.2E-06	7.4E-06	1.1E-05
760	**PC16:0/18:1**	2.8E-05	1.1E-05	2.5E-05	2.7E-05	2.0E-05	1.6E-05	2.5E-05	4.2E-05
786	**PC18:0/18:2**	1.3E-06	5.3E-07	1.4E-06	1.5E-06	5.5E-07	4.6E-07	7.0E-07	2.0E-05
788	**PC18:0/18:1**	1.4E-06	5.0E-07	1.0E-06	8.4E-07	2.9E-07	2.6E-07	3.5E-07	1.2E-05

Table AII.39- Amounts (nmoles/cell) of most abundant species of endogenous PC class fatty acid chains for control cultures used in Figure III.19.

		Time/hours							
MW /amu	**Fatty acid species**	**0**	**3**	**6**	**9**	**12**	**15**	**18**	**21**
732	**PC16:0/16:1**	2.9E-06	6.7E-07	2.6E-06	2.9E-06	5.2E-07	6.5E-07	1.2E-06	4.3E-06
746	**PC16:0a/18:1**	4.5E-06	9.2E-07	3.1E-06	2.8E-06	1.0E-06	4.8E-07	2.1E-06	4.8E-06
760	**PC16:0/18:1**	1.5E-05	3.7E-06	1.2E-05	1.2E-05	2.5E-06	3.0E-06	5.7E-06	1.9E-05
786	**PC18:0/18:2**	7.0E-07	3.0E-07	6.0E-07	7.7E-07	6.7E-08	6.6E-08	2.0E-07	8.5E-06
788	**PC18:0/18:1**	6.6E-07	3.2E-07	4.5E-07	2.9E-07	3.8E-08	3.3E-08	6.7E-08	4.4E-06

Table AII.40- Standard deviation for amounts (nmoles/cell) of most abundant species of endogenous PC class fatty acid chains for control cultures used in Figure III.19.

AII.2.2.3.2. **Endogenous PE**

		Time/hours							
MW /amu	**Fatty acid species**	**0**	**3**	**6**	**9**	**12**	**15**	**18**	**21**
716	**PE16:0/18:2**	1.86	1.70	2.45	2.10	2.48	2.32	2.23	1.74
718	**PE16:0/18:1**	9.62	10.01	11.01	8.90	12.02	11.29	11.47	8.42
732	**PE18:0a/18:1**	6.69	1.75	1.57	1.11	1.32	1.29	1.52	1.48
742	**PE18:1/18:2**	2.33	1.74	3.24	3.93	3.80	3.51	3.30	2.56
744	**PE18:0/18:2**	21.84	24.87	21.91	21.49	23.34	25.06	23.36	17.93
746	**PE18:0/18:1**	22.79	21.26	23.92	18.81	21.01	22.69	22.13	19.64
748	**PE18:0/18:0**	0.20	0.37	0.22	0.28	0.00	0.00	0.03	0.08
764	**PE16:0/22:6**	1.03	0.97	1.03	1.27	1.11	0.97	0.86	1.21
766	**PE18:1/20:4**	2.17	0.00	1.78	3.02	2.77	1.63	2.80	3.81
768	**PE18:0/20:4**	8.09	1.85	4.81	9.77	8.34	7.06	7.12	14.01
770	**PE18:0/20:3**	3.23	4.01	3.58	3.91	3.83	3.78	4.01	4.89
772	**PE18:0/20:2**	5.79	5.58	6.26	5.23	5.32	6.62	6.36	5.20
774	**PE18:0/20:1**	1.25	2.46	1.87	1.70	1.18	1.27	1.31	1.33
788	**PE18:0a/22:1**	0.29	2.29	1.60	1.36	0.31	0.42	0.41	0.51
790	**PE18:0a/22:0**	0.90	6.09	3.52	2.30	1.47	1.11	1.28	2.10
792	**PE18:0/22:6**	5.06	5.69	4.61	5.96	4.97	4.30	4.63	6.81
794	**PE18:0/22:5**	3.45	2.92	2.49	3.13	3.14	2.33	3.18	3.59
796	**PE18:0/22:4**	1.00	0.83	0.77	1.48	1.11	0.97	0.93	1.54
798	**PE18:0/22:3**	0.85	2.06	1.16	1.52	0.95	1.27	1.06	0.99
800	**PE18:0/22:2**	1.47	1.82	1.77	2.44	1.37	1.98	1.82	1.83
814	**PE20:4/22:5**	0.08	0.61	0.04	0.02	0.09	0.10	0.11	0.08
816	**PE20:3/22:5**	0.02	1.13	0.38	0.27	0.06	0.03	0.08	0.26

Table AII.41- Percentage data of endogenous PE class fatty acid chains per sample for control cultures used in Figure III.16.

		Time/hours							
MW /amu	**Fatty acid species**	**0**	**3**	**6**	**9**	**12**	**15**	**18**	**21**
716	**PE16:0/18:2**	0.42	0.33	0.41	0.12	0.26	0.26	0.77	0.52
718	**PE16:0/18:1**	0.56	1.23	0.34	0.37	1.71	2.15	0.93	1.23
732	**PE18:0a/18:1**	4.41	1.23	0.06	0.08	0.06	0.04	0.13	0.23
742	**PE18:1/18:2**	0.15	0.46	0.34	0.65	0.16	0.18	0.33	0.34
744	**PE18:0/18:2**	2.24	8.35	1.16	0.96	1.44	2.08	3.06	2.54
746	**PE18:0/18:1**	1.24	2.40	0.58	2.24	1.05	0.37	1.26	3.15
748	**PE18:0/18:0**	0.23	0.63	0.26	0.42	0.00	0.00	0.05	0.14
764	**PE16:0/22:6**	0.20	0.17	0.13	0.66	0.12	0.08	0.10	0.07
766	**PE18:1/20:4**	1.04	0.00	1.64	1.52	0.82	1.63	0.34	0.99
768	**PE18:0/20:4**	1.88	0.94	3.86	4.03	1.84	2.85	1.45	4.43
770	**PE18:0/20:3**	0.38	0.98	0.18	0.38	0.27	0.12	0.45	0.75
772	**PE18:0/20:2**	0.24	0.73	0.29	0.53	0.28	0.91	0.50	1.33
774	**PE18:0/20:1**	0.11	0.99	1.54	0.69	0.36	0.17	0.28	0.17
788	**PE18:0a/22:1**	0.09	0.57	2.18	0.87	0.06	0.14	0.16	0.29
790	**PE18:0a/22:0**	0.48	2.72	3.91	0.67	0.17	0.35	0.42	1.02
792	**PE18:0/22:6**	2.23	2.97	0.37	0.17	0.58	0.95	1.12	1.76
794	**PE18:0/22:5**	1.12	0.23	0.99	0.32	0.75	0.64	1.37	0.79
796	**PE18:0/22:4**	0.30	0.59	0.30	0.32	0.19	0.09	0.32	0.57
798	**PE18:0/22:3**	0.20	0.44	0.19	0.54	0.06	0.09	0.05	0.58
800	**PE18:0/22:2**	0.30	0.23	0.20	0.66	0.25	0.40	0.12	0.47
814	**PE20:4/22:5**	0.05	0.58	0.07	0.04	0.08	0.11	0.10	0.13
816	**PE20:3/22:5**	0.01	1.10	0.51	0.42	0.11	0.05	0.07	0.42

Table AII.42- Standard deviation for percentage data of endogenous PE class fatty acid chains per sample for control cultures used in Figure III.16.

		Time/hours							
MW /amu	**Fatty acid species**	**0**	**3**	**6**	**9**	**12**	**15**	**18**	**21**
718	**PE16:0/18:1**	1.8E-06	2.0E-06	2.2E-06	2.6E-06	2.8E-06	2.8E-06	2.8E-06	1.7E-06
732	**PE18:0a/18:1**	8.5E-07	3.3E-07	3.1E-07	3.2E-07	3.1E-07	3.1E-07	3.8E-07	2.9E-07
744	**PE18:0/18:2**	4.4E-06	4.2E-06	4.7E-06	5.3E-06	4.9E-06	5.5E-06	5.4E-06	4.1E-06
746	**PE18:0/18:1**	2.1E-08	6.5E-08	4.1E-08	5.3E-08	0.0E+00	0.0E+00	6.8E-09	1.2E-08
768	**PE18:0/20:4**	1.7E-06	4.0E-07	9.8E-07	3.0E-06	1.9E-06	1.6E-06	1.7E-06	2.8E-06
772	**PE18:0/20:2**	1.1E-06	1.1E-06	1.2E-06	1.5E-06	1.2E-06	1.6E-06	1.6E-06	1.1E-06
790	**PE18:0a/22:0**	4.3E-08	1.1E-07	1.3E-07	1.3E-07	6.9E-08	5.4E-08	6.2E-08	4.0E-07
792	**PE18:0/22:6**	2.4E-07	1.1E-07	1.8E-07	3.5E-07	2.3E-07	2.0E-07	2.3E-07	1.5E-06

Table AII.43- Amounts (nmoles/cell) of most abundant species of endogenous PE class fatty acid chains for control cultures used in Figure III.21.

		Time/hours							
MW /amu	**Fatty acid species**	**0**	**3**	**6**	**9**	**12**	**15**	**18**	**21**
718	**PE16:0/18:1**	1.3E-06	3.3E-07	2.7E-07	8.7E-07	4.6E-07	1.3E-06	4.6E-07	6.4E-07
732	**PE18:0a/18:1**	2.3E-07	2.0E-07	2.0E-08	1.0E-07	1.9E-08	1.0E-07	6.5E-08	7.0E-08
744	**PE18:0/18:2**	3.3E-06	7.7E-07	4.4E-07	1.7E-06	4.4E-07	1.6E-06	3.4E-07	2.0E-06
746	**PE18:0/18:1**	2.3E-08	1.1E-07	4.5E-08	6.8E-08	0.0E+00	0.0E+00	1.2E-08	2.1E-08
768	**PE18:0/20:4**	1.7E-06	3.1E-07	8.0E-07	1.9E-06	4.7E-07	3.0E-07	2.4E-07	9.5E-07
772	**PE18:0/20:2**	7.9E-07	1.8E-07	1.6E-07	5.0E-07	9.1E-08	7.2E-07	2.7E-07	6.5E-07
790	**PE18:0a/22:0**	5.2E-08	3.6E-08	1.4E-07	6.6E-08	1.0E-08	2.0E-08	1.5E-08	1.2E-07
792	**PE18:0/22:6**	2.7E-07	6.0E-08	3.2E-08	1.3E-07	3.6E-08	2.3E-08	4.3E-08	8.6E-07

Table AII.44- Standard deviation for amounts (nmoles/cell) of most abundant species of endogenous PE class fatty acid chains for control cultures used in Figure III.21.

AII.2.2.3.3. **Newly synthesised PC**

		Time/hours							
MW /amu	**Fatty acid species**	**0**	**3**	**6**	**9**	**12**	**15**	**18**	**21**
687	**d9PC14:0/14:0**	4.22	0.22	0.10	0.09	0.13	0.12	0.11	0.14
715	**d9PC14:0/16:0**	3.12	1.64	1.01	1.46	2.02	1.85	1.69	1.99
727	**d9PC16:0a/16:1**	0.92	1.03	1.44	1.24	1.62	1.49	1.69	1.65
729	**d9PC16:0a/16:0**	3.85	1.71	1.49	1.64	1.99	1.59	1.82	1.77
741	**d9PC16:0/16:1**	4.29	5.32	6.47	4.46	5.34	5.37	5.48	5.23
743	**d9PC16:0/16:0**	5.06	4.09	2.29	3.41	4.37	3.73	3.26	4.16
753	**d9PC16:0a/18:2**	2.15	1.21	1.51	1.67	1.89	1.88	1.76	1.74
755	**d9PC16:0a/18:1**	3.97	4.24	5.14	5.56	5.90	5.50	6.22	5.53
757	**d9PC16:0a/18:0**	4.34	0.91	0.62	1.17	0.98	0.84	1.04	1.13
767	**d9PC16:0/18:2**	2.31	4.51	6.15	5.38	4.66	4.32	4.26	4.59
769	**d9PC16:0/18:1**	8.06	28.20	26.96	25.09	28.81	29.97	29.36	29.28
771	**d9PC16:0/18:0**	4.52	2.02	0.65	1.04	1.18	0.94	0.98	1.08
777	**d9PC16:0a/20:4**	2.36	0.85	0.86	1.87	0.78	0.53	0.67	1.13
779	**d9PC18:1a/18:2**	1.17	0.73	0.95	1.22	0.95	0.86	0.95	1.02
781	**d9PC18:0a/18:2**	5.12	1.68	2.46	2.19	2.50	2.51	2.74	2.22
783	**d9PC18:0a/18:1**	5.31	2.13	2.38	2.54	2.64	2.64	2.94	2.41
791	**d9PC16:0/20:4**	2.39	1.18	0.97	2.33	1.04	0.88	0.89	1.66
793	**d9PC18:1/18:2**	2.48	2.41	3.04	3.96	2.45	2.23	2.14	2.68
795	**d9PC18:0/18:2**	4.41	15.10	17.18	12.59	14.79	15.94	15.82	12.24
797	**d9PC18:0/18:1**	3.18	10.18	8.93	7.73	7.76	8.50	7.52	7.93
803	**d9PC18:1a/20:4**	3.01	1.08	0.99	1.89	0.81	0.60	0.87	1.32
805	**d9PC18:0a/20:4**	2.49	0.67	0.71	1.43	0.55	0.43	0.54	0.97
809	**d9PC18:0a/20:2**	3.30	1.09	1.09	0.81	1.07	1.19	1.25	0.95
815	**d9PC16:0/22:6**	5.14	0.88	0.56	1.30	0.58	0.46	0.53	0.82
817	**d9PC18:1/20:4**	3.68	1.52	1.05	2.48	1.06	0.86	0.94	1.65
819	**d9PC18:0/20:4**	2.65	1.37	1.01	2.09	0.87	0.77	0.75	1.45
821	**d9PC18:0/20:3**	2.94	1.57	1.41	1.46	1.09	1.22	1.18	1.23
823	**d9PC18:0/20:2**	3.56	2.48	2.57	1.89	2.17	2.80	2.58	2.02

Table AII.45- Percentage data of newly synthesised PC class fatty acid chains per sample for control cultures used in Figure III.17.

		Time/hours							
MW /amu	**Fatty acid species**	**0**	**3**	**6**	**9**	**12**	**15**	**18**	**21**
687	**d9PC14:0/14:0**	3.07	0.18	0.01	0.01	0.02	0.01	0.00	0.03
715	**d9PC14:0/16:0**	1.13	0.29	0.03	0.09	0.32	0.32	0.19	0.03
727	**d9PC16:0a/16:1**	0.87	0.19	0.06	0.29	0.05	0.08	0.15	0.25
729	**d9PC16:0a/16:0**	1.24	0.87	0.03	0.10	0.12	0.21	0.13	0.37
741	**d9PC16:0/16:1**	2.85	0.53	0.55	0.19	0.18	0.10	0.30	0.17
743	**d9PC16:0/16:0**	2.03	2.51	0.02	0.76	0.73	1.04	0.63	0.25
753	**d9PC16:0a/18:2**	0.81	0.33	0.05	0.52	0.16	0.04	0.07	0.12
755	**d9PC16:0a/18:1**	1.48	0.41	0.16	1.20	0.45	0.66	0.63	0.79
757	**d9PC16:0a/18:0**	2.07	0.50	0.23	0.10	0.06	0.10	0.19	0.13
767	**d9PC16:0/18:2**	0.43	0.37	0.17	0.65	0.07	0.24	0.08	0.61
769	**d9PC16:0/18:1**	4.82	3.11	1.27	1.41	0.50	0.13	0.85	1.41
771	**d9PC16:0/18:0**	1.66	2.12	0.10	0.26	0.23	0.20	0.10	0.13
777	**d9PC16:0a/20:4**	1.11	0.14	0.13	0.61	0.04	0.09	0.18	0.45
779	**d9PC18:1a/18:2**	1.01	0.10	0.05	0.29	0.06	0.04	0.08	0.17
781	**d9PC18:0a/18:2**	2.52	0.30	0.06	0.47	0.24	0.32	0.23	0.30
783	**d9PC18:0a/18:1**	1.79	0.23	0.09	0.37	0.17	0.45	0.15	0.46
791	**d9PC16:0/20:4**	1.15	0.19	0.16	0.42	0.10	0.27	0.37	0.64
793	**d9PC18:1/18:2**	1.77	0.34	0.32	0.59	0.22	0.37	0.38	0.58
795	**d9PC18:0/18:2**	1.67	3.34	0.05	0.75	0.40	0.91	1.67	1.07
797	**d9PC18:0/18:1**	0.63	2.29	0.29	0.76	0.30	0.75	0.39	1.46
803	**d9PC18:1a/20:4**	1.29	0.26	0.18	0.56	0.10	0.05	0.15	0.35
805	**d9PC18:0a/20:4**	0.61	0.06	0.14	0.36	0.05	0.08	0.27	0.28
809	**d9PC18:0a/20:2**	0.76	0.20	0.09	0.08	0.09	0.18	0.17	0.15
815	**d9PC16:0/22:6**	1.88	0.08	0.12	0.13	0.03	0.13	0.26	0.22
817	**d9PC18:1/20:4**	0.71	0.23	0.26	0.49	0.10	0.22	0.48	0.57
819	**d9PC18:0/20:4**	1.29	0.14	0.22	0.41	0.08	0.21	0.40	0.41
821	**d9PC18:0/20:3**	0.54	0.05	0.13	0.07	0.06	0.03	0.03	0.04
823	**d9PC18:0/20:2**	1.31	0.53	0.28	0.15	0.15	0.38	0.16	0.37

Table AII.46- Standard deviation for percentage data of newly synthesised PC class fatty acid chains per sample for control cultures used in Figure III.17.

		Time/hours							
MW /amu	**Fatty acid species**	**0**	**3**	**6**	**9**	**12**	**15**	**18**	**21**
741	**d9PC16:0/16:1**	5.0E-09	6.4E-07	4.3E-06	2.7E-06	3.8E-06	4.2E-06	8.7E-06	6.7E-06
755	**d9PC16:0a/18:1**	6.1E-09	5.1E-07	3.4E-06	3.2E-06	4.2E-06	4.2E-06	9.9E-06	7.0E-06
767	**d9PC16:0/18:2**	3.8E-09	5.5E-07	4.1E-06	3.3E-06	3.3E-06	3.4E-06	6.7E-06	6.1E-06
769	**d9PC16:0/18:1**	1.3E-08	3.4E-06	1.8E-05	1.5E-05	2.0E-05	2.4E-05	4.6E-05	3.8E-05
795	**d9PC18:0/18:2**	7.4E-09	1.8E-06	1.1E-05	7.7E-06	1.0E-05	1.2E-05	2.5E-05	1.5E-05
797	**d9PC18:0/18:1**	4.9E-09	1.2E-06	5.9E-06	4.5E-06	5.4E-06	6.6E-06	1.2E-05	1.0E-05

Table AII.47- Amounts (nmoles/cell) of most abundant species of newly synthesised PC class fatty acid chains for control cultures used in Figure III.23.

		Time/hours							
MW /amu	**Fatty acid species**	**0**	**3**	**6**	**9**	**12**	**15**	**18**	**21**
741	**d9PC16:0/16:1**	1.2E-09	2.6E-07	1.8E-06	1.1E-06	3.5E-07	9.0E-07	2.2E-06	3.1E-06
755	**d9PC16:0a/18:1**	3.6E-09	2.1E-07	1.3E-06	8.1E-07	5.7E-07	4.1E-07	2.8E-06	3.4E-06
767	**d9PC16:0/18:2**	2.5E-09	2.3E-07	1.6E-06	1.6E-06	2.3E-07	9.2E-07	1.4E-06	3.4E-06
769	**d9PC16:0/18:1**	9.3E-09	1.4E-06	7.1E-06	6.6E-06	1.3E-06	5.0E-06	1.1E-05	1.7E-05
795	**d9PC18:0/18:2**	6.5E-09	9.4E-07	4.0E-06	3.3E-06	9.0E-07	2.2E-06	7.4E-06	6.4E-06
797	**d9PC18:0/18:1**	3.1E-09	4.5E-07	2.2E-06	1.6E-06	2.4E-07	9.3E-07	1.9E-06	4.9E-06

Table AII.48- Standard deviation for amounts (nmoles/cell) of most abundant species of newly synthesised PC class fatty acid chains for control cultures used in Figure III.23.

AII.2.2.3.4. **Rate of new PC synthesis**

Time /hours	**Rate of new PC synthesis /nmoles.h^{-1}**	**Standard deviation**
0	4.03E-06	1.51E-06
3	1.10E-05	3.94E-06
6	6.65E-06	2.62E-06
9	5.86E-06	3.48E-07
12	5.23E-06	1.12E-06
15	8.71E-06	1.80E-06
18	6.17E-06	2.90E-06
21	4.03E-06	1.51E-06

Table AII.49- Data used in Figure III.25.

AII.2.3. HDPC

AII.2.3.1. Cell viability

	HDPC 10.50 μM		HDPC 5.25 μM		HDPC 2.63 μM	
Time /hours	**% dead cells**	**SD**	**% dead cells**	**SD**	**% dead cells**	**SD**
0	13.61	3.54	13.61	3.54	13.61	3.54
3	9.31	3.40	9.64	0.48	8.21	1.66
6	11.09	3.81	9.51	1.79	9.37	1.03
9	12.48	3.45	16.05	3.92	10.85	2.00
12	8.27	2.32	17.48	13.21	8.29	0.44
15	13.22	8.96	9.42	2.15	8.22	1.44
18	5.77	1.63	11.38	1.55	10.34	3.00
21	8.47	0.34	3.61	0.77	9.13	2.31

Table AII.50- Data used in Figure III.26.

AII.2.3.2. Total lipid content by ESI-MS

	HDPC 10.50 μM		HDPC 5.25 μM		HDPC 2.63 μM	
Time /hours	**Amount /nmoles per cell**	**SD**	**Amount /nmoles per cell**	**SD**	**Amount /nmoles per cell**	**SD**
0	7.42E-05	3.86E-05	7.42E-05	3.86E-05	7.42E-05	3.86E-05
3	5.74E-05	3.11E-05	6.86E-06	1.50E-06	1.74E-05	5.25E-06
6	7.60E-05	4.60E-05	1.37E-05	4.39E-06	4.44E-05	1.83E-05
9	6.63E-05	2.76E-05	1.69E-05	7.69E-06	1.88E-05	5.02E-06
12	8.59E-05	2.18E-05	3.25E-05	1.47E-05	4.32E-05	1.46E-05
15	5.01E-05	1.02E-05	3.46E-05	1.18E-05	4.94E-05	2.16E-05
18	3.56E-05	1.80E-05	3.88E-05	4.74E-06	3.31E-05	7.39E-06
21	1.03E-04	2.29E-05	7.55E-05	3.96E-05	1.14E-04	3.99E-05

Table AII.51- Endogenous PC data used in Figure III.27.

	HDPC 10.50 μM		HDPC 5.25 μM		HDPC 2.63 μM	
Time /hours	**Amount /nmoles per cell**	**SD**	**Amount /nmoles per cell**	**SD**	**Amount /nmoles per cell**	**SD**
0	1.68E-05	1.20E-05	1.68E-05	1.20E-05	1.68E-05	1.20E-05
3	2.01E-05	6.82E-07	4.52E-06	1.13E-06	8.16E-06	6.96E-07
6	1.84E-05	7.12E-06	8.54E-06	4.15E-06	1.04E-05	1.79E-06
9	2.13E-05	3.52E-06	3.24E-06	1.23E-06	4.48E-06	1.75E-06
12	2.50E-05	1.80E-06	7.39E-06	1.44E-06	5.81E-06	5.88E-07
15	3.48E-05	2.35E-05	1.19E-05	1.91E-06	1.40E-05	7.42E-06
18	1.22E-05	3.89E-06	8.86E-06	1.08E-06	1.03E-05	2.95E-06
21	1.05E-05	6.13E-07	1.12E-05	5.55E-06	1.55E-05	8.34E-06

Table AII.52- Endogenous PE data used in Figure III.28.

	HDPC 10.50 μM		HDPC 5.25 μM		HDPC 2.63 μM	
Time /hours	**Amount /nmoles per cell**	**SD**	**Amount /nmoles per cell**	**SD**	**Amount /nmoles per cell**	**SD**
0	1.53E-07	8.36E-08	1.53E-07	8.36E-08	1.53E-07	8.36E-08
3	4.77E-05	2.37E-05	2.15E-06	5.18E-07	8.35E-06	3.20E-06
6	4.18E-05	3.10E-05	1.15E-05	5.49E-06	2.50E-05	1.26E-05
9	5.87E-05	2.56E-05	8.85E-06	5.24E-06	1.09E-05	4.42E-06
12	1.11E-04	3.74E-05	2.14E-05	1.15E-05	2.43E-05	6.60E-06
15	6.65E-05	1.56E-05	3.31E-05	1.17E-05	4.22E-05	1.82E-05
18	4.20E-05	2.22E-05	3.28E-05	7.60E-06	4.02E-05	9.07E-06
21	7.93E-05	1.63E-05	6.59E-05	3.82E-05	7.97E-05	2.73E-05

Table AII.53- Newly synthesised PC data used in Figure III.29.

AII.2.3.3. Drug content by ESI-MS

	HDPC 10.50 μM		HDPC 5.25 μM		HDPC 2.63 μM	
Time /hours	**Amount /nmoles per cell**	**SD**	**Amount /nmoles per cell**	**SD**	**Amount /nmoles per cell**	**SD**
3	1.41E-06	5.35E-07	4.54E-06	6.62E-06	2.94E-07	1.38E-07
6	2.97E-06	9.69E-07	1.75E-06	1.29E-06	7.95E-07	2.23E-07
9	4.56E-06	4.00E-07	2.72E-07	1.45E-07	1.88E-07	9.44E-08
12	6.49E-06	1.93E-06	1.67E-06	1.50E-07	9.15E-07	4.29E-08
15	8.03E-06	4.59E-06	2.46E-06	7.30E-07	1.79E-06	6.01E-07
18	4.70E-06	5.46E-07	2.90E-06	4.23E-07	1.84E-06	9.02E-07
21	4.38E-06	1.37E-06	4.35E-06	1.15E-06	2.25E-06	2.94E-07

Table AII.54- HDPC drug in membrane data used in Figure III.30.

	HDPC 10.50 μM		HDPC 5.25 μM		HDPC 2.63 μM	
Time /hours	**k /arb**	**SD**	**k /arb**	**SD**	**k /arb**	**SD**
3	0.0066	0.0036	0.0143	0.0105	0.0028	0.0012
6	0.0157	0.0074	0.0245	0.0146	0.0067	0.0029
9	0.0192	0.0089	0.0050	0.0023	0.0031	0.0015
12	0.0805	0.0279	0.0600	0.0016	0.0315	0.0060
15	0.0545	0.0383	0.0883	0.0456	0.0578	0.0300
18	0.0295	0.0119	0.1021	0.0101	0.0781	0.0507
21	0.0244	0.0055	0.0749	0.0222	0.0244	0.0037

Table AII.55- Partition coefficient k for HDPC drug in membrane data used in Figure III.31.

AII.2.3.4. Fatty acid membrane composition by ESI-MS

For reasons of brevity, percentage values and standard deviation are only shown for the most abundant species. For all other species, see attached data CD.

AII.2.3.4.1. **Endogenous PC**

		Time/hours							
MW /amu	**Fatty acid species**	**0**	**3**	**6**	**9**	**12**	**15**	**18**	**21**
732	**PC16:0/16:1**	4.38	5.08	5.21	4.19	4.88	4.60	4.49	3.88
746	**PC16:0a/18:1**	7.09	6.30	7.10	7.36	8.19	8.55	8.64	8.27
758	**PC16:0/18:2**	2.92	4.67	4.85	4.14	3.61	3.17	3.38	3.90
760	**PC16:0/18:1**	24.96	23.70	23.42	22.78	26.85	27.41	27.02	24.13
786	**PC18:0/18:2**	13.49	14.79	16.25	12.21	13.70	13.43	13.40	14.65
788	**PC18:0/18:1**	8.27	7.91	7.21	9.91	7.98	8.16	7.73	7.35

Table AII.56- Amounts (nmoles/cell) of most abundant species of endogenous PC class fatty acid chains for HDPC 10.50 μM used in Figures III.33 to III.36.

		Time/hours							
MW /amu	**Fatty acid species**	**0**	**3**	**6**	**9**	**12**	**15**	**18**	**21**
732	**PC16:0/16:1**	1.13	0.95	0.34	0.32	0.09	0.18	0.24	0.12
746	**PC16:0a/18:1**	0.39	0.38	0.18	0.80	0.47	0.14	0.32	1.24
758	**PC16:0/18:2**	0.46	0.27	0.33	0.46	0.10	0.17	0.14	0.47
760	**PC16:0/18:1**	1.99	0.80	0.61	0.98	0.35	0.34	0.55	1.41
786	**PC18:0/18:2**	4.66	1.86	4.19	0.15	0.69	0.15	0.61	0.29
788	**PC18:0/18:1**	1.11	1.34	1.92	0.06	0.40	0.27	0.39	0.14

Table AII.57- Standard deviation for amounts (nmoles/cell) of most abundant species of endogenous PC class fatty acid chains for HDPC 10.50 μM used in Figure III.33 to III.36.

		Time/hours							
MW /amu	**Fatty acid species**	**0**	**3**	**6**	**9**	**12**	**15**	**18**	**21**
732	**PC16:0/16:1**	4.38	5.08	5.21	4.19	4.88	4.60	4.49	3.88
746	**PC16:0a/18:1**	7.09	6.30	7.10	7.36	8.19	8.55	8.64	8.27
760	**PC16:0/18:1**	24.96	23.70	23.42	22.78	26.85	27.41	27.02	24.13
786	**PC18:0/18:2**	13.49	14.79	16.25	12.21	13.70	13.43	13.40	14.65
788	**PC18:0/18:1**	8.27	7.91	7.21	9.91	7.98	8.16	7.73	7.35

Table AII.58- Amounts (nmoles/cell) of most abundant species of endogenous PC class fatty acid chains for HDPC 5.25 μM used in Figures III.33 to III.36.

		Time/hours							
MW /amu	**Fatty acid species**	**0**	**3**	**6**	**9**	**12**	**15**	**18**	**21**
732	**PC16:0/16:1**	1.13	0.95	0.34	0.32	0.09	0.18	0.24	0.12
746	**PC16:0a/18:1**	0.39	0.38	0.18	0.80	0.47	0.14	0.32	1.24
760	**PC16:0/18:1**	1.99	0.80	0.61	0.98	0.35	0.34	0.55	1.41
786	**PC18:0/18:2**	4.66	1.86	4.19	0.15	0.69	0.15	0.61	0.29
788	**PC18:0/18:1**	1.11	1.34	1.92	0.06	0.40	0.27	0.39	0.14

Table AII.59- Standard deviation for amounts (nmoles/cell) of most abundant species of endogenous PC class fatty acid chains for HDPC 5.25 μM used in Figure III.33 to III.36.

		Time/hours							
MW /amu	**Fatty acid species**	**0**	**3**	**6**	**9**	**12**	**15**	**18**	**21**
732	**PC16:0/16:1**	4.38	5.06	5.05	4.27	5.10	4.43	4.10	4.33
746	**PC16:0a/18:1**	7.09	6.21	7.23	7.74	8.52	8.62	9.58	6.48
760	**PC16:0/18:1**	24.96	21.97	23.00	22.79	27.52	26.09	25.68	23.82
774	**PC18:0a/18:1**	4.65	3.87	3.70	3.83	5.02	4.72	5.48	3.33
786	**PC18:0/18:2**	13.49	11.82	13.13	11.63	13.11	13.05	11.87	12.33
788	**PC18:0/18:1**	8.27	10.26	8.79	10.07	8.08	8.33	8.75	6.89

Table AII.60- Amounts (nmoles/cell) of most abundant species of endogenous PC class fatty acid chains for HDPC 2.63 μM used in Figures III.33 to III.36.

		Time/hours							
MW /amu	**Fatty acid species**	**0**	**3**	**6**	**9**	**12**	**15**	**18**	**21**
732	**PC16:0/16:1**	1.13	0.26	0.34	0.30	0.28	0.31	0.25	0.18
746	**PC16:0a/18:1**	0.39	0.13	0.96	0.55	0.21	0.18	0.08	0.42
760	**PC16:0/18:1**	1.99	1.94	1.45	1.17	0.52	0.83	0.15	1.20
774	**PC18:0a/18:1**	1.31	0.77	0.72	0.06	0.32	0.15	0.21	0.07
786	**PC18:0/18:2**	4.66	0.10	1.63	0.41	0.38	0.17	0.45	0.41
788	**PC18:0/18:1**	1.11	0.91	2.05	0.18	0.30	0.48	0.68	0.26

Table AII.61- Standard deviation for amounts (nmoles/cell) of most abundant species of endogenous PC class fatty acid chains for HDPC 2.63 μM used in Figure III.33 to III.36.

AII.2.3.4.2. **Newly synthesised PC**

		Time/hours						
MW /amu	**Fatty acid species**	**3**	**6**	**9**	**12**	**15**	**18**	**21**
741	**d9PC16:0/16:1**	6.43	5.14	4.99	4.70	4.58	4.43	4.91
743	**d9PC16:0/16:0**	6.43	5.14	4.99	4.70	4.58	4.43	4.91
755	**d9PC16:0a/18:1**	4.80	4.88	4.39	5.25	5.71	6.46	5.99
767	**d9PC16:0/18:2**	4.88	5.99	6.43	4.59	4.45	5.16	5.35
769	**d9PC16:0/18:1**	30.60	29.04	28.13	31.94	32.57	28.80	31.16
795	**d9PC18:0/18:2**	14.42	12.86	14.10	14.31	14.66	15.12	16.26
797	**d9PC18:0/18:1**	9.67	8.31	7.92	7.84	8.33	7.51	7.45

Table AII.62- Amounts (nmoles/cell) of most abundant species of newly synthesised PC class fatty acid chains for HDPC 10.50 μM used in Figures III.38 to III.39.

		Time/hours						
MW /amu	**Fatty acid species**	**3**	**6**	**9**	**12**	**15**	**18**	**21**
741	**d9PC16:0/16:1**	1.26	0.79	0.52	0.20	0.28	0.15	0.25
743	**d9PC16:0/16:0**	1.43	1.19	0.63	0.45	0.25	0.07	0.25
755	**d9PC16:0a/18:1**	0.37	1.01	0.67	0.11	0.84	0.30	0.48
767	**d9PC16:0/18:2**	0.50	0.78	0.18	0.13	0.14	0.30	0.15
769	**d9PC16:0/18:1**	1.52	2.36	1.27	0.10	1.36	1.25	1.13
795	**d9PC18:0/18:2**	1.89	1.34	0.89	0.33	0.15	0.42	0.46
797	**d9PC18:0/18:1**	2.43	0.84	0.28	0.40	0.43	0.53	0.65

Table AII.63- Standard deviation for amounts (nmoles/cell) of most abundant species of newly synthesised PC class fatty acid chains for HDPC 10.50 μM used in Figures III.38 to III.39.

		Time/hours						
MW /amu	**Fatty acid species**	**3**	**6**	**9**	**12**	**15**	**18**	**21**
741	**d9PC16:0/16:1**	6.88	6.89	5.33	6.43	5.85	5.44	4.73
755	**d9PC16:0a/18:1**	4.43	5.59	5.76	6.38	6.60	7.22	6.56
767	**d9PC16:0/18:2**	6.62	6.81	5.77	4.97	4.20	4.28	4.91
769	**d9PC16:0/18:1**	27.29	28.20	27.23	32.32	34.15	33.11	30.14
795	**d9PC18:0/18:2**	15.44	16.21	14.51	15.03	13.66	14.08	15.42
797	**d9PC18:0/18:1**	6.45	6.35	8.84	8.26	8.62	8.08	7.28

Table AII.64- Amounts (nmoles/cell) of most abundant species of newly synthesised PC class fatty acid chains for HDPC 5.25 μM used in Figures III.38 to III.39.

		Time/hours						
MW /amu	**Fatty acid species**	**3**	**6**	**9**	**12**	**15**	**18**	**21**
741	**d9PC16:0/16:1**	1.30	0.25	0.41	0.16	0.12	0.29	0.17
755	**d9PC16:0a/18:1**	0.16	0.05	0.69	0.56	0.25	0.16	0.65
767	**d9PC16:0/18:2**	0.63	0.26	0.45	0.10	0.10	0.19	0.25
769	**d9PC16:0/18:1**	2.03	2.68	1.55	0.46	0.46	0.34	0.29
795	**d9PC18:0/18:2**	0.43	0.89	0.19	0.59	0.37	0.67	1.21
797	**d9PC18:0/18:1**	0.66	1.12	0.17	0.52	0.39	0.27	0.41

Table AII.65- Standard deviation for amounts (nmoles/cell) of most abundant species of newly synthesised PC class fatty acid chains for HDPC 5.25 μM used in Figures III.38 to III.39.

		Time/hours						
MW /amu	**Fatty acid species**	**3**	**6**	**9**	**12**	**15**	**18**	**21**
741	**d9PC16:0/16:1**	6.70	6.31	5.36	6.40	5.50	4.95	4.76
755	**d9PC16:0a/18:1**	4.01	5.37	6.69	6.87	7.33	7.85	6.17
767	**d9PC16:0/18:2**	6.30	6.29	5.11	4.25	3.79	3.52	5.32
769	**d9PC16:0/18:1**	25.28	26.97	26.16	33.23	32.12	32.09	27.93
795	**d9PC18:0/18:2**	15.31	15.32	13.65	13.93	14.31	13.45	13.09
797	**d9PC18:0/18:1**	8.99	7.90	8.67	8.43	8.93	9.19	6.49

Table AII.66- Amounts (nmoles/cell) of most abundant species of newly synthesised PC class fatty acid chains for HDPC 2.63 μM used in Figures III.38 to III.39.

		Time/hours						
MW /amu	**Fatty acid species**	**3**	**6**	**9**	**12**	**15**	**18**	**21**
741	**d9PC16:0/16:1**	0.69	0.63	0.26	0.27	0.39	0.26	0.26
755	**d9PC16:0a/18:1**	0.37	0.71	0.70	0.33	0.07	0.29	0.37
767	**d9PC16:0/18:2**	0.26	0.14	0.16	0.17	0.25	0.31	0.15
769	**d9PC16:0/18:1**	0.98	1.54	0.83	0.09	0.52	0.51	1.51
795	**d9PC18:0/18:2**	0.66	0.50	0.23	0.61	0.37	0.68	0.22
797	**d9PC18:0/18:1**	0.62	1.64	0.46	0.33	0.65	0.96	0.14

Table AII.67- Standard deviation for amounts (nmoles/cell) of most abundant species of newly synthesised PC class fatty acid chains for HDPC 2.63 μM used in Figure III.38 to III.39.

AII.2.3.4.3. **Endogenous PE**

		Time/hours							
MW /amu	**Fatty acid species**	**0**	**3**	**6**	**9**	**12**	**15**	**18**	**21**
718	**PE16:0/18:1**	10.07	14.58	10.65	10.53	11.68	12.58	10.98	11.73
744	**PE18:0/18:2**	16.70	22.34	23.14	22.82	24.11	24.24	23.53	23.25
746	**PE18:0/18:1**	13.79	25.58	21.82	21.63	25.15	26.65	24.24	24.77
766	**PE18:1/20:4**	7.22	0.28	2.08	2.01	2.02	1.22	2.70	2.87
768	**PE18:0/20:4**	11.29	2.33	7.12	6.82	5.62	3.77	7.33	6.31
772	**PE18:0/20:2**	6.11	5.62	5.31	4.81	6.77	7.23	5.84	5.85
792	**PE18:0/22:6**	3.11	5.09	4.65	4.89	4.56	4.05	4.06	4.24

Table AII.68- Amounts (nmoles/cell) of most abundant species of endogenous PC class fatty acid chains for HDPC 10.50 μM used in Figures III.41 to III.42.

		Time/hours							
MW /amu	**Fatty acid species**	**0**	**3**	**6**	**9**	**12**	**15**	**18**	**21**
718	**PE16:0/18:1**	4.82	3.87	1.55	1.74	0.50	2.51	0.57	0.58
744	**PE18:0/18:2**	8.71	1.45	2.01	1.04	1.19	0.62	0.26	0.92
746	**PE18:0/18:1**	2.59	3.16	1.19	1.78	0.56	1.21	1.76	1.07
766	**PE18:1/20:4**	1.05	0.35	1.78	1.10	0.22	1.06	0.48	0.50
768	**PE18:0/20:4**	8.98	1.51	3.72	0.76	0.35	3.26	0.67	0.19
772	**PE18:0/20:2**	2.87	1.21	0.94	0.91	0.11	1.01	0.33	0.31
792	**PE18:0/22:6**	3.28	1.71	0.26	0.73	0.23	0.91	0.69	0.50

Table AII.69- Standard deviation for amounts (nmoles/cell) of most abundant species of endogenous PC class fatty acid chains for HDPC 10.50 μM used in Figure III.41 to III.42.

		Time/hours							
MW /amu	**Fatty acid species**	**0**	**3**	**6**	**9**	**12**	**15**	**18**	**21**
718	**PE16:0/18:1**	7.89	9.08	11.06	10.76	15.81	16.26	15.20	10.94
744	**PE18:0/18:2**	21.78	21.58	21.16	21.27	25.38	25.75	23.16	22.74
746	**PE18:0/18:1**	13.07	17.90	19.09	27.09	28.22	27.86	28.59	22.82
766	**PE18:1/20:4**	5.01	5.29	5.27	1.08	1.15	0.94	1.08	3.40
768	**PE18:0/20:4**	5.80	11.20	10.28	4.92	3.09	3.35	5.53	8.24
772	**PE18:0/20:2**	7.56	3.87	3.93	4.97	6.28	6.47	6.47	5.79
790	**PE18:0a/22:0**	5.29	2.17	1.78	3.03	0.68	0.29	0.40	1.03
792	**PE18:0/22:6**	4.56	7.49	6.36	4.29	2.70	2.62	2.94	4.35

Table AII.70- Amounts (nmoles/cell) of most abundant species of endogenous PC class fatty acid chains for HDPC 5.25 μM used in Figures III.41 to III.42.

		Time/hours							
MW /amu	**Fatty acid species**	**0**	**3**	**6**	**9**	**12**	**15**	**18**	**21**
718	**PE16:0/18:1**	4.39	0.49	2.15	1.79	0.28	0.34	0.72	1.55
744	**PE18:0/18:2**	8.76	1.56	0.87	2.05	1.10	0.21	0.39	3.18
746	**PE18:0/18:1**	2.24	0.93	1.21	2.14	1.29	1.02	2.36	1.79
766	**PE18:1/20:4**	4.44	0.68	0.81	0.43	1.02	0.77	0.24	1.80
768	**PE18:0/20:4**	9.26	1.05	2.03	1.29	1.41	0.15	0.50	3.48
772	**PE18:0/20:2**	2.71	0.48	0.41	0.80	0.23	0.24	0.09	1.49
790	**PE18:0a/22:0**	3.34	0.43	0.40	0.89	0.18	0.04	0.12	0.16
792	**PE18:0/22:6**	2.97	0.39	0.60	1.53	0.29	0.22	0.47	0.59

Table AII.71- Standard deviation for amounts (nmoles/cell) of most abundant species of endogenous PC class fatty acid chains for HDPC 5.25 μM used in Figure III.41 to III.42.

		Time/hours							
MW /amu	**Fatty acid species**	**0**	**3**	**6**	**9**	**12**	**15**	**18**	**21**
718	**PE16:0/18:1**	7.89	8.83	11.76	11.34	16.58	15.10	17.56	7.59
744	**PE18:0/18:2**	21.78	18.23	19.35	20.49	24.69	25.20	23.66	17.59
746	**PE18:0/18:1**	13.07	22.25	22.59	25.56	27.70	27.27	28.43	18.42
766	**PE18:1/20:4**	5.01	2.53	2.05	1.46	0.60	1.33	1.00	5.94
768	**PE18:0/20:4**	5.80	7.60	8.54	4.64	3.64	3.90	3.64	18.03
772	**PE18:0/20:2**	7.56	3.69	4.22	5.00	6.60	6.64	6.71	4.01
790	**PE18:0a/22:0**	5.29	6.37	3.24	4.21	0.37	0.42	0.38	1.34
792	**PE18:0/22:6**	4.56	6.41	6.48	5.46	2.58	2.87	2.27	5.81

Table AII.72- Amounts (nmoles/cell) of most abundant species of endogenous PC class fatty acid chains for HDPC 2.63 μM used in Figures III.41 to III.42.

		Time/hours							
MW /amu	**Fatty acid species**	**0**	**3**	**6**	**9**	**12**	**15**	**18**	**21**
718	**PE16:0/18:1**	4.39	1.43	2.78	2.32	0.83	0.94	1.48	0.93
744	**PE18:0/18:2**	8.76	3.03	1.33	2.34	0.97	0.39	2.39	1.21
746	**PE18:0/18:1**	2.24	1.67	2.82	2.81	0.64	0.81	0.45	2.77
766	**PE18:1/20:4**	4.44	1.42	1.35	1.35	0.51	0.29	0.18	1.52
768	**PE18:0/20:4**	9.26	0.96	2.54	4.02	0.28	0.41	0.84	0.87
772	**PE18:0/20:2**	2.71	0.21	0.32	0.50	0.63	0.61	0.78	0.37
790	**PE18:0a/22:0**	3.34	1.34	0.36	2.43	0.13	0.20	0.17	0.49
792	**PE18:0/22:6**	2.97	0.55	0.99	0.40	0.14	0.10	0.27	0.94

Table AII.73- Standard deviation for amounts (nmoles/cell) of most abundant species of endogenous PC class fatty acid chains for HDPC 2.63 μM used in Figure III.41 to III.42.

AII.2.3.4.4. **Rate of new PC synthesis**

	HDPC 10.50 μM		**HDPC 5.25 μM**		**HDPC 2.63 μM**	
Time /hours	**Rate /nmoles. h^{-1}**	**SD**	**Rate /nmoles. h^{-1}**	**SD**	**Rate /nmoles. h^{-1}**	**SD**
3	1.59E-05	7.90E-06	7.17E-07	1.73E-07	2.78E-06	1.07E-06
6	6.96E-06	5.16E-06	1.91E-06	9.15E-07	4.17E-06	2.11E-06
9	6.53E-06	2.84E-06	9.83E-07	5.82E-07	1.21E-06	4.91E-07
12	9.27E-06	3.12E-06	1.78E-06	9.58E-07	2.02E-06	5.50E-07
15	3.83E-06	1.04E-06	1.86E-06	7.79E-07	2.66E-06	1.21E-06
18	2.52E-06	1.23E-06	1.87E-06	4.22E-07	1.81E-06	5.04E-07
21	3.78E-06	7.76E-07	3.14E-06	1.82E-06	3.80E-06	1.30E-06

Table AII.74- Data used in Figure III.42.

AII.2.4. CTAB

AII.2.4.1. Cell viability

	CTAB 3.00 μM		**CTAB 1.50 μM**		**CTAB 0.75 μM**	
Time /hours	**% dead cells**	**SD**	**% dead cells**	**SD**	**% dead cells**	**SD**
0	13.61	3.54	13.61	3.54	13.61	3.54
3	12.76	1.97	8.36	0.83	8.43	3.00
6	10.82	2.40	9.70	1.58	8.86	1.16
9	9.78	1.31	9.28	4.48	13.62	6.37
12	8.18	1.36	7.24	1.99	9.02	2.30
15	7.82	2.16	11.96	2.94	*4.16*	*3.10*
18	6.71	0.50	8.97	2.05	7.78	1.54
21	15.76	6.95	9.21	1.40	7.17	1.39

Table AII.75- Data used in Figure III.43.

AII.2.4.2. Total lipid content by ESI-MS

	CTAB 3.00 μM		CTAB 1.50 μM		CTAB 0.75 μM	
Time /hours	**Amount /nmoles per cell**	**SD**	**Amount /nmoles per cell**	**SD**	**Amount /nmoles per cell**	**SD**
0	7.42E-05	3.86E-05	7.42E-05	3.86E-05	7.42E-05	3.86E-05
3	1.42E-05	1.02E-05	1.07E-04	2.30E-05	2.10E-05	8.25E-06
6	2.65E-05	2.35E-05	3.16E-05	1.96E-05	2.91E-05	1.80E-05
9	6.15E-05	2.71E-05	5.96E-05	1.81E-05	5.14E-05	1.99E-05
12	5.40E-05	1.92E-05	4.44E-05	2.85E-05	7.36E-05	4.49E-05
15	5.31E-05	3.65E-05	5.51E-05	4.47E-05	7.95E-05	6.42E-05
18	1.25E-04	9.88E-05	5.60E-05	2.93E-05	2.08E-05	1.58E-05
21	3.93E-05	3.33E-05	2.06E-05	1.53E-05	7.02E-05	1.62E-05

Table AII.76- Endogenous PC data used in Figure III.45.

	CTAB 3.00 μM		CTAB 1.50 μM		CTAB 0.75 μM	
Time /hours	**Amount /nmoles per cell**	**SD**	**Amount /nmoles per cell**	**SD**	**Amount /nmoles per cell**	**SD**
0	1.68E-05	1.20E-05	1.68E-05	1.20E-05	1.68E-05	1.20E-05
3	3.55E-06	2.41E-06	1.39E-05	6.91E-06	1.08E-05	1.93E-06
6	6.80E-06	6.05E-06	3.34E-06	1.70E-06	1.12E-05	4.57E-06
9	1.13E-05	3.20E-06	1.69E-05	6.42E-06	1.37E-05	1.66E-06
12	1.40E-05	5.00E-06	1.37E-05	5.38E-06	1.95E-05	4.05E-06
15	1.62E-05	9.26E-06	1.19E-05	8.22E-06	2.80E-05	1.71E-05
18	2.03E-05	9.56E-06	1.48E-05	2.19E-06	1.11E-05	8.86E-06
21	1.09E-05	5.28E-06	8.13E-06	5.47E-06	1.33E-05	3.33E-06

Table AII.77- Endogenous PE data used in Figure III.46.

	CTAB 3.00 μM		CTAB 1.50 μM		CTAB 0.75 μM	
Time /hours	**Amount /nmoles per cell**	**SD**	**Amount /nmoles per cell**	**SD**	**Amount /nmoles per cell**	**SD**
0	1.53E-07	8.36E-08	1.53E-07	8.36E-08	1.53E-07	8.36E-08
3	6.63E-06	4.79E-06	3.26E-05	7.75E-06	6.02E-06	2.91E-06
6	2.31E-05	2.16E-05	1.68E-05	9.81E-06	1.89E-05	1.39E-05
9	8.87E-05	4.08E-05	4.21E-05	1.61E-05	2.66E-05	1.22E-05
12	1.15E-04	3.30E-05	4.80E-05	3.95E-05	9.57E-05	5.25E-05
15	4.32E-04	1.11E-04	2.32E-04	1.58E-04	1.68E-04	1.54E-04
18	5.58E-04	4.45E-04	6.79E-05	4.46E-05	5.25E-05	4.04E-05
21	1.07E-04	1.06E-04	2.78E-05	2.06E-05	1.29E-04	3.91E-05

Table AII.78- Newly synthesised PC data used in Figure III.47.

AII.2.4.3. Drug content by ESI-MS

	CTAB 3.00 μM		CTAB 1.50 μM		CTAB 0.75 μM	
Time /hours	**Amount /nmoles per cell**	**SD**	**Amount /nmoles per cell**	**SD**	**Amount /nmoles per cell**	**SD**
3	8.30E-07	4.35E-07	1.32E-06	1.22E-06	7.00E-07	9.96E-08
6	2.98E-06	2.02E-06	3.53E-07	1.63E-07	1.82E-06	3.19E-07
9	6.12E-06	1.70E-06	3.88E-06	2.17E-06	3.01E-06	4.85E-07
12	5.84E-06	2.68E-06	2.22E-06	4.05E-07	2.37E-06	7.32E-07
15	1.51E-05	2.28E-06	5.41E-06	3.97E-06	1.96E-06	3.68E-07
18	5.83E-06	3.18E-06	2.33E-06	7.17E-07	1.09E-06	8.35E-07
21	5.37E-06	3.09E-06	3.11E-06	1.50E-06	1.85E-06	1.37E-06

Table AII.79- CTAB drug in membrane data used in Figure III.48.

	CTAB 3.00 μM		CTAB 1.50 μM		CTAB 0.75 μM	
Time /hours	**k /arb**	**SD**	**k /arb**	**SD**	**k /arb**	**SD**
3	0.0124	0.0083	0.0677	0.0625	0.0510	0.0118
6	0.0306	0.0128	0.0164	0.0035	0.0268	0.0027
9	0.1923	0.1471	0.0999	0.0208	0.2177	0.0559
12	0.1889	0.0636	0.1481	0.0476	0.2285	0.1224
15	0.0771	0.0285	0.1079	0.0987	1.0979	0.6011
18	0.2666	0.1514	0.1612	0.0643	0.1295	0.1045
21	0.0710	0.0496	0.1617	0.0787	0.0992	0.0450

Table AII.80- Partition coefficient k for CTAB drug in membrane data used in Figure III.49.

AII.2.4.4. Fatty acid membrane composition by ESI-MS

For reasons of brevity, percentage values and standard deviation are only shown for the most abundant species. For all other species, see attached data CD.

AII.2.4.4.1. **Endogenous PC**

		Time/hours							
MW /amu	**Fatty acid species**	**0**	**3**	**6**	**9**	**12**	**15**	**18**	**21**
732	**PC16:0/16:1**	4.38	6.27	6.24	7.57	6.16	6.71	6.76	4.12
734	**PC16:0/16:0**	3.22	4.27	5.41	4.01	3.60	3.59	3.19	3.68
746	**PC16:0a/18:1**	7.09	6.91	7.52	8.49	10.98	7.01	9.99	7.66
758	**PC16:0/18:2**	2.92	4.43	4.22	4.63	3.87	5.46	4.40	3.92
760	**PC16:0/18:1**	24.96	24.78	24.48	26.11	22.53	19.73	24.80	20.34
786	**PC18:0/18:2**	13.49	13.60	10.21	13.07	12.00	11.39	13.61	12.48
788	**PC18:0/18:1**	8.27	8.36	9.22	5.63	4.61	5.14	4.27	5.95

Table AII.81- Amounts (nmoles/cell) of most abundant species of endogenous PC class fatty acid chains for CTAB 3.00 μM used in Figures III.51 to III.52.

		Time/hours							
MW /amu	**Fatty acid species**	**0**	**3**	**6**	**9**	**12**	**15**	**18**	**21**
732	**PC16:0/16:1**	1.13	0.66	0.37	0.24	0.66	0.28	0.02	0.88
734	**PC16:0/16:0**	2.09	1.73	0.37	0.59	0.51	0.94	0.12	0.18
746	**PC16:0a/18:1**	0.39	0.78	0.12	0.63	1.48	0.46	0.93	0.62
758	**PC16:0/18:2**	0.46	0.27	0.17	0.22	0.37	0.53	0.32	0.55
760	**PC16:0/18:1**	1.99	3.45	0.73	1.29	1.37	2.07	0.39	3.22
786	**PC18:0/18:2**	4.66	2.84	0.27	0.40	0.57	1.01	0.21	1.12
788	**PC18:0/18:1**	1.11	2.44	0.14	0.91	0.19	0.54	0.22	1.28

Table AII.82- Standard deviation for amounts (nmoles/cell) of most abundant species of endogenous PC class fatty acid chains for CTAB 3.00 μM used in Figure III.51 to III.52.

		Time/hours							
MW /amu	**Fatty acid species**	**0**	**3**	**6**	**9**	**12**	**15**	**18**	**21**
732	**PC16:0/16:1**	4.38	6.55	6.11	5.78	5.34	4.20	5.04	3.81
746	**PC16:0a/18:1**	7.09	7.29	6.83	7.22	7.27	6.72	7.77	7.93
760	**PC16:0/18:1**	24.96	26.66	24.88	24.72	25.58	20.29	25.37	19.13
786	**PC18:0/18:2**	13.49	12.38	11.28	14.68	15.73	13.21	14.97	10.15
788	**PC18:0/18:1**	8.27	9.36	9.76	5.64	5.91	5.86	6.22	5.86
848	**PC20:0a/22:6**	2.16	0.23	0.78	0.79	0.92	4.60	1.03	7.49

Table AII.83- Amounts (nmoles/cell) of most abundant species of endogenous PC class fatty acid chains for CTAB 1.50 μM used in Figures III.51 to III.52.

		Time/hours							
MW /amu	**Fatty acid species**	**0**	**3**	**6**	**9**	**12**	**15**	**18**	**21**
732	**PC16:0/16:1**	1.13	0.59	0.16	0.18	0.18	0.41	0.59	0.32
746	**PC16:0a/18:1**	0.39	0.74	0.63	1.01	0.35	0.51	1.08	0.18
760	**PC16:0/18:1**	1.99	0.83	0.70	0.47	0.52	0.95	2.20	1.59
786	**PC18:0/18:2**	4.66	1.89	0.52	0.97	0.65	1.03	0.83	0.87
788	**PC18:0/18:1**	1.11	2.28	0.18	0.56	0.95	0.90	1.01	0.73
848	**PC20:0a/22:6**	0.27	0.06	0.17	1.03	0.76	5.86	1.50	6.89

Table AII.84- Standard deviation for amounts (nmoles/cell) of most abundant species of endogenous PC class fatty acid chains for CTAB 1.50 μM used in Figure III.51 to III.52.

		Time/hours							
MW /amu	**Fatty acid species**	**0**	**3**	**6**	**9**	**12**	**15**	**18**	**21**
732	**PC16:0/16:1**	4.38	5.49	5.20	4.87	4.95	4.45	4.75	4.80
746	**PC16:0a/18:1**	7.09	6.24	5.92	5.49	6.80	6.16	6.49	6.51
758	**PC16:0/18:2**	2.92	4.52	4.62	5.16	4.00	3.79	3.76	4.04
760	**PC16:0/18:1**	24.96	20.97	21.32	23.23	24.51	24.94	24.71	24.31
774	**PC18:0a/18:1**	13.49	10.55	10.94	14.95	14.84	16.45	14.83	15.02
786	**PC18:0/18:2**	8.27	8.23	7.58	7.64	6.82	7.83	6.65	6.46

Table AII.85- Amounts (nmoles/cell) of most abundant species of endogenous PC class fatty acid chains for CTAB 0.75 μM used in Figures III.51 to III.52.

		Time/hours							
MW /amu	**Fatty acid species**	**0**	**3**	**6**	**9**	**12**	**15**	**18**	**21**
732	**PC16:0/16:1**	1.13	0.50	0.40	0.18	0.21	0.17	0.19	0.11
746	**PC16:0a/18:1**	0.39	0.16	0.32	0.24	0.42	1.79	1.16	0.96
758	**PC16:0/18:2**	0.46	0.15	0.21	0.43	0.23	0.98	0.45	0.12
760	**PC16:0/18:1**	1.99	2.26	1.06	0.74	0.26	1.22	0.38	1.03
774	**PC18:0a/18:1**	4.66	0.67	0.29	0.29	0.28	2.51	1.20	0.79
786	**PC18:0/18:2**	1.11	0.89	0.46	0.61	0.10	0.96	1.38	0.53

Table AII.86- Standard deviation for amounts (nmoles/cell) of most abundant species of endogenous PC class fatty acid chains for CTAB 0.75 μM used in III.51 to III.52.

AII.2.4.4.2. **Newly synthesised PC**

		Time/hours						
MW /amu	**Fatty acid species**	**3**	**6**	**9**	**12**	**15**	**18**	**21**
741	**d9PC16:0/16:1**	8.78	8.37	8.94	7.72	8.73	8.42	5.61
743	**d9PC16:0/16:0**	3.91	5.65	3.27	3.50	3.07	2.81	2.96
755	**d9PC16:0a/18:1**	4.14	5.43	7.32	9.68	5.62	8.27	6.89
767	**d9PC16:0/18:2**	6.72	6.23	6.11	5.20	7.48	5.65	5.45
769	**d9PC16:0/18:1**	27.95	27.05	29.35	27.23	23.51	29.37	25.40
795	**d9PC18:0/18:2**	16.37	12.86	15.20	13.94	13.78	15.36	15.96
797	**d9PC18:0/18:1**	6.71	7.60	4.89	4.71	4.62	4.47	5.51

Table AII.87- Amounts (nmoles/cell) of most abundant species of newly synthesised PC class fatty acid chains for CTAB 3.00 μM used in Figures III.54 to III.55.

		Time/hours						
MW /amu	**Fatty acid species**	**3**	**6**	**9**	**12**	**15**	**18**	**21**
741	**d9PC16:0/16:1**	0.33	0.29	0.21	0.73	0.59	0.21	0.62
743	**d9PC16:0/16:0**	0.86	0.32	0.17	0.55	0.74	0.22	0.37
755	**d9PC16:0a/18:1**	0.93	0.31	0.35	0.82	0.31	0.47	0.39
767	**d9PC16:0/18:2**	0.39	0.27	0.43	0.54	0.06	0.16	0.95
769	**d9PC16:0/18:1**	3.90	0.31	0.92	1.46	1.45	0.38	2.86
795	**d9PC18:0/18:2**	1.17	0.47	0.23	0.25	1.08	0.28	1.51
797	**d9PC18:0/18:1**	1.32	0.63	0.11	0.46	0.20	0.39	0.65

Table AII.88- Standard deviation for amounts (nmoles/cell) of most abundant species of newly synthesised PC class fatty acid chains for CTAB 3.00 μM used in Figures III.54 to III.55.

		Time/hours						
MW /amu	**Fatty acid species**	**3**	**6**	**9**	**12**	**15**	**18**	**21**
741	**d9PC16:0/16:1**	8.41	7.64	6.95	6.24	5.31	5.90	4.91
755	**d9PC16:0a/18:1**	5.53	5.42	6.67	6.60	6.74	6.64	7.98
767	**d9PC16:0/18:2**	5.84	6.38	5.25	5.14	5.18	4.77	4.49
769	**d9PC16:0/18:1**	29.32	27.06	28.48	28.56	25.10	28.00	24.71
795	**d9PC18:0/18:2**	15.22	13.58	16.36	16.39	16.55	16.66	13.31
797	**d9PC18:0/18:1**	7.90	8.35	5.74	5.72	6.43	6.31	6.02

Table AII.89- Amounts (nmoles/cell) of most abundant species of newly synthesised PC class fatty acid chains for CTAB 1.50 μM used in Figures III.54 to III.55.

		Time/hours						
MW /amu	**Fatty acid species**	**3**	**6**	**9**	**12**	**15**	**18**	**21**
741	**d9PC16:0/16:1**	0.55	0.52	0.57	0.11	0.26	0.64	0.09
755	**d9PC16:0a/18:1**	0.60	0.37	1.09	0.13	0.39	0.29	0.48
767	**d9PC16:0/18:2**	0.21	0.50	0.45	0.12	0.21	0.42	0.08
769	**d9PC16:0/18:1**	0.58	1.35	0.27	1.34	1.01	0.57	0.37
795	**d9PC18:0/18:2**	1.46	0.16	0.64	1.21	0.58	0.66	0.86
797	**d9PC18:0/18:1**	1.32	0.16	0.37	0.88	0.20	0.42	0.11

Table AII.90- Standard deviation for amounts (nmoles/cell) of most abundant species of newly synthesised PC class fatty acid chains for CTAB 1.50 μM used in Figures III.54 to III.55.

		Time/hours						
MW /amu	**Fatty acid species**	**3**	**6**	**9**	**12**	**15**	**18**	**21**
741	**d9PC16:0/16:1**	6.90	5.47	5.38	5.70	5.10	5.50	5.44
755	**d9PC16:0a/18:1**	4.43	5.01	4.67	6.00	4.98	5.74	5.57
767	**d9PC16:0/18:2**	6.54	6.51	5.97	5.17	4.48	4.42	4.78
769	**d9PC16:0/18:1**	24.67	24.82	25.44	27.65	28.65	27.86	28.22
795	**d9PC18:0/18:2**	12.72	12.26	15.92	17.35	17.27	17.03	16.84
797	**d9PC18:0/18:1**	8.82	7.55	7.74	6.84	7.97	7.31	6.68

Table AII.91- Amounts (nmoles/cell) of most abundant species of newly synthesised PC class fatty acid chains for CTAB 0.75 μM used in Figures III.54 to III.55.

		Time/hours						
MW /amu	**Fatty acid species**	**3**	**6**	**9**	**12**	**15**	**18**	**21**
741	**d9PC16:0/16:1**	0.42	0.50	0.73	0.12	0.16	0.26	0.10
755	**d9PC16:0a/18:1**	0.21	0.81	0.84	0.34	0.95	0.50	0.24
767	**d9PC16:0/18:2**	0.13	0.46	0.44	0.47	0.85	0.65	0.15
769	**d9PC16:0/18:1**	2.12	0.94	1.35	0.80	2.31	1.53	0.20
795	**d9PC18:0/18:2**	1.03	0.59	0.59	1.01	2.24	1.29	1.38
797	**d9PC18:0/18:1**	0.55	0.32	0.37	0.50	1.17	0.67	0.28

Table AII.92- Standard deviation for amounts (nmoles/cell) of most abundant species of newly synthesised PC class fatty acid chains for CTAB 0.75 μM used in Figure III.54 to III.55.

AII.2.4.4.3. **Endogenous PE**

		Time/hours							
MW /amu	**Fatty acid species**	**0**	**3**	**6**	**9**	**12**	**15**	**18**	**21**
718	**PE16:0/18:1**	7.89	12.09	11.01	14.76	16.16	6.28	15.86	10.28
744	**PE18:0/18:2**	21.78	20.22	18.37	22.25	24.59	17.62	27.19	15.78
746	**PE18:0/18:1**	13.07	19.87	23.51	20.07	19.80	14.59	17.26	15.32
766	**PE18:1/20:4**	5.01	2.80	3.10	3.09	2.75	7.04	2.49	2.26
768	**PE18:0/20:4**	5.80	10.14	11.19	9.44	7.29	17.39	6.20	4.05
772	**PE18:0/20:2**	7.56	5.23	4.16	4.39	4.55	2.55	5.15	4.62
790	**PE18:0/20:4**	5.29	1.30	0.99	0.89	1.02	1.86	0.90	9.54
792	**PE18:0/22:6**	4.56	4.76	5.75	4.29	3.44	7.13	3.71	3.90
794	**PE18:0/22:5**	1.42	3.52	4.00	3.46	2.41	5.33	2.72	2.12

Table AII.93- Amounts (nmoles/cell) of most abundant species of endogenous PC class fatty acid chains for CTAB 3.00 μM used in Figures III.57 to III.59.

		Time/hours							
MW /amu	**Fatty acid species**	**0**	**3**	**6**	**9**	**12**	**15**	**18**	**21**
718	**PE16:0/18:1**	4.39	1.94	0.38	1.56	0.39	0.76	1.67	5.42
744	**PE18:0/18:2**	8.76	3.79	1.50	0.93	0.76	2.20	0.94	5.21
746	**PE18:0/18:1**	2.24	4.18	2.81	1.04	1.51	0.87	0.19	6.71
766	**PE18:1/20:4**	4.44	0.75	0.86	0.41	0.50	1.28	0.55	1.98
768	**PE18:0/20:4**	9.26	3.16	1.43	1.23	1.12	3.38	1.19	2.72
772	**PE18:0/20:2**	2.71	1.54	0.50	0.31	0.55	1.25	0.48	1.22
790	**PE18:0/20:4**	3.34	0.61	0.48	0.34	0.19	0.66	0.24	6.89
792	**PE18:0/22:6**	2.97	0.78	0.42	0.62	0.27	0.80	0.29	3.42
794	**PE18:0/22:5**	1.60	0.85	0.98	0.34	0.41	1.44	0.97	0.66

Table AII.94- Standard deviation for amounts (nmoles/cell) of most abundant species of endogenous PC class fatty acid chains for CTAB 3.00 μM used in Figure III.57 to III.59.

		Time/hours							
MW /amu	**Fatty acid species**	**0**	**3**	**6**	**9**	**12**	**15**	**18**	**21**
718	**PE16:0/18:1**	7.89	12.46	10.54	12.35	12.86	6.95	12.65	8.78
744	**PE18:0/18:2**	21.78	20.99	18.28	20.40	22.38	14.32	20.15	20.53
746	**PE18:0/18:1**	13.07	24.88	23.38	19.57	19.08	15.65	18.61	19.90
766	**PE18:1/20:4**	5.01	2.90	4.01	0.78	0.00	3.36	0.66	1.85
768	**PE18:0/20:4**	5.80	10.77	13.27	6.29	3.36	7.06	1.81	6.34
772	**PE18:0/20:2**	7.56	5.07	3.77	4.27	5.67	5.07	5.46	5.53
774	**PE18:0/20:1**	2.49	1.25	0.87	1.56	1.58	5.31	1.52	1.53
790	**PE18:0a/22:0**	5.29	0.81	0.71	4.19	5.62	5.08	10.78	4.85
792	**PE18:0/22:6**	4.56	4.33	5.24	5.80	5.75	9.19	4.24	4.79

Table AII.95- Amounts (nmoles/cell) of most abundant species of endogenous PC class fatty acid chains for CTAB 1.50 μM used in Figures III.57 to III.59.

		Time/hours							
MW /amu	**Fatty acid species**	**0**	**3**	**6**	**9**	**12**	**15**	**18**	**21**
718	**PE16:0/18:1**	4.39	1.53	2.37	2.03	1.94	2.31	4.57	0.41
744	**PE18:0/18:2**	8.76	1.48	2.28	3.32	1.58	7.74	7.89	0.72
746	**PE18:0/18:1**	2.24	0.99	1.60	2.55	1.63	7.49	2.21	2.61
766	**PE18:1/20:4**	4.44	0.25	0.36	1.29	0.00	3.89	1.14	0.46
768	**PE18:0/20:4**	9.26	2.35	3.34	1.61	2.87	3.05	2.69	1.89
772	**PE18:0/20:2**	2.71	0.79	0.79	0.59	1.20	0.58	0.77	0.66
774	**PE18:0/20:1**	1.62	0.14	0.31	0.73	0.19	5.91	0.28	0.20
790	**PE18:0a/22:0**	3.34	0.43	0.38	1.04	1.29	3.60	12.63	0.55
792	**PE18:0/22:6**	2.97	0.62	0.98	1.64	0.95	7.75	0.17	1.31

Table AII.96- Standard deviation for amounts (nmoles/cell) of most abundant species of endogenous PC class fatty acid chains for CTAB 1.50 μM used in Figure III.57 to III.59.

		Time/hours							
MW /amu	**Fatty acid species**	**0**	**3**	**6**	**9**	**12**	**15**	**18**	**21**
718	**PE16:0/18:1**	7.89	7.03	5.46	7.55	12.17	10.02	9.68	8.80
744	**PE18:0/18:2**	21.78	16.24	15.95	22.63	22.43	24.12	14.29	21.06
746	**PE18:0/18:1**	13.07	19.23	15.56	17.28	20.19	17.88	16.99	20.41
766	**PE18:1/20:4**	5.01	5.81	7.44	1.02	1.18	0.61	2.05	2.15
768	**PE18:0/20:4**	5.80	20.94	21.56	5.31	6.35	5.28	1.98	4.84
772	**PE18:0/20:2**	7.56	2.65	2.65	5.20	5.40	6.14	4.18	3.99
790	**PE18:0a/22:0**	5.29	1.03	1.09	5.75	3.71	4.54	7.88	6.95
792	**PE18:0/22:6**	4.56	6.64	5.93	5.81	4.96	6.25	4.78	5.67
800	**PE18:0/22:2**	2.74	0.92	1.23	2.00	1.45	2.17	7.35	0.85

Table AII.97- Amounts (nmoles/cell) of most abundant species of endogenous PC class fatty acid chains for CTAB 0.75 μM used in Figures III.57 to III.59.

		Time/hours							
MW /amu	**Fatty acid species**	**0**	**3**	**6**	**9**	**12**	**15**	**18**	**21**
718	**PE16:0/18:1**	4.39	1.11	0.98	1.11	1.69	3.59	3.47	0.55
744	**PE18:0/18:2**	8.76	0.67	1.06	0.56	0.16	1.41	11.32	0.87
746	**PE18:0/18:1**	2.24	2.62	1.86	0.96	1.37	4.06	6.12	0.64
766	**PE18:1/20:4**	4.44	0.94	1.26	0.90	1.51	0.73	2.02	1.26
768	**PE18:0/20:4**	9.26	2.91	2.94	3.37	1.37	1.35	3.18	3.91
772	**PE18:0/20:2**	2.71	0.70	0.59	0.83	1.20	1.30	2.85	0.16
790	**PE18:0a/22:0**	3.34	0.18	0.49	2.84	0.73	4.08	3.67	3.54
792	**PE18:0/22:6**	2.97	0.77	0.70	0.78	0.40	1.25	0.80	2.98
800	**PE18:0/22:2**	0.77	0.23	0.37	0.69	0.40	0.22	9.18	0.37

Table AII.98- Standard deviation for amounts (nmoles/cell) of most abundant species of endogenous PC class fatty acid chains for CTAB 0.75 μM used in Figure III.57 to III.59.

AII.2.4.4.4. **Rate of new PC synthesis**

	CTAB 3.00 μM		**CTAB 1.50 μM**		**CTAB 0.75 μM**	
Time /hours	**Rate /nmoles. h^{-1}**	**SD**	**Rate /nmoles. h^{-1}**	**SD**	**Rate /nmoles. h^{-1}**	**SD**
3	2.21E-06	1.60E-06	1.09E-05	2.58E-06	2.01E-06	9.69E-07
6	3.86E-06	3.60E-06	2.80E-06	1.64E-06	3.15E-06	2.31E-06
9	9.86E-06	4.54E-06	4.68E-06	1.79E-06	2.95E-06	1.36E-06
12	9.59E-06	2.75E-06	4.00E-06	3.30E-06	7.98E-06	4.38E-06
15	1.01E-05	7.39E-06	1.26E-05	1.05E-05	1.12E-05	1.02E-05
18	1.96E-05	2.11E-05	5.47E-06	2.48E-06	2.92E-06	2.24E-06
21	5.08E-06	5.06E-06	1.32E-06	9.81E-07	6.12E-06	1.86E-06

Table AII.99- Data used in Figure III.59.

AII.3. Data tables for PFK-1 results (Chapter IV)

AII.3.1. BsPFK-1 kinetics as a function of time

Time /minutes	Percentage conversion	Standard deviation
0.5	9.49	0.69
2	11.11	1.34
4	13.61	1.01
6	12.64	0.70
8	12.19	2.16
14	12.23	1.22
16	14.65	1.83
18	15.75	4.20
20	16.66	2.25
25	20.67	0.97

Table AII.100- Assay 68 data used in Figure IV.8.

AII.3.2. BsPFK-1 kinetics as a function of enzyme concentration

	No lipid (Assay 98)		100% DOPC (Assay 99)		50% OA (Assay 100)	
[BsPFK-1] /(mu/mL)	Activity /nmoles.min^{-1}.mg^{-1}	SD	Activity /nmoles.min^{-1}.mg^{-1}	SD	Activity /nmoles.min^{-1}.mg^{-1}	SD
0	-8.35	0.60	-9.28	0.21	-9.92	0.61
0.5	-113.68	109.31	173.14	591.15	14.97	1.81
1	-131.84	105.30	433.37	66.16	958.13	317.40
2.5	1240.18	105.00	3265.70	219.07	4166.84	224.59
5	2734.09	196.26	5280.57	262.86	7992.65	242.36
7.5	3944.24	287.82	8818.23	351.47	10507.55	143.01
10	4462.03	494.89	9001.94	619.80	11872.14	188.86
15	5982.13	518.62	11591.93	331.21	12766.62	1069.87

Table AII.101- Data used in Figure IV.9.

Note: Enzyme activity is quoted as 1 mu/mL of pure protein in the 50 μL assay, where 1 unit will convert 1.0 μmole of fructose 6-phosphate and ATP to fructose 1,6-diphosphate and ADP per minute at pH 9.0 at 30 °C.

AII.3.3. BsPFK-1 kinetics as a function of lipid concentration

	100% DOPC		50% OA	
[Lipid] /mM	**Activity /nmoles.min^{-1}.mg^{-1}**	**SD**	**Activity /nmoles.min^{-1}.mg^{-1}**	**SD**
0.01	3966.17	992.55	3738.25	774.61
0.055	5338.62	278.42	5371.02	324.99
0.1	6349.91	199.05	5922.49	645.30
0.55	6412.08	195.62	5634.56	462.65
1	7519.13	210.88	7483.78	566.59
5.5	7109.35	305.60	7603.28	188.92
10	7231.96	120.27	7595.03	113.73

Table AII.102- Assay 88 data used in Figure IV.10.

	100% DOPC		50% OA	
[Lipid] /μM	**Activity /nmoles.min^{-1}.mg^{-1}**	**SD**	**Activity /nmoles.min^{-1}.mg^{-1}**	**SD**
0	4112.68	1109.05	5391.00	173.78
0.5	4928.79	111.94	5511.56	365.07
1	5319.81	573.07	4886.46	65.00
5	5509.63	562.19	7425.87	682.02
10	7639.25	272.66	7814.99	1238.06
25	7632.35	321.48	9188.67	550.35
60	8115.93	621.30	9512.06	120.70
100	9232.78	658.58	10307.08	224.93
550	8694.10	211.18	10132.79	424.30
1000	8421.92	542.42	10120.91	651.69
5500	7504.54	793.59	10427.73	246.02
10000	6377.08	818.66	9686.79	290.60

Table AII.103- Assays 89 to 93 data used in Figure IV.11.

AII.3.4. BsPFK-1 kinetics as a function of ATP concentration

[ATP] /μM	Activity /nmoles.min^{-1}.mg^{-1}	Standard deviation
2	269.50	92.33
5	464.78	158.51
10	3068.55	182.34
20	2869.74	292.14
50	2300.75	432.58
100	2301.63	445.90
200	1685.28	76.20
500	1672.32	135.19
1000	8804.73	292.47

Table AII.104- Assay 66 data used in Figure IV.13.

	10 μM ATP (Assay 72)		25 μM ATP (Assay 73)		50 μM ATP (Assay 74)	
Time /minutes	**Percentage conversion**	**SD**	**Percentage conversion**	**SD**	**Percentage conversion**	**SD**
0.5	2.74	0.53	2.98	0.73	2.52	1.29
3	3.56	1.11	2.89	0.63	3.62	0.92
5	4.74	0.78	4.46	1.38	1.42	0.60
10	7.12	0.29	3.14	0.68	1.26	0.36
15	5.68	1.09	5.05	0.18	3.25	0.59
20	8.82	0.85	5.13	1.41	4.47	2.01

Table AII.105- Data used in Figure IV.14.

AII.3.5. BsPFK-1 kinetics as a function of F6P concentration

[F6P] /mM	Activity /nmoles.min^{-1}.mg^{-1}	Standard deviation
0.01	343.25	228.13
0.05	3213.64	237.99
0.1	3831.66	154.43
0.2	4726.79	260.16
0.5	3928.71	326.82
1	3897.53	465.55
5	3290.03	344.27

Table AII.106- Assay 94 data used in Figure IV.15.

	No lipid (Assay 98)		100% DOPC (Assay 99)		50% OA (Assay 100)	
[F6P] /μM	Activity /nmoles.min^{-1}.mg^{-1}	SD	Activity /nmoles.min^{-1}.mg^{-1}	SD	Activity /nmoles.min^{-1}.mg^{-1}	SD
5	705.71	169.71	424.07	18.22	867.22	301.15
10	677.06	555.24	816.67	63.87	1115.20	283.20
50	3329.54	350.47	5113.55	275.16	7985.88	297.96
100	3843.01	186.14	5231.97	513.22	9101.60	313.24
250	4089.52	233.61	6046.08	556.79	9560.47	147.71
500	4319.33	76.89	6840.50	471.27	9479.03	351.64
1000	4174.61	745.77	6555.22	347.56	9796.42	397.55
1500	4361.14	897.06	6318.47	307.69	10003.89	165.53

Table AII.107- Data used in Figure IV.16.

AII.3.6. Inhibition of BsPFK-1 kinetics by PEP

[F6P] /mM	Activity /nmoles.min^{-1}.mg^{-1}	Standard deviation
10	391.73	78.31
25	1183.85	173.92
50	2592.85	41.73
75	3039.34	177.68
100	2662.39	373.94
150	2860.02	831.85

Table AII.108- Assay 111 data used in Figure IV.19.

	5 μM PEP (Assay 112)		25 μM PEP (Assay 113)		100 μM PEP (Assay 114)	
[F6P] /μM	**Activity /nmoles.min^{-1}.mg^{-1}**	**SD**	**Activity /nmoles.min^{-1}.mg^{-1}**	**SD**	**Activity /nmoles.min^{-1}.mg^{-1}**	**SD**
10	359.27	9.94	314.56	45.18	48.79	15.92
25	1141.56	48.52	506.21	181.38	88.68	28.16
50	1804.59	231.67	1321.55	41.49	447.86	73.35
75	1786.56	404.76	1379.22	563.36	828.86	238.56
100	1812.54	273.42	1352.38	189.19	1246.79	58.22
150	2187.89	309.35	2245.18	108.47	1779.32	133.53

Table AII.109- Data used in Figure IV.19.

	no PEP (Assay 101)		5 μM PEP (Assay 102)		25 μM PEP (Assay 103)	
[F6P] /μM	**Activity /nmoles.min^{-1}.mg^{-1}**	**SD**	**Activity /nmoles.min^{-1}.mg^{-1}**	**SD**	**Activity /nmoles.min^{-1}.mg^{-1}**	**SD**
0	72.32	58.71	106.70	28.58	59.50	9.73
5	121.72	88.26	181.92	N/A	80.09	N/A
10	435.99	290.62	581.21	N/A	118.59	47.33
50	1146.03	53.20	753.32	13.19	383.29	95.60
100	1194.11	82.36	1070.44	163.15	888.73	70.78
250	1182.93	154.80	1228.68	62.05	940.30	113.44
500	1248.88	127.61	1214.69	103.71	1076.19	63.39
1000	1075.34	96.24	1147.15	104.17	1271.64	64.58
1500	625.76	150.05	1368.98	204.07	1148.39	109.62

Table AII.110- Data used in Figure IV.20.

	5 μM PEP no lipid (Assay 112)		5 μM PEP 100% DOPC (Assay 116)		5 μM PEP 50% OA (Assay 120)	
[F6P] /μM	**Activity /nmoles.min^{-1}.mg^{-1}**	**SD**	**Activity /nmoles.min^{-1}.mg^{-1}**	**SD**	**Activity /nmoles.min^{-1}.mg^{-1}**	**SD**
10	359.27	9.94	117.36	80.05	335.51	88.89
25	1141.56	48.52	826.18	134.43	935.07	55.05
50	1804.59	231.67	1481.90	229.76	1308.70	189.30
75	1786.56	404.76	1602.37	34.95	1396.79	158.61
100	1812.54	273.42	1565.38	169.37	1860.90	182.30
150	2187.89	309.35	2041.56	39.75	2156.31	128.51

Table AII.111- Data used in Figure IV.21.

	5 μM PEP no lipid (Assay 102)		5 μM PEP 100% DOPC (Assay 105)		5 μM PEP 50% OA (Assay 108)	
[F6P] /μM	**Activity /nmoles.min^{-1}.mg^{-1}**	**SD**	**Activity /nmoles.min^{-1}.mg^{-1}**	**SD**	**Activity /nmoles.min^{-1}.mg^{-1}**	**SD**
0	106.70	28.58	-8.15	0.26	83.09	61.05
5	181.92	N/A	263.73	70.91	263.32	73.47
10	581.21	N/A	388.86	91.52	435.70	63.48
50	753.32	13.19	1869.16	304.71	2041.40	345.78
100	1070.44	163.15	2782.55	593.87	3221.09	186.43
250	1228.68	62.05	2941.76	214.40	3300.39	414.80
500	1214.69	103.71	3328.60	141.83	3154.65	73.00
1000	1147.15	104.17	3421.27	613.67	3490.58	272.27
1500	1368.98	204.07	3022.81	289.34	3773.13	344.63

Table AII.112- Data used in Figure IV.22.

	25 μM PEP no lipid (Assay 103)		25 μM PEP 100% DOPC (Assay 106)		25 μM PEP 50% OA (Assay 109)	
[F6P] /μM	**Activity /nmoles.min^{-1}.mg^{-1}**	**SD**	**Activity /nmoles.min^{-1}.mg^{-1}**	**SD**	**Activity /nmoles.min^{-1}.mg^{-1}**	**SD**
10	59.50	9.73	-103.43	45.33	408.59	121.28
25	80.09	N/A	565.47	11.60	683.49	99.63
50	118.59	47.33	-32.53	48.15	487.45	162.55
75	383.29	95.60	1076.31	1141.65	1697.77	158.59
100	888.73	70.78	1869.02	83.60	2588.83	373.74
250	940.30	113.44	2039.56	162.85	3133.47	274.78
500	1076.19	63.39	2148.79	283.13	2624.15	136.33
1000	1271.64	64.58	2375.25	9.80	2414.17	40.82
1500	1148.39	109.62	2362.59	455.02	2685.20	160.42

Table AII.113- Data used in Figures IV.23 to IV.24.

	100 μM PEP no lipid (Assay 114)		100 μM PEP 100% DOPC (Assay 118)		100 μM PEP 50% OA (Assay 122)	
[F6P] /μM	**Activity /nmoles.min^{-1}.mg^{-1}**	**SD**	**Activity /nmoles.min^{-1}.mg^{-1}**	**SD**	**Activity /nmoles.min^{-1}.mg^{-1}**	**SD**
10	48.79	15.92	320.47	206.46	172.29	67.32
25	88.68	28.16	284.97	240.58	248.64	80.25
50	447.86	73.35	617.82	195.88	-402.86	398.46
75	828.86	238.56	814.22	362.01	652.48	79.19
100	1246.79	58.22	1459.03	42.68	1069.15	347.18
150	1779.32	133.53	1468.98	131.70	1617.79	327.67

Table AII.114- Data used in Figure IV.25.

AII.3.7. Activation of BsPFK-1 kinetics by ADP

[F6P] /mM	Activity /nmoles.min^{-1}.mg^{-1}	Standard deviation
10	252.60	31.47
25	694.37	31.02
50	578.86	57.74
75	663.02	53.71
100	651.25	77.82
150	562.73	115.48

Table AII.115- Assay 123 data with no lipid and no PEP used in Figure IV.32.

	5 μM ADP (Assay 124)		25 μM PEP (Assay 125)		100 μM PEP (Assay 126)	
[F6P] /μM	Activity /nmoles.min^{-1}.mg^{-1}	SD	Activity /nmoles.min^{-1}.mg^{-1}	SD	Activity /nmoles.min^{-1}.mg^{-1}	SD
10	225.34	8.64	250.86	52.41	101.64	92.26
25	502.67	40.40	520.06	197.78	490.89	21.12
50	723.17	66.60	766.79	116.10	610.18	107.87
75	816.72	44.21	686.88	80.27	784.06	172.44
100	874.02	70.65	887.31	79.83	511.07	84.20
150	450.87	205.41	849.06	150.67	420.70	215.96

Table AII.116- Data used in Figure IV.33.

[F6P] /mM	Activity /nmoles.min^{-1}.mg^{-1}	Standard deviation
10	864.11	483.64
25	1616.27	146.62
50	1860.59	179.86
75	1748.47	236.87
100	1879.49	117.99
150	2096.02	176.04

Table AII.117- Assay 127 data with 100% DOPC and no PEP used in Figure IV.38.

	5 μM ADP 100% DOPC (Assay 128)		25 μM PEP100% DOPC (Assay 129)		100 μM PEP100% DOPC (Assay 130)	
[F6P] /μM	**Activity /nmoles.min-1.mg-1**	**SD**	**Activity /nmoles.min-1.mg-1**	**SD**	**Activity /nmoles.min-1.mg-1**	**SD**
10	480.62	108.44	667.90	81.72	957.42	47.87
25	1259.55	117.84	1586.57	114.04	3316.81	406.85
50	1617.76	138.96	1706.15	126.56	7902.18	1235.43
75	1619.03	274.30	1786.65	90.58	9319.07	225.31
100	1913.46	307.99	2024.28	200.99	9050.94	463.50
150	1937.94	114.83	2082.84	191.24	10103.85	434.19

Table AII.118- Data used in Figure IV.34, IV.35 and IV.38.

[F6P] /mM	**Activity /nmoles.min-1.mg-1**	**Standard deviation**
10	642.09	179.91
25	1598.33	60.07
50	2058.95	98.46
75	2455.49	277.78
100	2044.29	225.92
150	2432.43	287.80

Table AII.119- Assay 131 data with 50% OA and no PEP used in Figure IV.39.

	5 μM ADP 50% OA (Assay 132)		25 μM 50% OA (Assay 133)		100 μM 50% OA (Assay 134)	
[F6P] /μM	**Activity /nmoles.min-1.mg-1**	**SD**	**Activity /nmoles.min-1.mg-1**	**SD**	**Activity /nmoles.min-1.mg-1**	**SD**
10	606.19	194.91	326.39	143.75	597.15	85.28
25	1816.49	380.14	914.64	70.98	3097.36	370.15
50	1803.00	92.67	1707.14	205.24	3895.54	1252.93
75	1908.85	97.87	2383.80	372.19	4862.27	N/A
100	2157.69	282.91	2345.22	215.26	3720.08	N/A
150	3261.11	469.71	2638.77	321.28	9693.11	555.22

Table AII.120- Data used in Figure IV.34, IV.35 and IV.39.

Appendix III

Matlab code used for program used in Chapter III data analysis

(see attached data disc)